Magnavox Technical Report

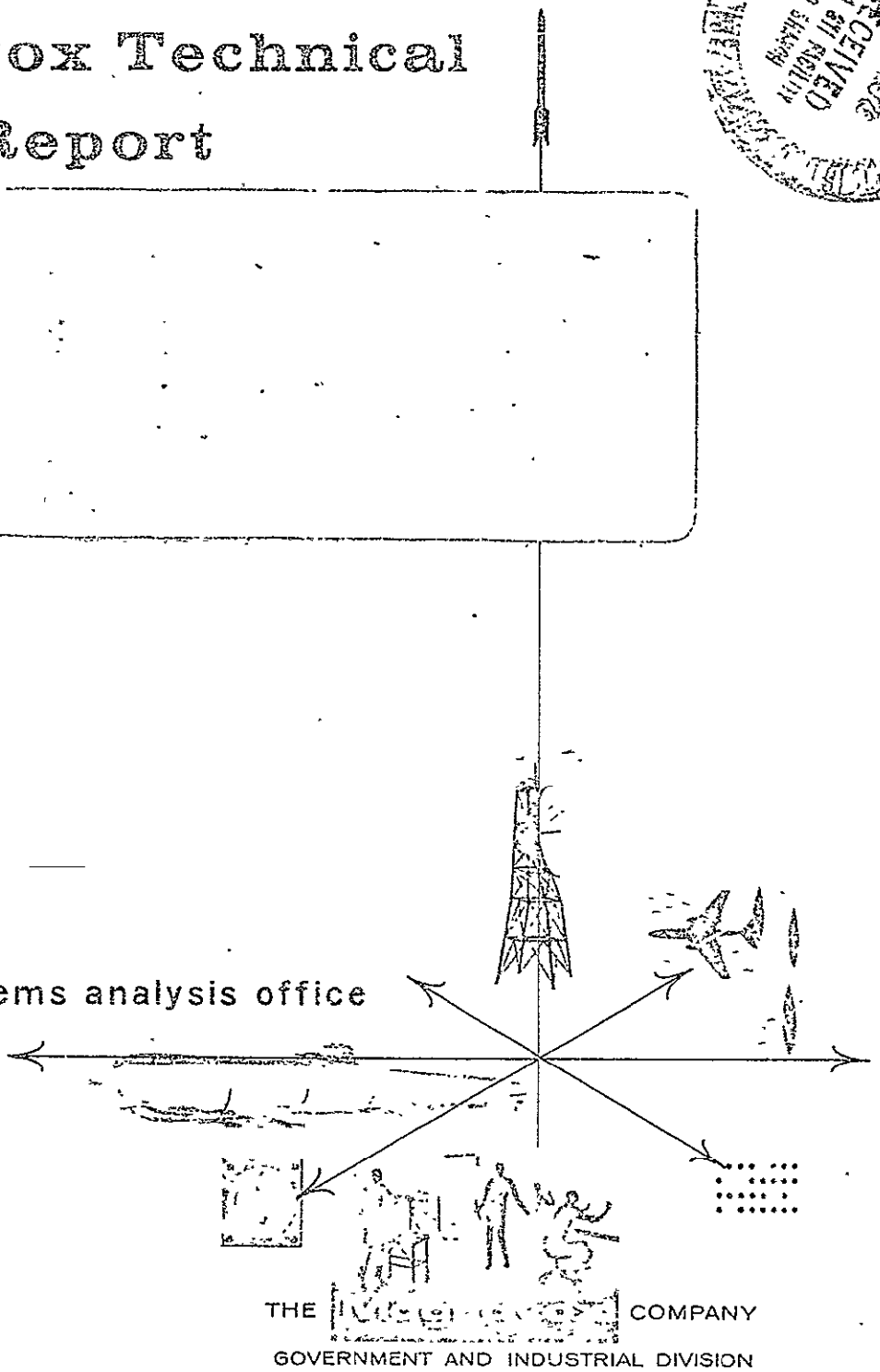

advanced systems analysis office

THE [redacted] COMPANY

GOVERNMENT AND INDUSTRIAL DIVISION

FINAL REPORT

MULTIPATH/MODULATION STUDY
for the
TRACKING AND DATA RELAY SATELLITE SYSTEM
(14 April 1969 - 12 January 1970)

Contract No.: NAS5-10744

Prepared by:

The Magnavox Company
Government and Industrial Division
Advanced Systems Analysis Office
Suite 1000, 8720 Georgia Avenue
Silver Spring, Maryland 20910

for

National Aeronautics and Space Administration
Goddard Space Flight Center
Greenbelt, Maryland

Prepared by: J. N. Birch
J. N. Birch

Acknowledgment

Magnavox wishes to acknowledge the help and cooperation the Company has received from NASA during this contract. In particular we wish to thank Dr. Kenneth E. Peltzer of GSFC, Greenbelt, Md., for his technical and administration guidance during the program. We also recognize the significant NASA contributions by John J. Schwartz, John Bryan, Paul Barritt, E. J. Habib, John Martin, James Cooley, Paul Heffernan, Marvin Maxwell, and T. S. Golden.

As major Magnavox contributors to this document we are grateful to C. R. Cahn, Robert Gold, Peter Nilsen, Don DeVito, Djimitri Wiggert, and Ceasar Filippi.

ABSTRACT OF FINAL REPORT

Introduction

This document is a Final Report which covers the Multipath Modulation Study of the Tracking and Data Relay Satellite System, conducted by The Magnavox Company's Advanced Systems Analysis Office for NASA Goddard.

The purpose of the study has been realized. The Magnavox Company has evolved a system as a result of many tradeoff analyses which will provide the users of Tracking and Data Relay Satellite Systems (TDRS) with the following capabilities:

- immunity to multipath
- multiple access through a wideband satellite in the presence of many other users
- interference rejection capability
- accurate range and range rate tracking by one or more ground stations
- simultaneous transfer of data and ranging information
- simultaneous contact between a ground station and many users

In addition to these gross capabilities, the approach provides for rapid synchronization between a user and ground station, and provides for all the required data rates and voice requirements. The system has built-in margins to insure successful operation.

Report Summary

The report begins with a statement of the objectives of the study and a complete requirement analysis. This requirement analysis sets the ground rules and goals of the study.

Prior to the technical discussions of the various candidate systems with potential anti-multipath, multiple access, and anti-interference capabilities we present in detail the significant parameters which govern the time varying channel between a user and the TDRS. These parameters are defined so that their particular roles in subsequent system performance evaluations are well understood. In addition to the propagation parameters such as fading bandwidths, coherent bandwidths, direct path doppler, etc., we have also discussed antenna anamolies which exist for unmanned user satellites as a result of its omni-directional pattern.

In order to provide tractable mathematical analyses and tradeoffs, Magnavox selected a limited but representative number of systems for actual analysis. This limited but representative number of candidate systems totals eleven separate techniques; their selection was based upon a signal design rationale which dictates that three generic approaches can be taken to the multipath problem; and these eleven systems are members of the three basic approaches.

Following the candidate system selections we determine the required bit error probability for a user to insure that the quantizing resolution employed in the user spacecraft is maintained through the noisy channel. Expressions are obtained and curves are presented which illustrate the maximum allowable bit error probability which can be tolerated and still maintain the desired A/D quantizing resolution. The analysis shows that the required bit error probability is a function of the amplitude statistics associated with the analog data prior to digital conversion.

Furthermore, the required bit error probability is a function of the number of bits utilized in the PCM system. For example, we have shown that the required bit error probability should be 10^{-5} for a 7-bit PCM system if the analog to digital conversion resolution of user spacecraft data is to be maintained. This analysis is considered essential to the study since by establishing the minimum acceptable bit error probability, the need for coding (e.g., forward error control) can be determined from individual performance analysis of candidate systems.

After selecting the systems we proceed to analyze them for their anti-multipath and multiple access capabilities. We have excluded from analysis, by direction from NASA, any system which requires time division multiple access or the accurate knowledge of time so that respective users can access the TDRS in a time coordinated fashion. The analyses are general and can be readily extended to situations where the repeater bandwidth and user power are not so restricted. We have emphasized the VHF link between the unmanned user and the TDRS in most of our analyses since this link appears to be the most difficult to support. It is both bandwidth and power starved. All of the analyses assumed worst case conditions and adequate system margins.

Of particular interest to TDRS and to other future NASA programs, is a section in this Final Report which discusses the correlation properties of pseudo-random codes which are known as Gold Codes. These codes are utilized for pseudo-noise multiplexing of a large number of simultaneous users through a common channel such as TDRS. This contribution is a significant result of our study, for this analysis determines for the

Once synchronization has been thoroughly analyzed we present a section on phase lock loop tracking for the efficient recovery of data and voice signals for the TDRS. We evaluate the impact of doppler and doppler rate on the ability of the user and G.S. to demodulate data at the designed bit error probability of 10^{-5}.

For manned applications of TDRS, there is a requirement for multiplexing voice and data. This requirement exists at S-band for the normal mode and at VHF for an emergency voice mode. Magnavox has surveyed various voice coding techniques to insure high quality voice, data multiplexing compatibility, and compatibility with various anti-multipath multiple access techniques. As a result of the survey we have recommended a voice coding technique for both the normal and emergency voice mode for the manned users which is economical in bandwidth, size, cost, and power, but renders high performance and degrades gracefully in noise.

Unfortunately the TDRS is plagued with RFI. Interference is seen by the relay satellite as well as by the user on both the VHF channels. Magnavox has devoted a complete section of this report to the evaluation of the RFI and determination of its impact on the modulation techniques investigated for the TDRS. We have included RFI data on a round the world basis to project the RFI environment in the frequency band of interest.

The hardware complexity of the user equipment is of prime concern. The hardware must be reliable, low power, cost effective, and lend itself to high density packaging. The various modulation techniques we have investigated have been reduced to block diagram form and in many cases

first time the expected number of users which can be supported by the TDRS when each user is assigned a pseudo-noise Gold Code for the purpose of multiple access and positive identification at the ground station.

To enhance the systems performance, independent of the modulation technique, and to insure a greater system margin, we discuss in detail the advantages of using a modest amount of forward error control for the power limited users of TDRS. We advocate the use of convolutional encoding at the user and sequential decoding at the ground station to enhance overall system performance. While forward error control in the past, has required complex circuitry, current circuit technology coupled with this particular forward error control approach, makes forward error control an attractive way of increasing the TDRS capacity and/or reliability with a minimal addition of hardware at the ground station.

A significant section in this Final Report deals with range and range rate considerations for TDRS. We discuss user position error in terms of the inaccuracies in tracking the TDRS, inaccuracies in the ground station position, and the tracking errors of a user by one or more tracking data relay satellites. Of particular importance is the conclusions we have reached that the ground stations can be located within a ten meter SEP absolute error using existing TRANSIT technology.

We also present a thorough discussion of the synchronization of various wideband and narrowband systems which were selected for their anti-multipath properties.

we have discussed the actual implementation of the various approaches in terms of their reliability, cost, size, weight, and power.

As a result of the many analyses and tradeoffs which range from anti-multipath performance to hardware designs, we present a recommended system and its block diagram design. The recommended approach is a "compromise optimum" system in that it has been evolved through a step-by-step evaluation process. In most instances the recommended approach is the best approach in a particular evaluation category. Overall the recommended system meets all of the goals of the study.

After recommending the final system we discussed impact of this system on existing Goddard instrumentation such as STADAN and the Manned Space Flight Network. We also discuss the similarity of the approach recommended by this study with other Goddard techniques already in existence.

We conclude our report with a set of recommendations. These recommendations advocate continued study in various problem areas uncovered as a result of our current study.

Recommendations

Based upon lengthy and detailed tradeoff analyses covering virtually every problem area existing between a low power user satellite and the Tracking and Data Relay Satellite, we have concluded that the pseudo-noise (PN) modulation system is the "best" compromise approach. We have shown that the PN system can support 40 unmanned users under the most adverse multipath conditions.

Furthermore, it is shown in this report that the pseudo-noise system will provide protection against multipath even at very low altitudes which are encountered during the initial launch phase of the mission. All other systems which were analyzed failed to meet one or more requirements with regard to protection of the signal in the presence of multipath.

We recommend, as an ancillary to the pseudo-noise system, forward error control of the convolutional encoding sequential decoding variety. We have shown that with a modest amount of hardware located at the ground station an improved system margin and/or capacity of 4 to 7 dB can be obtained through the use of forward error control.

To strengthen our choice of the pseudo-noise system as the basic approach for users of TDRS, we have shown that the pseudo-noise system can provide an excellent range and range rate tracking capability for these users. Specifically, it is shown that the pseudo-noise system will provide a 3 meter, one way ranging instrumentation error in the presence of 40 users and worst case multipath. Furthermore, it has been shown that the pseudo-noise system will provide a 4.5 meter accuracy for the ground station to user link. Range and range rate are virtually a fall-out of the instrumentation required to implement the pseudo-noise system, whereas other techniques investigated require the addition of range and range rate instrumentation to effect tracking of the users. We propose a pseudo-noise transponder at the user which provides a coherent turnaround doppler for 2-way range rate extraction.

The pseudo-noise system has been shown to synchronize with a 2-way sychronization probability of .9 and with worst case synchronization time of 16 secs; the average synchronization time is 8 secs for the complete 2-way link synchronization. The pseudo-noise system will provide unambiguous ranging between the user and the ground station out to the limits of the expected mission geometry.

It is shown that the pseudo-noise system can adequately track the doppler and doppler rate associated with the time-varying geometry between a user and the TDRS. The pseudo-noise system will provide accurate ranging between ground station and TDRS and provide accurate tracking of the TDRS, which is required in the final determination of the user's position. Furthermore, the pseudo-noise system will provide doppler compensation from the ground station to user link to insure that the doppler contribution from the motion of the TDRS will not degrade or bias the system's performance.

By using a pseudo-noise system in deference to other techniques investigated, the command link between ground station and user requires a single channel and all users in view of the TDRS can automatically synchronize to this single channel and thus provide the ground station continuous tracking of all users in view of a particular TDRS satellite.

A system margin of 6 dB has been included in all system calculations and the pseudo-noise system has been shown to provide the necessary data rates at the required bit error probability for a user power level of 2 watts. This power level includes the system margin of 6 dB.

Pulse duration modulation digital voice encoding is recommended for the manned space emergency and non-emergency modes. We have shown that the pulse duration modulation technique can be easily multiplexed with data and that it is very compatible with the pseudo-noise modulation approach. Furthermore, the pulse duration modulation technique outperforms both PCM, FM, and other modern voice encoding techniques in the region of critical signal to noise ratios. The encoding and decoding involved in the PDM modulation approach is extremely simple, low cost, and low power. During the manned emergency mode, it has been shown that pseudo-noise system combined with PDM voice and 4.8 kilobit multiplexed data can provide a very reliable channel between the manned user and the ground station. Furthermore, tracking the manned user during the emergency mode is effected. While the VHF channels are plagued by the presence of RFI from the earth, the pseudo-noise system is amenable to interference reduction techniques at ground station, and we have shown that a modest amount of interference reduction at ground station will completely negate the presence of the worst case of RFI.

With regard to hardware complexity the pseudo-noise system, because of the integrated nature of the waveform, provides simultaneous functions such as data transfer, range, etc. The pseudo-noise system is an integrated system, whereas other approaches which appear to be less complex with regard to hardware for anti-multipath protection, in fact require additional hardware to accomplish the range and range rate implementation. Thus we conclude that the relative complexity of the psuedo-noise system is low. A recent in-house study conducted by Magnavox shows that a transponder of

the type recommended in this report for a user (and ground station) can be implemented in 12 cubic inches. This packaged size includes the RF receiver at the user. Additional equipment at the ground station such as error control decoding and rapid and precision instrumentation require an additional 6 printed circuit boards per user.

The tracking concepts outlined in this report and the use of the PN system minimize the complexity of the TDRS repeater. A "bent pipe" repeater is shown to be quite feasible if PN is utilized with no forfeit of range or range rate accuracies.

In conclusion, the pseudo-noise system meets all of the desired goals of the multipath modulation study for the TDRS. Furthermore, the principles involved in the pseudo-noise system represent current technology now in use by NASA in the unified S-band system. These are khown techniques and provide virtual hands' free operation between the user and the ground station.

TABLE OF CONTENTS

LIST OF ILLUSTRATIONS

1.0 MULTIPATH MODULATION STUDY FOR THE TRACKING AND DATA RELAY SATELLITE SYSTEM TECHNICAL DISCUSSIONS

Section 1.0 is devoted entirely to technical discussions which relate to the Tracking and Data Relay Satellite System, and specifically, to the Multipath Modulation Study.

This document is a final report covering NASA Contract No. NAS5-10744, submitted by the Magnavox Advanced Systems Analysis Office, Silver Spring, Maryland.

This study addresses itself to several critical problem areas which exist within the current Tracking and Data Relay Satellite System (TDRS) objectives. The TDRS is an advanced concept, developed by NASA Goddard to

a) provide virtually real-time relay of up to forty unmanned scientific satellite data to a small number of ground stations

b) provide ranging between a user and ground station so that the user orbit or position can be determined

c) support a limited number of manned missions in real-time

The TDRS system capabilities should, from studies already conducted, far exceed the present ground station complex with regard to coverage, reliability, cost, etc. In order to realize these advantages, however, certain difficult problems must be solved and this report hopefully solves some of these problems.

1.1 REQUIREMENTS AND STUDY OBJECTIVES

The objectives of this study are based upon the requirements outlined by NASA which have been updated to include new requirements which are reflected in this summary of study objectives.

The primary objective of this study is to devise modulation techniques which can provide unmanned and manned users of the TDRS simultaneous communications and tracking in the presence of severe multipath and interference. The study was originally aimed to support ten unmanned users and two manned users. The unmanned users were required to transmit at a nominal digital data rate of 1 kilobit per second to the ground station (G.S.). The manned users must transmit up to a 51 kilobit data rate and the capacity for one full duplex voice channel. The study has now been expanded to support 40 unmanned users which are located in more or less random orbits between 100 mi and a 1000 mi above the earth. The manned requirements have not changed materially except except that an emergency voice mode has been included at VHF with a simultaneous requirement for 4.8 kilobit/sec data at VHF.

It is desirable for many reasons that the unmanned users utilize the standard VHF transmission frequencies for the ground station to user link as well as the user to ground station link. Specifically the user to ground station (G.S.) link shall employ the 136-138 MHz band and the ground station to user link will utilize the band between 148-149.9 MHz, if feasible.

The unmanned user spacecraft power levels are to be maintained at a minimum, that is, at average power levels between 1 watt and 10 watts. The antenna on board the unmanned user craft is omnidirectional, and as a result of this lack of directivity, a severe multipath situation is created between the unmanned user and the TDRS. The RFP specifies (and has been shown theoretically through previous studies) that one can expect a multipath signal power equal to or less than the direct signal power between user and the tracking and data relay satellite. Since the ground station to user and user to ground station links are symmetrical for the unmanned user situation then it is obvious that multipath will exist on both links. The unmanned user's omni-antenna does not have a perfect pattern. Actually deep nulls in the antenna pattern (18-25 dB) have been observed for linear polarization. These antenna anamolies have necessitated the use of polarization diversity in the existing system.

The ground station to user link, referred to as the command and control link, is used to command the unmanned missions and requires an overall data rate of 400 bits per second. At this rate each user should receive a command once every 10 seconds. This refresh rate is considered acceptable. Shown in Figure 1.1 is the projection of the requirements for various command techniques through 1980. Note that PCM command requirements increase rapidly while the other techniques remain constant or decrease with years.

Because the manned space flight vehicle is stabilized and uses a directional antenna at S-band, the multipath problem is virtually nonexistent when

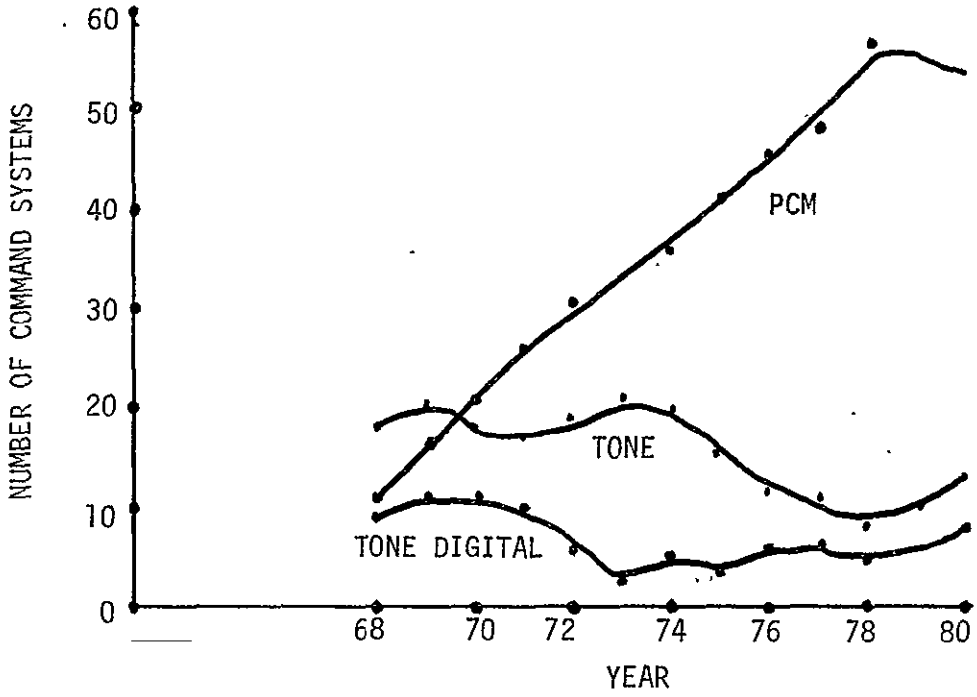

Fig. 1.1 -- Projected Command Type Requirement

the manned craft is functioning properly. In the case of emergencies the manned craft will use VHF for one full duplex voice channel and require a simultaneous 4.8 kilobit telemetry channel. During this mode, the manned craft will have 100 watts average power available for transmission. In the most dire circumstances, when the manned craft has lost its attitude controls and is tumbling, an omnidirectional antenna is assumed for the emergency voice and telemetry channel. Thus, in these circumstances, a multipath situation can be created. During emergency situations tracking of the manned mission is essential!

Because the VHF channel is power starved, bandwidth limited, and subject to intense interference, the primary emphasis of this study is placed on the unmanned user satellite requirements for the VHF channel. This does not mean we have neglected the manned requirements.

The pertinent requirements associated with the TDRS Multipath/ Modulation Study are summarized below.

Ground Station (GS)

System noise temperature - 150°K
Radiated power - 10 KW
Antenna gain - equivalent to 85' dish with efficiency of 0.7

Tracking and Data Relay Satellite (TDRS)

System noise temperature (GS to TDRS link) - 1200°K
Radiated power to GS - 10-20 W
Antenna gain (TDRS to GS link) - equivalent to 20° beamwidth with efficiency of 0.5
System noise temperature (TDRS/User Spacecraft Link) - 1200°K
Total Radiated power to User Spacecraft - 10-20W (S-band) 20W (VHF)
Antenna gain (TDRS to User) - equivalent to Earth coverage out to 1000 nmi (VHF) equivalent to 8' dish with efficiency of 0.5 (S-band)

User Spacecraft

(i) VHF (up to 40 unmanned users)
Receiver noise figure - 5 dB
Transmitted power - 1/2 W to 10 W
Antenna gain - omnidirectional (unstabilized circular polarized turnstile)

(ii) S-Band or K_u-band (2 manned users)
Receiver noise figure - 10 dB
Transmitted power - 10-100 W
Antenna gain - equivalent to a 3' to 10' dish with efficiency of 0.5

Frequency Plan - Data Rates

GS to TDRS - 13725 - 14200 MHz
TDRS to GS - 14875 - 15350 MHz
TDRS to User Spacecraft (unmanned) - VHF (148-149.9 MHz) - 400 bit/sec
User Spacecraft to TDRS (unmanned) - VHF (136-138 MHz) - 1000 bit/sec
User Spacecraft to TDRS (manned) - S-band (14400-14875 MHz) - 51 KB - voice full duplex
TDRS to User (manned) - S-band (13250-13725 MHz) - voice - data

	VHF	S-Band	K-Band
f_1 - DRS-User	148-149.9	2025-2120	13250-31725
f_2 - User-DRS	316-138	2200-2300	14400-14875
f_3 - Gnd=DRS			13725-14200
f_4 - DRS-Gnd			14875-15350

At S and K Band:

$$\frac{f_2}{f_1} = \frac{f_3}{f_4} = \frac{240}{221}$$

At K Band:

$$f_3 - f_1 = \frac{221}{240}(f_4 - f_2)$$

Emergency Mode

User (manned) to TDRS - VHF (136-138 MHz) Voice plus 4.8 KB/sec Data

The two possible TDRS configurations are illustrated in Figure 1.2 for three and four satellite geometries. Assuming a total of 40 unmanned users with each data relay satellite using an earth coverage plus 1000 mi antenna, it is easy to show that on the average each data relay satellite will see approximately 4/7 of the total number of users. This is true if the user satellites are randomly distributed between 100 miles and 1000 miles. We can expect the satellites to drift and in fact at some instances in time all the users will be crowded together.

Shown* in Table 1.1(a) is the projected satellite population vs. altitude for the years 1969 through 1980 and Table 1.1(b) is a similar projection of the inclination angles of the satellites in question.

Table 1.1(a) Satellite Population Projection

	1969	70	71	72	73	74	75	76	78	80
Altitude <3000 Km	54	48	52	57	53	56	54	54	50	45
3000-3600	24	30	27	27	28	26	23	23	18	19
Synchronous	7	7	6	5	8	8	14	14	23	23
>Synchronous	15	15	15	11	11	10	9	9	9	13

Note: eccentric satellites are accounted for above

Table 1.1(b) Satellite Inclination Projection

	1969	70	71	72	73	74	75	76	78	80
<30°	17	26	23	23	32	31	37	32	46	50
>30°,<60°	40	30	36	23	16	19	19	29	18	22
>60°,<90°	43	44	41	54	52	50	44	39	36	28

Note: the large number of low altitude (<3000 Km) and low inclination angle (<30°) satellite can be attributed to projected TDRS activities.

* E. J. Habib, "T&DS Mission Mode and Projected Spacecraft Support Requirement Through 1980", March 69, X-520-69-110

SATELLITES ARE IN SYNCHRONOUS INCLINED
ORBITS WITH INCLINATION ANGLES LESS THAN 20°

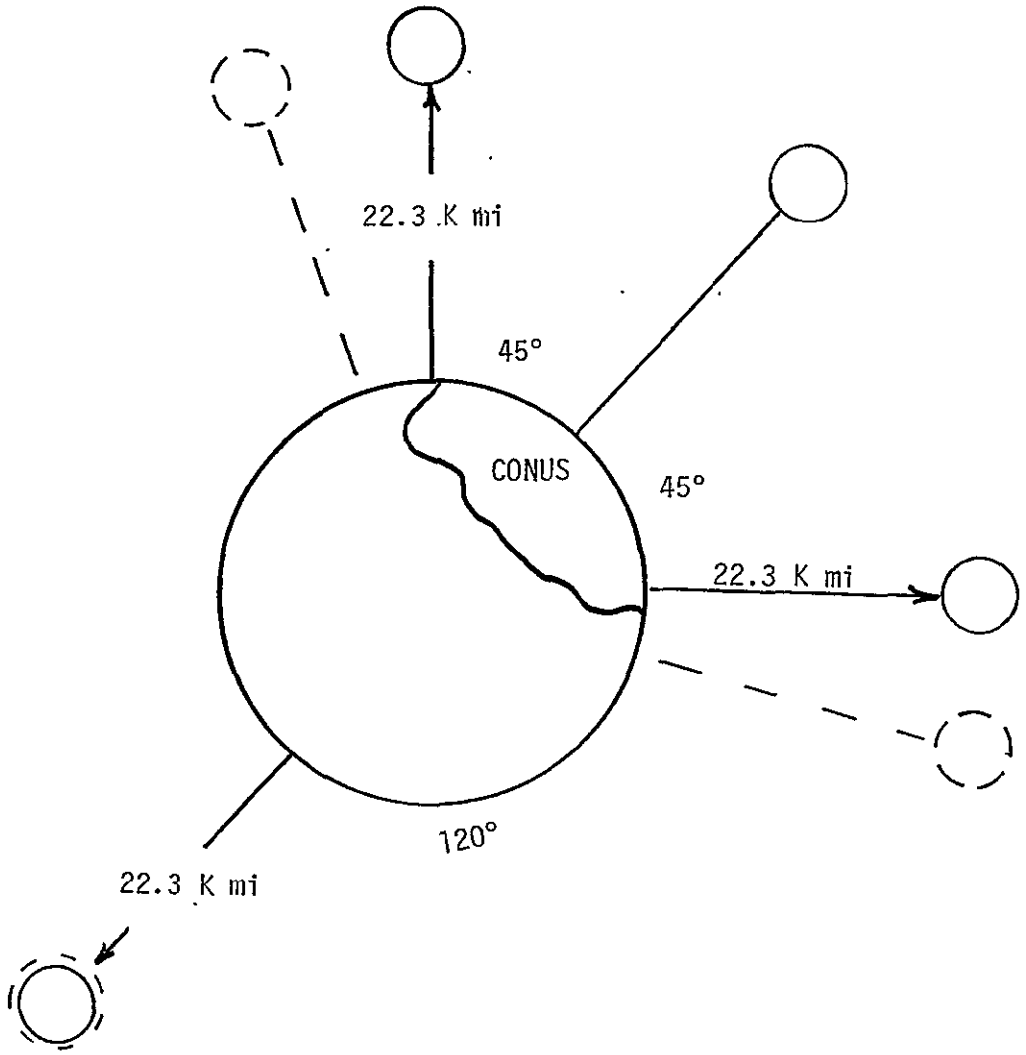

Fig. 1.2 -- TDRS Geometries

It is evident from Figure 1.2 that there are a number of problems associated with the TDRS which impact on the modulation system design. First there is the handover problem which is in effect a command and control problem. Secondly, if the four satellite TDRS is employed, three satellites can be within the field of view of a large number of users at certain times, complicating the multiple access problem. Recently, Delaney* has analyzed the 3 satellite TDRS vs. a G.S. complex such as Stadan. Delaney concluded that for a typical TDRS geometry (16° E, 88° E, 180° E, zero inclination, stationary) that 95% of the time each TDRS would be required to handle no more than 23 satellites from a total population of 40 satellites. This conclusion is not valid for the 4 satellite TDRS geometry but does illustrate the existence of a trade-off between the number of TDRS's employed and the system loading. The modulation technique chosen to provide anti-multipath/multiple access, anti-interference and tracking must also be compatible with all three (or two) satellites in view. In order to provide accurate tracking during critical phases of the mission it is necessary to have more than one TDRS to receive the same signal from one user, thus the signal design of the user must be compatible with any one or as many as three TDRS's simultaneously.

In addition to the multipath problem which exists between the user and the TDRS, there exists a potentially more severe problem created by the presence of unintentional interference sources located on the earth and found primarily within the VHF bands. In order to evaluate the potential problems associated with this interference we have solicited

*I.T.C. Proceeding, Vol. V, Sept. 1969

the aid of representatives of NASA, utilized existing NASA reports, and the services of ECAC to provide us with interference data covering CONUS. In addition to the CONUS RFI data, we have estimated the RFI intensity around the world from the International Telecommunications Union publication. If the four satellite TDRS geometry is employed CONUS based RFI will be seen by as many as three of the satellites. Thus we must provide modulation techniques which combat multipath and these techniques must also reject or avoid the interference. This last statement assumes that no other suitable frequency bands for TDRS can be found for the unmanned user applications.

The requirement for 40 unmanned users with simultaneous access through any one of the data relay satellites imposes a unique problem in that the user spacecraft and its equipment are to be of the low complexity and minimum transmitter power. Furthermore, the data relay satellite system itself is a restricted bandwidth repeater having a 2 MHz bandwidth for the 136-138 MHz link and 1.9 MHz bandwidth for the 148 to 149.9 MHz command band.

Finally, the modulation techniques which exhibit antimultipath properties, anti-interference properties and multiple access properties must also provide accurate range and range rate capabilities. With regard to user tracking, we discuss in this report the accuracy with which the ground stations can be located with existing TRANSIT technology. We also discuss the errors in locating and tracking a TDRS from the ground. Finally, we discuss the user's position error in light of instrumentation errors, both range and range rate.

In addition to the above goals NASA had authorized The Magnavox Company to study only asynchronous multiplexing techniques; that is, modulation techniques which do not require accurate knowledge of time by each of the users in order to gain access to the satellite, e.g., time division multiple accessing. Furthermore, we have been directed to assume that the data relay satellite is a linear side-stepping repeater with sufficient power to insure that the down link is essentially noiseless.

1.2 MATHEMATICAL DESCRIPTION OF THE USER TO DATA RELAY SATELLITE TRANSMISSION CHANNEL

Prior to any indepth analysis and selection of compromise antimultipath and multiple accessing communication techniques for the users of the data relay satellite system it is advisable to begin with a discussion of the nature of the transmission channel which exists between the user and the data relay satellite. Since the transmission link between the data relay satellite repeater and the ground station is a conventional k_u-band transmission link, we will not discuss in this section its characteristics but will assume that the link between the data relay satellite to ground station represent essentially a noiseless communication path.

Shown in Figure 1.3 is a data relay satellite and a potential user. Also shown are the direct paths between the user and the data relay satellite, the multipath created by the user, and the potential interference sources which reside on the earth and interfere with the data relay satellite and the user spacecraft at the VHF frequencies.

The user spacecrafts are low orbiting craft with orbits between 100 and 1000 miles above the earth*. These non-synchronous orbits insure that there will be a relative velocity of the spacecraft with respect to the earth and to the data relay satellite. Thus, the path between the user and the data relay satellite may be described in terms of a multiplicity of parameters which govern both the direct path and the multipath signal.

---

* Note that users need not be in circular orbits, elliptic orbits can be utilized.

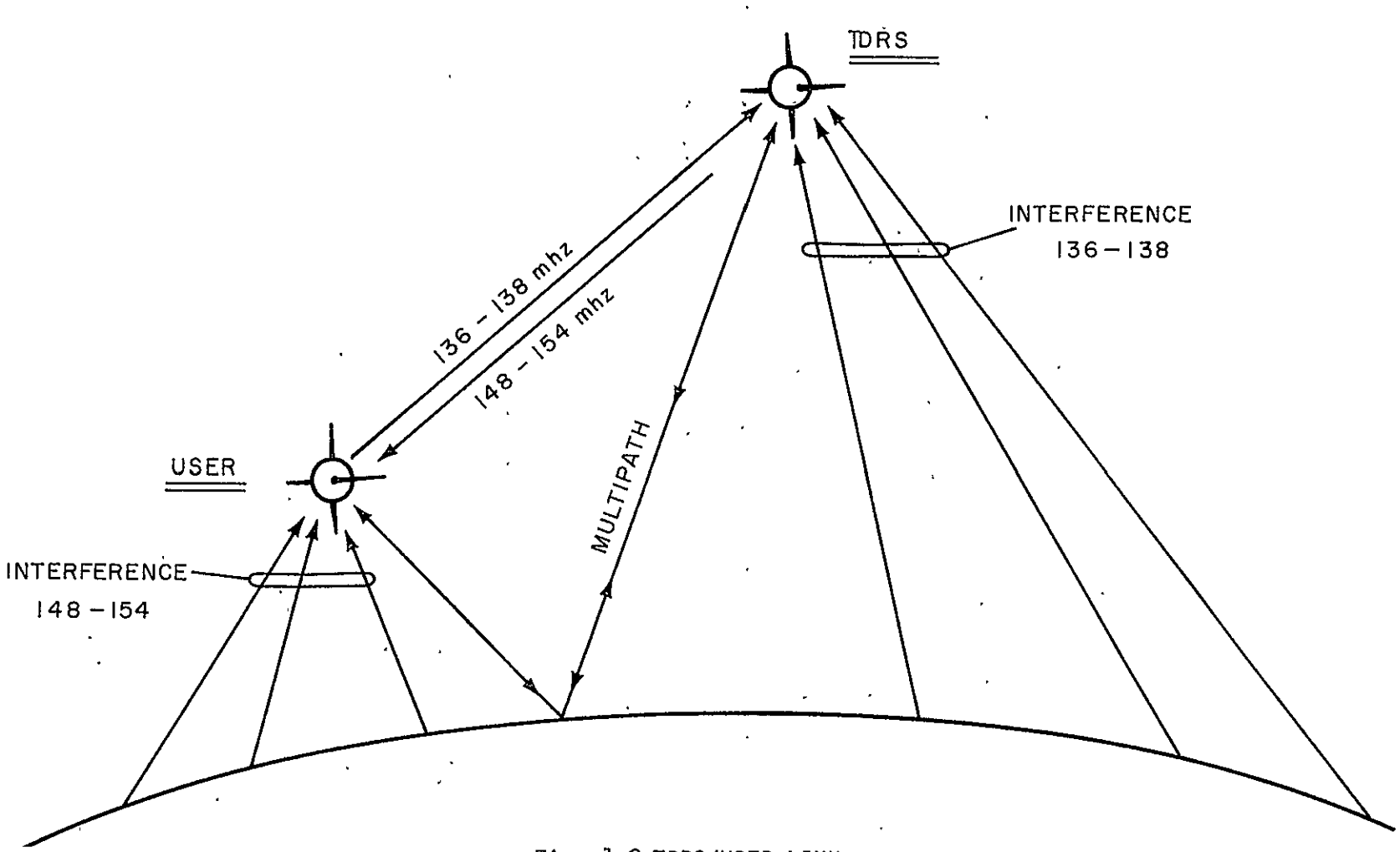

Fig. 1.3 TDRS/USER LINK

First of all there is a direct path Doppler between the user and the data relay satellite. We may consider the direct path to be a non-fading signal path. Variations in signal strength along the direct path will depend primarily on variations in distance between the user and the data relay satellite system and imperfections in the user onmidirectional antenna pattern. These variations in antenna patterns will be considered as additional margins required by the system.

The indirect or multipath signal channel may be described in terms of a multiplicity of parameters. These parameters will be discussed in some detail in the following paragraphs and utilized in the following sections of our analyses to determine the performance of antimultipath techniques.

The signal reflected off the earth is characterized by a time varying process which is statistically nonstationary because of the changing velocities and geometry between a user and the DRS. The short-term statistics of this link can be considered stationary. If a CW signal is transmitted from a user craft this signal will be reflected off the earth and will appear at the DRS as a fading signal (see Figure 1.4). The reflected signal can consist of a specular component and a diffuse component. The degree of specularity and diffuseness associated with the reflected signal will in turn depend upon a multiplicity of parameters, e.g., the grazing angle ψ, the roughness σ of the earth near the point of reflection, and the correlation length L across the surface of the earth. Roughness factor σ is a measure of the RMS height variations along the surface of the earth and the correlation length L is a measure of the degree of correlation between two

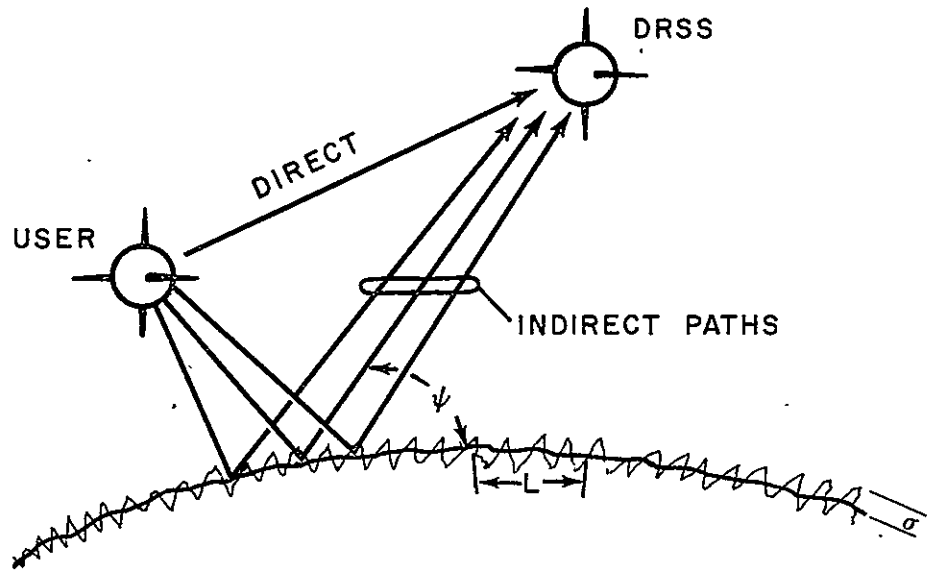

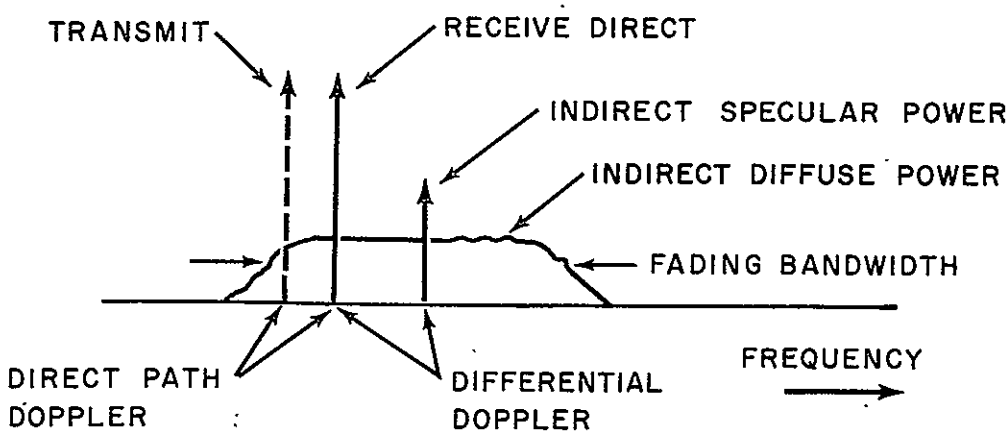

Fig. 1.4 CHANNEL CHARACTERISTICS

points along the surface of the earth. In general the amount of reflected specular energy can be expressed by the following equation.

$$S_{specular} = \langle \rho_s^2 \rangle D^2 |R_o|^2 S_d \qquad \text{eq.1.1}$$

$$\langle \rho_s^2 \rangle = e^{-\left(\frac{4\pi\sigma}{\lambda} \sin \psi\right)^2}$$

S_d is the direct power

λ is the wavelength

σ = rms height of the reflecting surface

D is the average divergence factor associated with the spherical earth,

$|R_o|^2$ is the mean squared reflection coefficent and ψ is the grazing angle.

The amount of diffuse power can be expressed by the equation derived by Duranni and Starras* and has the following form.

$$S_{diffuse} = D^2 |R_o|^2 F(\psi,h) S_d \qquad \text{eq.1.2}$$

h is the user height above the earth

$F(\psi,h) \leq 1$

The divergence factor is shown in Figure 1.5(a) as a function of the grazing angle for both a 100 mile orbit and a 1000 mile orbit. The relative expected specular and diffuse reflected power are illustrated in Figure 1.5(b), as a function of the grazing angle ψ for 136 mc and an average earth roughness and correlation distance.

* RCA Review - March 1968 pp. 77-105

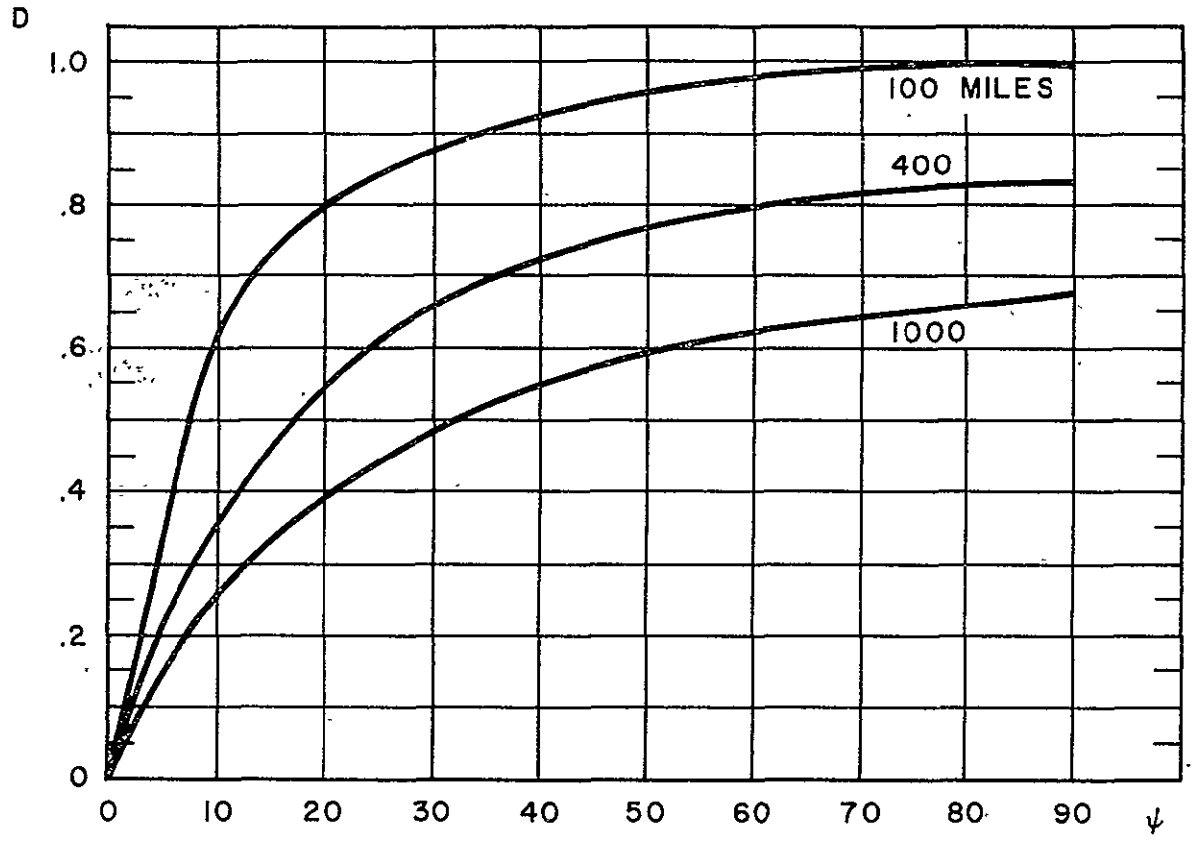

Fig. 1.5(a)

DIVERGENCE FACTOR

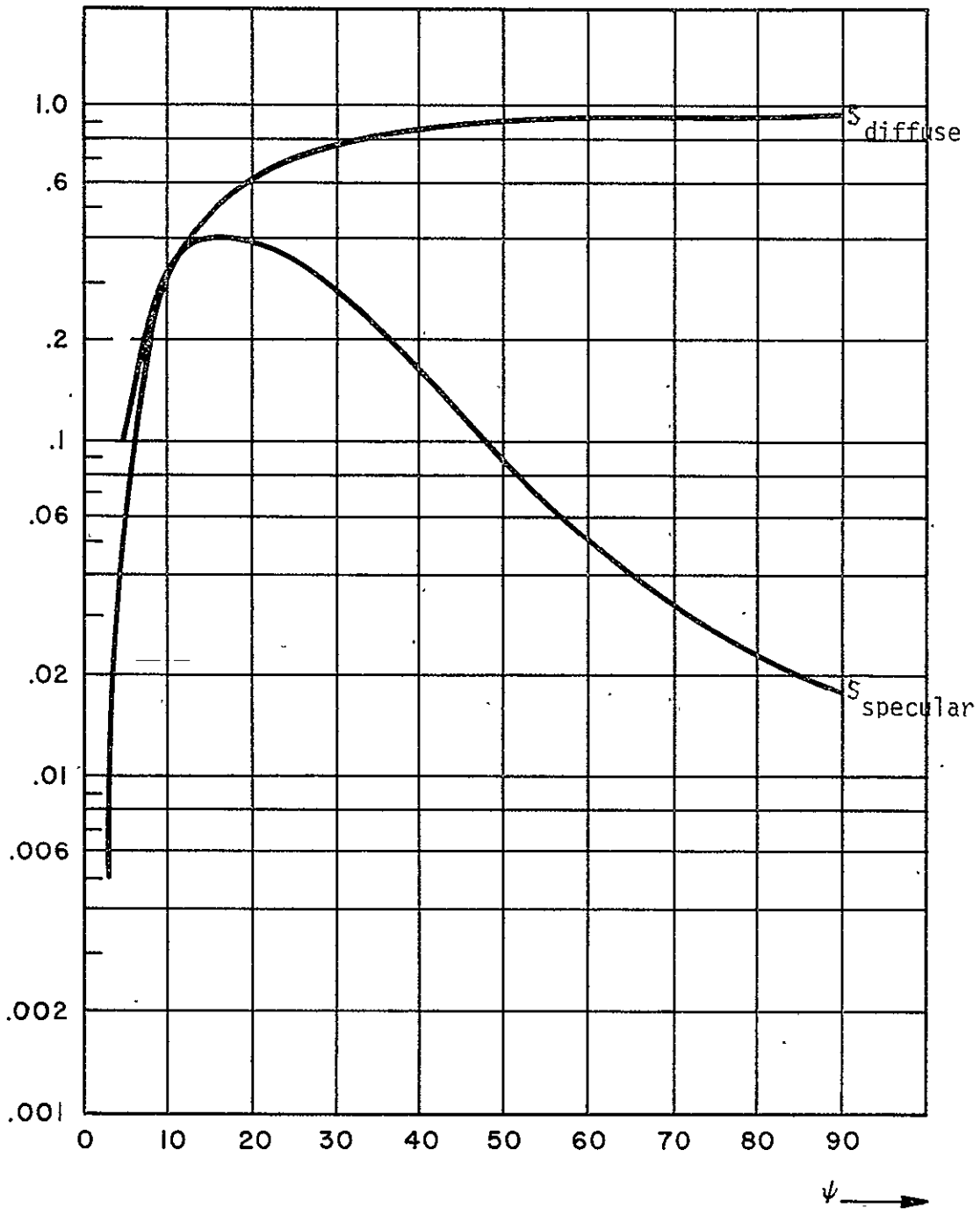

Fig. 1.5(b)

REFLECTED SPECULAR AND DIFFUSE POWER VS GRAZING ANGLE

We see that for low-grazing angles the divergence factor serves to diminish the multipath or reflected signal, while at high grazing angles the primary reflected energy is diffuse. Figure 1.5(b) is plotted for a 136 MHz signal. We can state that for reasonable roughness factors and correlation lengths, that the primary source of reflected power will be diffuse for grazing angles in excess of 20°. This represents the majority of a mission between a user and a particular TDRS.

The composite multipath or indirect signal power will normally be equal to or less than the direct path signal at VHF and S band when reflection coefficients of the earth are essentially unity and the grazing angles are in excess of 20°.

If we were able to separate the direct and the indirect signal paths at the DRSS when a CW signal is transmitted from a user we would observe that the envelope statistics associated with the indirect or reflected path would be Rician. This is true since the specular and diffuse components associated with the reflected path would constitute a fading signal consisting of a CW component and a diffuse component, thus the probability density governing the envelope would be Rician and is given by the following equation.

$$p(r_{indirect}) = \frac{r}{S_{diffuse}} \exp - \left(\frac{r^2+2S_{specular}}{2S_{diffuse}}\right) I_o \left(\frac{r\sqrt{2S_{spec}}}{S_{diffuse}}\right) \quad \text{eq. 1.3}$$

where

$$S_{scatter} = S_{diffuse} + S_{specular}$$

As the grazing angle increases beyond 20° the specular component diminishes rapidly and the probability density associated with the envelope of the received signal from the indirect path is essentially Rayleigh*.

Indirect path is also characterized by a differential Doppler relative to the direct path Doppler. The differential Doppler is illustrated in Figure 1.4.

In addition to differential Doppler the indirect signal when reflected from the earth's surface will fade. The fading bandwidth B_F is a function of the velocity of the user spacecraft relative to the earth, the ratio σ/L, and the grazing angle. This relationship is given in equation 1.4, and illustrated in Figure 1.4.

$$B_F = \frac{\nu}{\lambda} \sqrt{2} \ \frac{\sigma}{L} \sin \psi \qquad \text{eq. 1.4}$$

ν is the velocity of the user craft

We see that the fading bandwidth is maximized when the grazing angle is 90°, when the user is below the data relay satellite. At this point the reflected energy is completely diffuse and the fading bandwidth is maximum.

Another parameter which is of importance in the evaluation of anti-multipath systems is the coherent bandwidth of the user to data relay satellite link. The coherent bandwidth can be defined in a number of ways, but two preferred methods are illustrated in Figures 1.6(a) and 1.6(b).

---

* This result has been observed experimentally by K. L. Jordan, Measurement of Multipath Effects in a Satellite-Aircraft UHF Link - Proc IEEE June 67.

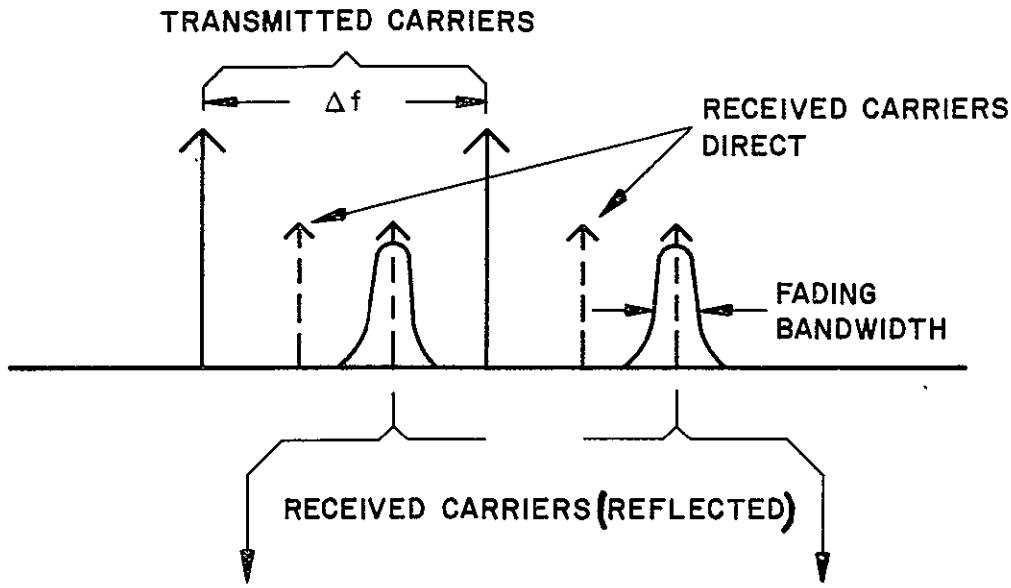

WHEN THE COMPLEX ENVELOPE CORRELATION FUNCTION BETWEEN THE TWO RECEIVED REFLECTED CARRIERS $\rho(\Delta f)$ IS EQUAL TO .5, THE VALUE OF Δf IS THE COHERENT BANDWIDTH.

Fig.1.6(a)

COHERENT BANDWIDTH (FREQUENCY DEFINITION)

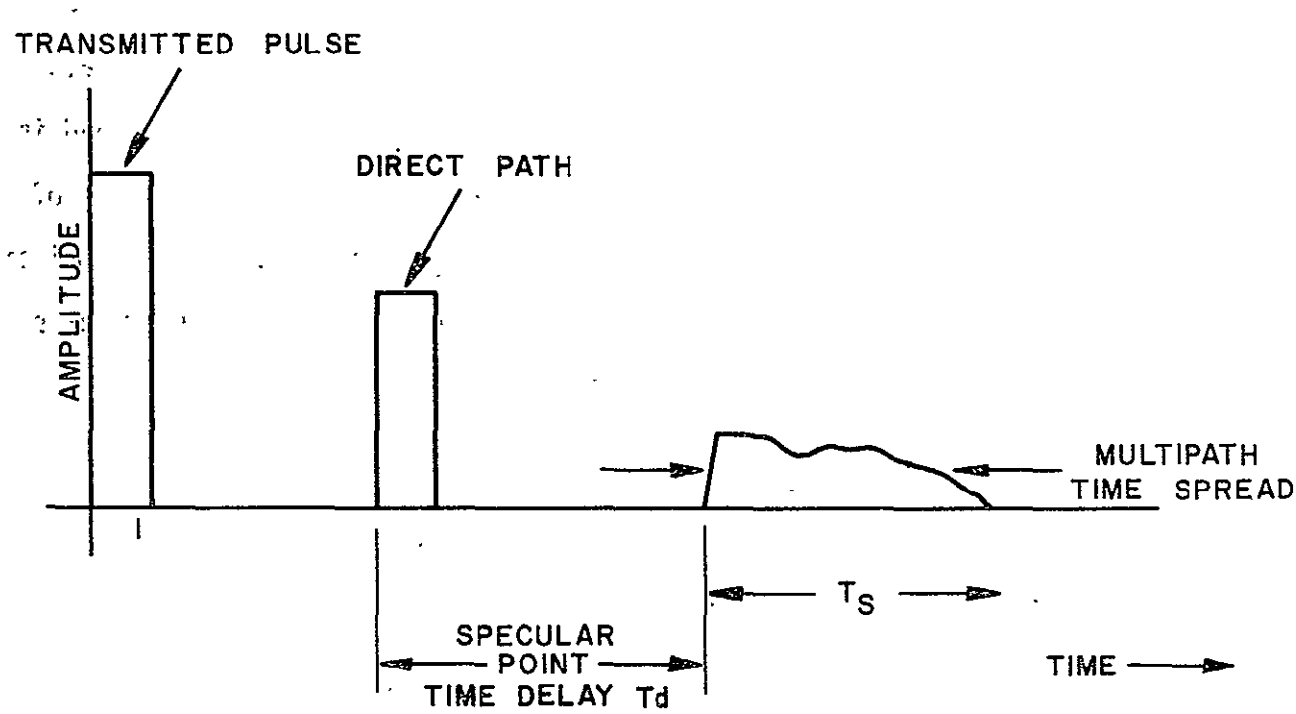

$$\text{AVERAGE MULTIPATH TIME SPREAD} = \frac{1}{\text{COHERENT B.W.}}$$

Fig. 1.6(b) COHERENT BANDWIDTH (TIME DEFINITION)

In Figure 1.6(a) we indicate that two transmitted carriers separated in frequency by ΔF are received at the TDRS from a user craft via the direct and the indirect paths. If the normalized correlation coefficient between the two received carriers arriving via the reflected path is computed then the correlation coefficient of ½ then the value of ΔF which is needed to produce this correlation value of ½, is defined as the coherent bandwidth B_C. This definition is independent of the direct path received signals. Definition of coherent bandwidths based on the transmission of two CW signals separated in frequency is an accepted definition in the literature and is a measure of the coherent bandwidth of a fading channel. In the case of the TDRS B_C does not necessarily limit the data capacity of the transmission link. The coherent bandwidth can be a limiting factor in the transfer of data over dispersive channels such as the HF radio or tropospheric scatter links.

If a pulse is transmitted by a user it will be received after some time via the direct path at the data relay satellite. At some time later the T_d multipath signal will arrive as illustrated in Figure 1.6(b). The multipath signal will be varying with time and will be characterized by an average multipath time spread. The coherent bandwidth or inverse of the multipath time spread associated with the indirect signal path has been derived by Durrani and Starras* and in their formulation is completely independent of the carrier frequency and primarily dependent on the separation ΔF of two CW components (Fig. 1.6(a)). Their result infers that the coherent bandwidth

---

* Op Cit

at S band is the same at UHF! On the other hand, frequency scaling from S band to VHF to obtain reduced values of B_C does not appear justified at all. From purely optical arguments, however, we conclude that the coherent bandwidth at VHF does not differ materially (order of magnitude) from the value at S band.

The onset of the multipath signal which arrives after the signal associated with the direct path constitutes the shortest differential time delay. This reflected energy comes essentially from the specular point on the earth. The remaining multipath signal which continues or persists after the specular point reflection signal arrival will, in most cases, be diffuse. Furthermore, for grazing angles in excess of 20° the entire multipath signal will probably be varying in time and show little or no specular components, even at VHF.

In summary, Table 1.2 lists the various parameters discussed above for the 136-138 MHz and 148-154 MHz links.

Table 1.2 Time Varying Parameter Governing 136-138 MHz Band

1. T_d - time delay between direct and indirect signals = .2 msec (100 mi orbit) to 10 msec (1000 mi orbit)
2. B_C - coherent bandwidth similar to S-band 5-30 KHz
3. Direct path Doppler $\sim$ 0 - 3.75 KHz maximum for 100 mi orbit
4. Differential Doppler $\sim$ 0 - 2 KHz
5. Fading bandwidth $\sim$ 0 - 2 KHz
6. Ratio of direct path power to indirect power $\geq$1 with indirect power primarily diffuse for $\psi > 20°$, (except when user antenna anamolies are considered)

Shown in Fig. 1.7 are the various parameters defined previously, which

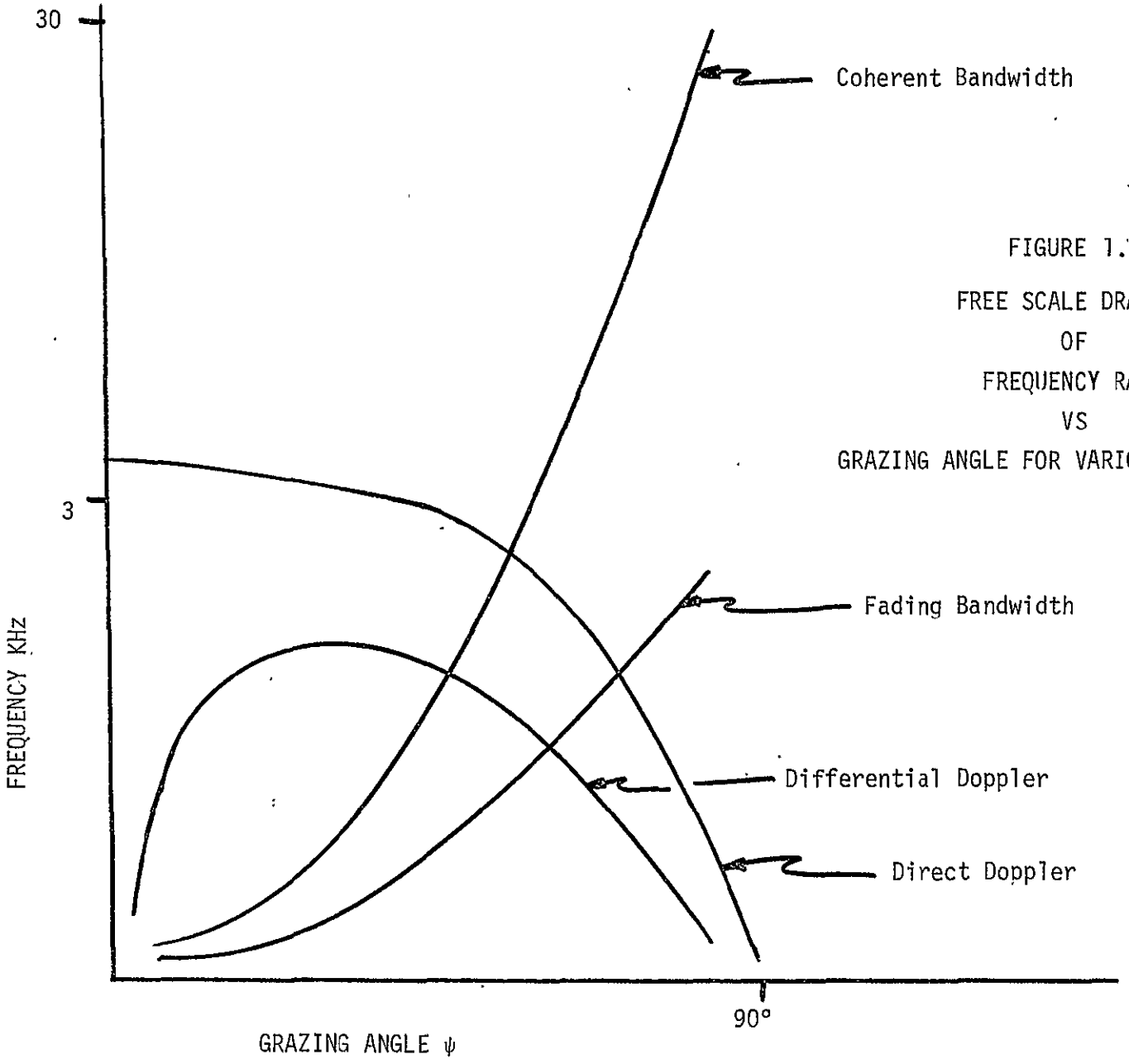

FIGURE 1.7

FREE SCALE DRAWING

OF

FREQUENCY RANGE

VS

GRAZING ANGLE FOR VARIOUS PARAMETERS

govern the user to TDRS channel, and illustrates their dependence on the grazing angle ψ.

In addition to the propagation parameters, there is another parameter which must be taken into account during subsequent evaluations. This is the variation in the user's antenna pattern at VHF. The users are not stabilized and can tumble during the mission. Deep nulls (17-25 dB) have been observed in these patterns when viewed by linearly polarized receiving antennas. Recent* work indicates that omni-pattern with as little as 3 dB ripple can be obtained if arrays are employed with element spacing of .8 wavelength.

The large antenna pattern variation have required the use of polarization diversity reception in STADAN. These variations can also serve to enhance the multipath while decreasing the desire signal of the user in the TDRS. Shown in Fig. 1.8 is the effect of a 3 dB ripple in the user's antenna pattern on the expected multipath to signal ratio (dB) for various user altitudes (calm sea at VHF grazing angle 90°).

1.3 SYSTEM SELECTION RATIONALE

In the previous section we have discussed briefly the nature of the transmission channel which exists between a user spacecraft and the satellite repeater. In that discussion we established that the channel was time variant, having parameters of differential Doppler, average multipath delay between the direct and indirect signal, a spread in multipath associated with the indirect signal, and that this spread in the indirect signal would be time varying, i.e., a function of the geometry between the user and repeater satellites, and the earth. Based on the previous discussion regarding the nature of the channel, let us now attempt to catalog various antimultipath

---

*Cockrell, C.R., NASA TN D2105, Oct. 1964
Croswell and Knop, I.E.E.E., Trans. Ants. & Prop., May 1966

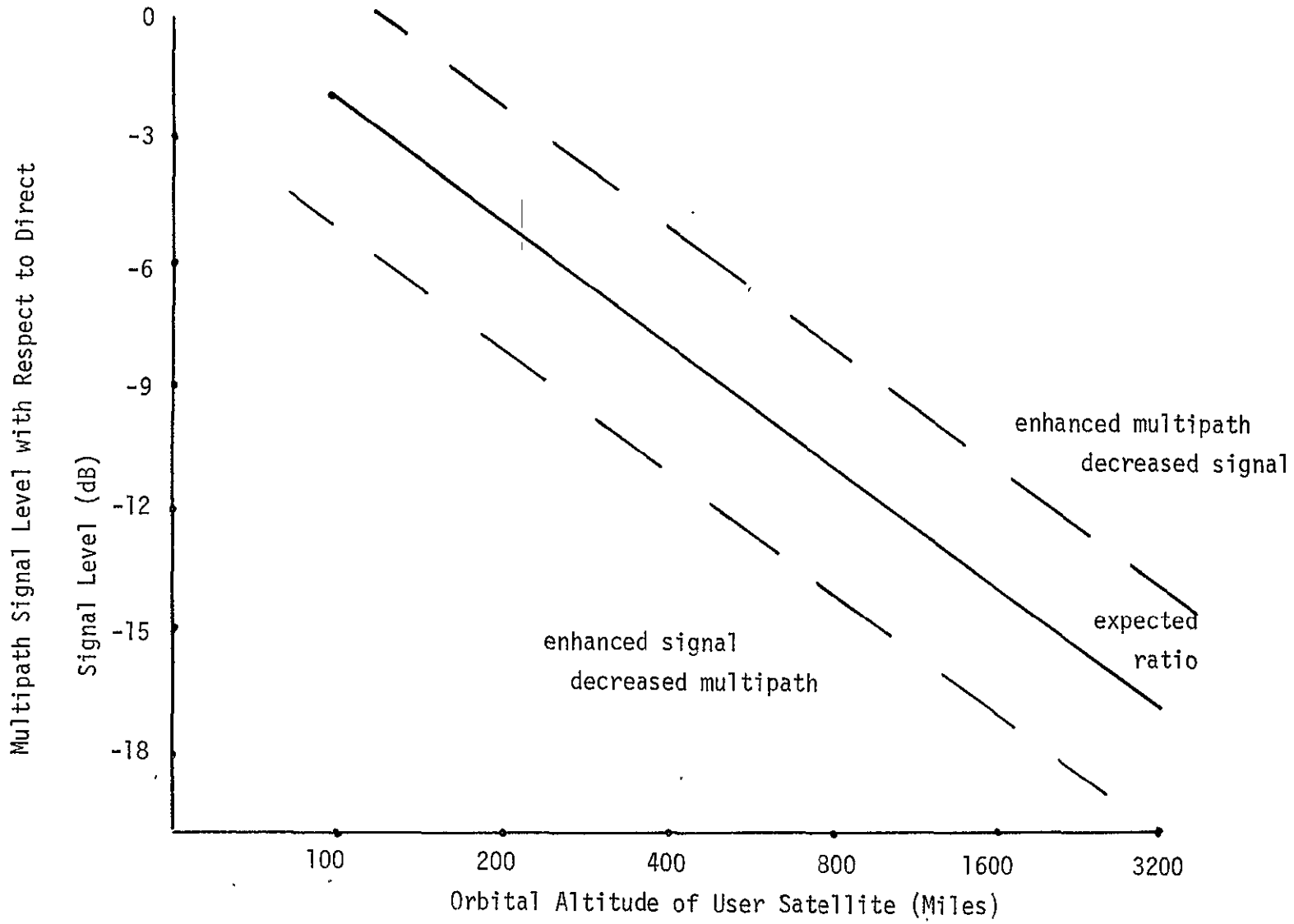

Fig. 1.8 -- Multipath/Direct Signal Ratio as a Function of Orbital Altitude

modulation techniques, and further to select a limited number of these techniques for further study.

It is obvious from purely practical reasoning that we have three alternatives to the multipath problem. These are, first devise a system which can utilize to the best possible extent, both the direct and the indirect paths, thus enhancing the detection reliability. Secondly, we can design a system which completely negates or circumvents the reflected signal, thus the entire system performance will be based upon the direct path alone. Finally, we can design systems which live with the reflected signal.

The theory of optimum antimultipath modulation techniques have been developed by Kalaith,* Price** and Seibert.*** However, the theory applies only to rather restricted and somewhat oversimplified models. For example, the theory of optimum antimultipath systems provided by Kalaith assumes a Gaussian multiplicative channel which is unrealistic for the TDRS in that the direct path is a non-fading line of sight channel.

In the absence of theory which defines the optimum antimultipath system for a channel with a direct nonfading path and multiplicity of indirect fading paths, we can hypothesize that the best system combines the direct and indirect path optimally to minimize the probability of error. Because of the limitation in the amount of power contained in the indirect path relative to the direct path, and the fact that it fades, make it doubtful that such an approach would show a significant increase in system performance over the direct path alone.

---

*T. Kalaith - ch 6 Lectures on Comm. System Theory McG.H. 1961

**R. Price - Trans IRE 1956 IT-2

***MIT Summer School Lecture Notes on Detection and Estimation Theory, June '63

The work of Barrow* has direct application to the question of the gains one can achieve when combining a non-fading direct channel with a fading indirect channel of equal average power. He has shown that the resultant bit error probability P_ε for such a combination (assume maximal ratio combining) is $P_\varepsilon = (2P_{\varepsilon_{direct}} \cdot P_{\varepsilon_{indirect}})$. If we choose a reasonable value for $E/N_o = 10$ dB $P_{\varepsilon_{direct}} \sim 10^{-5}$ for ΔPSK for the direct path and $P_{\varepsilon_{indirect}} \sim 10^{-1}$. Therefore little can be gained by combining the direct and indirect channels.

An alternate approach to the problem of multipath would be to design a transmitting waveform in cooperation with a receiver which rejects totally the presence of the multipath and does not attempt to use the multipath to enhance the detection probability. There are a number of signaling waveforms which of course satisfies this condition. For example, the frequency agile pulse system wherein data is transmitted by hopping the carrier over an ensemble of frequencies, programmed not to return to a specific frequency until the multipath signals have discontinued or died out. In effect, this type of transmission requires a coordinated activity between the transmitter and receiver. This type of transmission is optimum from a signal design point of view in that if we consider the multipath signal as noise or interference occupying essentially the same band as the transmission it can be shown that in order to enhance detection we designed the signal so as to minimize the effect of noise; that is, where noise is present in substantial amounts we minimize the signal power and in those regions where the noise is minimum we maximize the signal power density. Thus the theoretical point of view of signal design, a system which completely rejects the deleterious effects of multipath is optimum. It is not,

---

*B. B. Barrow, "Error Probabilities for Data Transmission Over Fading Radio Paths" Assen 1962 (Doctoral Thesis) Van Gorcum & Comp.

however, optimum in the sense of utilizing intelligently the energy contained in the multipath, as was pointed out in the previous paragraphs, where a system with optimum combining to minimize the probability of error for binary transmission was discussed.

Finally, there are a multiplicity of signaling schemes which live with the multipath but in some sense reduced its effect in the receiver through signal design or diversity. Perhaps the best known are those which utilize almost orthogonal sequences such as PN sequences which when observed over the duration of the data interval are almost orthogonal and because of this near orthogonal property discriminate against the multipath while introducing a small self noise through the correlation process. Other notable techniques which live with the multipath are frequency diversity systems, pseudo-random time hopped signals, pseudo-random frequency hopped signals and hybrid techniques such as frequency-time coded transmissions or random access discrete address signals.

1.4 SELECTION OF THE CANDIDATE ANTIMULTIPATH SYSTEMS FOR FUTHER STUDY

Thus far we have presented various antimultipath techniques ranging from the optimum approach to less optimum(but perhaps more practical approaches), all of which operate under constraint that the indirect path contains a total amount of power equal to or less than the power contained in the direct path,* and that the indirect path will probably be a fading channel, depending upon the grazing angle, and other reflection parameters.

---

*This constraint is relaxed in later sections to include the case where the multipath signal exceeds the direct path signal as a result of user antenna anamolies.

We have argued that the optimum antimultipath system consists of a signaling format which is a pulsed signal design followed by an optimum combining system using correlation techniques to determine the optimum weighting associated with the various branches in the combiner. This approach to optimum antimultipath signaling has been shown to provide little improvement over the direct path, and to the best of our knowledge, never been implemented or seriously attempted.

We have also argued that another approach to antimultipath systems would be to design the signaling waveform in cooperation with a receiver which would avoid the multipath upon reception; that is, by frequency agile or time hopping techniques. Such approaches are well within the state-of-the-art of the communications designers.

Finally we have suggested less optimum approaches to the multipath problem which include frequency diversity techniques and a variety of large time bandwidth product correlation techniques which reduce the effects of multipath in the receiver.

Based on our previous discussions we have chosen the following antimultipath techniques for more detailed analyses.

1. Frequency Diversity System
2. Pseudo-Random Time Hopped Signal

3. Random Access Discrete Address

   a) Small Address System (FH/TH Hybrid)

   b) Large Address System

4. Pseudo Noise Modulation

   a) Narrowband Pseudo Noise (Possible Frequency Agile)

   b) Wideband Pseudo Noise (Using Entire 2 MHz Repeater Bandwidth)

5. Programmed Systems

   a) Time Hopped Programmed System and Adaptive System

   b) Frequency Hopped Programmed System and Adative System

   c) Frequency Hopped/Time Hopped Programmed System for all Orbits and all Data Relay Satellites

The above systems will be analyzed for the 136-138 MHz user to TDRS link. It is valid to assume, at least with regard to multipath, that those techniques found suitable for the user to TDRS link will be quite suitable for the TDRS to user command link 148-149.9 MHz.

1.5 DETERMINATION OF THE REQUIRED BIT ERROR PROBABILITY VERSUS THE DESIRED QUANTIZATION RESOLUTION FOR TELEMETRY DATA

Prior to launching into detailed multipath analyses it is essential that we establish the required bit error probability for the user to TDRS link. This requirement will impact directly on the requirement for forward error correction, user power, etc.

Telemetry information from the unmanned users in the TDRS system is converted from an analog waveform to a digital waveform via conventional analog to digital conversion techniques. The digital stream is then transmitted from a user through the TDRS to a ground station utilizing an appropriate antimultipath multiple access and anti-interference modulation scheme. The binary data rate is assumed to be 1 kilobit per second. Furthermore, it is assumed that the quantization resolution can range between 5 and 9 bits per sample. The following analyses is directed toward the determination of the maximum allowable bit error probability which does not degrade the quantization resolution for the telemetry data. This analysis will assume that the initial telemetry analog waveform can be either Gaussian or is uniformly distributed over the limits of the PCM coder. We have selected these two amplitude probability densities since they should represent upper and lower bounds on the amplitude statistics normally associated with telemetry analog information. It will be shown that there are two sources of degradation in PCM systems. First, coder overload noise can occur when the waveform exceeds the coder limits. Second, noise contribution results from random errors in the telemetry

data stream. Graphs will be presented at the end of this section which show the required bit error probability to maintain the desired signal to quantizing resolution. It is understood that the data modulation systems have been appropriately combined with an antimultipath/anti-interference/ multiple accessing modulation scheme and therefore the required signal to noise into the final demodulator will be a function of the antimultipath etc. technique employed.

It is assumed that the PCM coder has a dynamic range extending from +A to -A volts, a total range of 2A volts. Given that there is an n bit description provided by the PCM system, the number of possible levels between -A and +A is 2^n. If each quantum step or separation between adjacent levels has a value q, then it follows that the quantizing noise N_Q is given by $Q^2/12$. Furthermore, if we define the signal power as σ^2 it follows that the signal to quantizing noise ratio is given by $3.2^{2n}\ (\sigma/A)^2$. The ratio (σ/A) is identified as a crest factor and represents a measure of how well the coder is loaded.

If the waveform to be coded is a sine wave then it follows that

$$\frac{\sigma^2}{N_Q} = 3/2 \times 2^{2n} \qquad \text{eq. 1.5}$$

If the waveform to be coded is uniformly distributed between the limits of A and -A, then it follows that the signal to quantizing noise is simply

$$\frac{\sigma^2}{N_Q} = 2^{2n} \qquad \text{eq. 1.6}$$

Furthermore, if we are coding a noise-like waveform to its $\pm 4\sigma$ values, then the resulting signal-to-noise ratio is given by:

$$\frac{\sigma^2}{N_Q} = \frac{3}{16} \times 2^{2n} \qquad \text{eq. 1.7}$$

In the previous paragraph we have considered the behavior of the signal to quantizing noise as a function of the loading of the PCM coder for various waveforms. What we have not considered as yet is the contribution to the noise if the coder is overloaded. What follows is an analysis to determine the overload noise when the signal encoded is Gaussian in amplitude. The mean squared error resulting from overload is calculated in the following equations:

$$N_{overload} = \int_A^{\infty} (x - A)^2 \, p(x)dx + \int_{-\infty}^{-A} (-x - A)^2 \, p(x)dx$$

Where

$$p(x) = \frac{\exp\left[-\frac{x^2}{2\sigma^2}\right]}{\sqrt{2\pi\sigma^2}}$$

$$\frac{\sigma^2}{\text{Noise overload}} = 2\left[\left(\frac{A}{\sigma}\right)^2 + 1\right] \Phi(Z) - \sqrt{\frac{2}{\pi}}\left(\frac{A}{\sigma}\right) e^{-\frac{A^2}{2\sigma^2}} \qquad \text{eq. 1.8}$$

Where

$$\Phi(Z) = \frac{1}{2\pi} \int_Z^{\infty} \exp - \frac{Z^2}{2} \, dz$$

$$Z = \frac{A}{\sigma}$$

Again we see that the crest factor plays an important role in the determination of the signal to overload noise. It is assumed that the contribution to the total noise power can be represented as follows:

$$\frac{\sigma^2}{N\ \text{total}} = \frac{1}{\frac{NQ}{\sigma^2} + \frac{N\ \text{overload}}{\sigma^2}} \qquad \text{eq.1.9}$$

When the above noise-to-signal ratios are plotted as a function of the crest factor, we find that there exists a minimum in the total noise-to-signal ratio as indicated in Figure 1.9.

In a recent paper by Whelan*, PCM decoding in the presence of digital errors is considered. A resultant output signal-to-noise ratio $(S/N)_R$ consisting of contributions to the noise power from quantizing as well as digital errors, was derived. Whelan found that the signal-to-noise ratio due to errors is given by:

$$\left(\frac{S}{N}\right)_E = \frac{(1-2P)^2}{4P(1-P)} \qquad \text{(PCM)} \qquad \text{eq.1.10}$$

P = Prob of error

If one considers that the contribution to the total output signal-to-noise ratio is an additive process, that is, the noise due to errors, the noise due to quantizing, and overload noise are additive, we have

$$\left(\frac{S}{N}\right)_R = \frac{1}{\left(\frac{N}{S}\right)_E + \left(\frac{N}{S}\right)_{total}} \qquad \text{eq. 1.11}$$

* Whelan, P.G.C.T. June, 1966

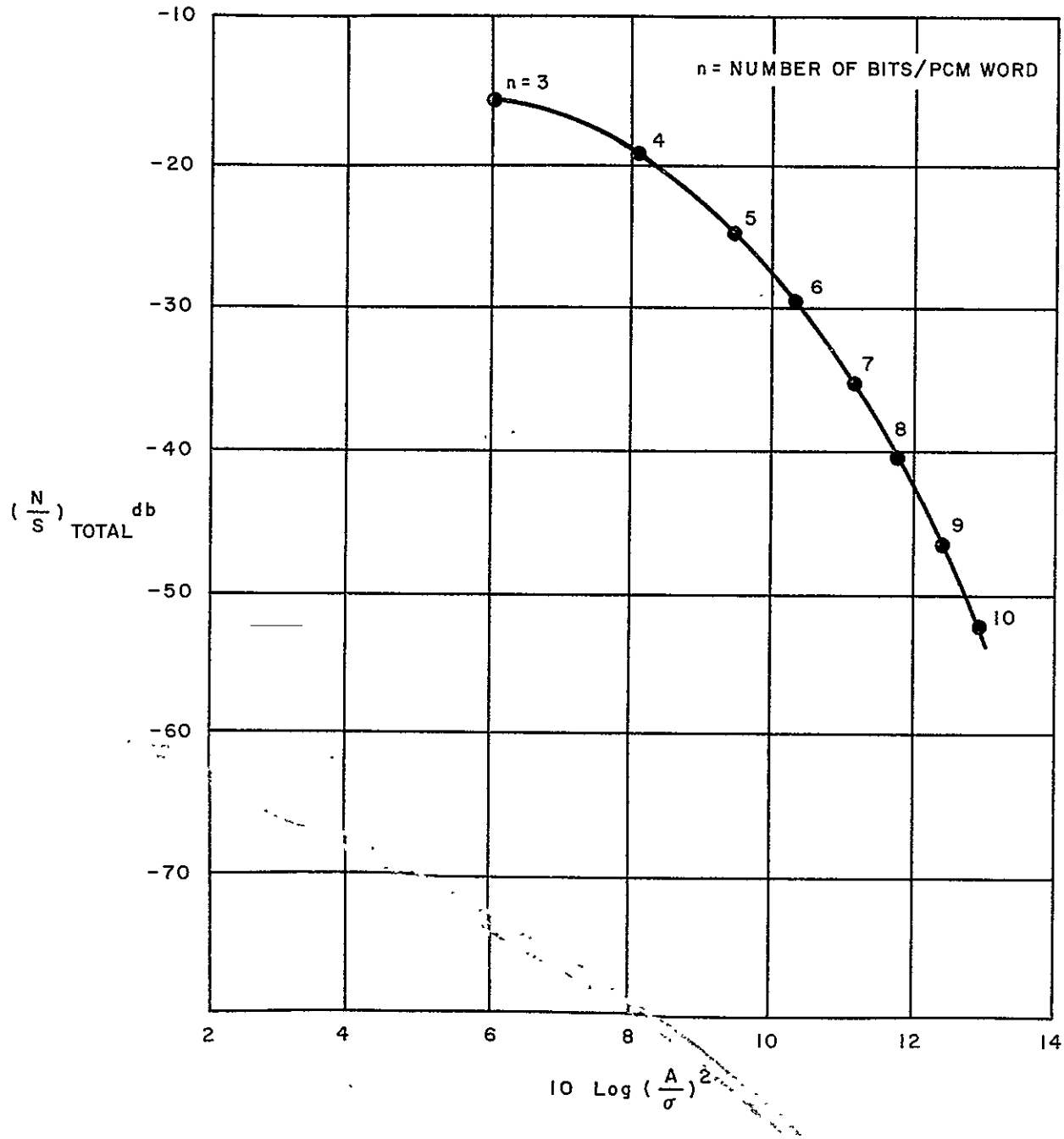

Fig. 1.9 MAXIMUM OUTPUT $\left(\frac{S}{N}\right)$ FOR PCM WITH GAUSSIAN INPUT

Figure 1.10 illustrates the resultant or total signal-to-noise ratio for PCM systems as a function of the predetection signal-to-noise ratio. The number of bits per sample or the number of bits per PCM code word, for both the optimum PSK and differentially coded PSK are given.

From Figure 1.10 we conclude that the desired bit error probability for a practical PSK system ($P_\varepsilon \cong 2\ P_{cPSK}$) should be on the order of 10^{-5} so as not to degrade the quantizing resolution for a 7 bit PCM telemetry system. This value of P_ε corresponds to a predetection (S/N) of 10 dB. In analyses to follow a 10^{-5} bit error will be used as the target error probability for all the candidate systems.

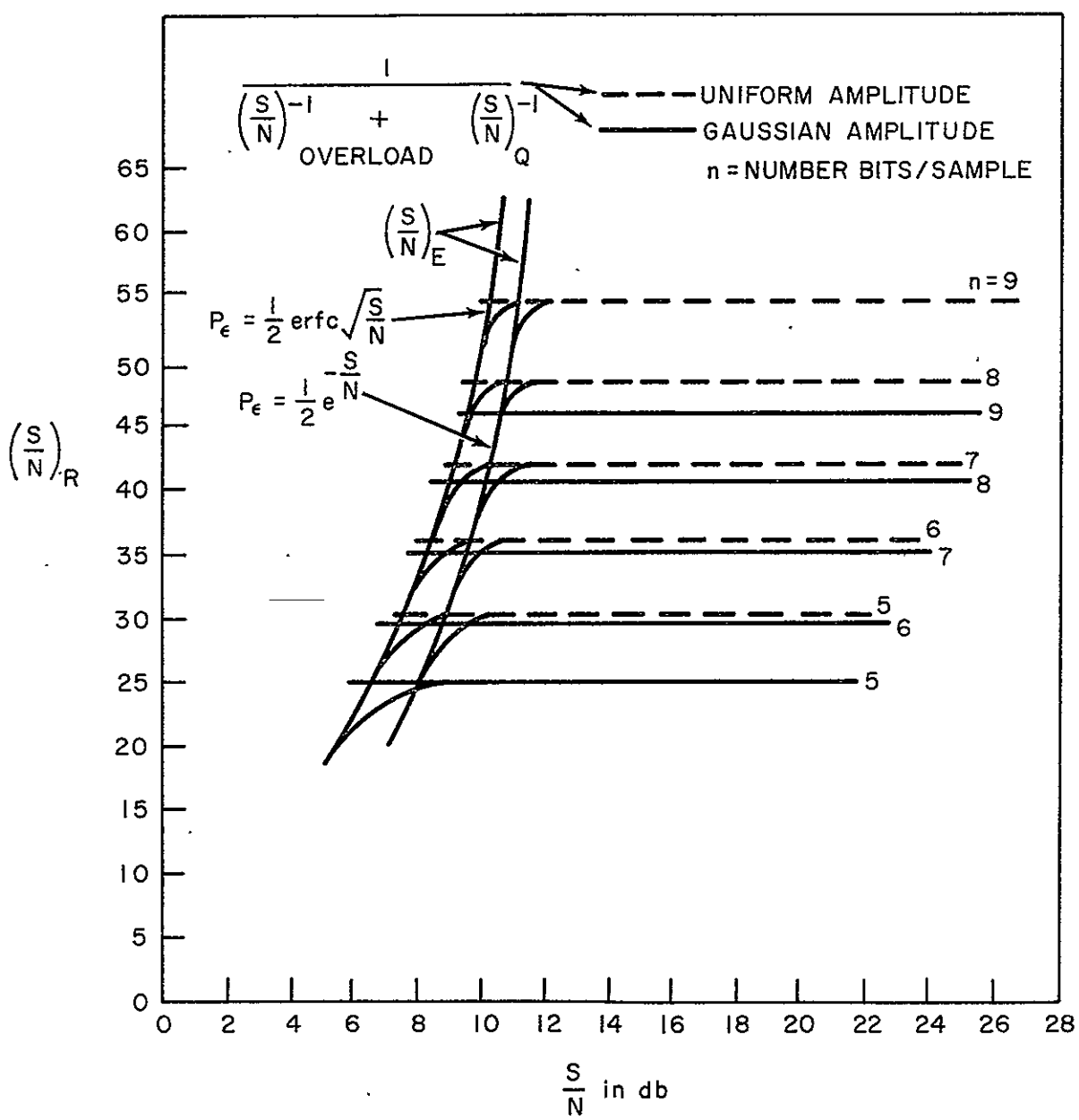

Fig. 1.10 $\left(\frac{S}{N}\right)_R$ PCM WITH ERRORS

1.6 ANTIMULTIPATH SYSTEMS ANALYSES

1.6.1 Frequency Diversity System

In accordance with the program specifications it is highly desirable to obtain reliable communications for the 136-138 MHz band and support simultaneously up to 40 users, with a minimum of user equipment complexity. Furthermore, the system should operate reliably within the constraints of 2 MHz total repeater RF bandwidth and within the power limitations imposed on the user satellite. We are obliged to consider the use of diversity techniques in order to obtain a reasonably simplified system for the 136-138 MHz link.

In a previous section we have argued that the major contribution to the multipath should result from the diffuse component and that this diffuse component can be appreciable for grazing angles in excess of 20°. For all practical purposes the diffuse component can be considered maximum for grazing angles above 40° and the power in the diffuse component may equal the power in the direct path signal under worse case multipath conditions. (Multipath power can actually exceed the desired signal power at low orbits as a result of user antenna variations).

A single channel ΔPSK transmission in the presence of diffuse multipath, the power of which is equal to the desired signal power, will experience a bit error probability of .18*. Furthermore, this value is approached at reasonably low input signal to Gaussian noise ratios (10 dB). In order to obtain diversity action it is necessary to transmit the same

* This result is obtained for a $\left(\frac{E_b}{N_o}\right)$ = 10 dB and a ΔPSK $P_\varepsilon = 2P_{CPSK}$ (see Appendix I)

information on a number of independent carriers. The frequency separation of these carriers for proper diversity action must exceed the coherent bandwidth (otherwise the fading is correlated). For the TDRS satellite geometry the coherent bandwidth should be between 5 KHz and 30 KHz depending upon the height of the user vehicle above the earth.

For the time being we will not consider the effects of interference or the requirements for emergency voice for the manned missions at VHF, rather confine our attention to the performance of a diversity system in the presence of multipath. We assume that there are 40 users, a data rate/user of 1 KBit/sec, a repeater bandwidth of 2 MHz between 136-138 MHz and that the users are transmitting on independent frequencies located within the 2 MHz spectrum. A four-frequency system which illustrates the frequency locations of various users is shown in Figure 1.11. The carriers associated with one user are separated sufficiently in frequency so as to be in excess of the largest expected coherent bandwidth. Furthermore, the frequency bands which are allocated to a particular user are sufficient to accommodate Doppler and differential Doppler and frequency uncertainties in the TDRS. system. It is assumed that forward error control can be applied simultaneously to the redundant data transmission system of a user. Furthermore, the power which is divided among the carriers is assumed to be divided equally. We have allocated 12.5 KHz to each frequency or subcarrier associated with each user. Such an allocation imposes a maximum number of independent carriers for each user; that is, we find that the total bandwidth of 2 MHz can support a four-frequency diversity system for each user, assuming 40 users and 12.5 KHz for each carrier per user.

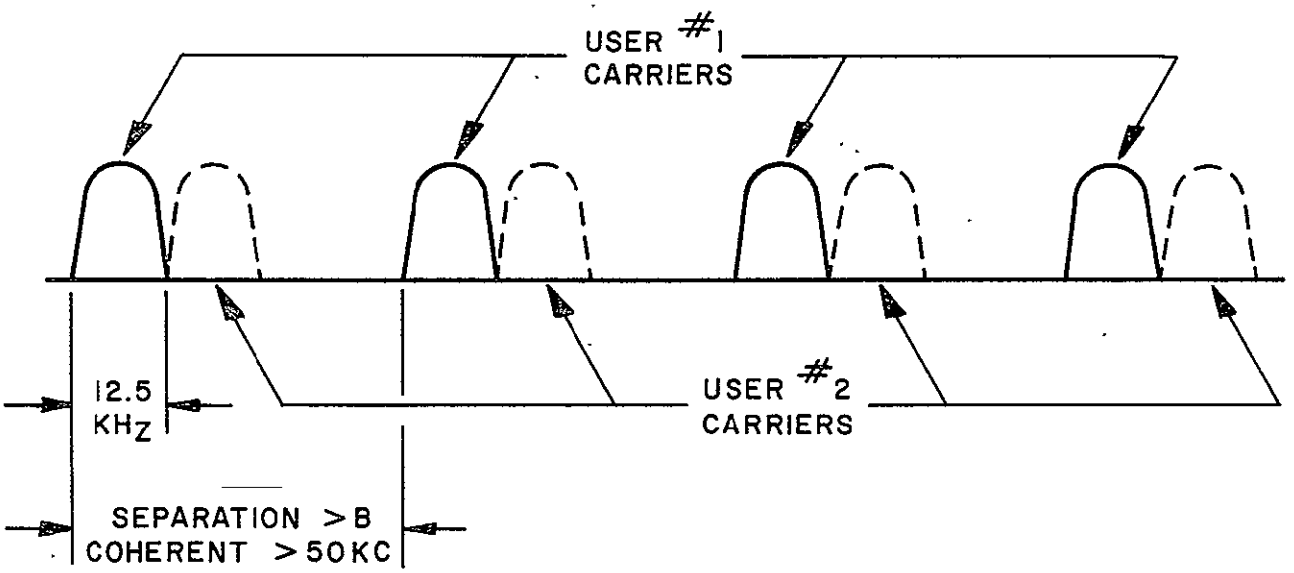

Fig. 1.11

FREQUENCY DIVERSITY SYSTEM

Table 1.3 indicates the power budget and link calculations required to determine system performance for various user power levels per diversity channel.

Table 1.3 User to TDRS Link (Ideal)

Required S/N_o	40 dB Hz	$P_\epsilon = 10^{-5}$
System Margin	10 dB	antenna and system losses
N_o	-167.8 dbm	$T_s = 1200°K$
P_u Required at Satellite	-117.8 dbm	
G_t = User Antenna Gain	0 dB	
G_r = TDRS Antenna Gain	16 dB	
L_p = Path Loss	167.8 dB	
P_t = User Power	34 dbm = 2.5 watts*	

* if 6 dB system margin is used then $P_t \simeq 1$ watt

Assuming that the average signal-to-noise ratios are equal in all four diversity branches and that maximal ratio combining is employed in the ground station, we find that the expected raw bit error probability is 4×10^{-3} for the four-frequency optimum diversity system, when the signal-to-multipath power ratio is unity. Furthermore, we find that this bit error probability can be obtained at a power level per diversity channel of between 1 to 2.5 watts or a total user power of 4 to 10 watts, depending on the assumed system margin 6-10 dB.

Further increase in the amount of user power in the presence of multipath does not improve system performance for this particular approach. The raw bit error probability of 4×10^{-3} is not acceptable for most cases, since it has been shown that a bit error probability of 10^{-5} is normally required to preserve the quantizing resolution of the telemetered data. This result infers that forward error control techniques must be applied in order to further reduce the raw bit error probability to an acceptable level of 10^{-5}. The encoding techniques are usually simple. The decoders are at the ground station where additional complexity can be tolerated. Using convolutional encoding and sequential decoding a raw bit error probability of .005 can be readily reduced to 10^{-5}*. Forward error control is discussed in detail in Section 1.7 of this report.

In summary, we have shown that it is feasible to operate a four-frequency diversity system to obtain a desired bit error probability 10^{-5} when forward error control techniques are employed in conjunction with the diversity system. The upper limit on the number of diversity frequencies is four and this is predicated on 40 users, 12.5 KHz per diversity channel allocated to each user. Furthermore, it assumes that the diversity channel frequencies are separated in excess of the coherent bandwidth in order to obtain full diversity action in the receiver. No attempt has been made to evaluate the diversity system in the presence of interference. The 12.5 KHz channel bandwidth is probably a bit optimistic and should probably be increased to about 16 KHz which in turn will reduce the order of diversity to three instead of four. However, even at an order of diversity of three

---

* (based on a rate ½ convolutional encoder/sequential decoder and, reasonable constraint lengths, and storage.)

the resultant error probability will be 1.2×10^{-2} which can still be reduced to 10^{-5} by forward error correction, if large constraint lengths are employed.

1.6.2 Multipath Model for Large Time Bandwidth Product Signals

In several following sub-sections we will analyze large time bandwidth signal designs for their antimultipath properties. In order to do this an accurate multipath model is required.

The multipath properties of the user/TDRS channel have been discussed in section 1.2. There it was shown that the reflected signal would have average time delays relative to the direct path between 200 usec to and 10 msec depending on the height of the user's orbit. Actually these delays will range between 1 msec to 10 msec for most cases. Since the large time bandwidth signals to be analyzed will operate at 1 Kbit/sec frame rate, which corresponds to the 1 Kbit/sec user rate, it is reasonable to treat the multipath signal as another user signal which after 1 msec is uncorrelated with its direct signal. For large TW signals the chip durations (symbol durations) will be such to overshadow the fading bandwidths, Doppler and differential Doppler. The multipath signal generated by a large TW product signal can cause symbol errors in other user signals as well as its own direct signal during subsequent data frames, and it is easy to show that specular or diffuse multipath cause equal symbol error probabilities when the signal to multipath ratio is unity.

The failing feature of this multipath model is that it does not allow for time spread effects and thus represents a conservative model rather than an optimistic model.

Based on the above arguments, the multipath analyses of large TW product signals which follow will assume that the signal to multipath ratio is unity and that the multipath effectively increases the number of simultaneous users by a factor of two. Thus these analyses will also cover the multiple accessing of large TW product signals through a common linear repeater of bandwidth 2 MHz for the user to TDRS link.

1.6.3 Pseudo-random Time Hop System (PRTH)

A potential candidate for the DRSS is a pseudo-random time hop system. The primary advantages of such an approach is that it requires no net synchronization and the implementation is quite simple. Furthermore, it can provide (with complex instrumentation) range and range rate between user and ground station. The pseudo-random time hop system employs RF pulses with an extremely low duty factor. We assume that there is perfect synchronization between the transmitter and receiver and that there are a number of users equal to K. Furthermore, the duty factor is given by α where α is much less than unity. We will further assume that the effects of multipath are accurately represented by doubling the number of users through the linear repeating satellite. The various users are not coordinated in time and the emissions of pulsed carriers from each user are random. Furthermore, on the average the time hop pulse is pseudo-randomly time hopped over an information interval T_F such that α is given by the duration of the pulse divided by the frame time. This system has been proposed by Cahn* for multiple access through repeating satellites. The PRTH waveform is illustrated in Figure 1.12. Cahn has shown that the worst case bit error

* J. M. Aein etal, Multiple Access to a Comm. Sat, with a Hard Limiting Repeater Vol. II April 65 AD465-789

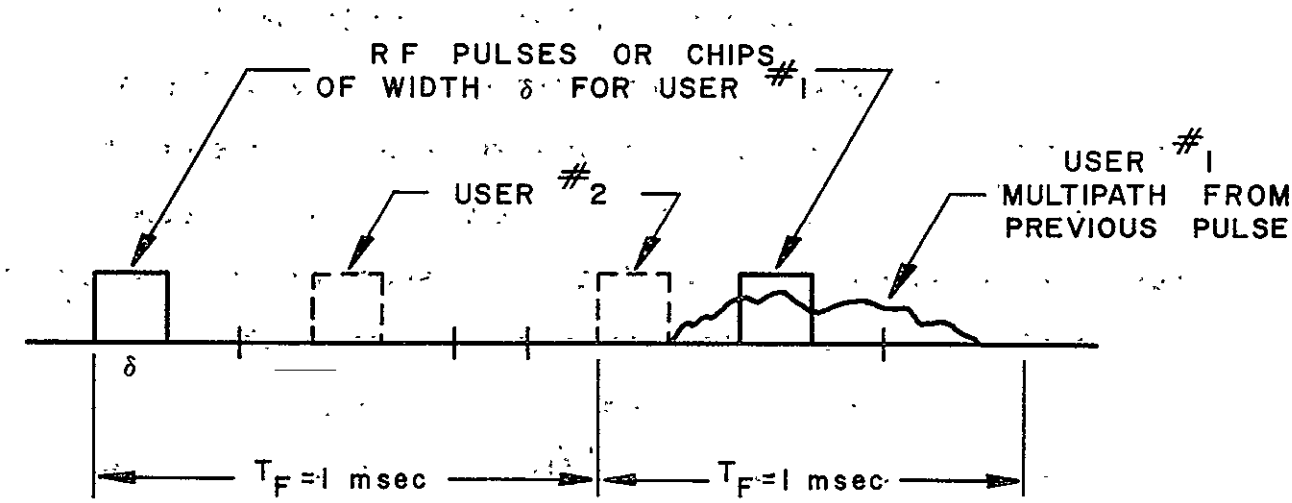

$$\alpha = \frac{\delta}{T_F}$$

Fig. 1.12: PRTH WAVEFORM

probability is given by eq. 1.12.

$$P_\varepsilon = (1-\alpha)^{K-1} P_{\Delta PSK} + \gamma\left[1-(1-\alpha)^{K-1}\right] \qquad \text{eq.1.12}$$

$.18<\gamma<\frac{1}{2}$ $\therefore$ $\gamma=\frac{1}{2}$ worst case

$P_{\Delta PSK}$ is the bit error probability resulting from noise

The above equation assumes that when a pulse is received in the presence of another interfering user pulse or multipath whose strength is equal to that of the desired signal we obtain a bit error probability of ½. Furthermore, when a pulse is received without the presence of multipath or another user, we obtain a bit error probability given by the theoretically largest value obtained via ΔPSK modulation.

When applied to the TDRS system wherein the 136-138 MHz band is confined to a 2 MHz RF bandwidth then it follows that the duty factor α has a minimum value which is regulated by this RF bandwidth and by the minimum binary data rate. For a data rate of 1 kilobit per second it follows that the value of α must be equal to or greater than $.5 \times 10^{-3}$.

The bit error probability given in equation 1.12 can be minimized by properly choosing the duty factor within the constraints of the DRSS channel. This is, in general, a difficult task to accomplish. However, we can obtain an approximation to the bit error probability assuming that the duty factor is small, and that the two parts of equation 1.12 are equal.

$$P_\varepsilon \cong \alpha(K-1) \qquad \text{eq. 1.12}$$

$$\simeq 4 \times 10^{-2} \text{ for the TDRS}$$

(multipath + users = 80 users)

We can solve the above equation under the constraints of the 136-138 MHz TDRS channel and the desired bit error probability which has been determined to be on the order of 10^{-5}. We find that it is impossible to obtain a bit error probability under the constraints of the duty factor α which can be obtained through the TDRS, and the number of required users equal to 40.

Thus it can be concluded that while the pseudo-random time hop system is indeed attractive from an implementation point of view, it will not in general provide the desired bit error probability for the number of users required.

Again, as with the diversity system previously analyzed, forward error correction can be relied upon to reduce the bit error rate to 10^{-5} if large constraint length convolutional encoding/sequential decoding is employed.

Note that the Gaussian noise contribution to the error probability need only be on the order $P_{\varepsilon Gaussian} = .02$ which corresponds to a symbol or chip $E/N_0 = 4.2$ dB. Assuming a system margin of 10 dB this corresponds to an <u>average</u> user power $\simeq .6$ watts and a peak power of <u>1200 watts</u>!

1.6.4 Hybrid Frequency Hopped/Time Hopped Signal Scheme

As in the previous sub-section, we assume that each user's multipath appears as another user. In this context, the multipath analysis reduces to a multiple access problem. We therefore focus attention on a multiple access communication system: a hybrid frequency/time hopping (FH/TH) scheme which is actually a generalization of the PRTH system. The system relies basically on the division of the time-frequency plane into MN cells

as indicated in Figure 1.13; each cell represents a chip, with some specified combination of chips representing a symbol from the alphabet being used to encode the data (in the binary case, this could be 0 and 1, or mark and space). An important constaint is that during any time frame (of fixed duration T_F), the same number of chips is transmitted. These may be distributed in any chosen manner in the corresponding time-frequency plane.

In the frequency/time-hop system each user sends to exactly one ground station (GS) although the latter may be able to receive from more than one user. User and GS are synchronized in the sense that the GS knows which arrangement of cells in the time-frequency plane corresponds to a mark and which to a space (or more generally, to any symbol of an m-ary alphabet). The GS then "looks" only in the appropriate cells. Such a signaling scheme has been analyzed by Wittman* and Reiffen**, among others.

Wittman's analysis includes the effects of unequal signal amplitudes and RF phase cancellation at the GS as well as noise in both the user-to-TDRS ("up") and TDRS-to-GS ("down") links. He assumes a perfectly linear, frequency-translating satellite with bandwidth W_s. Both up- and down-link noise is additive, white, and Gaussian. The transmission media have no other effect on the signals. A typical user transmits at data rate R bits/sec, where R is some sub-multiple of the maximum system data rate. The user (and synchronized GS) independently and pseudorandomly selects a chip configuration

---

* Wittman, John H., "Analysis of a Hybrid Frequency-Time Hopping Random-Access Satellite Communication System," IEEE Trans., COM-16, no. 2, April 1968, pp. 303-310.

** Reiffen, Barney, "On the Use of Non-Coherent Pulse-Address Modulation for Multiple Access to a Hard-Limiting Satellite Repeater," App. VA in Aein, J.M., et al., Multiple Access to a Communication Satellite with a Hard-Limiting Repeater, v. II, IDA Rept. R-108 (AD 465-789), April 1965.

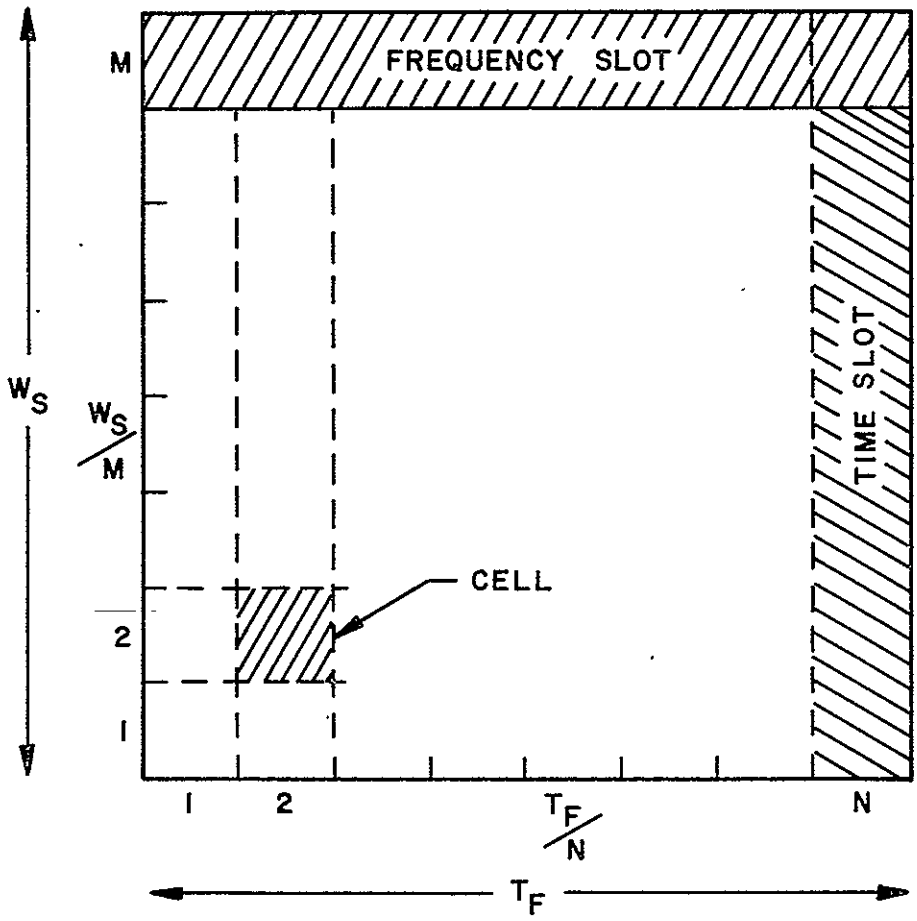

Fig. 7.13

PARTITIONING OF THE FREQUENCY-TIME PLANE

for a mark by selecting b distinct cells from each of η successive time frames, along with another, non-overlapping set of ηb cells for a space. Each chip then consists of a constant-amplitude pulsed sinusoid which is matched-filter envelope detected*. The decision as to mark or space (i.e., data bit = 0 or 1) is then made on the basis of ηb mark vs space chip decisions at the receiver, with the bit decision based simply on a majority of the chip decisions. Thus, the probability of a bit error is just the probability that more than $\eta b/2$ chip errors have been made. The two factors contributing to chip error in this model are noise and interference from up to K-1 other users of the same cell. Under the assumption that the number of cells per frame is very much less than the total number of cells in the time-frequency plane (i.e., $b/MN<<1$), individual chip decisions can be taken as independent. With marks and spaced assumed equally probable a priori, one can view the chip decisions as successive outputs of a binary symmetric channel operating at capacity. The bit error probability P_e is then related to the chip error probability p_e through the familiar binomial expansion

$$P_e = \sum_{\Delta=[\eta b/2]}^{\eta b} \binom{\eta b}{\Delta} p_e^{\Delta} (1-p_e)^{\eta b-\Delta} \qquad \text{eq. 1.13}$$

Here [x] denotes the smallest integer larger than x.

Reiffen's model is almost identical to Wittman's, the only significant difference being the assumption of a hard-limiting instead of a linear satellite.

* Note that for this analysis we have dropped the ΔPSK signaling technique, but this is necessary to make the analysis tenable. The results will still illustrate the performance of the system and will not be dramatically different from the ΔPSK system.

In both analyses, evaluation of the relevant expressions for bit error probability leads to the conclusion that the FH/TH scheme is inadequate as an antimultipath technique unless used in conjunction with some form of forward error control (e.g., with sequential decoding using a fairly short, rate ½ convolutional code, a raw P_e of .005 can be converted to an output P_e of 10^{-5}). In particular, Table 1.4 gives trade-offs obtained from Wittman's results. Using Reiffen's model and analysis, similar results are obtained.

Table 1.4 FH/TH Trade-Offs

$MN=1000$, $W_s \approx 2X10^6$ Hz

R(bps)	K	nb	E_{bit}/N_o, db	P_e(raw)
1000	15	2	14	$>10^{-3}$
300	80	7	19.4	10^{-5}
1000	10	4	23	10^{-5}

Note: K=2X (actual no. of users), in our multipath model

In the next section, we shall discuss a multiple access scheme which does achieve the required bit error probability $P_e = 10^{-5}$ for 80 users, an information rate per user of 1000 bps, and total bandwidth of 2 MHz. This is accomplished, however, at the price of increased complexity (i.e., m-ary coding with large m).

1.6.5 RADA System

A random access, discrete address (RADA) system differs from the hybrid time-hop/frequency-hop system described in the previous section mainly in the way in which a user/ground station pair (i.e., transmitter and receiver) is determined and communication established between them. Specifically, any user and ground station (GS) can communicate. This is accomplished by having the user send out an address uniquely to a particular GS. This address is determined by a combination of k cells from the MN-cell time-frequency plane and is detected at the GS as a k-fold coincidence (see Figure 1.14).

In the RADA system to be described, we consider an extension of this technique to the case in which each GS has not one but m addresses, all unique with respect to the other GS's in the system. Note that a separate coincidence circuit is required for each address which is not a time translation of another address for that GS. A unique feature of this system is that each address serves also as an alphabet symbol for the GS. This m-ary alphabet may be viewed as a kind of error correction technique because of the distance it provides between symbols when the latter are viewed on a chip-by-chip basis.

Furthermore, noise will be neglected*, and interference will appear as a false k-fold coincidence but not as pulse cancellations. (This model and the analysis which follows are due to Chesler**.) In view of

---

* This assumption is justified by virtue of the often-used rule of thumb that equal contributions to the total bit error probability are made by pulse interference and multipath on the one hand and by noise on the other. As in the preceding section, we account for multipath by considering twice the number of actual users. Then the error probabilities obtained here should be roughly doubled to account for effects of noise.

** Chesler, David, "Performance of a Multiple Address RADA System," IEEE Trans., COM-14, no. 4, August 1966, pp. 369-372.

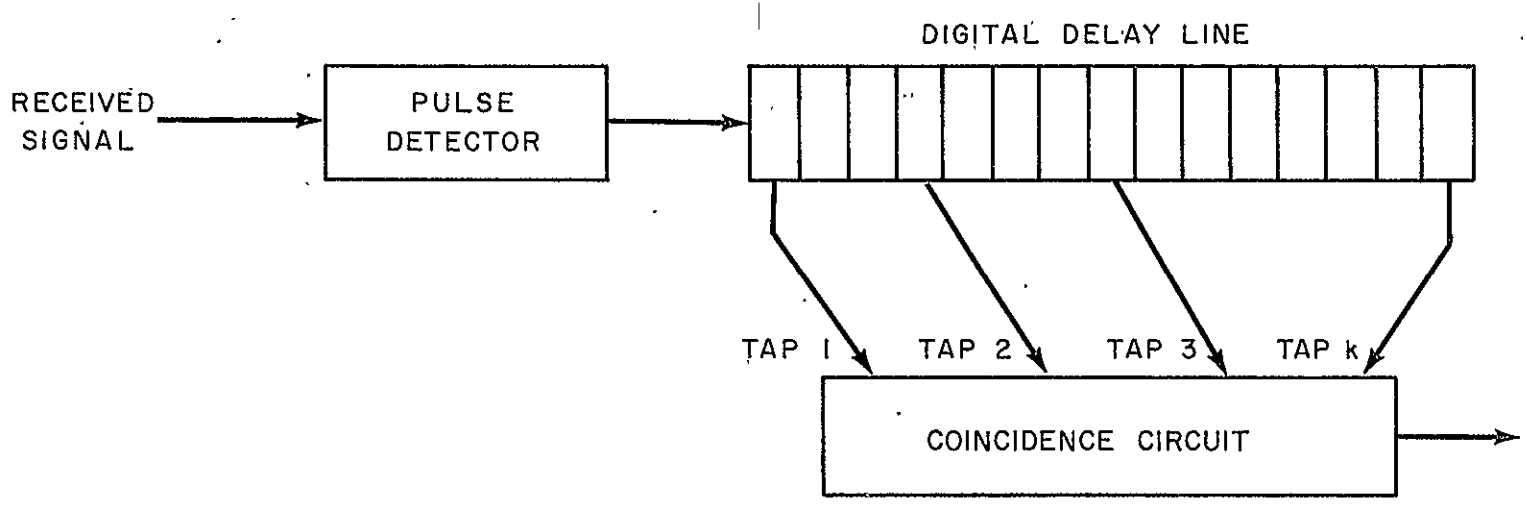

Fig. 1.14 RADA RECEIVER

these assumptions, it is natural to evaluate performance in terms of the probability $\overline{P}$ of a false k-fold coincidence of at least one of the m addresses of a given GS. The two parameters of prime interest are the channel utilization F and the size MN of the time-frequency plane, where F is defined by $F = \overline{R}/W_s$, with $\overline{R}$ being the average total information rate and W_s the channel bandwidth defined in the previous sub-section.

Without loss of generality, we can assume that only one time frame (which Chesler calls a matrix period) is necessary to transmit an address. It will be stated without further discussion that whether or not user and GS are initially synchronized, there is the same probability of error per decision as to which, if any, of the GS's addresses was transmitted. We wish to point out that some of the approximations made in the analysis which follow are definitely restricted in their validity by the size of certain quantities, particularly exponents. We will not enter into a discussion of these points, however, since we consider the final results as adequate guidelines for our own conclusions.

Let $P(k|K)$ be the probability that K users will cause a false k-fold coincidence of at least one of the m addresses of a particular GS. We calculate $P(k|K)$ as follows. Assuming that the k pulses which determine an address are chosen at random from the time-frequency plane of MN cells, the probability that a particular interfering user has a pulse in any cell is

$$p_1 = k/MN \qquad \text{eq. 1.14}$$

Then the probability that none of K users has a pulse in that cell is

$$p_2 = (1-p_1)^K \qquad \text{eq. 1.15}$$

and the probability of a coincidence of all k pulses of a particular address is approximately

$$p_3 = (1-p_2)^k \qquad \text{eq. 1.16}$$

Finally, since the probability of no coincidence at any of m addresses is $(1-p_3)^m$, we have

$$p(k|K) = 1-(1-p_3)^m \approx m\, p_3 = m[1-(1-k/MN)^K]^k \qquad \text{eq. 1.17}$$

Now we assume that the active status of a user is an event independent of all other users. Then the number K of active users will have a Poisson distribution

$$P(K) = (\overline{K})^K e^{-\overline{K}}/K! \qquad K = 0,1,2,... \qquad \text{eq. 1.18}$$

Thus, $\overline{P}$, the average probability of error per decision, is given by

$$\overline{P} = \sum_{K=0}^{\infty} P(k|K)P(K) = \sum_{K=0}^{\infty} m[1-(1-k/MN)^K]^k (\overline{K})^K e^{-\overline{K}}/K! \qquad \text{eq. 1.19}$$

This result is of little use to us unless we can relate it to the parameters F and MN defined earlier. This we will now do. As already noted, $F = \overline{R}/W_s$, while $MN = W_s T$, where T is the length of a time slot. Now the average information rate, in bits per second, is the information per

symbol (=address) times the average number of users divided by the length of a time slot; i.e.,

$$\overline{R} = \overline{K}(\log_2 m)/T \qquad \text{eq. 1.20}$$

Thus the channel utilization is

$$F = \overline{K}(\log_2 m)/MN \qquad \text{eq. 1.21}$$

Solving 1.21 for $\overline{K}$ and substituting in 1.19 gives

$$\overline{P} = \sum_{K=0}^{\infty} m[1-(1-k/MN)^K]^k (F\,MN/\log_2 m)^K (1/K!)\exp(-FMN/\log_2 m) \qquad \text{eq. 1.22}$$

This expression is quite unwieldy, so that in order to obtain a measure of the performance of a multiple-address RADA system, we argue as follows. From 1.21 we get

$$\overline{K} = FMN/\log_2 m, \qquad \text{eq. 1.23}$$

from which it is clear that the average number of users is proportional to MN; thus for fixed F and m, $\overline{K}$ becomes large with MN. Since the standard deviation of the Poisson distribution (1.18) is $\sqrt{\overline{K}}$, it can be argued that the relative variation in K approaches zero as $K \to \infty$, so that for very large MN, we let $K=\overline{K}$. This eliminates the need for averaging over K in (1.19) and permits us to use (1.17) directly for calculating $\overline{P}$:

$$\overline{P} = m[1-(1-k/MN)^{\overline{K}}]^k \qquad \text{eq. 1.24}$$

A further approximation from (1.24) can be obtained by noting that for $k/MN \ll 1$, $(1-k/MN)^{\overline{K}} \approx e^{-k\overline{K}/MN}$, so that

$$\overline{P} \approx m(1-e^{-k\overline{K}/MN})^k \qquad \text{eq. 1.25}$$

Now k may be chosen to minimize $\overline{P}$ in (1.25). It turns out that this optimum value of k satisfies $e^{k\overline{K}/MN}=2$, giving

$$\overline{P}_{opt} = m2^{-MN(\ell n2)/\overline{K}} = 2^{-\log_2 m[(\ell n2)/F-1]} \qquad \text{eq. 1.26}$$

from which we see that $\overline{P}_{opt}$ can be made arbitrarily small by increasing the number of addresses m per receiver, as long as channel utilization F is less than about 70% ($\ell n2 \approx 0.69$).

Figure 1.15 (due to Chesler) represents the optimum performance of a multiple access RADA system as a function of MN with F as a parameter. (The dashed line approximate for $n=.04$, corresponding to our $\overline{K}$ of 80.) Here performance $\overline{P}$ has been optimized with respect to both k, the number of pulses per address, and alphabet size m. The relation between MN and the approximate optimizing value of m is given in Table 1.5. These values have been used in obtaining Figure 1.16, which is a necessary step in compiling Table 1.5.

To relate the expressions developed in the foregoing analysis of the multiple access RADA system to our multiple access (alias multipath) model, we must note several important facts. Our data rate of 1000 bps is for <u>each</u> user, so that

$$\begin{aligned} \overline{R} &= 1000 \text{ X (no. of users)} \\ &= 1000\ \overline{K} \\ &= 1000\ K, \text{ for large MN} \end{aligned} \qquad \text{eq. 1.27}$$

TABLE 1.5

OPTIMUM VALUES OF ALPHABET SIZE AS A FUNCTION OF MATRIX SIZE

Matrix Size N	Approx. Optimum Values of $\log_2 m$
50	4
100	6
500	12
1000	20

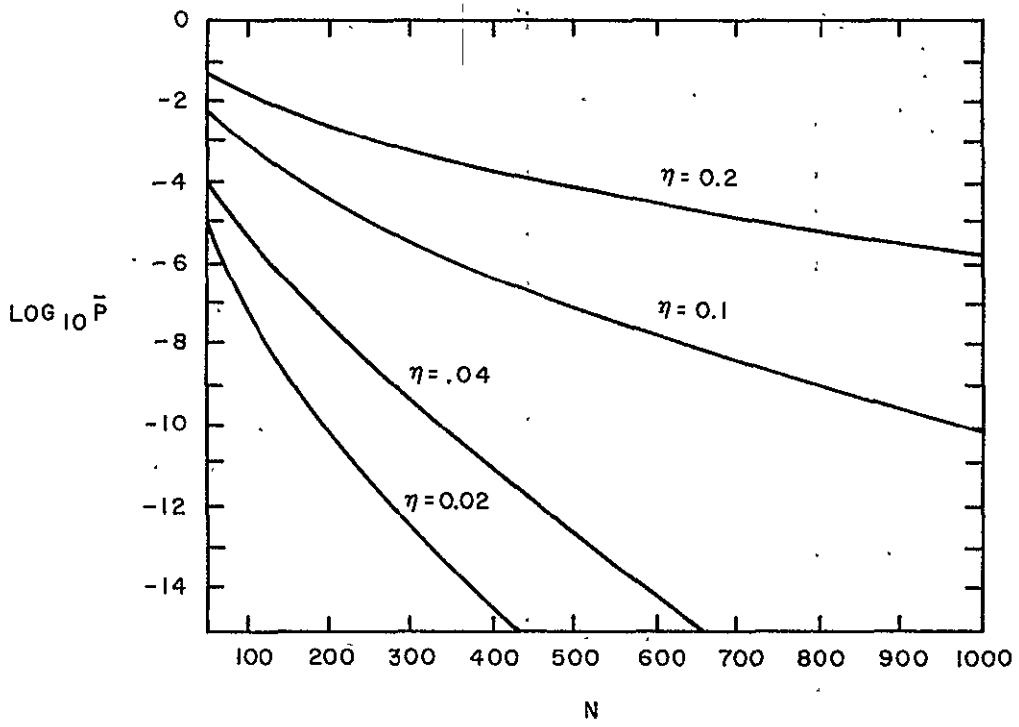

Fig. 1.15

PROBABILITY OF ERROR VS MATRIX SIZE (OPTIMUM SIZE OF ALPHABET)

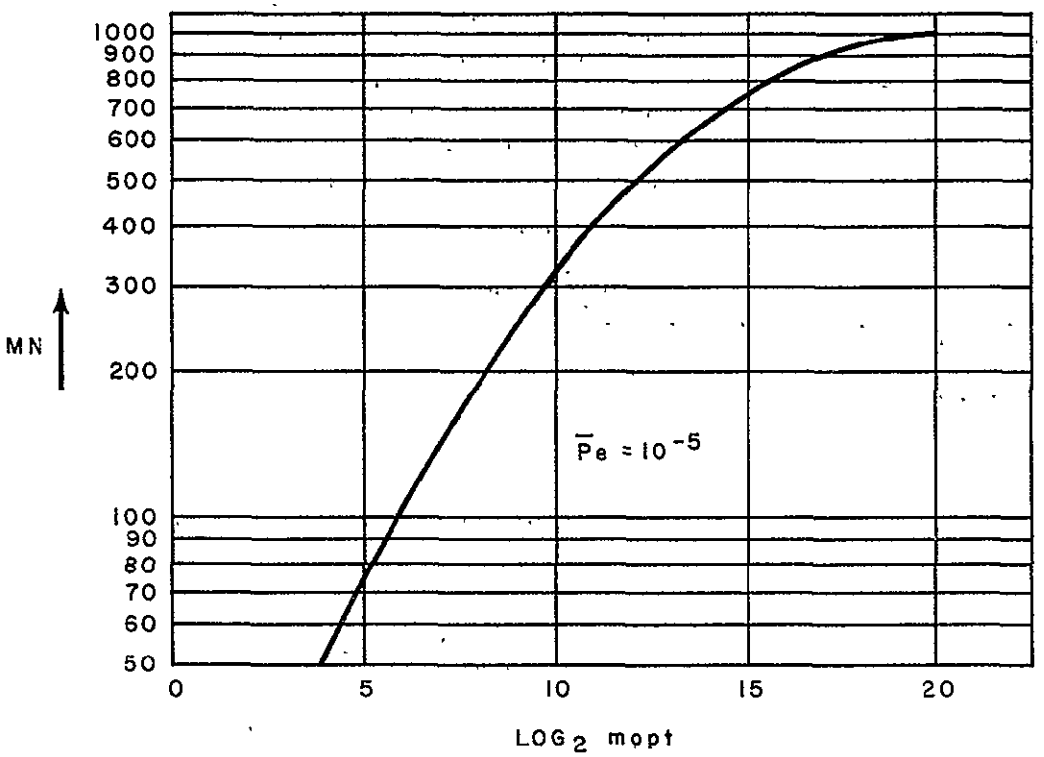

Fig.1.16

NUMBER OF CELLS IN TIME-FREQUENCY PLANE VS ALPHABET SIZE

On the other hand, all users are pushing data through the same 2 MHz channel, so

$$F = 1000\ \overline{K}/(2 \times 10^6) = 0.5\ \overline{K} \times 10^{-3} \qquad \text{eq. 1.28}$$

The value of the optimum k is found from 1.23:

$$k = MN\ \ell n2/K \qquad \text{eq. 1.29}$$

Table 1.6 was obtained in the following manner. We set $\overline{P} = 10^{-5}$ and entered Figure 1.15 to get pairs of values of MN and F. Values of $\log_2 m$ were obtained from Figure 1.16 while K was obtained from 1.28. Finally, 1.29 gives the corresponding k.

It is amply clear that the required bit error probability, viewed now as probability of error per m-ary symbol, is easily achieved with the allotted bandwidth, but only at the price of a 64-symbol alphabet. The time-frequency plane contains a modest 100 cells. It is interesting to note that only 1 pulse per address optimizes $\overline{P}$ for a wide range of numbers of user pairs.

Table 1.6 RADA System Parameters

System parameters giving $\overline{P} = 10^{-5}$ (W_s = 2 MHz, R_{user} = 1000 bps) optimized over m and k.

F	MN	$\log_2 m$	m	$\overline{K}$	k
.2	730	14.7	26,700	400	1.27
.1	240	8.8	440	200	0.83
.04	100	6	64		0.87
.02	50	4	16	40	0.87

1.6.6 PN SYSTEMS FOR TDRS

Up to this point in the report we have considered only systems which operate in the presence of multipath and do not attempt to avoid it. We will now analyze the last technique which "lives" with the multipath. This system can take on various configurations but basically uses pseudonoise (PN) coding to combat multipath, decrease the effects of interference, provide multiple access through the TDRS, provide user addressing, and accurate range and range rate data.

The PN analyses to follow will emphasize:

(1) PN multiplexing
(2) repeater considerations
(3) multipath performance
(4) maximizing the processing gain for the TDRS

The effects of interference on the performance and choice of the PN approach is discussed in section 1.12 (RFI Considerations for the TDRS).

1.6.6.1 PN Multiplexing Techniques for the Data Relay Satellite System

Binary sequences form the basis for PN communication systems which have antimultipath, anti-interference, and multiple access capabilities. Specifically, the maximal length linear sequence generator has been the primary source of control for such communication systems in the past because of its almost ideal autocorrelation properties. The autocorrelation properties of a maximal length linear sequence consisting of n stages is defined by eq.1.30.

$$R_{11}(\tau) = \frac{\text{agreements - disagreements}}{\text{agreements + disagreements}}$$

$$= 1, \ \tau = 0$$

$$= -\frac{1}{2^n-1} \quad \tau \geq 1 \text{ chip} \qquad \text{eq. 1.30}$$

The autocorrelation function of a maximal length code is two-valued and the residual autocorrelation coefficient $\tau > 1$ chip is slightly negative, having a value of $-\frac{1}{2^n-1}$

There are a number of ways of providing unambiguous multiplexing on a non-coordinated basis for the TDRS system. Non-coordination means the simultaneous presence of a number of signals in the TDRS passband with no synchronous time division accessing.

(1) Each user is assigned a different Gold sequence from a family of equal length sequences.

(2) Users are assigned different maximal length sequences of different lengths.

(3) All users utilize the same maximal length code but use frequency offsets in each user carrier to allow user discrimination in the receiver located at the ground station.*

(4) Users are assigned equal length codes, from a very limited number of codes (e.g., eight codes) and are frequency multiplexed as in (3) (e.g., five frequencies), such that the product of codes X frequency slots equal forty.

(5) Because of the interference problem and the range and range rate requirement another approach to PN multiplexing is to use separate non-overlapping channels for each user and allow each user to utilize the same PN code. The PN code rate would be high enough to protect a user against his own multipath and provide the required range and range rate now obtained with the present GRARR 20 KHz side tone system.

*This technique has been proposed by the Jet Propulsion Labs.

At this time there is very little known about the cross-correlation properties of maximal length codes of different lengths. Therefore, technique number 2 for PN multiplexing will not be discussed in this study. This section will emphasize technique (1) and a comparison of the variou techniques will be given in section 1.6.6.6.

Consider technique (1), the use of different codes of equal length for the TDRS to user link. Given that each user employs a shift register of length n, there are Φ_N/n maximal length sequences of period 2^n-1 which can be generated from the n-state register. Φ_N is the number of positive integers less than n and relatively primed to n. This number, the Euler number, is well approximated by $2^n-1/n$ for reasonably large values of n. It is obvious that for n large (>10) there are an adequate number of maximal length codes of length 2^n-1 which are available for the expected number of users in the TDRS.

It is necessary to minimize the cross-correlation values between user codes to prevent false synchronization and provide maximum processing gain. Gold* has shown that it is possible to select pairs of maximal length codes which are generated from a n-stage register which have the following cross-correlation properties.

$$|R_{ij}(\tau)| \leq \frac{1}{2^{(n+2)/2}+1} \qquad n \text{ even}$$

$$\leq \frac{1}{2^{(n+1)/2}+1} \qquad n \text{ odd} \qquad \text{eq. 1.31}$$

*R. Gold, Trans, I.T. Oct. 67

The selection of their pairs result in minimum cross-correlation between code pairs. Other codes selected from the family of maximals can produce very high cross-correlation values.

Gold has also devised a technique for generating large numbers of these minimum cross-correlation codes utilizing linear sequence generators. The procedure for generating these families is given through the following theorem. Let F1 and F2 be preferred pairs of primative polynomials of degree n whose corresponding shift registers generate maximal linear sequences of period 2^n-1 and whose cross-correlation function satisfies the inequality.

$$|R_{12}(\tau)| \leq \frac{1}{2^{(n+2)/2}+1} \qquad n \text{ even}$$

$$\leq \frac{1}{2^{(n+1)/2}+1} \qquad n \text{ odd} \qquad \text{eq. 1.32}$$

Then the shift register corresponding to the product polynomial F1·F2 will generate 2^n+1 different sequences each of period 2^n-1, such that the cross-correlation function of any pair of such sequences satisfies the above inequality. The autocorrelation function of any of the above non-maximal codes, however, is no longer ideal but has the following form

$$R_{11}(0) = 1 \quad \tau = 0$$

$$|R_{11}(\tau)| \leq \frac{1}{2^{(n+2)/2}+1} \qquad n \text{ even}$$

$$\leq \frac{1}{2^{(n+1)/2}+1} \qquad n \text{ odd} \qquad \text{eq. 1.33}$$

We can state that the generation of such code sequences with minimum cross-correlation coefficients still produce an upper bound on the maximum obtainable processing gain for a PN multiplex system. For example, one must choose a value of n sufficiently large such that the cross-correlation coefficient between the desired code and another user code is not high enough to produce false synchronization. On the other hand, it can be shown that for the same length sequences even purely random code words will produce higher cross-correlation properties than those obtained through the encoding technique just described. Thus we may consider this particular approach to generating large families of essentially orthogonal code words as being near otpimum, if one averages over the code length. The above discussions are based on averaging over the entire code length; however, when averaging over an interval equal to a data bit duration, the partial correlation properties of the Gold codes enter into the final multiplexing performance analysis. Specifically for low data users of the TDRS who employ PN for anti-multipath, tracking, multiple access, etc.; that might use chip rates as high as 2 mega chips/sec and PN code lengths of 8191 or 16383 chips, it is obvious that the integration time for each bit decision is 1 msec. At a 2 mega chip/sec code rate the code will repeat every 4^{+} msec or 8^{+} msec depending on the code length 8191 chips or 16364 chips. The receiver integrates for only 1/4 of the code length for each binary decision (1000 bps, 8191 code length, 2 mega chips/sec code rate). The later case is of particular interest to the TDRS, i.e., the

40 or more unmanned users (if PN is the choice system) would transmit at 1000 bps, use code rates close to 2 mega chip/sec at VHF, and use code lengths like 8191 or 16383 chip. The ability to multiplex simultaneously 40 or more TDRS users through a common 2 megahertz channel at VHF is primarily governed by the cross correlation properties of the PN Gold codes employed by the users. The length of the integration time for each data bit (e.g., 1 msec) spans a number of PN chips and this number is referred to as the window size w in the following analyses.

1.6.6.1.1 Partial Correlation Function of Pseudo Random Codes

In this section we discuss various statistical models for use in the determination of the partial correlation function of linear pseudo random codes. The ultimate objective is the determination of the distribution function of the partial correlation function of pseudo random codes and in particular the Gold Codes. We approach this goal in this document insofar as we present a model for the partial correlation function with known distribution function whose second order moments are equal to those of the unknown distribution.

In 1.6.6.1.2 we review the binomial model for the partial correlation function and apply this to balanced and unbalanced binary codes. This model becomes poor for increasing correlation window length w since the variance of the actual random variable approaches zero while the variance of the binomial model increases with increasing correlation window. In 1.6.6.1.5-6 we compute the second order moments of the unknown distribution function of maximal linear codes and for the family of Gold codes. The

hypergeometric distribution is shown to have second order moments equal to these of the linear codes and hence to be an improved model for the unknown partial correlation distribution function. These second order moments equal to these of the linear codes and hence to be an improved model for the unknown partial correlation distribution function. These second order moments are derived in 1.6.6.1.7 together with a normal approximation to the hypergeometric distribution.

1.6.6.1.2 Binomial Model for Partial Correlation Function

General Binomial Formula

We now derive an expression for the distribution function of the partial correlation function based on a binomial model. In particular we show

$$\text{prob}\left[|\theta| < \frac{k}{w}\right] \sim N\left(\frac{w\left(\frac{1}{2} - p\right) + \frac{k}{2}}{\sqrt{w\,p\,q}}\right) - N\left(\frac{w\left(\frac{1}{2} - p\right) - \frac{k}{2}}{\sqrt{w\,p\,q}}\right) \quad \text{eq. 1.34}$$

θ = correlation coefficient

In the above expression:

N = Gauss's distribution

w = length of correlation window

p = number of ones/sequence length

q = 1 - p

proof: prob $\left[|\theta| < \frac{k}{w}\right]$ $1 \leq k \leq w$

$$\text{prob}\left[\left|\frac{w-2n_1}{w}\right| < \frac{k}{w}\right] \quad n_1 = \text{number of ones in correlation window}$$

$$\text{prob}\left[|w-2n_1| < k\right]$$

$$\text{prob}\left[-k < w - 2n_1 < k\right]$$

$$\text{prob}\left[-w-k < -2n_1 < -w + k\right]$$

$$\text{prob}\left[w - k < 2n_1 < w + k\right]$$

$$\text{prob}\left[\frac{w}{2} - \frac{k}{2} < n_1 < \frac{w}{2} + \frac{k}{2}\right]$$

$$\text{prob}\left[\frac{w}{2} - w\,p - \frac{k}{2} < n_1 - w\,p < \frac{w}{2} - w\,p + \frac{k}{2}\right]$$

$$\text{prob}\left[\frac{w\left(\frac{1}{2} - p\right) - \frac{k}{2}}{\sqrt{w\,p\,q}} < \frac{n_1 - w\,p}{\sqrt{w\,p\,q}} < \frac{w\left(\frac{1}{2} - p\right) + \frac{k}{2}}{\sqrt{w\,p\,q}}\right]$$

$$\sim N\left(\frac{w\left(\frac{1}{2} - p\right) + \frac{k}{2}}{\sqrt{w\,p\,q}}\right) - N\left(\frac{w\left(\frac{1}{2} - p\right) - \frac{k}{2}}{\sqrt{w\,p\,q}}\right) \quad \text{QED} \qquad \text{eq. 1.34}$$

q_s a balanced code we have $p \sim \frac{1}{2}$ and hence

$$\text{prob}\left[|\theta| < \frac{k}{w}\right] \sim N\left(\frac{k}{\sqrt{w}}\right) - N\left(\frac{-k}{\sqrt{w}}\right) \qquad \text{eq. 1.35}$$

1.6.6.1.3 Application of Binomial Model to Gold Code

In this section we apply the binomial model to an unbalanced Gold Code. The number of ones in such a code is given by $\sim 2^{n-1} + 2^{\frac{n-1}{2}}$ where 2^n-1 is the length of the code. Thus, the probability of selecting a one is given by $\sim \frac{1}{2} + \frac{1}{2^{\frac{n+1}{2}}}$. Using the binomial model for the distribution function of the partial correlation function we find

$$\text{prob}[|\theta| > \frac{k}{w}] = 1 - N\left(\frac{\sqrt{w}}{2^{\frac{n-1}{2}}} + \frac{k}{w}\right) + N\left(\frac{\sqrt{w}}{2^{\frac{n-1}{2}}} - \frac{k}{w}\right) \qquad \text{eq. 1.36}$$

Computation: $\text{prob}[|\theta| > \frac{k}{w}]$

$$\sim 1 - N\left(\frac{w\frac{1}{2} - p + \frac{k}{2}}{\sqrt{w\,p\,q}}\right) + N\left(\frac{w\frac{1}{2} - p - \frac{k}{2}}{\sqrt{w\,p\,q}}\right)$$

$$\text{Now } p\,q \sim \left(\frac{1}{2} + \frac{1}{2^{\frac{n+1}{2}}}\right)\left(\frac{1}{2} - \frac{1}{2^{\frac{n+1}{2}}}\right) = \frac{1}{4} - \frac{1}{2^{n+1}} \sim \frac{1}{4}$$

Thus we have:

$$1 - N\left(\frac{\sqrt{w}}{2^{\frac{n-1}{2}}} + \frac{k}{\sqrt{w}}\right) + N\left(\frac{\sqrt{w}}{2^{\frac{n-1}{2}}} - \frac{k}{\sqrt{w}}\right)$$

1.6.6.1.4 Approximate Difference Formula for Balanced and Unbalanced Codes

The difference in the probability distributions of the unbalanced Gold code and a balanced code may be approximated by:

$$\text{prob}\left[|\theta| > \frac{k}{w}\right]_{\text{Gold Code}} - \text{prob}\left[|\theta| > \frac{k}{w}\right]_{\text{Balanced Code}}$$

$$\sim \frac{1}{2^{\frac{n-2}{2}}} \sqrt{\frac{w}{\pi}}\, e^{-\frac{k^2}{w}} \qquad \text{eq. 1.37}$$

Computation: $\text{prob}\left[|\theta| > \frac{k}{w}\right]_{\text{Gold Code}} - \text{prob}\left[|\theta| > \frac{k}{w}\right]_{\text{Balanced Code}}$

$$\left[1 - N\left(\frac{\sqrt{w}}{2^{\frac{n-1}{2}}} + \frac{k}{\sqrt{w}}\right) + N\left(\frac{\sqrt{w}}{2^{\frac{n-1}{2}}} - \frac{k}{\sqrt{w}}\right)\right] - \left[1 - N\left(\frac{k}{\sqrt{w}}\right) + N\left(\frac{-k}{\sqrt{w}}\right)\right]$$

$$\left[N\left(\frac{\sqrt{w}}{2^{\frac{n-1}{2}}} - \frac{k}{\sqrt{w}}\right) - N\,\frac{-k}{\sqrt{w}}\right] - \left[N\left(\frac{\sqrt{w}}{2^{\frac{n-1}{2}}} + \frac{k}{\sqrt{w}}\right) - N\,\frac{k}{\sqrt{w}}\right]$$

$$\left(\frac{\sqrt{w}}{2^{\frac{n-1}{2}}}\right) N'\left(\frac{-k}{\sqrt{w}}\right) + \frac{\sqrt{w}}{2^{\frac{n-1}{2}}}\, N'\left(\frac{k}{\sqrt{w}}\right)$$

$$\frac{2\sqrt{w}}{2^{\frac{n-1}{2}}}\, \frac{1}{\sqrt{2\pi}}\, e^{-\frac{k^2}{w}}$$

$$\frac{1}{2^{\frac{n-2}{2}}} \sqrt{\frac{w}{\pi}}\, e^{-\frac{k^2}{w}}$$

1.6.6.1.5 Moments of Distribution Functions

In this section we derive the second order moments of the unknown distribution function of the partial correlation function of linear codes.

Maximal Linear Codes

We show that the mean and variance for maximal linear sequences are given respectively by the formulas:

$$\bar{\theta} = -\frac{w}{n} \quad \text{and} \quad v(\theta) = w\left[1 - \frac{w-1}{n}\right] - \left[\frac{w}{n}\right]^2 \qquad \text{eq. 1.38}$$

The number of agreements minus the number of disagreements in a correlation window of length w, starting at the nth term of the maximal linear sequence a is given by:

$$\theta_n = \sum_{i=o}^{w-1} a(n+i) \quad \text{where the sequence is represented by } \pm 1\text{'s} \qquad \text{eq. 1.39}$$

averaging this quantity over all starting positions we have

$$\bar{\theta} = \frac{1}{n}\sum_{n=o}^{n-1} \theta_n = \frac{1}{n}\sum_{n=o}^{n-1}\sum_{i=o}^{w-1} a(n+i)$$

$$= \frac{1}{n}\sum_{i=o}^{w-1}\sum_{n=o}^{n-1} a(n+i) \qquad \frac{1}{n}\sum_{i=o}^{w-1}(-1) \cdot \cdot - \frac{w}{n} \qquad \text{eq. 1.40}$$

We next establish the above formula for the variance of θ. The second control moment $\overline{\theta^2}$ of θ_n is given by:

$$\overline{\theta^2} = \frac{1}{n} \sum_{n=o}^{n-1} \theta_n^2 =$$

$$\frac{1}{n} \sum_{n=o}^{n-1} \left[\sum_{i=o}^{w-1} a\,(n+i) \right]^2 \quad \text{using the definition of } \theta_n$$

$$\frac{1}{n} \sum_{n=o}^{n-1} \sum_{i=o}^{w-1} \sum_{j=o}^{w-1} a\,(n+j) \quad \text{by squaring}$$

$$\frac{1}{n} \sum_{n=o}^{n-1} \left[\sum_{i=o}^{w-1} a^2\,(n+i) + \sum_{i \neq j} a\,(n+i)\; a\,(n+j) \right]$$

$$\frac{1}{n} \sum_{n=o}^{n-1} \left[w + \sum_{i \neq j} a\,(n+i)\; a\,(n+j) \right]$$

$$w + \frac{1}{n} \sum_{i \neq j} \sum_{n=o}^{n-1} a\,(n+i)\; a\,(n+j)$$

$$w + \frac{1}{n} \sum_{i \neq j}^{w-1} (-1) \quad \text{Since a is maximal linear sequence.}$$

$$w + \frac{w^2 - w}{n} \cdot w \left[1 - \frac{w-1}{n} \right] \qquad \text{eq. 1.41}$$

The second control moment θ^2 of θ_n is then given by

$$\overline{\theta}^2 = w\left[1 - \frac{w-1}{n}\right] \text{ and} \qquad \text{eq. 1.41}$$

$$v(\theta) = w\left[1 - \frac{w-1}{n}\right] - \left[\frac{w}{n}\right]^2 \qquad \text{eq. 1.42}$$

Gold Codes

We next compute $\overline{\theta}$ and $v(\theta)$ for the family of Gold codes. The averages are taken here over all possible starting positions and over all possible codes. We show that $\overline{\theta} = -\frac{w}{2^{2n}-1}$ where 2^n-1 is the period of the code and that $v(\theta) = w\left[1 - \frac{w-1}{2^{2n}-1}\right] - \left[\frac{w}{2^{2n}-1}\right]^2$ we let $\theta_{n\,m} = \sum_{i=o}^{w-1} a_m(n+i)$. Then

$$\overline{\theta} = \frac{1}{2^{2n}-1} \sum_{m=o}^{2^n} \sum_{n=o}^{2^n-2} \theta_{n\,m} =$$

$$= \frac{1}{2^{2n}-1} \sum_{m=o}^{2^n} \sum_{n=o}^{2^n-2} \sum_{i=o}^{w-1} a_m(n+i)$$

$$= \frac{1}{2^{2n}-1} \sum_{i=o}^{w-1} (-1) = \left[\frac{-w}{2^{2n}-1}\right] \qquad \text{eq. 1.43}$$

The second control moment $\overline{\theta}^2$ of θ taken over all windows of the family of gold codes is given by:

$$\overline{\theta}^2 = \frac{1}{2^{2n}-1} \sum_{m=o}^{2^n} \sum_{n=o}^{2^n-2} (\theta_{n\,m})^2$$

$$= \frac{1}{2^{2n}-1} \sum_{m=o}^{2^n} \sum_{n=o}^{2^n-2} \left[\sum_{i\ o}^{w-1} a_m (n+i) \right]^2$$

$$= \frac{1}{2^{2n}-1} \sum_{m=o}^{2^n} \sum_{n=o}^{2^n-2} \left[\sum_{i=o}^{w-1} a_m^2 (n+i) + \sum_{i \pm j} a_m (n+i)\, a_m (n+j) \right]$$

$$= \left(\frac{1}{2^{2n}-1} \right) \left[(w) \left(2^{2n}-1 \right) + \sum_{i \pm j} \sum_{m=o}^{2^n} \sum_{n=o}^{2^n-2} a_m (n+i)\, a_m (n+j) \right]$$

$$w + \sum_{i \pm j} \sum_{m=o}^{2^n} \theta_m (i-j) \qquad \text{eq. 1.44}$$

We now use the following property of Gold Codes: If we take the autocorrelation sequence of each gold code for a fixed phase shift then the result is the same set of Gold Codes. Thus we have

$$\bar{\theta}^2 = w + \frac{1}{2^{2n}-1} \sum_{i \pm j} (-1)$$

$$w + \frac{w\,(w-1)}{2^{2n}-1}$$

$$= w \left[1 + \frac{w-1}{2^{2n}-1} \right] \qquad \text{eq. 1.45}$$

1.6.6.1.7 Hypergeometric Model for Partial Correlation Function

In this section we use a hypergeometric model for the partial correlation process. The second order statistics of this model are identical with those of the unknown distribution function for maximal linear codes. Hence, this model should give improved performance over that of the binomial model discussed in Section II in the estimation of the partial correlation function. We show below that for the hypergeometric model = E (θ)

$$\overline{\theta} = \left(\frac{w}{n} \cdot n_1 - n_{-1}\right)$$

where n is the sequence period

n_1 is the number of ones in the sequence

n_{-1} is the number of minus ones in the sequence

w is the length of the correlation window.

$$E(\theta) = \overline{\quad}$$

$$E\left[\sum_{j=j}^{w-1} a(i)\right]$$

$$= \sum_{j=o}^{w-1} E(a(i))$$

$$= \sum_{j=o}^{w-1} \left(1\left[\text{prob } a(i) = 1\right] + (-1) \quad \text{prob}\left[a(i) = -1\right]\right)$$

$$\sum_{j=o}^{w-1} \frac{n_1}{n} - \frac{n_{-1}}{n}$$

$$w\left(\frac{n_1 - n_{-1}}{n}\right) = w\ \alpha \quad \text{where } \alpha \left(\frac{n_1 - n_{-1}}{n}\right) \qquad \text{eq. 1.46}$$

We next obtain the formula for variance of θ

$$\text{Var } \theta = w\left(1 - \alpha^2\right)\left(1 - \frac{w-1}{n-1}\right)$$

proof: Var (θ)

$$\text{Var}\left[\sum_{i=o}^{w-1} a\ (i)\right]$$

$$\sum_{i=o}^{w-1} \text{Var } (a\ (i)) + 2 \sum_{\substack{i_1 j \\ i<j}}^{w-1} \left[\overline{a\ (i)\ .\ a\ (j)} - a\ (i)\ .\ \overline{a\ (j)}\right]$$

Now:

$$\text{Var } a\ (i) = a^2\ (i) - \left[\overline{a\ (i)}\right] = 1 - \left[a\ (i)\right]^2 = 1 - \alpha^2$$

Also

$$a\ (i) \times a\ (j) - \text{prob } (a\ (i)\ a\ (j) = 1\ ) - \text{prob}\left[\ a\ (i)\ a\ (j) = -1\ \right]$$

$$\frac{n_1 \cdot n_1 - 1}{(n)\ (n-1)} + \frac{(n_{-1}\ (n_{-1} - 1)}{(n)\ (n-1)} - \frac{2\ n_{-1}\ n_1}{(n)\ (n-1)}$$

$$\frac{(n_1 - n_{-1})^2 - n}{(n)\ (n-1)}$$

$$\frac{n\ \alpha^2 - 1}{n}$$

Thus $V(\theta)$

$$\sum_{i=o}^{w-1} (1 - \alpha^2) \quad + 2 \sum_{\substack{i_1 j=o \\ i<j}}^{w-1} \left(\frac{n\ \alpha^2 - 1}{n-1} \quad - \alpha^2 \right)$$

$$w(1 - \alpha^2) \quad + \quad (w) \quad (w-1) \left(\frac{n\ \alpha^2 - 1}{n-1} \quad - \alpha^2 \right)$$

$$w\ (1 - \alpha^2) \left(1 - \frac{w-1}{n-1} \right) \qquad \text{eq. 1.47}$$

Using these values of mean and variance, the hypergeometric distribution can be approximated by a normal distribution for different values of α determined by the unbalance of the codes used. Specifically we drew that prob $\left[|\theta| < \beta \right] =$

$$N \left(\frac{-\sqrt{w}\,(\alpha - \beta)}{\sqrt{\left(1-\alpha^2\right)\left(1 - \frac{w}{n}\right)}} \right) - N \left(\frac{-\sqrt{w}(\alpha + \beta)}{\sqrt{\left(1-\alpha^2\right)\ 1 - \frac{w}{n}}} \right)$$

$$\text{prob} \left[|\theta| < \beta \right] \qquad \beta > 0$$

$$\text{prob} \left[\left| \frac{w - 2\,n1}{w} \right| < \beta \right] \qquad \theta \text{ defined as } \frac{w - 2\,n\,1}{w}$$

$$\text{prob}\ [-\beta w < w - 2n_1 < \beta w]$$

$$\text{prob}\ [-w - \beta w < -2n_1 < w\beta - w]$$

$$\text{prob}\ [(w - \beta w) < 2n_1 < (w + \beta w)]$$

$$\text{prob}\left[\left(\frac{w}{2} - \frac{\beta w}{2}\right) < n_1 < \left(\frac{w}{2} + \frac{w\beta}{2}\right)\right]$$

$$\text{prob}\left(\frac{w}{2} - \frac{\beta w}{2} - \bar{n}_1\right) < \left(n_1 - \bar{n}_1\right) < \left(\frac{w}{2} + \frac{w\beta}{2} - \bar{n}_1\right)$$

$$\text{prob}\left[\left(-\frac{w\alpha}{2} - \frac{\beta w}{2}\right) < n_1 - \bar{n}_1 < \left(-\frac{w\alpha}{2} + \frac{\beta w}{2}\right)\right] \qquad n_1 = \frac{w}{2}(1+\alpha)$$

$$\text{prob}\left[\left(-\frac{w}{2}\right)(\alpha+\beta) < \left(n_1 - \bar{n}_1\right) < \left(-\frac{w}{2}\right)(\alpha-\beta)\right]$$

Now

$$V(\theta) \sim \frac{\sqrt{w}}{2}\sqrt{1-\alpha^2}\sqrt{1-\left(\frac{w}{n}\right)}$$

$$\text{prob}\ \frac{(-\sqrt{w})(\alpha+\beta)}{\sqrt{\left(1-\alpha^2\right)\left(1-\frac{w}{n}\right)}} < \frac{n_1 - \bar{n}_1}{\sqrt{V(\theta)}} < \frac{-\sqrt{w}(\alpha-\beta)}{\sqrt{\left(1-\alpha^2\right)\left(1-\frac{w}{n}\right)}}$$

$$N\left(\frac{-\sqrt{w}(\alpha-\beta)}{\sqrt{\left(1-\alpha^2\right)\left(1-\frac{w}{n}\right)}}\right) - N\left(\frac{-\sqrt{w}(\alpha+\beta)}{\sqrt{\left(1-\alpha^2\right)\left(1-\frac{w}{n}\right)}}\right) \qquad \text{eq. 1.48}$$

From the preceding math (eq. 1.45) we have arrived at an extremely important result which allows us to predict the performance of PN multiplexing for TDRS at VHF for the unmanned users. With Gold multiplexing of K users through a TDRS (2 MHz bandwidth), we have a single user output (S/N) in the presence of K other users as given by

$$\left(\frac{S}{N}\right)_{\text{ith user}} = \frac{P_u[P.G.]}{\frac{P_u}{2}(K-1)\ 1-\frac{W-1}{N^2}} \qquad \text{eq. 1.49}$$

Where N = code length 2^n-1, P_u user power seen at the satellite, P.G. = processing gain or the ratio of chip rate to bit rate, and w = chip rate X data bit duration. For most TDRS unmanned application $\frac{w-1}{N^2} << 1$.

The effects of thermal noise, multipath, and R.F.I. will be included as we proceed through subsequent sections. The main result obtained in this section is that by using Gold coding (one unique code assigned to each user) we have shown that interference noise seen by one user from the other users (K-1) is

$$\frac{P_u}{2}\ \frac{(K-1)}{P.G.}\ \left[\ 1-\frac{w-1}{N^2}\ \right] \qquad \text{eq. 1.50}$$

This result says that Gold Coding results in 3 dB less noise than would be experienced by a user if the user were interfered with by (K-1) C.W. signals each of power P_u .

1.6.6.2 Repeater Considerations for PN Multiplexing

The data relay satellite must accomodate up to 40 simultaneous users, employing one of the multiplexing schemes discussed in 1.6.6.1. The data relay satellite is assumed to be a linear repeater having an average power limitation; in other words, a slow-acting automatic gain control is assumed for the repeater and this gain control maintains the linear operation of the repeater.

Assuming that the up-link power for each user is given by P_u measured at the satellite, then the amount of power measured at the ground station which is available to the i^{th} user is given by $P_i = P_{sat}\left(\frac{P_u}{P_{tot}}\right)$ where P_{sat} is the total satellite power measured at the ground station and $P_{tot}=KP_u + W_sN_u + I$, where

I = total interference
W_s = repeater bandwidth
N_u = uplink noise
K = # of users

} measured at the input to the TDRS satellite

If the PN signal occupies the entire bandwidth (W_s) of the repeater, then the output signal to noise for the i^{th} receiver at the ground station is given by the following equation

$$\left(\frac{S}{N}\right)_{ith} = \frac{(\text{Proc. Gain})\, P_{sat}\, (P_u/P_{tot})}{W_sN_r + P_{sat}(1 - P_u/P_{tot})} \qquad \text{eq. 1.51}$$

N_r = noise density at GS

$\left(\frac{S}{N}\right)_{ith} \simeq P.G.(P_u/P_{tot})$ for a noiseless TDRS to GS link

The above equation should be modified when the PN signals entering the data relay satellite are frequency division multiplex in contiguous bands or in frequency bands where interference does not exist. Under these assumptions, the above equation becomes:

$$\left(\frac{S}{N}\right)_{ith} = \frac{P_u P.G.'}{N_u W' + P_u} \quad \text{TDRS to GS noiseless} \qquad \text{eq. 1.52}$$

Where P.G.' is the processing gain of the PN/FDM system W' is the spread bandwidth of one of the PN/FDM signals.

1.6.6.3 PN Correlation Receiver Output in the Presence of Multipath

Since much of the analysis to follow depends upon an accurate knowledge of the output noise components of a correlation system, we will spend a few moments discussion these noise components.

The input to a correlation receiver of the type used in a PN system can consist of a variety of interference sources. These include Gaussian background noise, unintentional interference from earth located sources, as well as self noise or multipath generated from reflected signals off the earth's surface.

We will consider for the purpose of analysis that the output of a correlation receiver, having some processing gain (PG) or an equivalent time bandwidth product TW, in response to Gaussian noise and uncorrelated

interference is essentially Gaussian, or in other words, the input noise and interference is suppressed by the P.G. of the receiver and this amount of noise represents the Gaussian noise which contributes to the degradation of the system.

In addition to the Gaussian noise, multipath can produce non-Gaussian noise at the output of the correlator. For example, if the multipath signal is essentially specular and the differential time delay between the direct and the indirect signal path is less than the duration of PN chip, the output of the correlation receiver will consist of two components one of which is Gaussian and the other is non-Gaussian. That portion of the reflected signal which is within the time correlation aperture (PN chip duration) will produce a randomly phased component which can be represented as a constant envelope term whose power is proportional to the square of the correlation coefficient between paths times the power in the reflected path. That portion of the reflected signal which remains outside the correlation aperture produces essentially Gaussian noise which is suppressed by the P.G. of the receiver and this noise can be added directly to the Gaussian noise resulting from ambient noise and interference.

Since a differential Doppler between the direct and indirect path exists for the user to TDRS link, the postulation that the non-Gaussian component at the output of the correlation receiver will be a randomly phased constant envelope component for the specular reflection is reinforced.

When the reflection from the earth's surface is completely diffuse and the differential time delay between the direct and indirect path is less

than the correlation aperture (PN chip duration), the output components of a correlation receiver will be all Gaussian. The ambient noise and interference will be reduced by the P.G. of the receiver as will the Gaussian noise produced by the reflected signal which lies outside the correlation aperture. That portion of the reflected signal which lies inside the correlation aperture will produce a Gaussian noise component whose power is proportional to the square of the correlation coefficient between the direct and indirect signal paths times the amount of power in the indirect path and this term will not be diminished by the P.G. of the receiver.

1.6.6.4 The Effects of Multipath on PN Systems

When we consider the indirect path to be a perfect reflection, we are able to approach a reasonably accurate solution to the degradations imposed on PN systems by multipath.

For the purpose of analysis let us assume that the data is PSK* and that the system is a four-phase PN coded system. The amount of noise power which will be found in the post-correlation filter is given by the following terms.

$$\text{Noise in Post correlation filter} = \underbrace{\frac{N_{in}}{P.G.} + \frac{(1-\rho^2)S_{ind}}{P.G.}}_{\sigma^2} + \overbrace{\rho^2 S_{ind}}^{\text{C.W. term}} \qquad \text{eq. 1.53}$$

σ^2 = Gaussian noise term

S_{ind} is the power in the indirect path

* as stated previously, the ΔPSK signal is the more practical approach and the bit error probability for ΔPSK = $2P_{PSK}(1-P_{PSK})$ where P_{PSK} is the error probability for coherent PSK

The noise power is seen to consist of the ambient Gaussian noise reduced by the processing gain plus a Gaussian noise resulting from partial decorrelation with the reflected path diminished by the processing gain and finally a constant envelope term which represents the partial correlation of the direct and indirect path. The factor ρ is a number which lies between 0 and 1 and the amount of energy in the indirect path is a function of polarization, ground conductivity, grazing angle, etc.

After a few algebraic manipulations a conditional binary error probability is obtained with the following form.

$$P_\varepsilon(\theta) = \frac{1}{2}\,\mathrm{erfc}\left[\frac{\sqrt{2S_d}}{\sqrt{2\sigma}}\left(1 + \frac{\rho\sqrt{2S_{ind}}}{\sqrt{2S_d}}\left|\frac{\sin\Delta\omega\frac{T}{2}}{\Delta\omega\frac{T}{2}}\right|\cos\phi\right)\right] \qquad \text{eq. 1.54}$$

$\phi=\theta - \frac{\Delta\omega T}{2}$, θ is a random phase angle

$\sqrt{2S_d}$ = signal strength of the direct path

$\sqrt{2S_{ind}}$ = signal strength of the indirect path

T = duration of the binary symbol

$\Delta\omega$ = differential Doppler radian frequency

Under the assumption that the phase angle associated with the specular multipath interference is a random variable we are free to determine the average binary error probability by averaging the conditional density over a uniform density in phase. This results in

$$\overline{P}_\varepsilon = \frac{1}{2\pi}\int_{-\pi}^{\pi}\frac{1}{2}\,\mathrm{erfc}\left[\sqrt{\frac{S_d}{\sigma^2}}\,(1+\zeta\cos\phi)\right]d\phi \qquad \text{eq. 1.55}$$

The average bit error probability vs ρ is illustrated in Figure 1.17, under the assumption that the direct and indirect signal path ratio is unity, the input signal to Gaussian noise is unity, and the P.G. is 12 dB. Note that the Gaussian noise power from the interfering path changes as a function of ρ, that is, the Gaussian noise contribution resulting from partial correlation approaches zero as correlation improves, whereas the constant envelope interference component increases as the correlation between direct and indirect path increases. Keep in mind that ζ is the product of the ratio of direct and indirect signal strength times the path correlation coefficient ρ.

At the other extreme the multipath signal is completely diffuse, and to evaluate its effects on a PN system we assume that the diffuse reflected energy can be broken down into discrete paths. Each path is assumed to fade according to a Rayleigh amplitude statistic and each path will be uncorrelated.

The total time spread in the indirect path is assumed either equal to the duration of 1 PN chip or the time spread is assumed to be much greater than the duration of 1 chip. Furthermore, it is assumed that the paths comprising the total indirect path contains equal power and that the sum of the powers associated with the separate paths equal the total power contained in the reflected signal. With these assumptions it is possible to determine the performance of a PN system in diffuse multipath interference.

Case 1 - The time spread in the indirect path is assumed to be such that confined to the original correlation function of the PN sequence and the

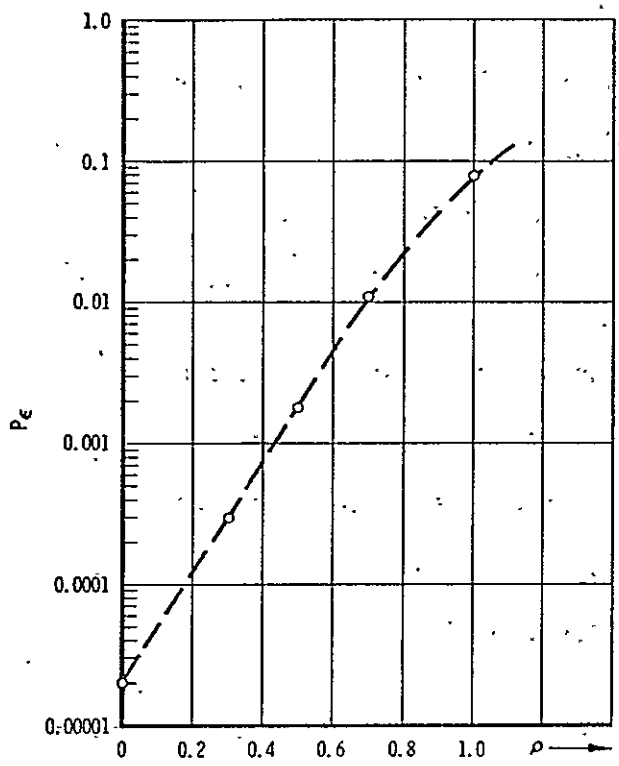

Fig. 1.17

BIT ERROR PROBABILITY VS ρ FOR P.G. = 12 dB,

$\frac{S_d}{S_{ind}} = 1$

indirect signal is diffuse. Under these circumstances the amount of noise power produced at the correlator output and seen by a detector (PSK) is given by eq. 1.56 .

$$\text{Noise Total} = \underbrace{\frac{Nin}{P.G.} + \frac{(1-\rho^2)S_{ind}}{P.G.}}_{\text{all Gaussian noise terms}} + \rho^2 S_{ind} \qquad \text{eq. 1.56}$$

ρ = degree of correlation or signal overlap, $0 \leq \rho \leq 1$

S_{ind} = amount of power in the indirect path

We see that as the indirect and the direct path becomes more correlated, the amount of noise power which confronts a binary decision increases as the square of the correlation coefficient and the noise will be essentially Gaussian since the diffuse path is fading according to a Rayleigh statistic. The amount of interference due to the reflected energy associated with the indirect path which remains uncorrelated is suppressed by P.G. of the system as is the input noise which is always associated with the system. The post-correlation or predetection signal-to-noise ratio, therefore, will in effect approach 0 dB when the correlation coefficient is 1 and the direct and indirect paths are equal.

The resulting binary error probability (PSK) is given by

$$P_\varepsilon = \frac{1}{2}\,\text{erfc}\sqrt{\frac{S_{direct}}{\frac{Nin}{P.G.} + \frac{(1-\rho^2)S_{ind}}{P.G.} + \rho^2 S_{ind}}} \qquad \text{eq. 1.57}$$

diffuse (no time spreading)

Case II - Now let us assume that the multipath signal is time spread such that the total reflected signal is distributed over a spread in time which is large compared with the correlation aperture (chip duration) δ of the binary sequence. We can expect that a fraction of the reflected power will be contributed directly to the Gaussian noise in the receiver, the rest will remain uncorrelated and suppressed by P.G. Thus, as a function of the correlation coefficient we have noise terms which have the following form.

$$N_{total} = \frac{Nin}{P.G.} + \frac{\left(1-\rho^2\frac{\delta}{T}\right)S_{ind}}{P.G.} + \rho^2 S_{ind}\left(\frac{\delta}{T_{spread}}\right) \qquad \text{eq. I.58}$$

Without further formalism we can state that time spreading in the multipath signal is a benefit since time spreading forces more energy outside the correlation aperture and therefore this energy is subject to suppression by the P.G.

Perhaps we have over analyzed the effects of multipath for the PN system for the TDRS application, in that the multipath signal delay relative to the direct path signal is between .2 msec and 10 msec. The minimum differential delay of .2 msec however establishes the lower bound on the required chip rate for a PN system so as to avoid rapid degradations resulting from correlated noise in the receiver when the user satellite is at its lowest orbital altitude. When the user is in the launch phase of the mission very short differential time delays can be expected $\sim$ 20 usec requiring at least 40-50 kilochip/sec PN rates.

When the chip rate is in excess of 40-50 kilochips/sec then a users signal and multipath can be considered uncorrelated since the minimum signal delay for launch is 20 usec. When large processing gain are employed the differential Doppler etc. are of no concern and the PSK error probabilities given in 1.54 and 1.57 are identical, i.e.,

$$P_{\epsilon_{PSK}} = \frac{1}{2} \operatorname{erfc} \sqrt{\frac{S_{direct}(P.G.)}{(Nin + S_{indirect})}} \qquad \text{eq. 1.59}$$

Equation 1.59 is an exact equation for the performance of an optimum PSK/PN signal in noise and its own multipath. The more practical ΔPSK error probability is approximately $2P_{\epsilon_{PSK}}$. It is evident that if P.G. is sufficiently large P_{ϵ} can be made quite small.

Before we can compare the PN/FDM system with the PN system which uses the entire TDRS repeater bandwidth (or a large portion such as the JPL approach, i.e., chip rates 400 K chips/sec) we must determine the maximum P.G. obtainable through the 2 MHz TDRS channel.

1.6.6.5 Determination of the Maximum Processing Gain Obtainable through the DRSS 2 MHz Band-Limited Repeater

It is of interest to determine, for a fixed 1 kilobit data rate, the maximum processing gain that can be expected through the user to ground station 2 megacycle band-limited channel. In the analysis that follows we consider this channel as a 2 MHz rectangular filter. This assumption is justified since restrictive filters must be utilized to remove interference sources which are immediately adjacent to the 136 and 138 MHz band. The solution to the problem is obtained by determining the optimum chip rate for the 2 megacycle band-limited channel which in turn provides the maximum available processing gain. As mentioned above, the data rate is assumed to be 1 kilobit per second and the PN carrier will be located in the center of the 2 MHz bandwidth channel, i.e., 137 MHz.

The system model is illustrated in Figure 1.18 of this section and the mathematics required to determine the correlation function at the output of the receiver described by Figure 1.18 follows. It should be pointed out that a reference filter is employed in the receiver in order to maximize the processing gain. This is done because match filter receivers require references which are identical to the signal applied to the receiver and since the PN signal has been processed through the band-limited channel then the reference in the receiver should be identically band limited.

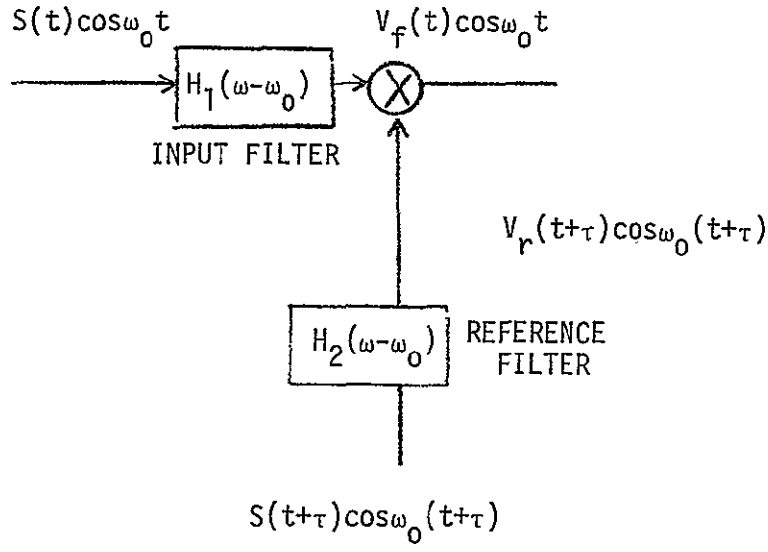

Figure 1.18 System Model

The cross correlation function can be determined by using an equivalent low pass model for analysis then using the shifting theorem to yield the results for the bandpass case. The signal due to the pseudorandom modulation can be represented by the inverse Fourier transform of its amplitude spectral density function.

$$s(t) = \frac{1}{2\pi} \int_{-\infty}^{\infty} S(\omega)\, e^{j\omega t} d\omega \qquad \text{eq. 1.60}$$

The signal at the output of the input filter is

$$v_f(t) = \frac{1}{2\pi} \int_{-\infty}^{\infty} H_1(\omega) S(\omega)\, e^{j\omega t} d\omega \qquad \text{eq. 1.61}$$

In the same manner the output of the reference filter is

$$v_r(t) = \frac{1}{2\pi} \int_{-\infty}^{\infty} H_2(\omega) S(\omega)\, e^{j\omega t} d\omega \qquad \text{eq. 1.62}$$

Their cross-correlation function is,

$$R_{fr}(\tau) = \overline{v_f(t)v_r(t+\tau)}$$

$$= \lim_{T\to\infty} \frac{1}{2T} \int_{-T}^{T} v_f(t)v_r(t+\tau)dt \qquad \text{eq. 1.63}$$

$$= \lim_{T\to\infty} \frac{1}{2T} \int_{-T}^{T} \frac{1}{(2\pi)^2} \left[\int_{-\infty}^{\infty} S(\omega)H_1(\omega)e^{j\omega t}d\omega\right]$$

$$\cdot\left[\int_{-\infty}^{\infty} S(\rho)H_2(\rho)e^{j\rho(t+\tau)}d\rho\right] dt \qquad \text{eq. 1.64}$$

$$R_{fr}(\tau) = \lim_{T\to\infty} \frac{1}{2\pi} \left[\int_{-\infty}^{\infty}\int_{\infty}^{\infty} S(\omega)S(\rho)H_1(\omega)H_2(\rho)e^{j\rho\tau}d\omega d\rho\right]$$

$$\left[\frac{1}{2\pi 2T} \int_{-T}^{T} e^{j(\omega+\rho)t}dt\right]$$

but $$\frac{1}{2\pi 2T} \int_{-T}^{T} e^{j(\omega+\rho)t}dt \longrightarrow \delta(\omega+\rho).$$

then $$R_{fr}(\tau) = \frac{1}{2\pi} \int_{-\infty}^{\infty}\int_{-\infty}^{\infty} S(\omega)S(\rho)H_1(\omega)H_2(\rho)\delta(\omega+\rho)e^{j\rho\tau}d\rho\, d\omega$$

$$= \frac{1}{2\pi} \int_{-\infty}^{\infty} S(\omega)S(-\omega)H_1(\omega)H_2(-\omega)e^{j\omega\tau}d\omega \qquad \text{eq. 1.65}$$

Since the reference filter, $H_2(\omega)$, and the amplitude spectrum, $S(\omega)$, are symmetrical, the above equation becomes

$$R_{fr}(\tau) = \frac{1}{2\pi} \int_{-\infty}^{\infty} S(\omega)S^*(\omega)H_1(\omega)H_2{}^*(\omega)e^{j\omega\tau}d\omega \qquad \text{eq. 1.66}$$

It can be shown by use of the shifting theorem that for the bandpass system

$$R_{fr}(\tau) = 2\pi \int_{-\infty}^{\infty} S(\omega)S^*(\omega)H_1(\omega)H_2^*(\omega)e^{j(\omega+\omega_0)\tau}d\omega \qquad \text{eq. 1.67}$$

The cross correlation function can be determined from equation 1.65 assuming rectangular filters for $H_1(\omega)$ and $H_2(\omega)$.

$$H_1(\omega) = 1, \ \omega \leq \omega_1$$
$$= 0 \text{ elsewhere}$$
$$H_2(\omega) = 1, \ \omega \leq \omega_1$$
$$= 0 \text{ elsewhere}$$

The power spectral density of a pseudorandom signal is

$$S(\omega)S^*(\omega) = T\left(\frac{\sin\omega T/2}{\omega T/2}\right)^2$$

where T = chip width $\qquad$ eq. 1.68

Deleting for now the $\cos\omega_0\tau$ term, the cross correlation is

$$R_{fr}(\tau) = \frac{1}{2\pi}\int_{-\omega_1}^{\omega_1} T\left(\frac{\sin\omega T/2}{\omega T/2}\right)^2 e^{j\omega\tau}d\omega$$

$$= \frac{2}{\pi}\int_{-\omega_1}^{\omega_1} T\left(\frac{\sin\omega T/2}{\omega T}\right)^2 e^{j\omega\tau}d\omega$$

Since the $\left(\frac{\sin x}{x}\right)^2$ is an even function the integral becomes

$$R_{fr}(\tau) = \frac{4}{\pi}\int_{0}^{\omega_1} T\left(\frac{\sin\omega T/2}{\omega T}\right)^2 \cos\omega\tau d\omega$$

$$= \frac{4}{\pi} \int_0^{\omega_1 T} \left(\frac{\sin \omega T/2}{\omega T}\right)^2 \cos \omega\tau \, d\omega T$$

$$= \frac{2}{\pi} \int_0^{\omega_1 T} \frac{\cos\omega\tau - \frac{1}{2}\cos\omega(T+\tau) - \frac{1}{2}\cos(T-\tau)\, d\omega T}{(\omega T)^2}$$

integrating by parts yields

$$R_{fr}(\tau) = \frac{2}{\pi} \frac{\cos\omega_1\tau}{\omega_1 T} + \frac{1}{\pi} \frac{\cos\omega_1(T+\tau)}{\omega_1 T}$$

$$+ \frac{1}{\pi} \frac{\cos\omega_1(T-\tau)}{\omega_1 T} - \frac{2}{\pi} \frac{\tau}{T} \int_0^{\omega_1\tau} \frac{\sin x \, dx}{x}$$

$$+ \frac{T+\tau}{\pi T} \int_0^{\omega_1(T+\tau)} \frac{\sin}{x} x \, dx + \frac{T-\tau}{\pi T} \int_0^{\omega_1(T-\tau)} \frac{\sin x}{x} \, dx$$

$$R_{fr}(\tau) = -\frac{2}{\pi} \frac{\cos\omega_1\tau}{\omega_1 T} + \frac{1}{\pi} \frac{\cos\omega_1(T+\tau)}{\omega_1 T} + \frac{1}{\pi} \frac{\cos\omega_1(T-\tau)}{\omega_1 T}$$

$$- \frac{2\tau}{\pi T} \, Si(\omega_1\tau) + \frac{T+\tau}{\pi T} \, Si\left[\omega_1(T+\tau)\right]$$

$$= \frac{T-\tau}{\pi T} \, Si\left[\omega_1(T-\tau)\right] \qquad \text{eq. 1.69}$$

The cross correlation function was plotted versus the delay τ. The PN chip width is normalized to one

$$T = 1$$

$$\alpha = \frac{\omega_1 T}{2\pi}$$

$$= \frac{\omega_1}{2\pi}$$

which defines the portion of the PN power spectrum which is filtered. As an example with α=1, the power between the first nulls of $\frac{\sin^2 x}{x^2}$ is passed.

In Figure 1.19 we have plotted the receiver cross-correlation function for various values of α. At $\tau=0$, the maximum processing gain is $R_{fr}(0)$.

The above analysis has served to determine the maximum P.G. for a band-limited PN system. The peak of the cross-correlation function for $\tau=0$ represents the reduction in the processing gain for a PN system, thus a plot of this reduction vs the ratio of the chip rate to 2 MHz represents the amount of band-limited loss to PN system for the TDRS channel. This is shown in Figure 1.20. Also shown in Figure 1.21 is a plot of the maximum processing gain that one can expect using a PN system through the 2 MHz band-limited TDRS user to ground terminal channel. This is based upon a comparison between the infinite bandwidth channel and the 2 MHz channel. It is seen that a chip rate of approximately 2 megachips will realize a theoretical maximum usable processing gain of 32 dB when a 1 kilobit per second data rate is utilized. Chip rates in excess of 2 MHz do not provide any increase in processing gain. Chip rates below this factor reduce the available processing gain.

1.6.6.6 Comparison of PN Multiplexing Techniques

In section 1.6.6.5 we obtained a theoretical maximum P.G. for a PN system which uses the entire TDRS 2 MHz repeater bandwidth. The theoretical maximum P.G. is 32 dB for a 1 kilobit/sec user data rate.

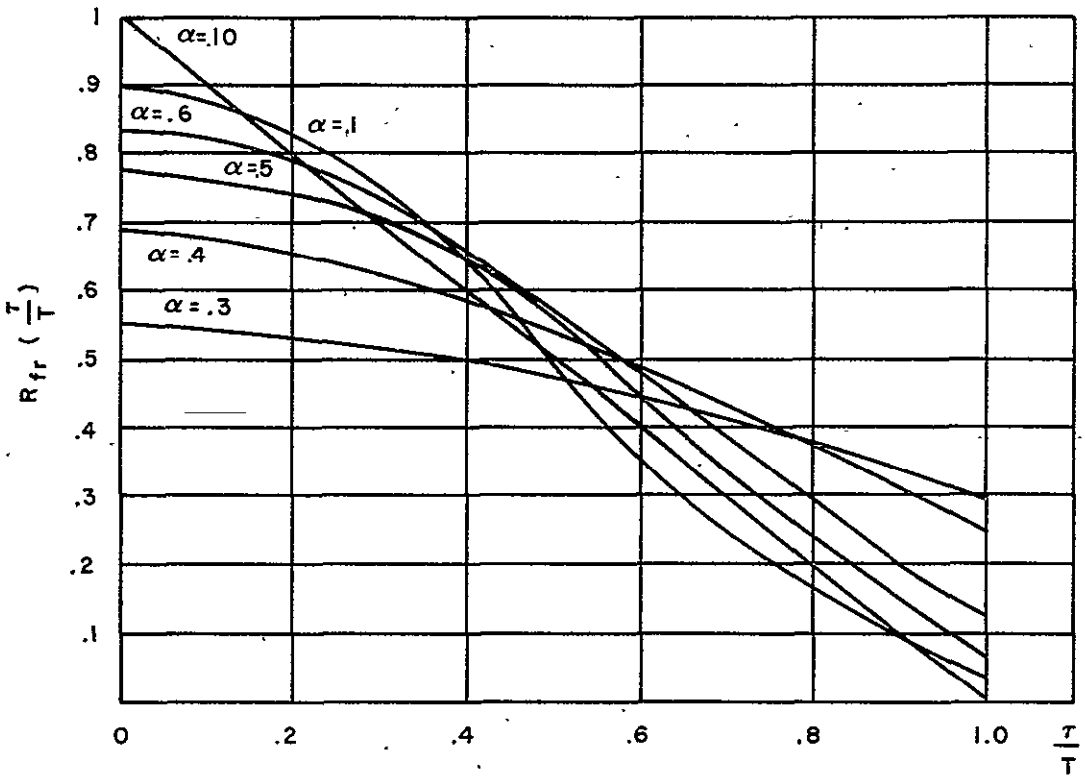

Fig. 1.19 CROSS CORRELATION FUNCTION

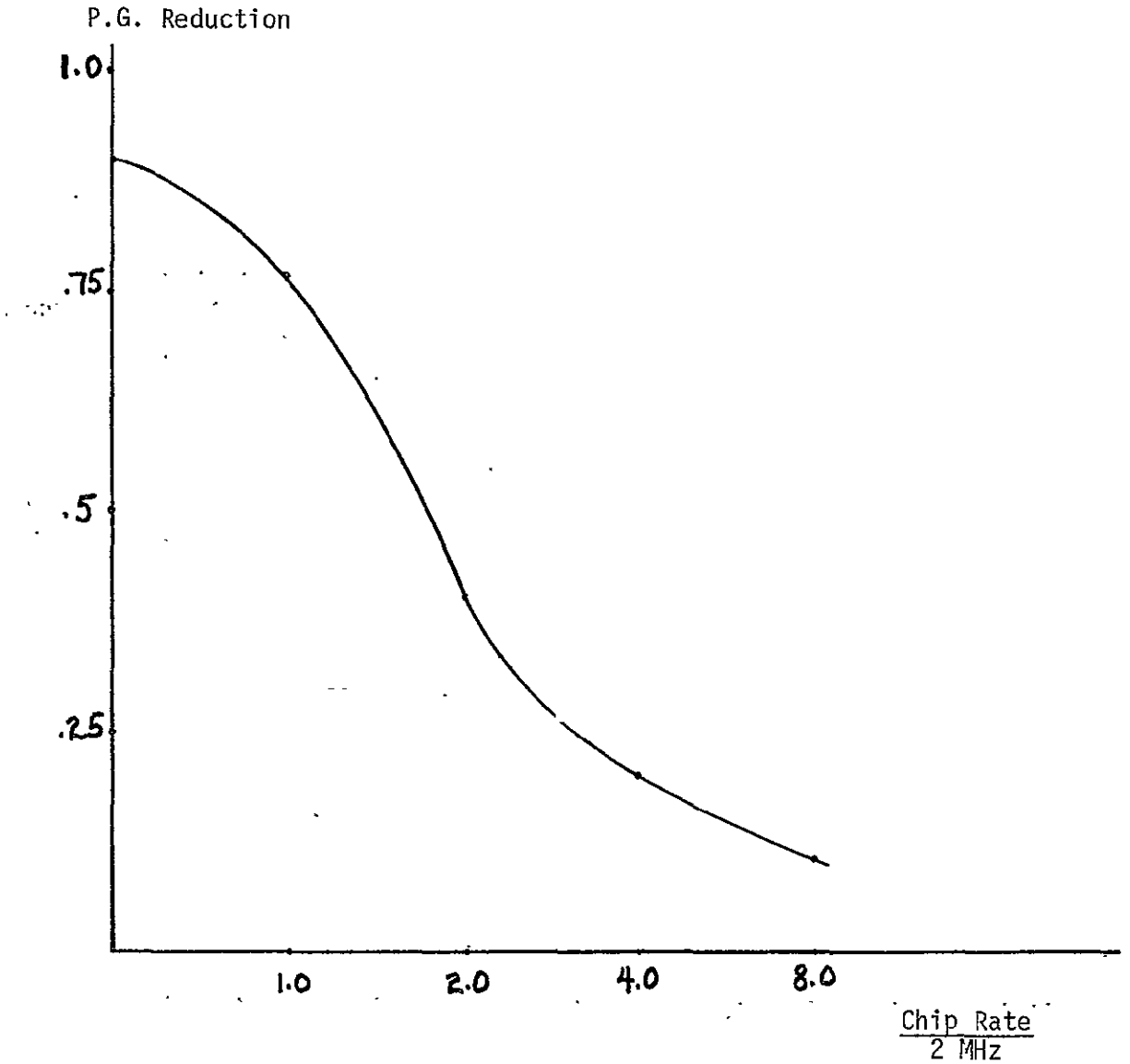

Fig. 1.20 PROCESSING GAIN REDUCTION FACTOR VS $\frac{\text{Chip Rate}}{2\ \text{MHz}}$

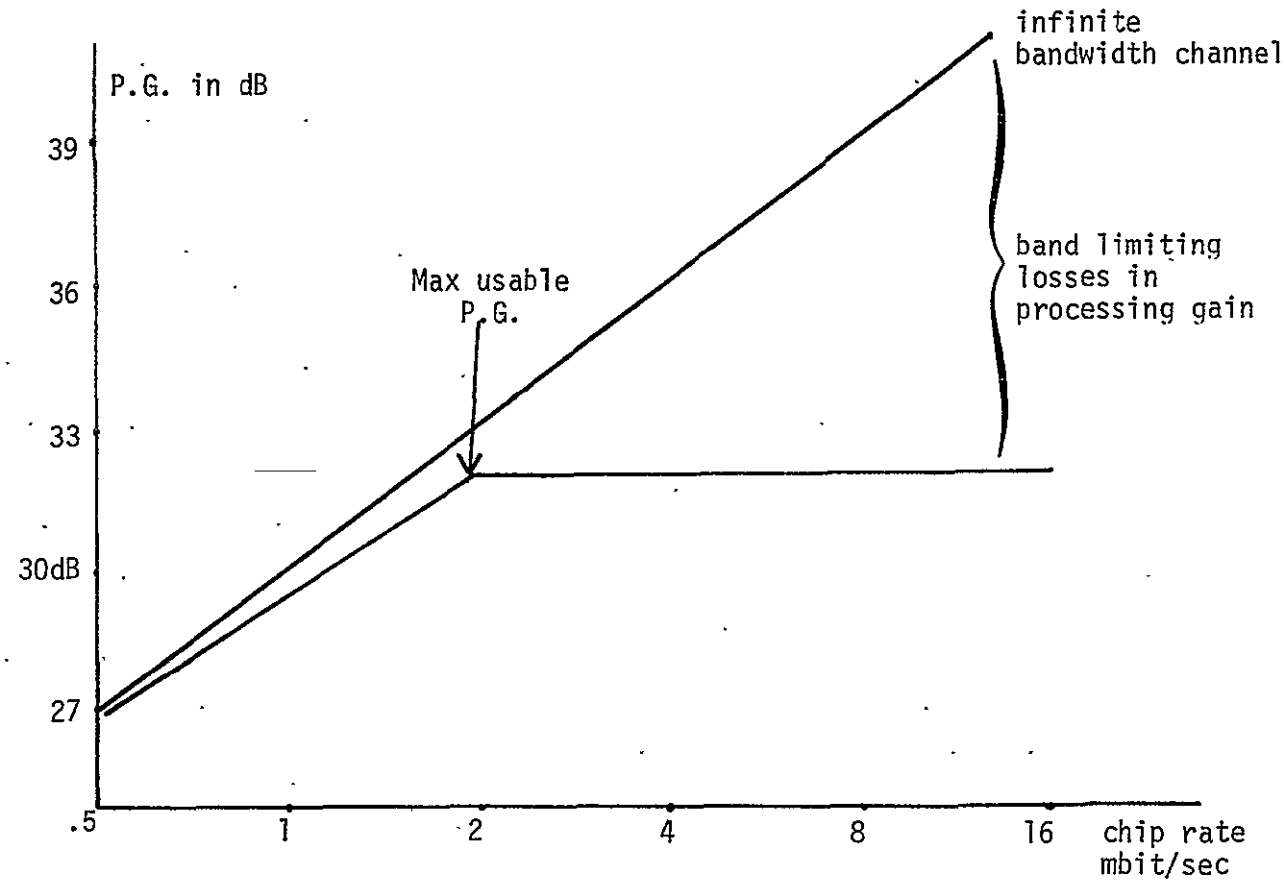

Fig. 1.21 P.G. VS CHIP RATE FOR FIXED RF CHANNEL 2 MHz
DATA RATE 1KB/SEC

In this section we compare the performance of the multiplexing PN techniques put forth in section 1.6.6.5. For purpose of analysis we assume that the wideband system can attain the 32 dB processing gain and that the chip rate for the narrowband channelized PN system is 40 Kchip/sec and the carriers are spaced by 50 KHz to avoid Doppler overlap. Thus each narrowband PN signal has a processing gain of 15 dB. We assume that each user can radiate .5, 1, 2, 4, or 8 watts. The receiver (TDRS) is assumed to have an operating temperature of 1200°K. In Table 1.7 the link parameters are summarized. Forty users are assumed with each user's multipath equal to his signal power. The user's multipath signals are noise like and can be added directly to the gaussian noise at the repeater. The additional noise resulting from the other 39 users direct path signals, however, has been shown to produce a noise at the output of the ith user's correlation receiver of approximately $\sim \frac{P_u}{2}(K-1)$ when the users employ Gold codes.

Thus the wideband PN system performance is governed by

$$\left(\frac{S}{N}\right)_{WBPN} = \frac{P_u\ P.G.}{N_u + P_u K + \frac{P_u}{2}(K-1)} \sim \frac{P_u\ P.G.}{N_u + \frac{3}{2} P_u K} \qquad \text{eq. 1.70}$$

N_u input noise to the satellite and K is the number of user. The narrowband PN system is confronted by its own multipath and ambient noise N_u' but no other users and no other user's multipath, thus

$$\left(\frac{S}{N}\right)_{NBPN} = \left(\frac{P_u\ P.G.'}{P_u + N_u'}\right) \qquad \text{eq. 1.71}$$

The wideband and narrowband PN systems performance under worst case multipath and noise are summarized in Table 1.7(c).

Table 1.7(a) Wideband PN Parameters

Received Signal at TDRS (one user)	Power (watts)	Noise (2 mc)	Users + Multipath
-124 dbm	.5	-105 dbm	-106 dbm
-121 dbm	1	-105 dbm	-103 dbm
-118 dbm	2	-105 dbm	-100 dbm
-115 dbm	4	-105 dbm	- 97 dbm
-112 dbm	8	-105 dbm	- 94 dbm

Table 1.7(b) Narrowband PN Parameters

Received Signal at TDRS (one user)	User Power (Watts)	Noise (40 KHz)	Multipath
-124 dbm	.5	-122 dbm	-124 dbm
-121 dbm	1	-122 dbm	-121 dbm
-118 dbm	2	-122 dbm	-118 dbm
-115 dbm	4	-122 dbm	-115 dbm
-112 dbm	8	-122 dbm	-112 dbm

Table 1.7(c) Wide PN vs Narrowband PN Performance

Power (watts)	(S/N_0)WBPN dB	(S/N_0)NBPN dB
.5	9.5	$\sim$11
1	11.5	12.5
2	12.5	13.75
4	13	14.5
8	13.5	$\sim$14.75

Table 1.7(c) indicates that both systems operate equally well for a user output power >1 watt. Furthermore, both systems rapidly become user limited for P_t>1 watt. The wideband system appears to operate with .5 watts for each user with no system margin. If a 10 dB margin is included, then both systems will perform well if the P_t = 5 watts. Correspondingly, if a system margin of 6 dB is required, then the user power is only 2 watts.

If user spacecraft output power cannot exceed 1 watt for practical reasons, then a $P_\varepsilon = 10^{-5}$ can still be obtained if convolutional encoding and sequential decoding are employed. The encoder is extremely simple (several IC's) and Magnavox can now fabricate the complete sequential decoder, at the G.S., on two 4"×6" PC boards using T^2L logic. The benefits which can be achieved by forward error control are discussed in a later section of this report, but as an example of these benefits the wideband PN user power can be further reduced in the above table to .8 watts while maintaining 6 dB system margin if forward error control is used.

It would appear from the above comparison that wideband PN multiplex using Gold codes with good cross-correlation properties will support 40 TDRS users and that a user power level between .8 to 5 watts will provide 6 to 10 dB of system margin depending on whether or not forward error control is employed. The narrowband PN/FDM technique will also work at the above power level and all users can use the same PN code and are identified by their carrier frequencies.

The JPL multiplexing scheme uses wideband PN with each user carrier separate by 10 KHz. All users use the same PN code at a rate of 40 Kchips/sec.

The JPL processing gain is 6 dB less than the theoretical maximum and in our opinion the JPL chip rates could easily be increased 1 mchip/sec. At this increased chip rate and the addition of forward error control, the JPL system should operate in a manner comparable to the PN systems compared above. A higher chip rate for the JPL system than the one now contemplated make both wideband PN techniques attractive. The narrowband PN system on the other hand is susceptible to interference and is subject to degradations resulting in variations in the user's antenna pattern. Thus the choice of approach to the TDRS problem now seems to hinge on interference effects and overall ranging performance requirements.

1.6.7 Programmed and Adaptive Antimultipath Systems

The objective of this section is to analyze various multiple access techniques which completely avoid the multipath and to determine the bandwidth, data rate, and data storage requirements necessary for their implementation. The techniques presented herein will be of the following generic types:

- Pre-programmed - whereby user satellite timing and data rates are preset to a fixed value prior to launch to compensate for the maximum and minimum differential time delays imposed by the selected satellite orbital altitude.
- Adaptive - having the user satellite timing and data rates controlled remotely by the ground station. The framing intervals, storage, etc., are continuously adjusted in accordance with the satellite's position relative to the DRSS, thereby providing for an optimal level of signal energy.

The modes of signal transmission under consideration will be Time Hop (TH), Frequency Hop (FH), and Time Hop/Frequency Hop (TH/FH). Such transmission will be constrained by a multipath signal delay ranging from 0.2 msec to 10 msec for circular orbital heights of 100 mi to 1000 mi respectively and grazing angles of 16° to 90°; furthermore, the presence of a differential Doppler of 0 to 2 KHz, a direct path Doppler of 0 to 3.75 KHz, and a fading bandwidth of 0 Hz to 2 KHz, must be taken into consideration, and an average data rate of 1 kb/s must be maintained; in addition, crystal oscillator stability of 1×10^{-7} shall be assumed in all calculations. In the sections that follow, the various accessing techniques will be evaluated in light of the aforementioned constraints and performance requirements. For the purpose of this report it will be assumed that system synchronization has been established; those systems employing the "pre-programmed" mode of

transmission will be analyzed only in a "worst case" sense. It should be noted that the 136-138 MHz link is treated exclusively. In addition, synchronization and tracking, and hardware limitations will not be discussed here but will be deferred to a later section.

1.6.7.1 Programmed Time Hop

For a time hopping system to achieve an average data rate of 1 kb/s while providing multipath protection for a .2 to 10 msec duration, the following data format might be imposed. For the 100 mi orbit with multipath delays on the order of 200 μsec to 1 msec, the system is permitted to transmit for 200 μsec and then is "quiet" for 1 msec. Referring to Figures 1.22 and 1.23, it can be seen that to maintain the required data rate, two pulses must be sent during a 200 μsec time interval which is followed by 1.8 msec of no transmission, then two more pulses and the same process is repeated. If it is assumed that the maximum duration of each pulse is 100 μsec the minimum transmission bandwidth required for one user is 10 KHz. Allowing 4 KHz for direct path Doppler and 2 KHz for fading per user, the bandwidth needed for 20 users (assuming they are all in a 100 mi orbit) is a minimum of 320 KHz (likewise, a 640 KHz bandwidth is needed for 40 users).

The "worst case" condition for TH transmission occurs when the user satellite is at the 1000 mi altitude. Differential time delays arising from such an orbit range from 1 to 10 msec (grazing angle 16° to 90°). To maintain an average data rate of 1 kb/s the user must transmit 12 bits of data in 1 msec.

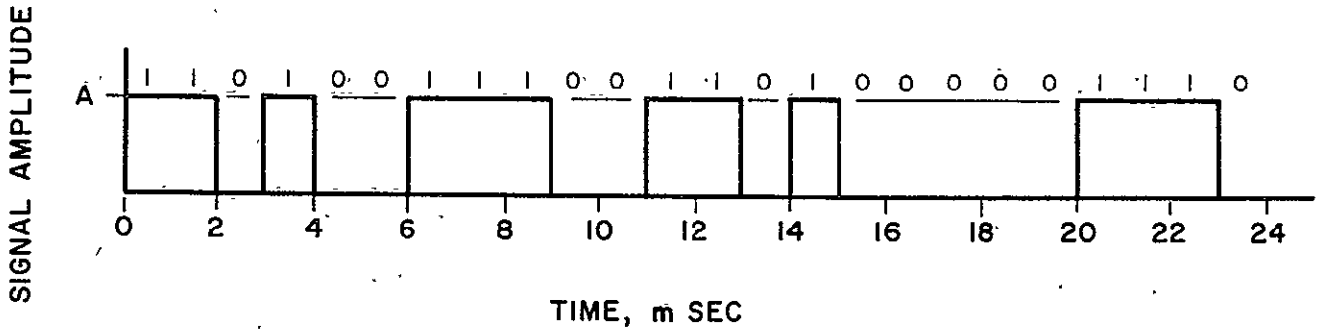

Fig. 1.22 TYPICAL BINARY SEQUENCE

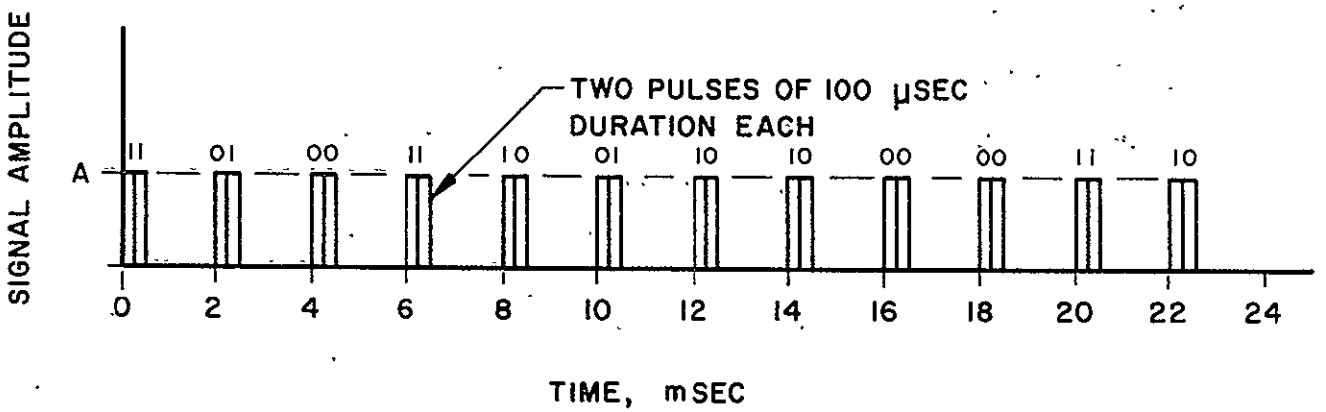

Fig. 1.23 PRE-PROGRAMMED TH FOR A 100 MI CIRCULAR ORBIT

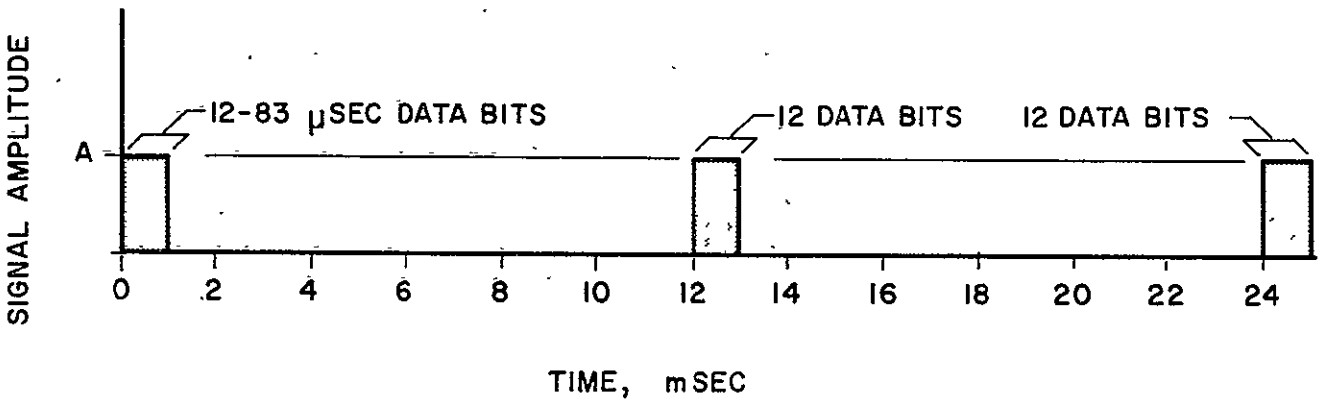

Fig. 1.24 PRE-PROGRAMMED TH FOR A 1000 MI CIRCULAR ORBIT

As an illustrative example of the technique consider the diagram of Figure 1.24 in which twelve bits of binary information are transmitted during a 1 msec interval and repeated again every 12 msec. Each data bit is 83.5 μsec in length and the resulting signal bandwidth is 12 KHz per user. Allowing for a 3 KHz direct Doppler per user and 2 KHz each for differential Doppler and fading the total repeater bandwidth required for 20 users (in a 1000 mi orbit) is 380 KHz (760 KHz for 40 users).

It should be emphasized here that for the systems described herein the orbits of the user spacecraft are assumed circular. If the satellites were to be put into elliptical orbits (at least 15 are predicted to be launched in the 1970-1980 time period)* the following considerations must be given to the signaling format:

1. For the programmed system the transmitted signal format must be changed to comply with the minimum and maximum multipath delays encountered in such an orbit. For a TDRS stationed over the equator and a user in an elliptical polar orbit with the plane of the ellipse being normal to the line between the TDRS and the major axis of the ellipse; the minimum and maximum time delays are 200 μsec and 10 msec, respectively. In this case, to avoid the multipath, the user must transmit 12-16.7 μsec data pulses every 12 msec.

2. If more than one (say three) TDRS is in use by a single user satellite, then the signaling format considered to by optimum (in that it negates the effect of multipath and minimizes the signal bandwidth requirement for one user) would not, because of the relative position of the elliptical plane and the other TDRS's, necessarily be optimum for the remaining user-TDRS links.

3. Similarly, the adaptive signaling system operates with the same disadvantage as the programmed system. A user satellite which, upon command from a ground station, changes the duration of its transmitted signal to maintain the most desirable communication with the TDRS, has by the very nature of this signal design rendered its link with any other TDRS non-desirable.

4. As the duty factor is varied to accommodate the multipath time delay variation the peak power must be changed to maintain a constant average power.

*T&DS Mission Model and Projected Spacecraft Support requirements through 1980, E.J.Habib, Study Manager, March 1969. X-520-69-110.

1.6.7.2 Adaptive Time Hop

Adaptive time hopping requires the duration and the repetition period of the transmitted signal to vary in accordance with the relative position between the user satellite (at some fixed altitude) and the TDRS. For the 1000 mi orbit the user transmits (at low grazing angles) continuously at a 500 Hz rate a 1 msec pulse; as the grazing angle increases towards its maximum the duration of the transmission increases. Conversely, the signaling rate decreases allowing a 50% duty cycle to be maintained. The technique is illustrated in the timing diagram of Figures 1.25 to 1.28 where a typical digital sequence is shown along with the user satellite data transmission formats for 1, 5, and 10 msec differential delays in Figures 1.26, 1.27, and 1.28 respectively. The maximum bandwidth required per user for this type of signaling is 8 KHz (1 KHz signal bandwidth, 3 KHz direct Doppler and 2 KHz each for differential Doppler and fading). The 50% duty factor can be maintained at orbital altitudes below 1000 mi; however, the signal power level must continually be changed to maintain a constant average energy per data bit.

The adaptive TH system is essentially a store and forward technique; therefore, the user satellite must have the capability of continuous storage of up to 20 binary data bits.

1.6.7.3 Pre-programmed Frequency Hop

For a user satellite at a 100 mi altitude sufficient protection from the deleterious effects of multipath propagation will be achieved by transmitting a 200 μsec data bit at a 1 kb/s rate with the carrier switching between two preset frequencies on alternate data pulses. The bandwidth required for reception 10 KHz (two RF channels each of which

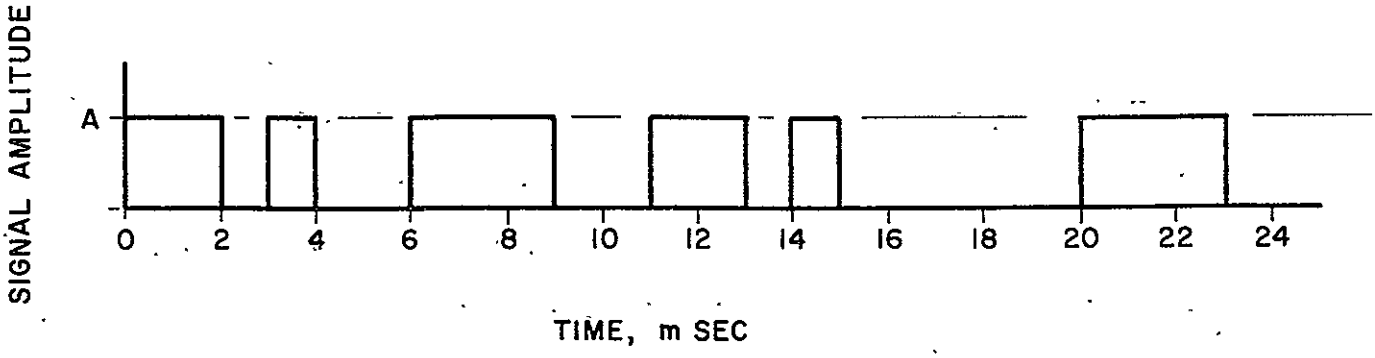

Fig. 1.25 TYPICAL DIGITAL SEQUENCE

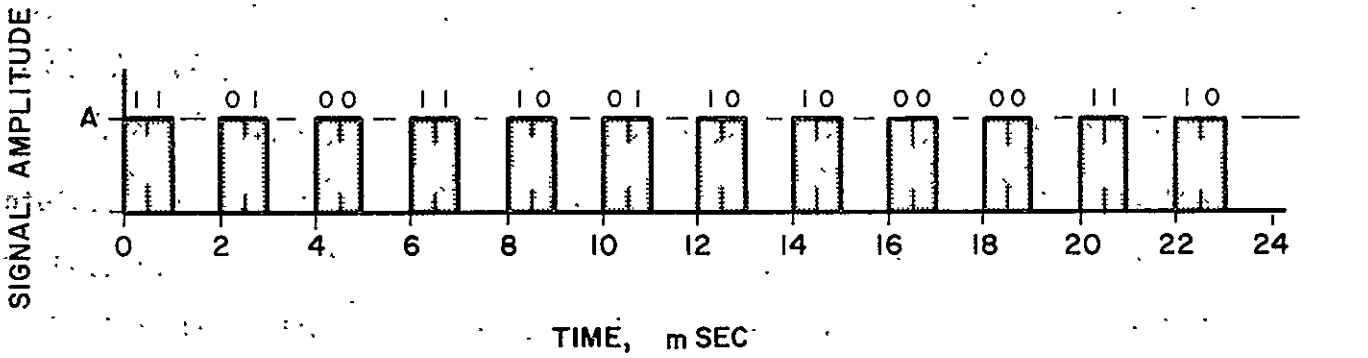

Fig. 1.26 ADAPTIVE TH FOR 1 MSEC DELAYED MULTIPATH

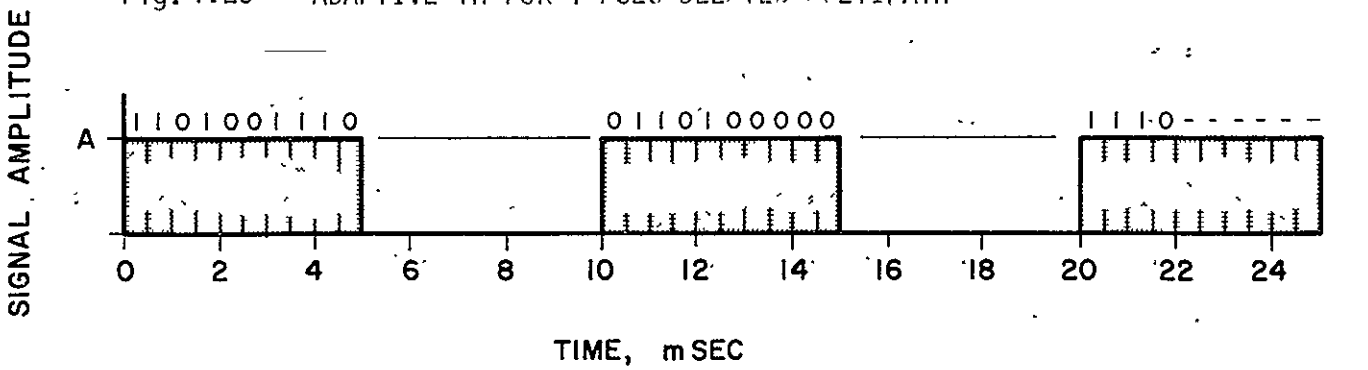

Fig. 1.27 ADAPTIVE TH FOR 5 MSEC DELAYED MULTIPATH

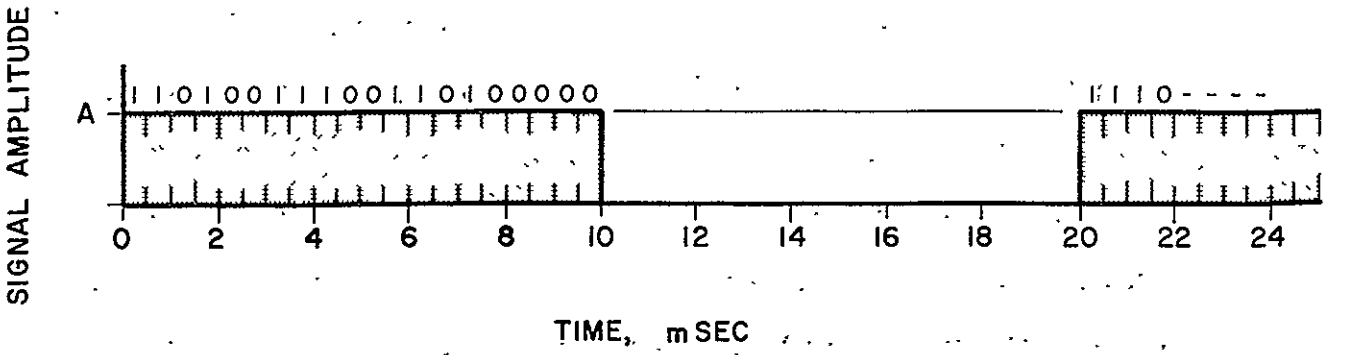

Fig. 1.28 ADAPTIVE TH FOR 10 MSEC DELAYED MULTIPATH

Allowing an additional 4 KHz per user to provide for the maximum direct path Doppler and 4 KHz for fading, the total system bandwidth required for 20 users is 360 KHz (720 KHz for forty users). The frequency-time chart of Figure 1.29 illustrates the pre-programmed FH system.

1.6.7.4 Adaptive Frequency Hop

In the adaptive frequency hop system the duration of each transmitted signal and the interval between them are adjusted to be optimum for the differential time delay imposed upon the user-to-DRSS link. For a user satellite in a 100 mi orbit the signal duration and the interval between signals will vary continuously from 200 μsec (for grazing angles of approximately 15°) to a maximum of 1 msec (and a 90° grazing angle). In the presence of 200 μsec multipath time delay the user will transmit 200 μsec signal at alternate frequencies every 200 μsec. The net effect is to provide a 50% duty cycle in both channels. The maximum bandwidth requirement is on the order of 18 KHz per user. At an altitude of 1000 mi the μsec spacecraft will transmit at alternate frequencies for signal durations of from 1 to 10 msec. Presented in Figures 1.30, 1.31 , and 1.32 are the frequency time diagrams for the 0.2, 1, and 10 msec multipath delays respectively. It should be noted that the maximum bandwidth per user for the 1000 mi orbit is approximately 10 KHz (4 KHz signal bandwidth + 2 KHz fading + 2 KHz differential Doppler + direct Doppler). The adaptive FH system must have (as in the adaptive TH system) the capability of storing continuously a maximum of 10 data bits.

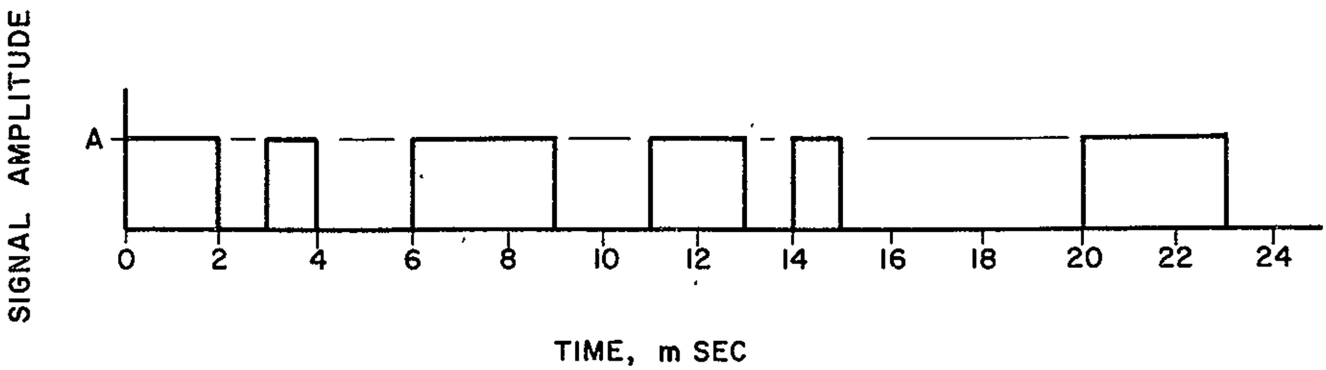

a) Typical Binary Sequence

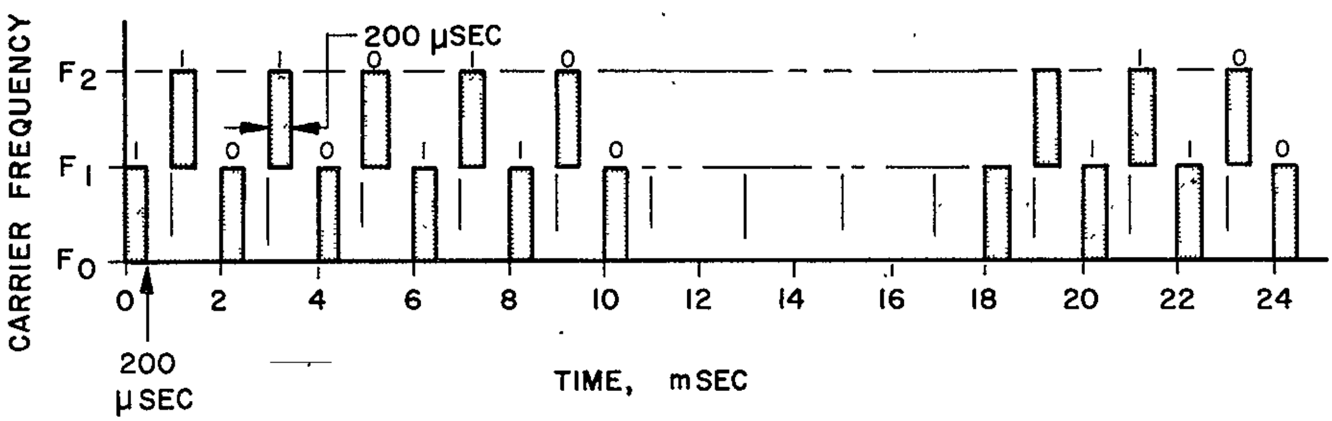

b) Timing For a 100 Mi Circular Orbit

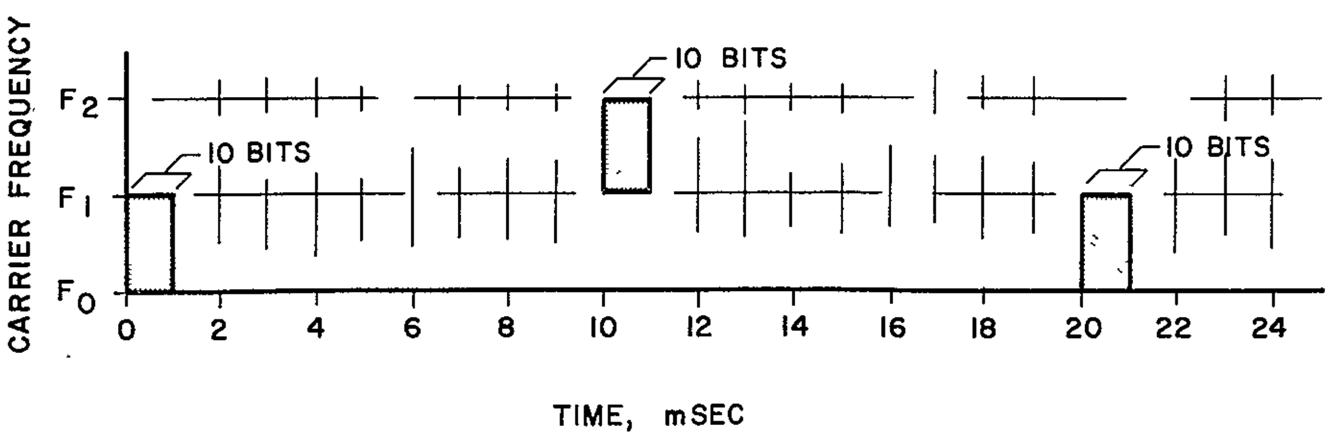

c) Timing For a 1000 Mi Circular Orbit

Fig. 1.29 PRE-PROGRAMMED FH TIMING DIAGRAMS

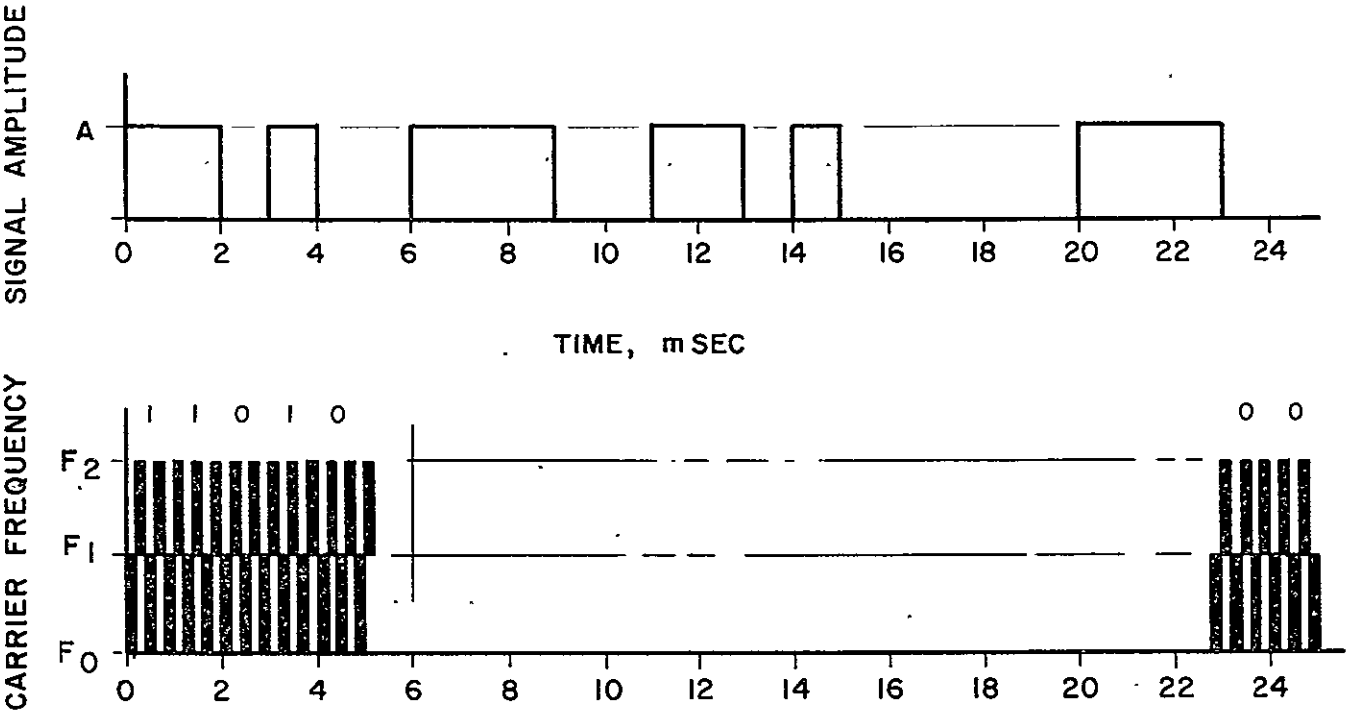

Fig. 1.30. ADAPTIVE FH FOR 0.2 MSEC DELAYED MULTIPATH

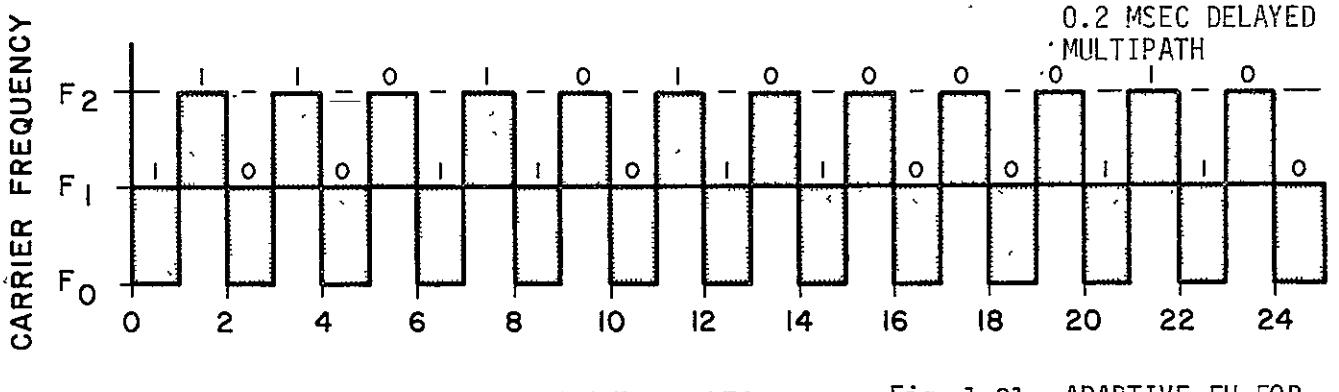

Fig. 1.31 ADAPTIVE FH FOR 1 MSEC DELAYED MULTIPATH

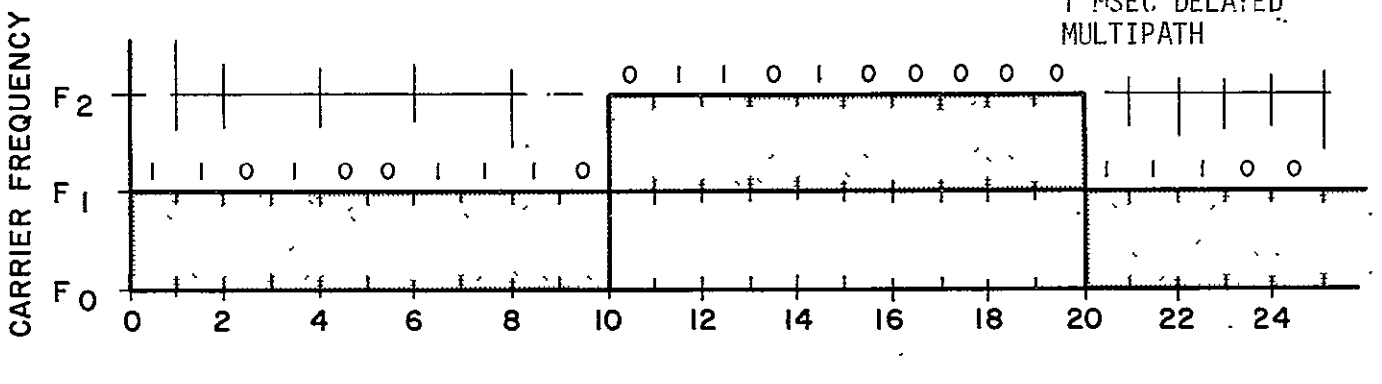

Fig. 1.32 ADAPTIVE FH FOR 10 MSEC DELAYED MULTIPATH

1.6.7.5 Time Hop/Frequency Hop (TH/FH)

Multipath protection can be achieved by the use of a time gated, frequency hopping system in which a signal, (S_1), is transmitted for a period of time equal to the minimum differential time delay (200 μsec in this case); at the end of that transmission the carrier (at say f_1) is shifted to an adjacent frequency (f_2) and another 200 μsec signal (S_2) is transmitted. The operation continues with each successive pulse ($S_3, S_4, \ldots, S_n$) transmitted at adjacent frequency (namely, $f_3, f_4, \ldots, f_n$) for a period equivalent to the maximum path delays to be encountered then the carrier is recycled so that the next transmission is again at f_1. The frequency vs time generating function is a staircase-sawtooth function (see Figure 1.33) which is recycled every 11 msec. The bandwidth required per user for a 200 μsec pulse transmitted in the manner described herein is approximately 77 KHz ((5 KHz signal BW + 2 KHz differential Doppler) X 11 frequency channels). For 20 and 40 users the required repeater bandwidth is 1.54 MHz and 3.1 MHz respectively.

1.6.7.6 Link Calculations for the Various Antimultipath Techniques

1.6.7.6.1 Ideal System

The ideal system as defined here is one in which multipath does not significantly degrade the performance of the system. With the TDRS at an altitude of 22,300 mi and the user satellite maintained in a fixed orbit ranging from 100 mi to 1000 mi, the distance of the user-TDRS link varies from 21,300 mi to 26,750 mi. The down link frequency is approximately 136 MHz; therefore, the maximum and minimum free space path

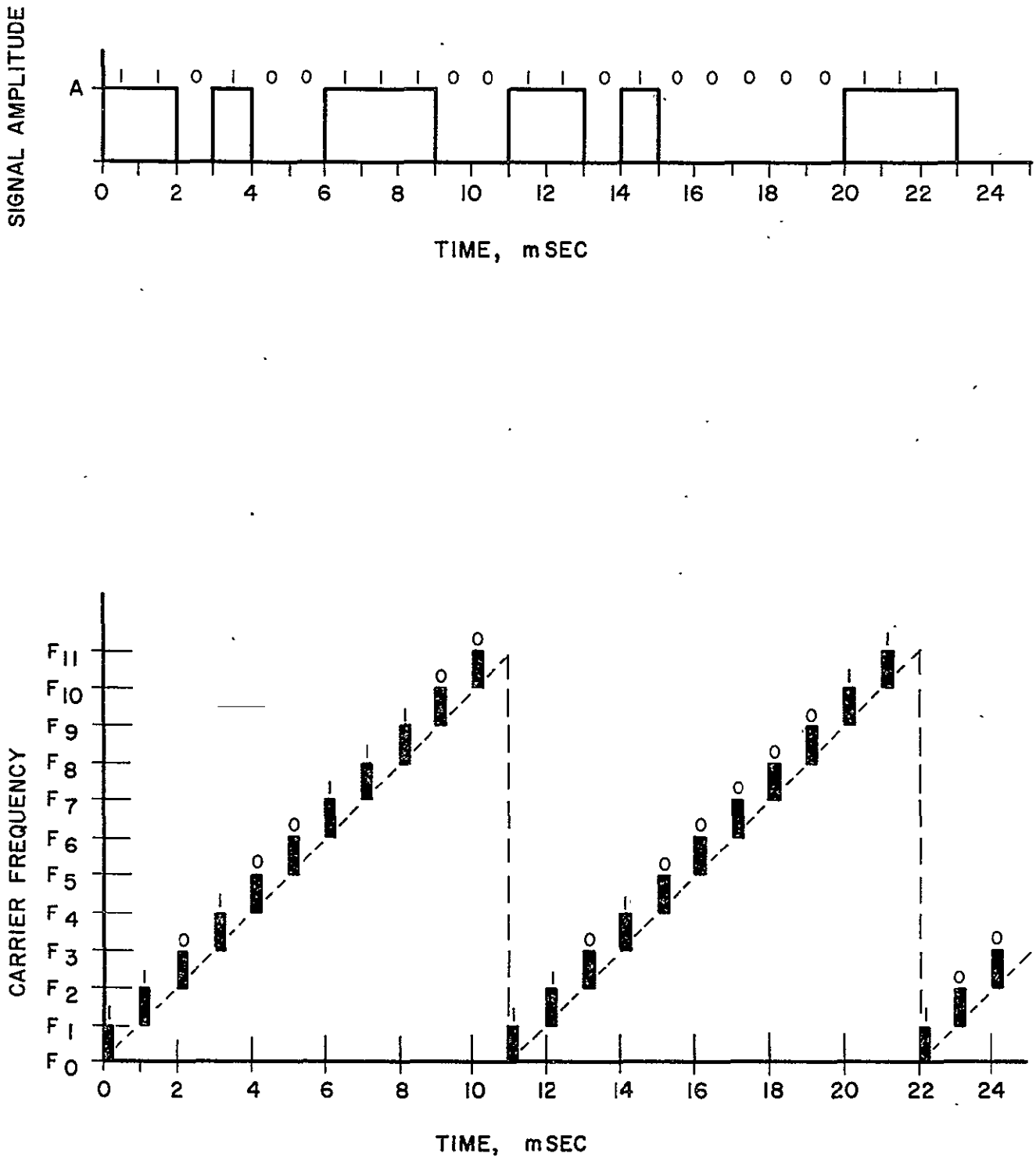

Fig. 1.33 TIME HOP/FREQUENCY HOP TIMING

length losses are 165.8 dB and 167.8 dB respectively. For an equivalent noise temperature of 1200°K (30.8 dB-°K) at the receiver the input noise power spectral density (kT) is - 167.8 dbm/Hz, (k = -198.6 dbm-sec/°K). To achieve a bit error probability, P_e, of 10^{-5} with Δ-PSK signaling, where $P_{e_{\Delta\text{-PSK}}} = 2 \cdot P_{e_{PSK}}(1 - P_{e_{PSK}})$, the required energy per bit to noise density ratio, E/N_o, is on the order of 10 dB; hence, the carrier to noise density ratio, C/N_o $(= \frac{E/T}{N_o})$ for a bit length, T of 1 msec (for a 1 kb/s data rate) is

$$\frac{C}{N_o} = 10 \log \frac{E}{N_o} - 10 \log T$$

$$= 10 + 30$$

$$= 40 \text{ dB - Hz}$$

The power requirements for the user-TDRS is summarized in Table 1.8. For the purposes of this presentation the minimum power requirements will be treated exclusively.

Table 1.8

Power Requirements For User-TDRS Link (Δ-PSK) Carrier frequency = 136 MHz			
Description	Max.	Min	Remarks
$\frac{C}{N_o}$ Desired (dB-Hz)	40.0	40.0	For $P_e=10^{-5}$ and T = 1 msec
Margin Needed (dB)	10	6	Including: Polarization, Equipment Loss and others.
N_o = Noise Spectral Density $\frac{dbm}{Hz}$	-167.8	-167.8	T_S = 1200°K
C = Carrier Power Required (dbm)	-117.8	-121.8	
G_t = User Antenna Gain (dB)	0	0	
G_r = DRSS Antenna Gain (dB)	16	16	
L_p = Path Loss (dB)	167.8	165.8	
P_t = Transmitter Power Required (dbm)	34.0	28.0	$P_t = C+L_p-G$
(watts)	2.5	.630	

1.6.7.6.2 Comparison of Systems Which Avoid Multipath

In this section link calculations will be performed for those antimultipath techniques analyzed in Section 1.6.7. A typical calculation is as follows. Consider a preprogrammed TH system for a satellite in low orbit (100 mi), where it was determined that the signal duration should be 100 μsec and the interpulse period 2 msec. The carrier-to-noise density ratio for this case is on the order of 50 dB-Hz (= 10 dB - 10 log 10^{-4}) and the required transmitter power computed in a manner similar to Table 1.8 is 40 dbm or 10w. Bearing in mind that two adjacent 100 μsec pulses are transmitted every 2 msec, the average signal power is

$$P_{avg} = \frac{200 \times 10^{-6}}{2 \times 10^{-3}} P_t$$

$$= (0.1) P_t$$

$$= 1 \text{ watt (30 dbm)}$$

A comparison of the selected antimultipath schemes in terms of the required bandwidth, carrier to noise density ratio, peak and average user power requirements is presented in Table 1.9.

We have summarized in the Abstract of the report the good and bad features of the anti-multipath techniques just discussed. Then we also present a summary of the ability of each system to meet all the basic TDRS/user requirements. Of particular concern to us is the ability to avoid multipath using the narrowband system just discussed when the altitude of the user is very low, such as in the case of the launch phase. During this critical phase, if communication is to be established between the G.S. and a user via a TDRS, the techniques just discussed are hard pressed to avoid the multipath.

Table 1.9 Comparison of Link Requirements for Various Antimultipath Techniques

Antimultipath Technique	Required Bandwidth/user	C/N_o for P_e -PSK $=10^{-5}$	$P_{t_{pK}}$ dbm	$P_{t_{pK}}$ W	$P_{t_{avg}}$ dbm	$P_{t_{avg}}$ W	Remarks
Ideal	1 KHz	40dB-Hz	28	.630	28	.630	
1. Time Hop:							
a) Adaptive	7 KHz	43dB-Hz	33	2	30	1	Multipath greater than 1 ms
b) Pre-programmed	18 KHz	50dB-Hz	40	10	30	1	100 mi orbit
2. Frequency Hop							
a) Adaptive	18 KHz	43dB-Hz					
b) Pre-programmed	13 KHz	47.2dB-Hz	33	2	30	1	Worst-Case (Low Orbit)
3. Time Hop/Freq. Hop Programmed for all orbital altitudes	77 KHz	47dB-Hz	37	5	30	1	

1.7 FORWARD ERROR CONTROL

In this report we have discussed various systems which combat multipath while simultaneously providing a multiple-access capability. We made frequent reference to the use of forward error control to enable a particular system to achieve the required performance levels or to provide additional system margins or increased user capacity. In particular, forward error control was shown to be a positive necessity for the four-frequency diversity, pseudo-random time hop, and frequency hop/time hop hybrid systems under the worst case assumptions, i.e., the multipath and desired signal were of equal strength and that all users were in low orbits which produce the greatest multipath.

Thus it appears timely to introduce forward error control concepts at this point in the report and to show the significant benefits that can be obtained with a modest amount of hardware located at the G.S.

1.7.1 Convolutional Encoding/Sequential Decoding

In this treatment of convolutional encoding and sequential decoding, we shall restrict our attention to rate - 1/2 and systematic codes. The physical channel which is assumed is the white Gaussian noise channel with equally like binary inputs. With hard decisions (i.e., no quantization or weighting) at the receiver, and the assumption of independent errors, the overall channel model is the familiar binary symmetric channel.

In convolutional encoding, we can think of the check digits being computed as the information digits slide past a code generator (i.e., a parity-computing network) and being inserted, as they are computed, into the transmitted sequence between information symbols.

Because encoding for convolutional codes proceeds in this manner, decoding must be done in the same way, i.e., one information bit at a time. For this reason, the concept of block length for block codes gives way to that of code constraint length, which is the maximum number of consecutive channel symbols (information and check digits) which can be related for a given code generator length.

For a binary convolutional code, Figure 1.34 shows schematically the encoding operation for rate R = 1/2 bit/binit and constraint length n = 10. For the encoder shown, the code is systematic, i.e., each information digit is transmitted unaltered, followed by a check digit. Each of the latter is computed by digital convolution in which information

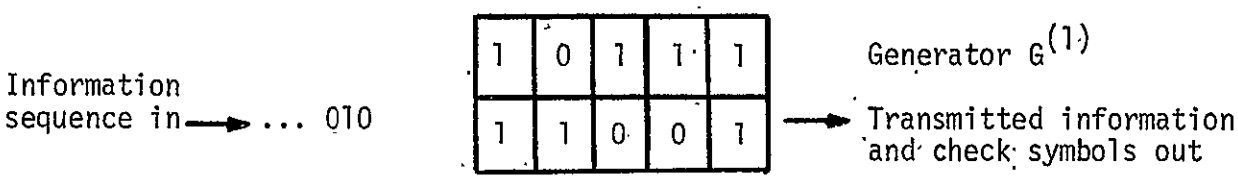

Figure 1.34

Binary Convolutional Encoding

digits and generator digits are multiplied position by position and the resulting products are added modulo 2. For the situation shown in Fig. 1.34 convolution with G gives (starting at the left) $1\cdot1 + 1\cdot0 + 0\cdot1 + 0\cdot1 + 1\cdot1 = 0 \pmod 2$. Thus, the sequence 10, the right-most information digit and a check digit, would be transmitted. The information sequence then shifts one position to the right and the entire operation is repeated.

It is instructive to use Huffman's delay operator notation and write input, generator, and output sequences as polynomials in the delay operator D:

$$I(D) = i_0 + i_1 D + i_2 D^2 + \ldots$$

$$G(D) = g_0 + g_1 D + g_2 D^2 + \ldots + g_m D^m$$

$$T^{(j)}(D) = t_0^{(j)} + t_1^{(j)} D + t_2^{(j)} D^2 + \ldots \qquad j = 1,2 \qquad \text{eq. 1.72}$$

Here D^u represents a delay of u time units relative to the time origin chosen; thus i_u enters the encoder at time u, and if the code is systematic, $T^{(1)}(D) = I(D)$, while each digit of the other transmitted sequence (the check sequence) is a linear combination of digits of I(D):

$$T^{(2)}(D) = G(D)\cdot I(D)$$

where

$$t_0^{(2)} = g_0 i_0$$

$$t_1^{(2)} = g_0 i_1 + g_1 i_0$$

$$t_2^{(2)} = g_0 i_2 + g_1 i_1 + g_2 i_0$$

and in general

$$t_u^{(2)} = \sum_{\ell=0}^{u} g_\ell \, i_{u-\ell}, \text{ mod } 2 \qquad \text{eq. 1.73}$$

where

$$u = 0,1,2,\ldots ;$$

and

$$g_\ell = 0 \text{ for } \ell > m.$$

This operation is digital convolution as described above. The polynomial G(D) is a code-generating polynomial. The quantity m is the degree of G. Thus, m + 1 represents the maximum number of time units over which any information digit can affect the encoder output. A detailed example is shown in Fig. 1.35 with the encoder shift register and tap connections for check digit calculation appearing in Fig. 1.36.

The set of sequences generated by all possible choices of the information digits can be represented as a tree. Referring to Fig. 1.37 we see that corresponding to each new information digit, there is a node in the message tree; from this node, two branches emanate, one corresponding to a value of 0 and one to a value of 1 for the new bit. For a systematic code, proceeding from oldest to newest digits in a left-to-right direction in the tree, gives an information digit followed by a check digit on each branch. Each check digit was computed by encoding the current information digit and all other information digits encountered in tracing the most direct path back through the tree to its base. Adding another branch to a path through the tree corresponds to supplying a new information digit to the encoder of Figs. 1.35 and 1.36.

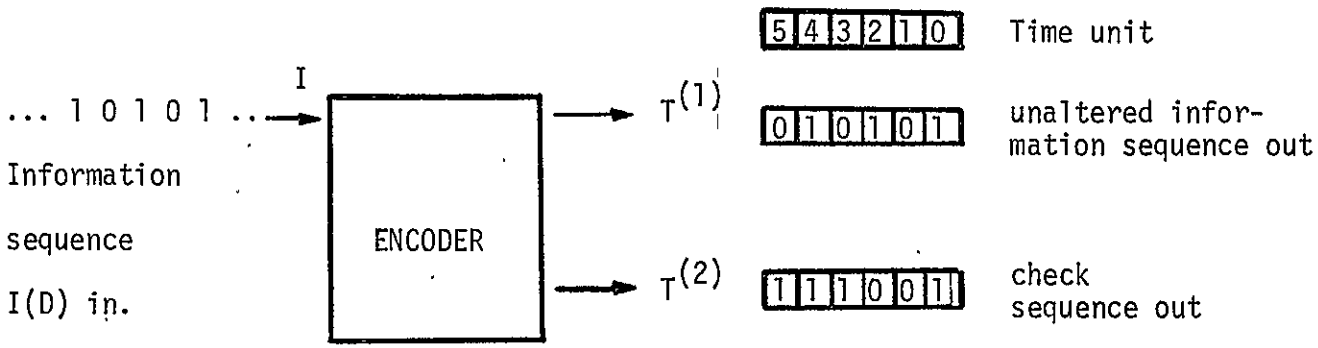

$$I(D) = 1 + D^2 + D^4 + D^6 + \ldots$$

$$G(D) = 1 + D^2 + D^3 + D^4$$

$$T^{(1)}(D) = I(D) = 1 + D^2 + D^4 + D^6 + \ldots$$

$$T^{(2)}(D) = G(D) \cdot I(D) = 1 + D^3 + D^4 + D^5 + \ldots$$

Figure 1.35

Encoder for rate 1/2, showing output and delay-operator computations for the first six time units

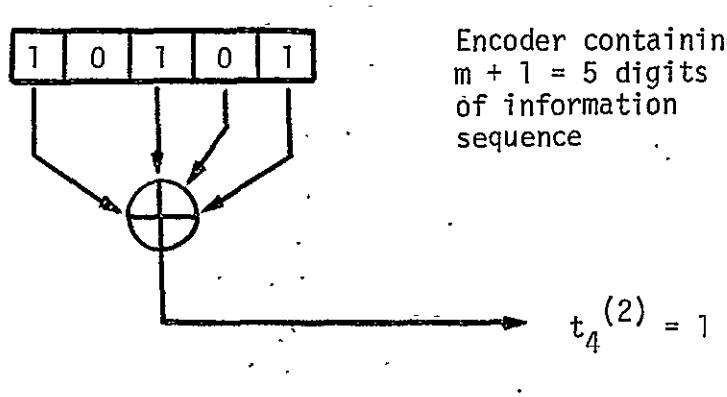

Figure 1.36

Tap connections for the encoder of Figure 1.35, showing check-digit computation at time unit 4.

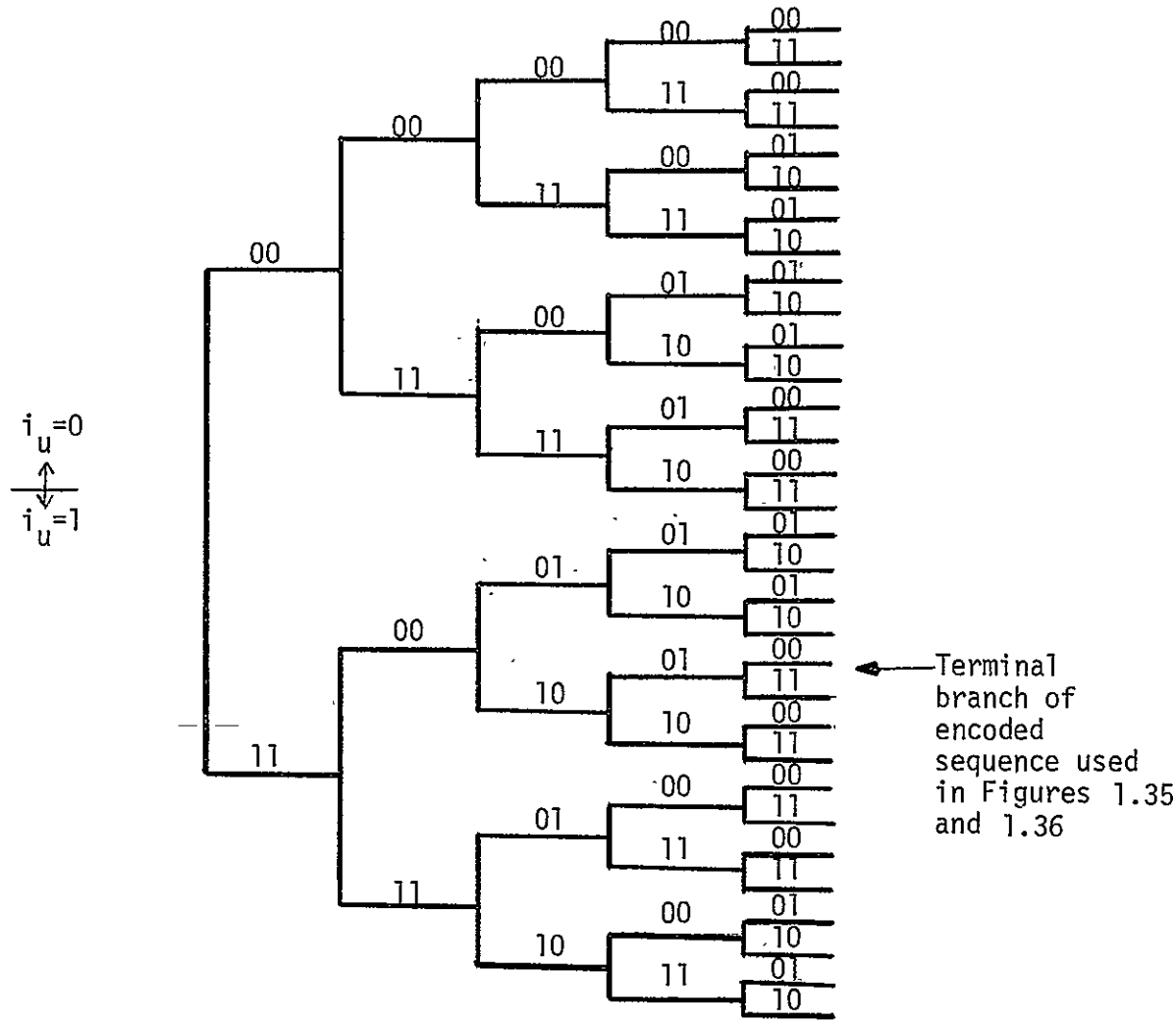

Figure 1.37

Message tree for the code of Figures 1.35 and 1.36

$$R = \frac{1}{2}, \quad n_A = 10,$$

The virtue of the tree is that it displays all possible encoded sequences of any length equal to or less than the maximum length included in the tree. Although the tree may be regarded as extending infinitely far to the right, it is usually truncated at the constraint length of the code.

Sequential decoding differs fundamentally from decoding schemes developed for block codes and from other algorithms developed for convolutional codes in being probabilistic rather than deterministic. The basic task in sequential decoding involves finding an information sequence whose encoded version (information and check digits) most closely matches in some sense the corrupted received sequence. The notion of "closely matching" sequences involves the concept of a decoding metric, the simplest of which is the well known Hamming distance. Other functions which may be used as decoding metrics in a hard-decision algorithm include the mutual information of a particular trial sequence (often referred to as a set of bit hypotheses) and the received sequence; and a simplification of this in which one of two fixed values $m_1>0$ and $-m_2<0$ is assigned to each hypothesized binit according to whether it agrees or disagrees with the corresponding received binit. Note that with Hamming distance one would seek to minimize the metric while with the other two examples one wants to maximize it.

As stated earlier, we shall consider decoding in which hard decisions (not necessarily correct) have already been made on the binits input to the decoder. Although this procedure destroys information (e.g., there is

no way of knowing the degree of confidence with which a 0 or 1 value was assigned to a channel output waveform) the resulting decreases in decoder storage and computational complexity more than make up for this. The metric chosen must therefore be one which is defined for sequences of binary digits.

The sequence of hypothesized binits is generated 2 digits (i.e., one information bit) at a time. As each new set of 2 digits is added to the existing sequence, the total distance of the new hypothesized sequence from the corresponding portion of the received sequence is computed. This distance is compared with a threshold or reject criterion, which is, in general, a function of the length of the trial sequence and (as we shall soon see) of the number and lengths of paths in the message tree which have already been tried and rejected. This threshold is, in fact, one value in a family of thresholds for the present degree of strictness. There are m + 1 values in each family (one for each possible length of the trial sequence) and some arbitrary number of families. Initially, the trial sequence is generated starting at the first node in the tree and terminating at the constraint length, at which time a decision is made as to whether the first hypothesized information bit was a 0 or a 1.

The decoder begins by selecting the first branch of the tree (i_0=0 or 1) and the corresponding check digit. Whenever possible, the chosen branch is nearer than the other one to the corresponding digits of the received sequence. In any case, the distance between the trial

and received branch is compared with a threshold value for that length. If the trial and received branches are close enough as determined by the threshold, the trial branch is accepted. If it is rejected, the other initial branch is tried. If it, too, is rejected, a new family of thresholds is adopted which allows acceptance of greater distances between trial and received sequences. When this first trial branch is accepted, the decoder moves to the next node and the process is repeated, always testing total distance between trial and received sequences. This time, however, and at all nodes other than the initial node in the tree, rejection of both trial branches results not in relaxation of the threshold but in going back toward the initial node of the tree just far enough to reach a node for which the other branch is untried for the current threshold family. If the total distance between trial and received sequences at this point is acceptable according to the corresponding threshold, the new trial branch is accepted. If it, too, is rejected, the process of backing up in the message tree is repeated. If this process results in reaching the base of the tree, the threshold is relaxed again.* Eventually (i.e., with probability 1 for a properly chosen set of thresholds) a sequence is accepted at the constraint length and the first information digit is decoded.

For continuing from this point, current versions of the algorithm proceed by retaining all but the initial branch of the trial sequence just accepted, merely generating a new terminal trial branch and moving

*In the Fano algorithm, back-searches of more than the constraint length are permitted, as long as the number of received binits is great enough at that point.

out one node in the tree. Only the distance between the sequences at the constraint length is tested against the threshold.

If the only changes in threshold were those just described as being necessary for accepting some trial sequence, the threshold would eventually become so loose as to allow acceptance of increasingly incorrect trial sequences, especially at times when the channel is causing very few errors in the received binits. For this reason, there is built into any sequential decoding algorithm a periodic tightening of the threshold. The details of the threshold tightening scheme may vary, and we shall not become any more specific here.

The sequential decoder to be described later differs somewhat from this description in that it utilizes a sequence called the syndrome as the basis for its operation. The syndrome is computed from the received binits and is ultimately a function of the channel noise alone. We can write, for j = 1,2:

$$R^{(j)}(D) = T^{(j)}(D) + E^{(j)}(D)$$

and

$$R^{(j)}(D) = r_0^{(j)} + r_1^{(j)} D + r_2^{(j)} D^2 + \ldots \qquad \text{eq. 1.74}$$

$$E^{(j)}(D) = e_0^{(j)} + e_1^{(j)} D + e_2^{(j)} D^2 + \ldots \qquad \text{eq. 1.75}$$

where R and E are the received and channel noise sequences, respectively. The first thing which the decoder's encoder does is to compute

$$S(D) = R^{(1)}(D) \cdot G(D) + R^{(2)}(D) \qquad \text{eq. 1.76}$$

In view of eqs. 1.74 and 1.75 and the fact that addition is mod 2, eq. 1.76 reduces to

$$S(D) = E^{(1)}(D) \cdot G(D) + E^{(2)}(D) \qquad \text{eq. 1.76}$$

Thus, calculating S(D) by processing the received binits turns out to be identical to operating in exactly the same way on the channel noise digits.

The way in which sequential decoding defeats both the storage and the computation problems should now be apparent. The former is minimized because the decoder generates and considers only one trial sequence at a time, compared with a possible maximum of $2^{n/2}$ for constraint length $n = 2(m+1)$. Thus active storage need only be provided for n received digits, n trial digits, roughly 2n bits for bookkeeping for the various paths tried in the message tree, and for a multiple of m + 1 values of threshold. In addition there must be some buffer storage to hold in-coming binits while decoding is taking place.

The average number of computations* per information bit can be shown to be bounded by a power of n for the binary symmetric channel. This bound is made possible by the fact that rejection of a trial sequence at some length $m_1 < m+1$ information digits means that 2^{m+1-m_1} sequences of length n are removed from consideration for that family of thresholds. Unfortunately, this is a bound on the <u>average</u> number of computations;

*A computation is defined as consisting of the following operations: computing a branch in the message tree, computing its distance from the received branch, testing against the threshold, and deciding on which direction to move from there.

that is, there will be times when a particularly noisy received sequence will cause a search deep into the message tree, with the input buffer filling up in the meantime. If this search is long enough, the buffer will fill completely and subsequent binits will be lost unless measures are taken to prevent buffer overflow (e.g., by terminating a search if the input buffer becomes full).

1.7.2 Gains Realizable Through Sequential Decoding

To obtain an idea of the improvement possible through the use of forward error control in general and sequential decoding in particular, consider first the data presented in Fig. 1.38. The curve labeled REF OPTIMUM BINARY gives the calculated probability of a bit error as a function of the ratio of received signal energy per information bit to noise spectral density for antipodal (coherent binary PSK) signaling waveforms. Similarly, the (24,12) Block curve has been calculated for the augmented (23,12) optimum BCH code, which corrects all triple errors and detects all combinations of an odd number of errors. The curve labeled Sequential Decoder was obtained by computer simulation of a sequential decoder having constraint length $n = 2K = 64$ binits and a random-access memory size of $L = 512$ words. This is a very modest size, as later details will show.

To obtain the desired bit error probability of 10^{-5}, we note that sequential decoding gives an improvement in E_b/N_o of about 2.2 dB over the BCH code and 4.3 dB over the optimum (uncoded) binary. Looked at another way, sequential decoding at rate 1/2 and length 64 enables us to

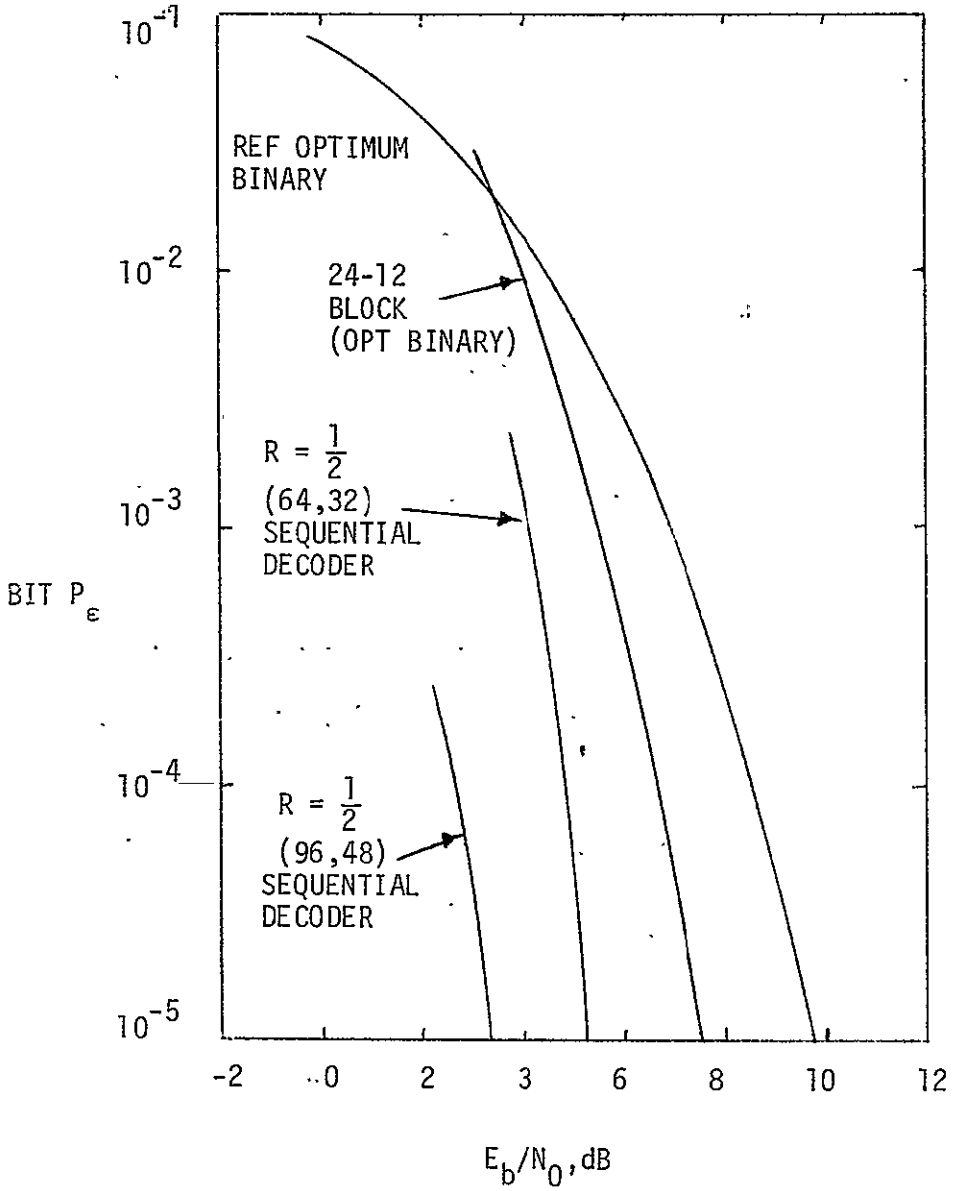

Figure 1.38: Performance of BCH and Sequential Decoders

convert a raw (i.e., uncoded) bit error probability of about 5×10^{-3} to the desired P_ε of 10^{-5}. Since P_ε decreases exponentially with constraint length, the value of 10^{-5} could be made orders of magnitude smaller, or the raw P_ε made larger for any given decoded P_ε, with only a modest increase in decoder size.

As a further comparison, consider Fig. 1.39 , which gives n, the ratio of total energy per bit for coded to uncoded systems, as a function of δ, the ratio of system data rate (bps) to carrier-tracking loop bandwidth, all for a bit error probability $P_\varepsilon = 10^{-5}$. In this case, there is a clear-cut (2.0-2.5 dB) advantage over the 8-bit biorthogonal code even for rate R = 1/2 sequential decoding.

The biorthogonal coding scheme provides error protection by representing each block of n consecutive bits of information by a sequence (code word) of 2^{n-1} binits. These code words have the property that any two distinct words are either orthogonal (i.e., agree in as many places as they disagree) or are complements of each other. For example, for n = 3, the code has the 8 words

0 0 0 0	1 1 1 1
0 0 1 1	1 1 0 0
0 1 0 1	1 0 1 0
0 1 1 0	1 0 0 1

Since 2^{n-1} chips must be transmitted for every n bits, there is a bandwidth expansion factor of $2^{n-1}/n$, which increases nearly exponentially as n becomes large. In addition to this penalty in bandwidth, equipment complexity

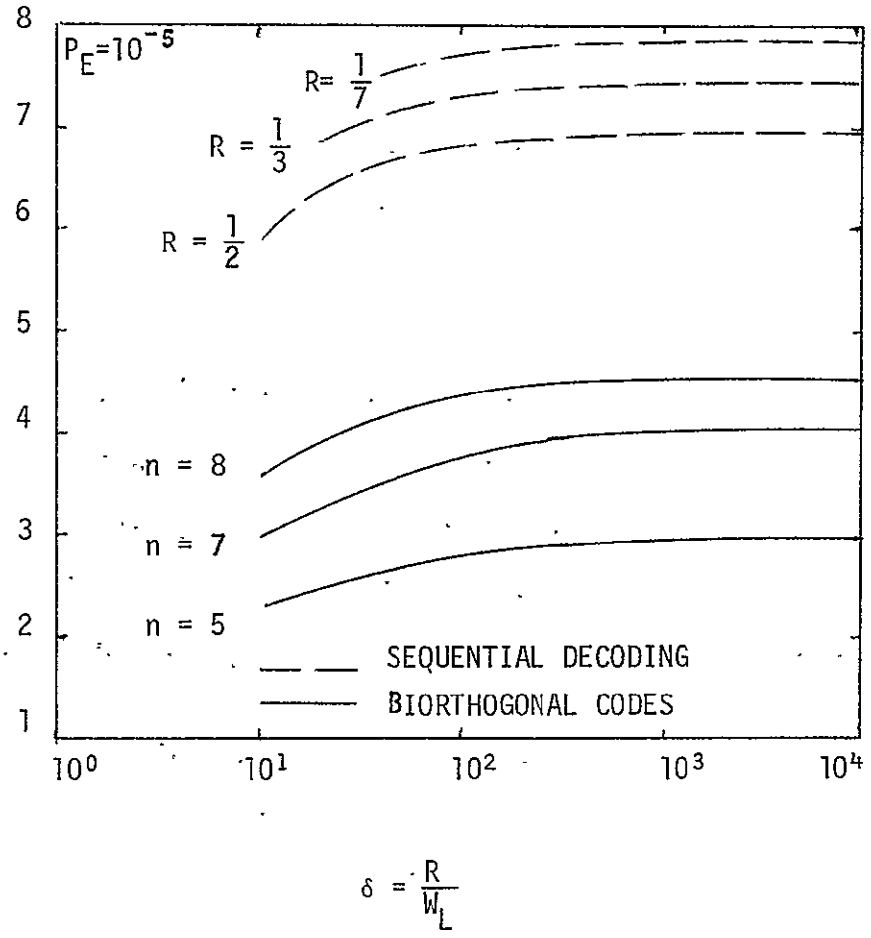

Figure 1.39: Improvement in Efficiency due to Coding versus $\delta = R/W_L$ at a Bit Error Probability of 10^{-5}

at the receiver also increases exponentially with n since 2^n correlators are required for decoding.

Contrasting with the bandwidth expansion behavior for biorthogonal codes is the expansion for sequential decoding by the factor 1/R.

1.7.3 Sequential Decoder Implementation

In this section we draw heavily on unclassified results recently reported by Magnavox Research Laboratories as part of a classified study*. Implementation was studied for the particular sequential decoder which has been discussed in the preceding sections: rate 1/2, systematic code, hard decisions on binits entering the decoder.

In gross form, the sequential decoder appears as in Fig. 1.40. Shown in detail is the replica of the transmitter's encoder whose function is the calculation of the syndrome, which is the key input to the decoder via the random-access memory (RAM). The decoding algorithm is similar to the Fano algorithm as far as its tree-searching strategy is concerned, but it differs from the Fano or other sequential decoding algorithms in its exploitation of the syndrome as the key to error correction.

---

* USC-( ) Study Report (Secret), 15 June 1969, prepared by Magnavox Research Laboratories, Torrance, California, for U.S. Army Satellite Communication Agency, Ft. Monmouth, N.J., under contract no. DAAB07-68-C-0263.

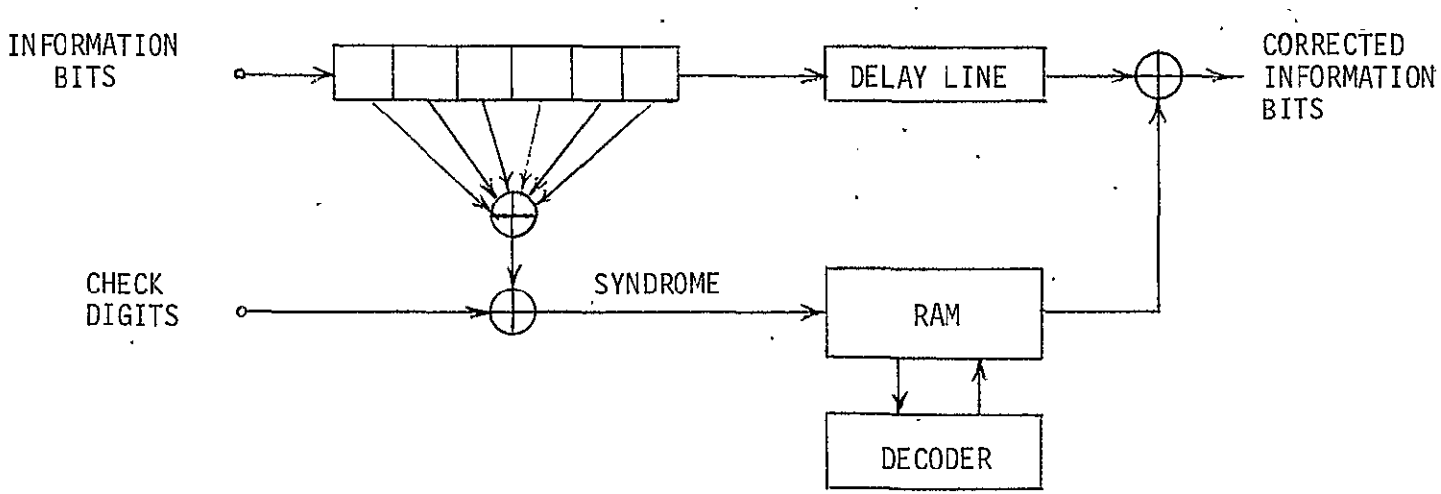

Figure 1.40: Sequential Decoder Block Diagram

A decoder of the size under consideration requires the use of semiconductor memory, since the decoder is not large enough to realize the economies of scale for core memories. One feature of the refined algorithm is that it allows specialization of the memory. The received information bits are shifted into an encoder that is a duplicate of the encoder used in the transmitter. The check bits generated by this encoder are mod 2 added to the received check bits. The result, the syndrome, contains all of the information required by the decoder to detect errors in the received information bits. The syndrome is then entered into the RAM. The information bits, which are not used directly in the decoding process, are delayed by an amount equal to the delay through the RAM. The output of the RAM, which contains 1's in the error locations, is mod 2 added to the delayed information bits, thus accomplishing the correction of errors.

---

* In general, constraint length m+1 would require $\left[\log_2 \left(\frac{m+1}{2}\right)\right]$ delays, where [x] represents the smallest integer $\geq x$.

The syndrome is buffered into the random-access memory. The error-corrected syndrome is buffered out of the RAM and mod 2 added to the delayed dirty information bits producing clean bits for output. The RAM is organized into L 2-bit words. Four 2-bit words are read in and out in parallel to provide an effective speed-up of four in memory access time. The memory address is selected from one of two counters. One counter contains the address of the input-output, while the other contains the address of the decoder.

The delay line may be implemented with MOS shift registers which offer considerably lower cost and higher density than fast random-access semiconductor memories. For example, dual 100-bit MOS shift registers are priced at $30 or 15 cents/bit, while 16-bit RAM's in Motorola MECL II logic are priced at $12 or 75 cents/bit. Thus, this decoder organization provides both a significant cost reduction and a significant package count reduction. The algorithm is also designed to accomplish a maximum amount of computation each clock cycle in order to obtain a greater effective speed factor in the decoder. This is another of the refinements mentioned above.

The I-O counter is incremented by one every fourth information bit, and a I-O read-write cycle is stolen from the decoder. The decoder counter is an up-down counter that is incremented by one each time the decoder moves ahead or behind four nodes.

There is a two-level buffer on the decoder side of the RAM. This is to enable the decoder to proceed at maximum speed in either direction or

reverse itself at any time without having to wait for an extra memory cycle. The second level buffer is also a right-left shift register. The syndrome in this buffer is shifted into an encoder. The decoder logic determines the presence of errors and inserts a "one" in the hypothesis register when errors are located. The decoder logic also computes the new value of the metric, the tilted distance function, and stores this in the metric register. This logic also decides whether to search forward or backward and raises and lowers the threshold when needed.

It should be noted that there is no separate back-up buffer; it has been included in the RAM. This was done because the RAM, which is constructed of MECL II circuits, is sufficiently fast that a separate back-up buffer is unnecessary, thus resulting in fewer packages.

It is estimated that the decoder logic and control together with the metric register can be implemented in about 40 flat packs of Motorola MECL II and MECL III, the latter being a newer family of logic which is about 5 times faster than MECL II. This figure is independent of buffer size and encoder constraint length. All the encoders are estimated at 3 flat packs per information bit of constraint length. For a constraint length of 10, this would amount to 30 flat packs. The RAM requires about 50 flat packs for 64 nodes of storage, including associated buffers and address counters. This adds up to a total of 120 flat packs or about the equivalent parts count of a BCH (24, 12) decoder. If the number of flat packs is increased to about 250, the constraint length can be increased to 32 and the memory size to 512 nodes.

It is estimated that the above decoder can be operated at a clock rate of 50 MHz. All speed critical circuits can be implemented with MECL III, while the less critical circuits and the memory use MECL II. The MECL III family provides logic delays of 1 nanosecond, while MECL II provides delays from 4-6 nanoseconds.

A computer program has been written at Magnavox Research Laboratories to simulate this decoder in order to evaluate its performance. Preliminary results have been obtained for the 250 flat pack decoder (K = 32, L = 512); they were shown in Figure

These results include both undetected errors and buffer overflows. Error rates of 10^{-5} are obtained at E_b/N_o of 5.3 dB. This is a result of great interest since nearly all of the possible sequential decoding gain for rate 1/2 with hard decisions has been achieved with a small amount of hardware compared to previous designs.

Magnavox Research Laboratories has conducted a detailed trade-off study for 5 megabit and 50 megabit/sec sequential decoders operating as just described. Clearly the speed requirements of that study exceeded those for TDRS by several orders of magnitude.

1.7.4 Summary

We have documented the superiority, in terms of achievable bit error rates and ease of implementation, of sequential decoding operating at dimensionless rate 1/2 with a systematic code and hard decisions on received binits, when compared with either a (24,12) optimum BCH block decoder or a biorthogonal code up to the (128,8) level.

We have also demonstrated the ease of implementation of such a sequential decoder using state-of-the-art technology. At the decoder operating speeds currently possible, the problem of input-buffer overflow, which usually is the chief operational difficulty, will be negligible if not non-existent at TDRS data rates. Specifically, an improvement, at $P_\varepsilon = 10^{-5}$, of better than 4 dB (a factor of 2.5) in E_b/N_o is possible using convolutional encoding/sequential decoding instead of uncoded coherent binary PSK. This improvement is obtained at a cost of two multi-layer PC boards located at the ground station using TTL, which implements decoder memory, logic, and control for a constraint length of 64 digits (information and check) and a backsearch capability of 96 nodes. Note that the encoder on board the user craft requires an insignificant amount of digital circuitry.

The 4 dB improvement over an uncoded binary signal can be used to increase the system's capacity or lower the required user power levels. Still further improvement is possible with larger constraint lengths, as may be seen from the curve for the rate - $\frac{1}{2}$ (96, 48) sequential decoder in Fig. 1.38.

1.8 TDRS POSITION LOCATION AND RANGE AND RANGE RATE CONSIDERATIONS FOR USER TRACKING

The following sub-sections are devoted to

a) determination of the position accuracy of a single TDRS

b) range and range rate implementations for the purpose of tracking TDRS user

c) comments on the position location of a TDRS user.

As outlined in the requirements Section 1.1 a user of the TDRS must be capable of being tracked by a G.S.'s via the TDRS. To do this the G.S. (or in some cases a small number of G.S.'s) must track a user through one or two TDRS's (perhaps three in rare instances). Multiple TDRS tracking of a user can be accomplished through the TDRS inter satellite relay or by observing two TDRS's separately at one G.S. via two antennas. The user's specific mission will dictate whether or not tracking is required during various phases, e.g., launch, insertion, or during critical portions of the orbit. Shown in figure 1.41 is the expected number of satellites vs years to 1980 which will require precise orbit determination.

Regardless of whether one or two TDRS's participate in the process of locating a user, orbit determination procedure must be used over several hours or even days if precise user position is to be obtained. This portion of the document does not address itself to the non-real-time data acquisition and smoothing required in orbit determination. It is beyond the scope of this study to attempt a user position error analysis that

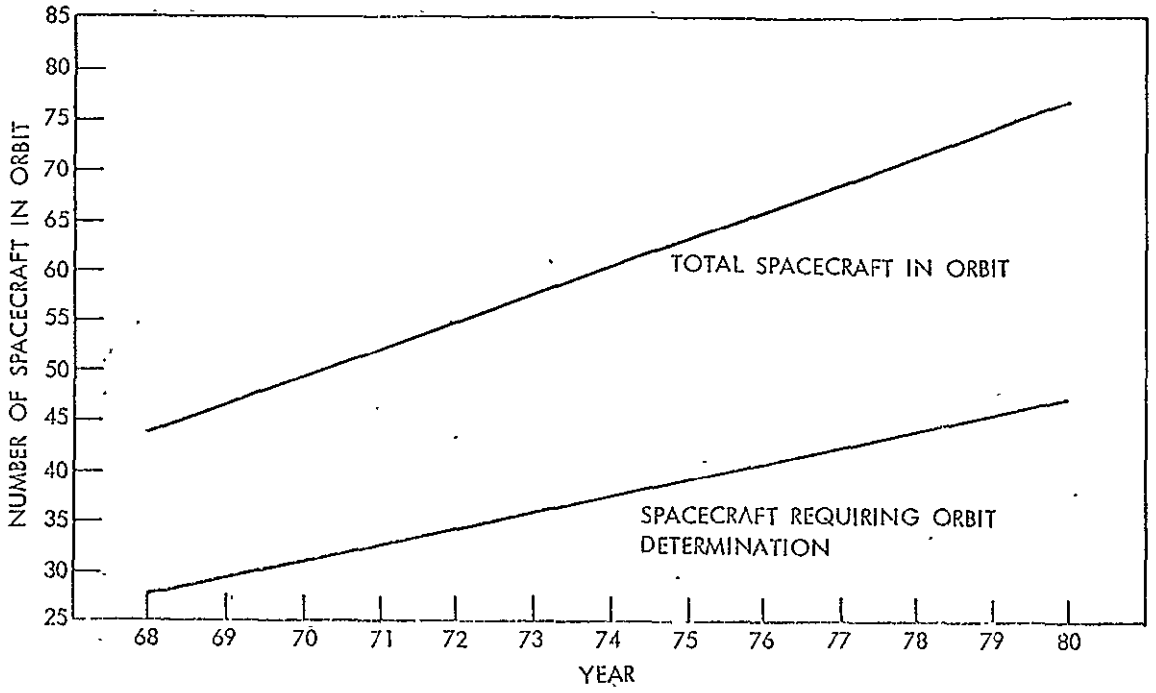

Fig. 1.41 Total Spacecraft Requiring Orbit Determination

includes these considerations; furthermore, NASA has already developed computer programs which estimate the user's position error when tracked by synchronous satellites and a repetition of the existing analysis is unnecessary.

What is appropriate, in this final report, is to document those errors which must be known by NASA in order to obtain the user's position error via the existing computer programs. These errors result from range and range rate instrumentation errors, R & $\dot{R}$ errors resulting from noise and interference, and the lack of precise knowledge of the location of the one or more TDRS's participating in the tracking of a user. The last error source is in turn dependent on the inherent errors in position location of the G.S. or G.S.'s and the instrumentation used to track the TDRS from the G.S.'s.

For purpose of analysis only, Magnavox has chosen to track, and thus determine, the position location of a TDRS by a 3 range difference scheme which involves 4 G.S.'s to tracking and position locate (in virtually real-time) the TDRS. There is nothing sacred about this approach, and it is recognized that a 3 station tri-lateration technique would represent a valid alternative. The approach does illustrate that the TDRS position location accuracy may become sensitive to the choice of location for the G.S.'s involved. Note that while we are not necessarily promoting the 3 ΔR technique, the 4 G.S.'s need not be complicated and can easily use ranging instrumentation like GRARR to accomplish the 3 ΔR measurements.

The geometry for tracking the TDRS by 4 G.S.'s is illustrated in figure 1.42 . The absolute position error of each G.S. is described

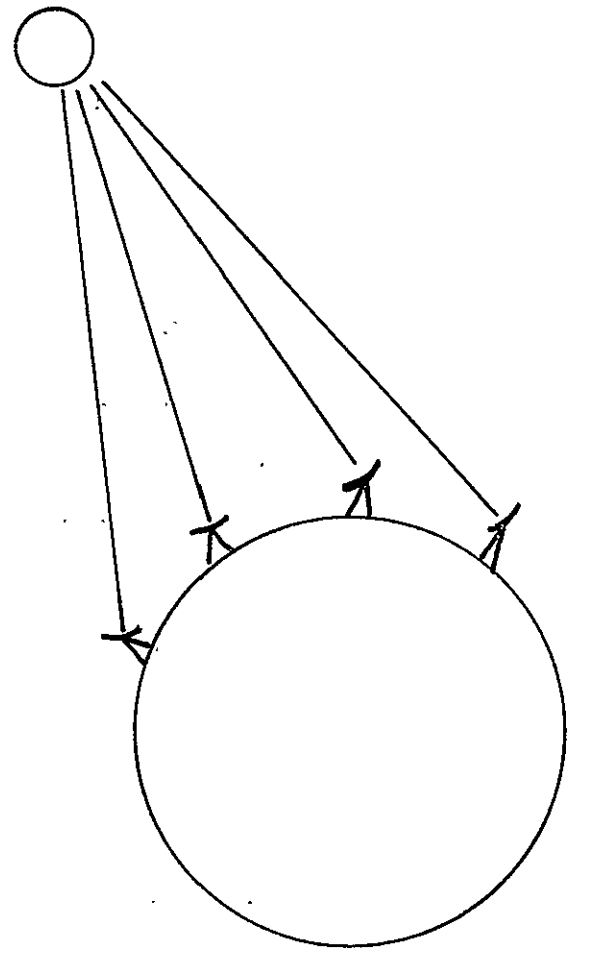

Fig. 1.42 G.S./TDRS Geometry for 3ΔR Measurement

by a spherical error probability (SEP) of 10 meters. We realize that a 10 m SEP absolute is not a currently accepted figure for the position location of S.G.'s, however, over the past year Magnavox has accumulated substantial data from its TRANSIT receiver/computer equipment which show conclusively that a 10 m SEP absolute error can be readily achieved by observing 12 usable passes (24 hrs.) of the TRANSIT Satellite. Measurements have been made over most of the world and the repeatability of the averaged data is within 2 meters. A description of the current instrumentation used in position fixing with TRANSIT is provided in Appendix II of this report.

We have been familiarized with the NASA computer program which calculates the SEP of a TDRS when tracked by precise ranging instrumentation (Laser) from two G.S.'s e.g., Rosman and Mojave. After a 24 hr tracking period the SEP has dimensions of 10m-30m-100m when the station position location error is a 10m SEP.

The TDRS position location error based on a $3\Delta R$ measurement procedure is discussed in the next subsection, where various satellite-station geometries are considered and representative error magnitudes are derived. For comparison purposes, we have included in Appendix 5 the analogous TDRS position error analysis based on a 3-range measurement procedure, again considering various geometries. The relative performance of the two measurement procedures in question is also discussed in the Appendix 5.

In the following subsections we discuss various aspects of range and range rate implementations for the TDRS and the unique R & $\dot{R}$ problems associated with the system. For purpose of analysis we often use the PN

code system as an example. We are justified in this favoritism since the PN system is shown in this report to have the following advantages:

a. provides precise ranging between one or more G.S.'s and a user via one or more TDRS's during the entire user mission,

b. provides coherent transponding at the user spacecraft which insures an accurate range rate signal for tracking the user.

The pseudorandom time hop signal has been shown, Section 1.6.3, to have the desired properties of a good range and range rate system. However, the PRTH signal requires excessively high peak power levels to guarantee adequate communications and R & $\dot{R}$ signal margin. High peak power levels present a serious problem for the user craft transmitters and can result in instantaneous satellite overloading. For this reason the PRTH is not a serious contender for the TDRS system.

Likewise the FH/TH or RADA signals, while theoretically capable of providing the required R & $\dot{R}$ accuracy, also require complex phase continuous frequency synthesizer to effect this accuracy. This requirement places the FH/TH or RADA signal in the doubtful category for applications to TDRS.

Adaptive time hop (ATH), discussed in Section 1.6.7, can be used in conjunction with narrowband (10KC side tone system) to accomplish range and range rate tracking of one user from one G.S., assuming that the proper timing and gating (50% duty factor with a changing signaling format vs grazing angle ψ or altitude) is employed by the G.S. and user. At very low altitudes which are representative of the initial launch phase, the signaling format cannot be arranged to avoid the multipath. In addition to this difficulty,

the ATH system's signal format (timing) which is appropriate to avoid the multipath between a user and a specific TDRS at normal orbital altitudes may not be appropriate (usable) by a second TDRS which is participating in the joint tracking of a user. Since the ATH system relies upon a changing signal structure to avoid the multipath, a similar signal structure must be used by the G.S. and the user being tracked. This dedication of the G.S.'s R & $\dot{R}$ signals to one user mean that simultaneous tracking of more than one user by the S.G. cannot be accomplished unless more than one G.S. to TDRS channel is employed (one for each user). To track a user with an ATH/side tone system by two TDRS's also presents a minor problem at the G.S. observing the two TDRS's since the signals from each TDRS are on the same frequency. Antenna discrimination must be relied upon to separate the ranging signals at the G.S.

Pre-programmed time hop or frequency hop signals, Section 1.6.7, avoid the multipath for all values of grazing angle $16° < \psi < 90°$ for a fixed circular orbit and require signal duty factor changes only for elliptical orbits. While the pre-programmed systems do not suffer the joint TDRS malady of the ATH system, it does suffer from the inability to protect against multipath at low altitudes and does impose the dedicated channel inflexibility required by the ATH system during tracking.

1.8.1 TDRS Position Error Analysis: 3 Range Differences

The purpose of this note is to derive a position error formulation for the case where a TDRS position is established from the range differences between four stations. The interest is to relate position error to range-measurement errors and station-location errors.

If the vehicle coordinates are denoted by $x_i (i=1,2,3)$ and the j-th station coordinates are denoted by $p_i^{(j)}$ $(i=1,2,3)$, then the range between the j-th station and the vehicle is given by

$$r_j = \{ \sum_{i=1}^{3} [x_i - p_i^{(j)}]^2 \}^{\frac{1}{2}} \qquad \text{eq. 1.77}$$

and the range difference between the j-th and (j+1)-th station is given by

$$d_j = r_j - r_{j+1} = \{ \sum_{i=1}^{3} [x_i - p_i^{(j)}]^2 \}^{\frac{1}{2}} - \{ \sum_{i=1}^{3} [x_i - p_i^{(j+1)}]^2 \}^{\frac{1}{2}}$$

$$(j=1,2,3) \qquad \text{eq. 1.78}$$

If we denote the directional cosines of the j-th station by $\alpha_{i,j}$, i.e.,

$$\alpha_{i,j} = \frac{x_1 - p_i^{(j)}}{r_j}$$

then the incremental equation to be used for small-error analysis is given by

$$\delta dj = \delta r_j - \delta r_{j+1} = \sum_{i=1}^{3} (\alpha_{i,j} - \alpha_{i,j+1}) \delta x_i - \sum_{i=1}^{3} \alpha_{i,j} \delta p_i^{(j)} + \sum_{i=1}^{3} \alpha_{i,j+1} \delta p_i^{(j+1)}$$

$$(j=1,2,3) \qquad \text{eq. 1.79}$$

or

$$\sum_{i=1}^{3} a_{i,j} \delta x_i = \delta d_j + \delta \varepsilon_j - \delta \mu_j \qquad (j=1,2,3)$$

where

$$a_{i,j} = \alpha_{i,j} - \alpha_{i,j+1}$$

$$\delta d_j = \delta r_j - \delta r_{j+1}$$

$$\delta \xi_j = \sum_{i=1}^{3} \alpha_{i,j} \delta p_i^{(j)}$$

$$\delta \mu_j = \delta \xi_{j+1} = \sum_{i=1}^{3} \alpha_{i,j+1} \delta p_i^{(j+1)}$$

and the results of Eq. 1.79 can be written in matrix form as follows

$$\underset{3\times 3}{A} \; \underset{3\times 1}{\delta x} = \underset{3\times 1}{\delta d} + \underset{3\times 1}{\delta \xi} - \underset{3\times 1}{\delta \mu} \qquad \text{eq. 1.80}$$

If the vehicle-station's geometry is such that the matrix A is nonsingular, the position error can then be expressed explicitly as

$$\underset{\sim}{\delta x} = A^{-1} (\underset{\sim}{\delta d} + \underset{\sim}{\delta \xi} - \underset{\sim}{\delta \mu}) \qquad \text{eq. 1.81}$$

The first term represents a range-measurement error contribution, while the second and third terms represent station-location error contributions. These last two terms are fixed bias errors for a given vehicle-station geometry (i.e., for given $\alpha_{i,j}$). Another bias error could be contributed by the range-measurement term $\underset{\sim}{\delta d}$ itself, e.g., if bias systematic errors exist.

If we assume a common location error $\delta p_i^{(j)} = \delta p$ for all coordinates i and stations j, then the bias position error caused by this effect is given by

$$(\underset{\sim}{\delta x})_{k,\substack{\text{station}\\\text{location}}} = \sum_{j=1}^{3} (A^{-1})_{kj}(\underset{\sim}{\delta\xi}-\underset{\sim}{\delta u})_j$$

$$= \delta p \sum_{j=1}^{3}\sum_{i=1}^{3} a_{ij}(A^{-1})_{kj}$$

$$= \delta p \sum_{i=1}^{3} (A\cdot A^{-1^T})_{ik} \qquad \text{eq. 1.82}$$

where the T stands for the transpose operation.

The variance of the position error caused by the range-measurement errors is now evaluated assuming a zero mean value due to this effect, i.e., the position error mean is assumed to be the station-location error contribution. Under these conditions, the covariance matrix of the position error is given by

$$K(\underset{\sim}{\delta x}) = E[(A^{-1}\underset{\sim}{\delta d})(A^{-1}\underset{\sim}{\delta d})^T]$$

$$= A^{-1}E[(\underset{\sim}{\delta d})(\underset{\sim}{\delta d})^T](A^{-1})^T = A^{-1}K(\underset{\sim}{\delta d})(A^{-1})^T \qquad \text{eq. 1.83}$$

where $K(\underset{\sim}{\delta d})$ is the covariance matrix of the range-difference errors. The elements of this last matrix are given by

$$[K(\underset{\sim}{\delta d})]_{ij} = E(\delta d_i \delta d_j) = E[(\delta r_i - \delta r_{i+1})(\delta r_j - \delta r_{j+1})]$$

$$= E(\delta r_i \delta r_j) + E(\delta r_{i+1}\delta r_{j+1}) - E(\delta r_i \delta r_{j+1}) - E(\delta r_{i+1}\delta r_j)$$

$$= \begin{cases} \sigma^2(\delta r_i) + \sigma^2(\delta r_{i+1}) & \text{if } i=j \\ -\sigma^2(\delta r_j) & \text{if } i=j-1 \\ -\sigma^2(\delta r_i) & \text{if } i=j+1 \\ 0 & \text{if } |i-j| = 2 \end{cases} \qquad \text{eq. 1.84}$$

or

$$K(\underset{\sim}{\delta d}) = \begin{bmatrix} \sigma_1^2 + \sigma_2^2 & -\sigma_2^2 & 0 \\ -\sigma_2^2 & \sigma_2^2 + \sigma_3^2 & -\sigma_3^2 \\ 0 & -\sigma_3^2 & \sigma_3^2 + \sigma_4^2 \end{bmatrix} \qquad \text{eq. 1.85}$$

where $\sigma_i^2 \triangleq \sigma^2(\delta r_i)$ for simplicity in notation. In the derivation, the range-measurement errors from different stations have been assumed to be statistically independent; otherwise, correlation terms will have to be included in Eq. 1.85.

The TDRS position error covariance matrix is thus specified by the matrices A and $K(\underset{\sim}{\delta d})$ through Eq. 1.83. The matrix A reflects the system geometry in question, and the matrix $K(\underset{\sim}{\delta d})$ reflects the ranging error contributions. An analogous formulation and interpretation exists in the case where the TDRS position is established from 3 range measurements: it is shown in Appendix 5 that the matrices C and $K(\underset{\sim}{\delta r})$ respectively play the role of A and $K(\underset{\sim}{\delta d})$. The main distinction is that $K(\underset{\sim}{\delta d})$ is non-diagonal even if statistically independent range measurements are assumed, while $K(\underset{\sim}{\delta r})$ is diagonal under such conditions.

The position-error covariance matrix of Eq. 1.83 can now be evaluated. Its general element is given by

$$[K(\underset{\sim}{\delta x})]_{ij} = \sum_{k=1}^{3} \sum_{\ell=1}^{3} (A^{-1})_{ik}(A^{-1})_{j\ell}[K(\underset{\sim}{\delta d})]_{k\ell} \qquad \text{eq. 1.86}$$

so the individual coordinate-error variances represented by the diagonal elements are

$$\sigma^2(\delta x_j) = [K(\underset{\sim}{\delta x})]_{jj}$$

$$= \sum_{k=1}^{3} [(A^{-1})_{jk}]^2(\sigma_k^2+\sigma_{k+1}^2) - 2 \sum_{k=1}^{2} (A^{-1})_{jk}(A^{-1})_{j,k+1}\sigma_{k+1}^2 \qquad \text{eq. 1.87}$$

or written in terms of the range-measurement-error variances of the individual stations:

$$\sigma^2(\delta x_j) = [(A^{-1})_{j1}]^2 \sigma_1^2 + [(A^{-1})_{j1} - (A^{-1})_{j2}]^2\sigma_2^2$$

$$+ [(A^{-1})_{j2} - (A^{-1})_{j3}]^2\sigma_3^2 + [(A^{-1})_{j3}]^2\sigma_4^2 \qquad \text{eq. 1.88}$$

Example 1

X(0,0,h+R)

$S_1(0,0,R)$ $\quad d_1^2 = h^2$

$S_2(0,R/\sqrt{2},R/\sqrt{2})$ $\quad d_2^2 = D^2$

$S_3(0,-R/\sqrt{2},R/\sqrt{2})$ $\quad d_3^2 = D^2$

$S_4(R/\sqrt{2},0,R/\sqrt{2})$ $\quad d_4^2 = D^2$

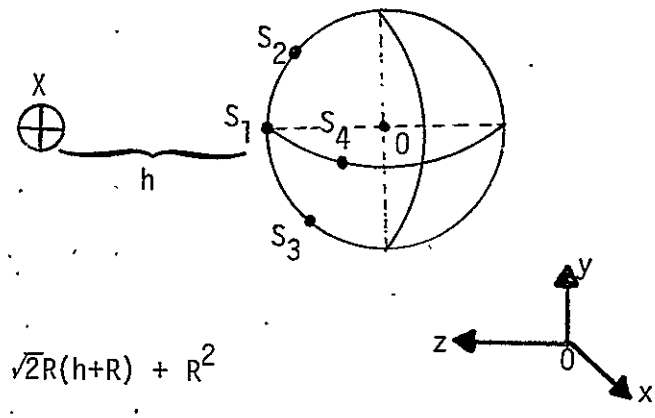

Directional Cosines: $D^2 \triangleq (h+R)^2 - \sqrt{2}R(h+R) + R^2$

$S_1(0,0,1)$

$S_2(0,-R/\sqrt{2}D, (h+R/\sqrt{2})/D)$

$S_3(0,R/\sqrt{2}D, (h+R-R/\sqrt{2})/D)$

$S_4(-R/\sqrt{2}D,0,(h+R-R/\sqrt{2})/D)$

Evaluation of A and A^{-1} matrices: $B \triangleq 1 - \frac{h+R-R/\sqrt{2}}{D}$

$$A = \begin{bmatrix} 0 & 0 & R/\sqrt{2}D \\ R/\sqrt{2}D & -2R/\sqrt{2}D & R/\sqrt{2}D \\ B & 0 & 0 \end{bmatrix}$$

$$|A| = \frac{BR^2}{D^2}$$

$$A^{-1} = \frac{D^2}{BR^2} \begin{bmatrix} 0 & 0 & R^2/D^2 \\ BR/\sqrt{2}D & -BR/\sqrt{2}D & R^2/2D^2 \\ 2BR/\sqrt{2}D & 0 & 0 \end{bmatrix}$$

$$= \begin{bmatrix} 0 & 0 & 1/B \\ D/\sqrt{2}R & -D/\sqrt{2}R & 1/2B \\ 2D/\sqrt{2}R & 0 & 0 \end{bmatrix}$$

Evaluation of $\sigma^2(\delta x_j)$:

$$\sigma^2(\delta x_1) = \frac{1}{B^2}(\sigma_3^2+\sigma_4^2)$$

$$\sigma^2(\delta x_2) = \frac{D^2}{2R^2}\sigma_1^2 + \frac{2D^2}{R^2}\sigma_2^2 + \left(\frac{D}{\sqrt{2}R} + \frac{1}{2B}\right)^2 \sigma_3^2 + \frac{1}{4B^2}\sigma_4^2$$

$$\sigma^2(\delta x_3) = \frac{2D^2}{R^2}\ (\sigma_1^2+\sigma_2^2)$$

Numerical Results: h = 22375 miles, R = 3985 miles

D = 23710 miles, β = 0.00717

$$\sigma^2(\delta x_1) \approx 1.9\times10^4(\sigma_3^2+\sigma_4^2)$$

$$\sigma^2(\delta x_2) \approx 17.7\ \sigma_1^2+71\sigma_2^2 + 5450\ \sigma_3^2 + 4850\ \sigma_4^2$$

$$\sigma^2(\delta x_3) \approx 71(\sigma_1^2+\sigma_2^2)$$

Example 2

$X(0,0,h+R)$

$S_1(0,R/2,\sqrt{3}R/2)$ $\quad d_1^2 = D_1^2$

$S_2(0,R/\sqrt{2},R/\sqrt{2})$ $\quad d_2^2 = D^2$

$S_3(0,-R/\sqrt{2},R/\sqrt{2})$ $\quad d_3^2 = D^2$

$S_4(R/\sqrt{2},0,R/\sqrt{2})$ $\quad d_4^2 = D^2$

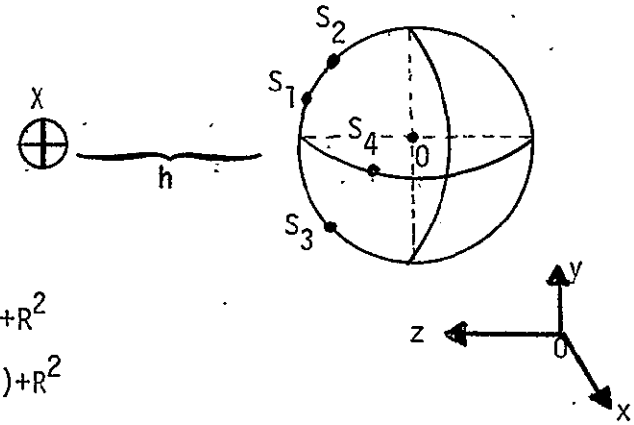

Directional Cosines: $D^2 \triangleq (h+R)^2 - \sqrt{2}R(h+R)+R^2$

$D1^2 \triangleq (h+R)^2 - \sqrt{3}R(h+R)+R^2$

$S_1(0,-R/2D^1;(h+R-\sqrt{3}R/2)/D^1)$

$S_2(0,-R/\sqrt{2}D,(h+R-R/\sqrt{2})/D)$

$S_3(0,R/\sqrt{2}D,(h+R-R/\sqrt{2})/D)$

$S_4(-R/\sqrt{2}D,0,(h+R-R/\sqrt{2})/D)$

Evaluation of A and A^{-1} matrices: $B^1 \triangleq \frac{h+R-\sqrt{3}R/2}{D^1} - \frac{h+R-R/\sqrt{2}}{D}$

$$A = \begin{bmatrix} 0 & 0 & R/\sqrt{2}D \\ R/\sqrt{2}D - R/2D^{1} & -2R/\sqrt{2}D & R/\sqrt{2}D \\ B^{1} & 0 & 0 \end{bmatrix}$$

$$|A| = \frac{B^{1}R^{2}}{D^{2}}$$

$$A^{-1} = \frac{D^{2}}{B^{1}R^{2}} \begin{bmatrix} 0 & 0 & R^{2}/D^{2} \\ B^{1}R/\sqrt{2}D & -B^{1}R/\sqrt{2}D & R^{2}/2D^{2} - R^{2}/2\sqrt{2}DD^{1} \\ 2B^{1}R/\sqrt{2}D & 0 & 0 \end{bmatrix}$$

$$= \begin{bmatrix} 0 & 0 & 1/B^{1} \\ D/\sqrt{2}R & -D/\sqrt{2}R & 1/2B^{1} - D/2\sqrt{2}D^{1}B^{1} \\ 2D/\sqrt{2}R & 0 & 0 \end{bmatrix}$$

Evaluation of $\overline{\sigma^{2}(\delta x_{j})}$:

$$\sigma^{2}(\delta x_{1}) = \frac{1}{B^{1}{}^{2}} (\sigma_{3}^{2} + \sigma_{4}^{2})$$

$$\sigma^{2}(\delta x_{2}) = \frac{D^{2}}{2R^{2}} \sigma_{1}^{2} + \frac{2D^{2}}{R^{2}} \sigma_{2}^{2} + \left(\frac{D}{\sqrt{2}R} + \frac{1}{2B^{1}} - \frac{D/D^{1}}{2\sqrt{2}B^{1}} \right)^{2} \sigma_{3}^{2} + \left(\frac{1}{2B^{1}} - \frac{D/D^{1}}{2\sqrt{2}B^{1}} \right)^{2} \sigma_{4}^{2}$$

$$\sigma^{2}(\delta x_{3}) = \frac{2D^{2}}{R^{2}} (\sigma_{1}^{2} + \sigma_{2}^{2})$$

Numerical Results: h = 22375 miles, R = 3985 miles

D = 23710 miles, D^{1} = 22995 miles

B^{1} = 0.00343

$$\sigma^2(\delta x_1) \approx 8.5\times10^4(\sigma_3^2+\sigma_4^2)$$

$$\sigma^2(\delta x_2) \approx 17.7\ \sigma_1^2 + 71\ \sigma_2^2 + 1910\ \sigma_3^2 + 1560\ \sigma_4^2$$

$$\sigma^2(\delta x_3) \approx 71(\sigma_2^2+\sigma_3^2)$$

Example 3

$X(0,0,h+R)$

$S_1(0,0,R)$	$d_1^2 = h^2$
$S_2(0,\sqrt{3}R/2,R/2)$	$d_2^2 = D^{11^2}$
$S_3(0,-\sqrt{3}R/2,R/2)$	$d_3^2 = D^{11^2}$
$S_4(\sqrt{3}R/2,0,R/2)$	$d_4^2 = D^{11^2}$

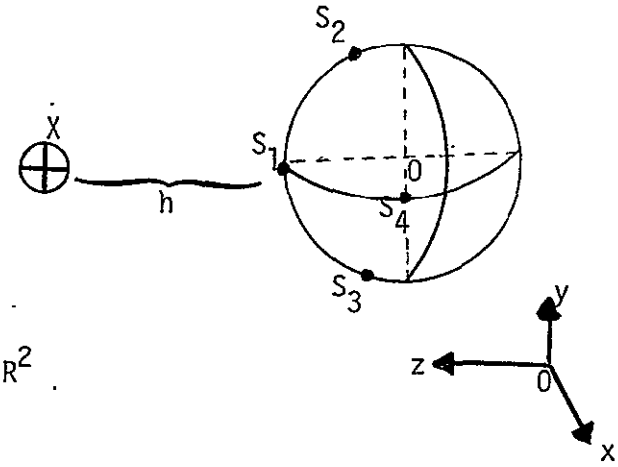

Directional Cosines: $D^{11^2} \triangleq (h+R)^2 - R(h+R) + R^2$

$S_1(0,0,1)$

$S_2(0,-\sqrt{3}R/2D^{11},(h+R-R/2)/D^{11})$

$S_3(0,\sqrt{3}R/2D^{11},(h+R-R/2)/D^{11})$

$S_4(-\sqrt{3}R/2D^{11},0,(h+R-R/2)/D^{11})$

Evaluation of A and A^{-1} matrices: $B^{11} \triangleq 1 - \frac{h+R/2}{D^{11}}$

$$A = \begin{bmatrix} 0 & 0 & \sqrt{3}R/2D^{11} \\ \sqrt{3}R/2D^{11} & -\sqrt{3}R/D^{11} & \sqrt{3}R/2D^{11} \\ B^{11} & 0 & 0 \end{bmatrix}$$

$$|A| = \frac{3B^{11}R^2}{2D^{11^2}}$$

$$A^{-1} = \frac{2D^{11^2}}{3B^{11}R^2} \begin{bmatrix} 0 & 0 & 3R^2/2D^{11^2} \\ \sqrt{3}RB^{11}/2D^{11} & -\sqrt{3}RB^{11}/2D^{11} & 3R^2/4D^{11^2} \\ \sqrt{3}RB^{11}/D^{11} & 0 & 0 \end{bmatrix}$$

$$\begin{bmatrix} 0 & 0 & 1/B^{11} \\ D^{11}/\sqrt{3}R & -D^{11}/\sqrt{3}R & 1/2B^{11} \\ 2D^{11}/\sqrt{3}R & 0 & 0 \end{bmatrix}$$

Evaluation of $\sigma^2(\delta x_j)$:

$$\sigma^2(\delta x_1) = \frac{1}{B^{11^2}} (\sigma_3^2+\sigma_4^2)$$

$$\sigma^2(\delta x_2) = \frac{D^{11^2}}{3R^2} \sigma_1^2 + \frac{4D^{11^2}}{3R^2} \sigma_2^2 + \left(\frac{D^{11}}{\sqrt{3}R} + \frac{1}{2B^{11}} \right)^2 \sigma_3^2 + \frac{1}{4B^{11^2}} \sigma_4^2$$

$$\sigma^2(\delta x_3) = \frac{4D^{11^2}}{3R^2} (\sigma_1^2+\sigma_2^2)$$

Numerical Results: h = 22375 miles, R = 3985 miles

D^{11} = 24615 miles, B^{11} = 0.01

$$\sigma^2(\delta x_1) \approx 10^4 (\sigma_3^2+\sigma_4^2)$$

$$\sigma^2(\delta x_2) \approx 12.7 \sigma_1^2 + 50.8 \sigma_2^2 + 2869 \sigma_3^2 + 2500 \sigma_4^2$$

$$\sigma^2(\delta x_3) \approx 50.8 (\sigma_1^2+\sigma_2^2)$$

1.8.1.1 Discussion of Examples

If we assume a common rms range error σ for all stations, the corresponding rms position errors of the TDRS for the three examples presented are as follows

	σ_{x_1}/σ	σ_{x_2}/σ	σ_{x_3}/σ
Example 1	200	101	12
Example 2	400	60	12
Example 3	141	74	10

It is evident from this simple case that the vehicle-stations geometry plays an important role in specifying the vehicle position error, and that no definite conclusions should be drawn from particular examples which may or may not represent actual operational conditions. Moreover, the previous analysis was based on a single-measurement error (ensemble-averaged over the random error contribution); as time elapses the vehicle-stations geometry varies and consecutive single-measurement rms errors may exhibit a relevant variation due to the changing geometry. Needless to say, smoothing of consecutive range measurement samples (say, using least-square error curve-fitting procedures) and/or the actual orbital determination techniques being used will affect the effective vehicle position error and should be included for a proper perspective under the circumstances. Still, an interesting feature exhibited by the three examples considered above is that: (a) when going from Ex. 1 to Ex. 2 the only effect was moving the first station closer to the second, and the location error was somewhat degraded by the doubling of the first-coordinate rms error (though σ_{x_2} was reduced), (b) when going from Ex. 1 to Ex. 3 the second, third and

fourth stations were separated further from the first one and from each other, and the location error was somewhat reduced in all three coordinates. Whether or not this is representative of a pattern linked to station separation considerations, and if so then whether or not the pattern is strongly linked to the use of range-difference methods, seem to be important questions that merit further examination in the future since perhaps station location principles and recommendations could arise from such a study.

With reference to the error contribution due to station location uncertainty, the formulation of Eq. 1.82 yields the following results for the case where a common location error δ_p (say, 10m) is assumed for all coordinates and all stations:

	δ_{x_1}/δ_p	δ_{x_2}/δ_p	δ_{x_3}/δ_p
Example 1	33	18	1
Example 2	69	10	0.3
Example 3	28	15	1

Again the results illustrate the strong dependence on the particular system geometry assumed. Also, the same error-variation pattern previously noticed in the rms range-error contribution tabulation can now be observed, which further suggests that attention be given to the station locations.

1.8.1.2 User Position Location Considerations

In general, we can consider two possible cases regarding the user position-location principles: (a) there are 3 relay satellites in real-time contact with the user, or (b) there are only 1 or 2 TDRS's participating.

The other case of more than 3 satellites is not expected to occur. In the first case, the user position can be established from conventional trilateration techniques (3 real-time, independent, range measurements). In the second-case, a non-real-time procedure is to be used if independent measurements are to be preserved, e.g., range and range rate measurements from a common satellite are not independent measurements (the errors themselves may be statistically independent as when deriving range information from a sidetone or PN code and range rate information from a carrier doppler, since different noise bands enter into the problem, but the range and range rate are related through the orbit involved).

The formulation and notation for the case where 3 satellites are involved is summarized in Table 1.10, where it has been assumed for simplicity that each satellite is also tracked by a trilateration procedure (a satellite tracking procedure based on 3 range differences from 4 stations only requires a re-interpretation of the B-matrices and the q-parameters). The basic results are Eqs. 1.89 and 1.90 of the table, which give an explicit user position error in terms of user and satellite ranging errors and ground station location errors. A covariance error analysis analogous to that presented for the satellite location problem now becomes extremely complex due to the multiple geometries involved.

It is understood that the case where only 1 or 2 satellites are in real-time contact with a given user will probably characterize most of the practical situations. In this case the use of non-real-time data processing is recommended for a more efficient orbital determination. Under such conditions, the interest is not to consider a position error analysis based on ensemble-averaging over a single measurement, but to

account for the non-real-time smoothing and specific orbital determination procedure to be employed. It should be evident that this represents a complex problem which merits further investigation.

1.8.1.3 Conclusion

In Section 1.8, we have presented a TDRS positive-location error analysis for the case where the TDRS coordinates are determined from three range differences involving four stations. In Appendix 5, we also present the analogous formulation and results for the case where three range measurements from three stations are used to determine the TDRS location. In both cases, expressions and numerical results have been derived for the single-measurement error contributions due to station location uncertainties and rms range measurement errors. For the specific examples considered, the resultant TDRS location errors corresponding to the range-differences procedure exhibited greater magnitudes than their counterparts on a 3-range procedure, as well as a stronger dependence on the particular stations-satellite geometry assumed. It should be understood these comments refer to single-measurement location errors, and should be revised for a given data smoothing or orbital determination principle actually used.

With reference to the user position location errors, the limitation of only 1 or 2 TDRS's being in real-time contact with a user (which is the expected operational situation) suggests a position error analysis based on more than one single measurement, and this introduces the need to account for the aforesaid non-real-time smoothing operations and orbital determination procedures employed, which is beyond the scope of the present report.

TABLE 1.10

Formulation

$$r_j = \{\sum_{i=1}^{3} [x_i - p_i^{(j)}]^2\}^{1/2}$$

$$\delta r_j = \sum_{i=1}^{3} A_{ij}[\delta x_i - \delta p_i^{(j)}]$$

$$\delta x_k = \sum_{j=1}^{3} (A^{-1})_{kj}[\delta r_j + \sum_{i=1}^{3} A_{ij}\delta p_i^{(j)}] \qquad \text{eq. 1.89}$$

$$\delta p_i^{(j)} = \sum_{\ell=1}^{3} [B^{(j)}]^{-1}_{i\ell} [\, S_\ell^{(j)} + \sum_{m=1}^{3} B_{m\ell}^{(j)}\, q_m^{(\ell)(j)}] \qquad \text{eq. 1.90}$$

Notation

x_i = i-th coordinate of user

$p_i^{(j)}$ = i-th coordinate of j-th satellite

r_j = user range measurement by j-th satellite

A_{ij} = i-th directional cosine of user with respect to j-th satellite

$B_{m\ell}^{(j)}$ = m-th directional cosine of j-th satellite with respect to ℓ-th station

$S_\ell^{(j)}$ = j-th satellite range measurement by ℓ-th station

$q_m^{(j)(\ell)}$ = m-th coordinate error of j-th satellite due to ℓ-th station location error

1.8.2 General Ranging System Considerations

The ranging operation involves measurement of the round-trip delay of the ranging event (e.g., sidetone zero crossing, PN code structure, r-f pulse edges) along the two propagation paths illustrated in Fig. 1.43 The GS-TDRS-GS path (P-I) provides direct ranging of the TDRS, while the GS-TDRS-user-TDRS-GS path (P-II) provides indirect ranging of the user. The path P-I is assumed to be free from channel disturbances (multipath, interference) other than additive noise, while the path P-II suffers from such disturbances in the TDRS-user-TDRS transmission link, plus has the added constraint of sustaining an asynchronous variable-loading, multiple-access, communication link.

1.8.2.1 Side-Stepping Repeater Characteristics

The simplest form of TDRS processor to be used in paths P-I and P-II consists of a side-stepping repeater that heterodynes the received signals with its own incoherent local oscillator. Such a repeater is compatible with a multiple-access operation and minimizes the TDRS system complexity. Also, such a repeater is compatible with wideband PN, PRTH, or adaptive time hop (side tone) ranging.

1.8.2.2 PN Code Range Rate Considerations

If the range rate is to be derived from the ranging signal itself, i.e., from the time-varying fluctuations of the PN-code round-trip delay, then again a side-stepping TDRS repeater is applicable and no carrier coherence is required from the TDRS or user transponders as a processing constraint; only the coherent code interchange (GS code by specific user code) is required at the user transponder. However, if

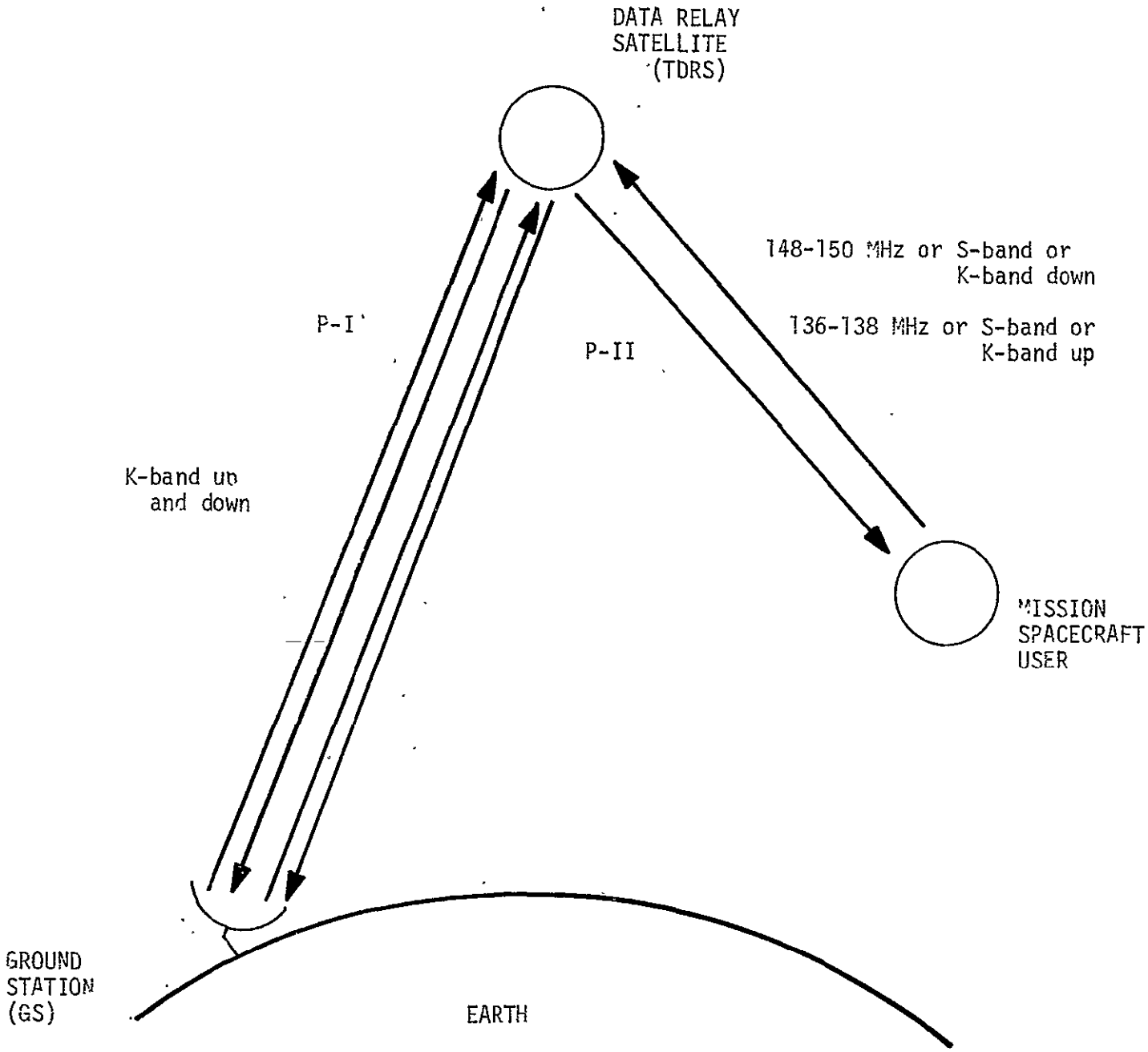

Fig. 1.43 Ranging Signal Propagation Paths

the range rate extraction is to be based on carrier doppler techniques, then the simple side-stepping configuration is somewhat limited in its performance capability, as is now made evident.

To illustrate the issues, consider the effective carrier processing that occurs when employing a side-stepping repeater configuration for the TDRS processing of both the GS and user signals. If the user is assumed to act as a coherent (phase-locked) transponder for the carrier as well, then the effective system processing is that indicated in Figure 1.44 where the net carrier processing is presented and the corresponding modulation processing is omitted for simplicity. The $\pm$ symbol is used to indicate that either of the two signs can be used in the analysis. For example, consider the case where the GS received carrier is given by

$$\underbrace{Nf_o - \frac{K}{M}(Mf_o - f_c)}_{\text{TDRS-GS carrier (down-link)}} + \underbrace{ND_o - \frac{K}{M}[M(D_o+2D_o')-(2D_c+2D_c')]}_{\text{path P-II doppler effect (neglecting 2nd-order effects)}} \qquad \text{eq. 1.91}$$

Note that the pertinent carrier frequencies are specified by f_c for the GS-TDRS transmission, $Mf_o - f_c$ for the TDRS-user transmission, $\frac{K}{M}(Mf_o - f_c)$ for the user-TDRS transmission, and $Nf_o - \frac{K}{M}(Mf_o - f_c)$ for the TDRS-GS transmission. Also note the primed symbols in the doppler term represent doppler acquired in the TDRS-user-TDRS baseline propagation, while unprimed terms represent path P-I doppler effects. In particular, the doppler effect may be decomposed as

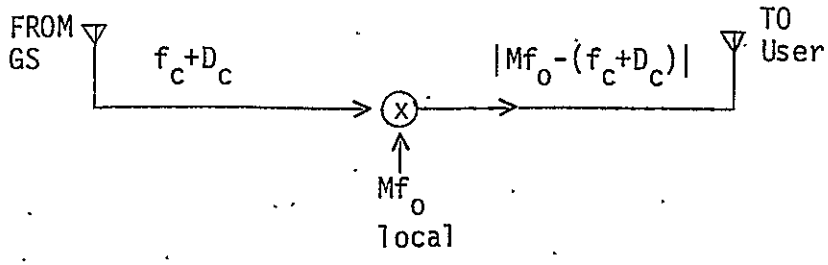

(a) TDRS side-stepping of GS signal

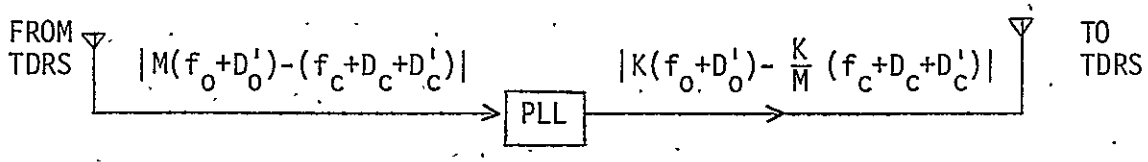

(b) User coherent turnaround of TDRS signal

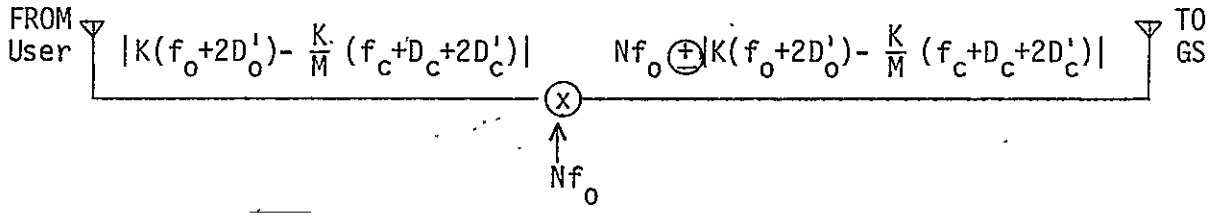

(c) TDRS side-stepping of User signal

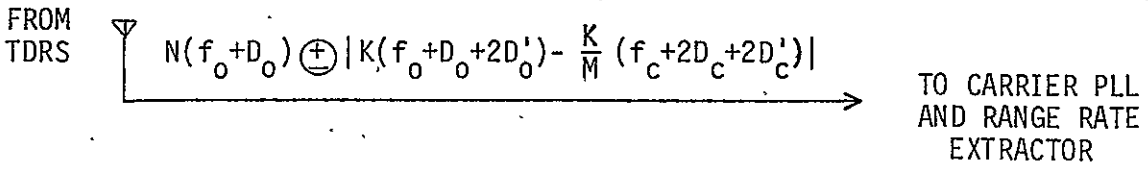

(d) GS receiver signal from TDRS

Figure 1.44: Carrier Processing over Path P-II using a Side-Stepping TDRS and a Coherent User Transponder

$$\underbrace{[ND_o - \frac{K}{M}(MD_o - 2D_c)]}_{\text{GS-TDRS link doppler effect}} \qquad \underbrace{[\frac{K}{M}(2MD_o' - 2D_c')]}_{\text{TDRS-user link doppler effect}} \qquad \text{eq. 1.92}$$

where the 1st term is approximately the 2-way GS carrier doppler around the GS-TDRS baseline, and the 2nd term is approximately the 2-way user carrier doppler around the TDRS-user baseline. For example, assuming the operational values f_c = 14 gHz, $Mf_o - f_c$ = 148 mHz, $\frac{K}{M}(Mf_o - f_c) = \frac{221}{240}$ (148 mHz), $Nf_o - \frac{K}{M}(Mf_o - f_c) = \frac{221}{240}$ (14 gHz), we have the doppler effect:

$$\underbrace{ND_o - \frac{K}{M}(MD_o - D_c)}_{\substack{\text{1-way doppler on} \\ \text{TDRS-GS baseline} \\ \text{at } \frac{221}{240} \text{ (14 gHz)}}} + \underbrace{\frac{K}{M} D_c}_{\substack{\text{1-way doppler on} \\ \text{GS-TDRS baseline} \\ \text{at } \frac{221}{240} \text{ (14 gHz)}}} - \underbrace{\frac{K}{M}(2MD_o' - 2D_c')}_{\substack{\text{2-way doppler on} \\ \text{user-TDRS baseline} \\ \text{at } \frac{221}{240} \text{ (150 mHz)}}} \qquad \text{eq. 1.93}$$

This composite doppler is first tracked by the GS receiver carrier loop, and then fed to the range rate extractor subsystem at the GS receiver. If the TDRS orbital dynamics are such that the GS-TDRS baseline doppler effects (at the GS carrier frequency) are negligible relative to the TDRS-user baseline doppler effects (at the user carrier frequency), then the unprimed terms can be neglected and the system processing of Fig. 1.44 will directly yield a useful measure of the TDRS-user baseline doppler. However, if the TDRS orbital dynamics are not negligible to this effect, then one must consider the possible ways in which the available path P-I measurement of $2D_c$ can be incorporated to solve the problem; otherwise, the simple side-stepping TDRS configuration of Fig.1.44 is not useful.

The orbital dynamics of a TDRS will depend upon the angle of inclination of the synchronous satellites. As stated in our requirements analysis section, there can be either a 3 or 4 satellite configuration for a TDRS system and we can expect that inclination angles of 10°-20° might be used to provide extended coverage and improved user position error performance. Depending upon the ground station location relative to the TDRS and the angle of inclination; e.g., 10°-20°, a TDRS's relative motion with respect to a ground station can produce significant doppler. The up and down links between a ground station and a TDRS are at K_u-band and, while the velocity of the spacecraft is only 300 to 1000 meters per second depending on angle of inclination, the motion can produce doppler on the ground station to TDRS link of the order of 14 KHz. It is obvious that this one-way doppler frequency between the ground station and the TDRS at K_u-band is significantly greater than the expected one-way doppler between the TDRS and the user at VHF.

A possible approach is to use the available 2-way doppler measurement on the path P-I carrier (say, 14 gHz) to compensate for the two $\frac{221}{240}$ (14 gHz) doppler terms. Thus the receiver would yield 2-way VHF doppler on the user-TDRS baseline. Also, the doppler measurement available from path P-I can be used to aid the user acquisition process by transmitting $f_c - D_c$ instead of f_c at the GS. The resultant doppler conditions for a side-stepping TDRS and a coherent user are illustrated in Fig.1.45 ; the D_c term is now absent from the doppler effect appearing at the user input, so only VHF doppler caused by user orbital dynamics relative to the TDRS need be considered for user acquisition purposes.

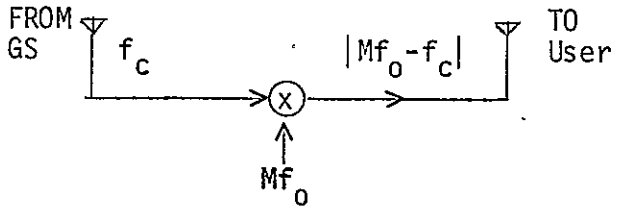

(a) TDRS side-stepping of GS signal

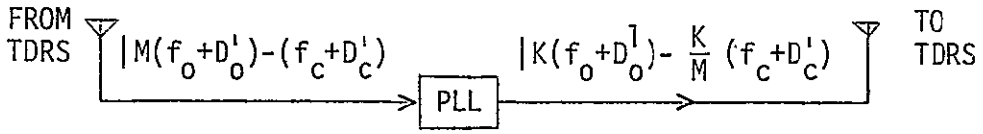

(b) User coherent turnaround of TDRS signal

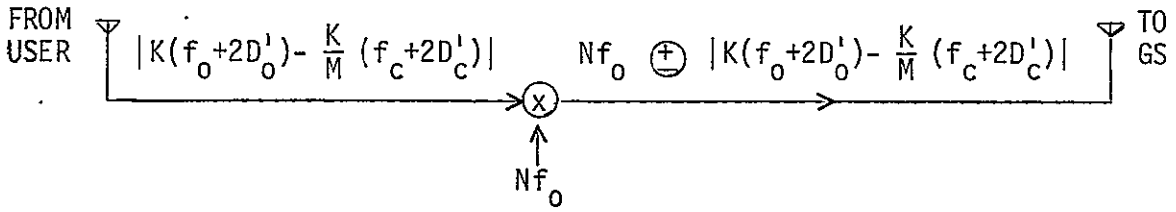

(c) TDRS side-stepping of user signal

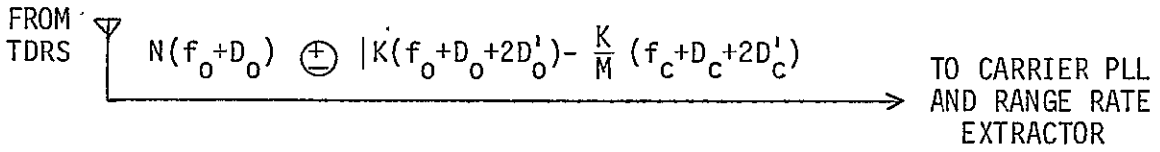

(d) GS receiver signal from TDRS

Figure 1.45 : Carrier Processing over Path P-II using a Side-Stepping TDRS and a Coherent User Transponder, plus Path P-I Doppler Aid

Also note that the GS receiver doppler effect only differs from that of Eq.1.93 by the absence of the $\frac{K}{M} D_c$ term, so the interest now is to compensate only one $\frac{221}{240}$ (14 gHz) doppler term with the available doppler measurements from path P-I.

Another possible approach is to attempt the measurement of $2D_c+2D'_c$ from the received doppler term, since then the available $2D_c$ data from path P-I can be used to yield $2D'_c$ (the 2-way TDRS-user baseline doppler at 14 gHz). The received doppler of Eq.1.93 can also be decomposed as

$$\underbrace{\frac{K(2D_c+2D'_c)}{M}}_{\substack{\text{2-way doppler on path P-II link of TDRS-GS carrier} \\ (\frac{221}{240} \times 14 \text{ gHz})}} - \underbrace{2\,KD'_o}_{\substack{\text{2-way doppler on TDRS-user baseline of user-TDRS carrier} \\ (\frac{221}{240} \times 148 \text{ mHz})}} \qquad \text{eq. 1.94}$$

where $ND_o = \frac{K(MD_o)}{M}$ was used in the derivation. It is evident that the desired compensation of the D'_o term will require propagation of an independent TDRS-generated reference (derived from f_o) through the TDRS-user baseline, but such an additive signal would be unprotected to the channel multipath and interference signals being added to its baseband, which would hinder its extraction (regardless of its point of detection). One could of course protect such a signal by modulating it with a TDRS-generated PN code, or by sending it as an added modulation on the GND-originated

carrier since the latter is PN-protected, but in neither case the simple side-stepping TDRS configuration will be preserved and we might as well consider the problem from scratch with a broader mind on the TDRS configuration. This is done in section 1.8.3 to illustrate the system complexity required if a feasible compensated extraction of the $2(D_c+D_c')$ term is implemented.

1.8.3 Range Rate Considerations: Two-Way Carrier-Doppler Systems

The range rate information can be established from two-way doppler measurements on a coherent carrier, or derived from the phase fluctuations of the ranging event itself. The first approach has a greater range rate resolution capability, and may be desirable if proven to be feasible. To this effect, it is of interest to consider the pertinent signal-processing alternatives at the TDRS and user transponder, and through them investigate the various coherent-carrier reproduction approaches and recognize their advantages and limitations.

The basic alternatives are illustrated in Fig. 1.46 , where the modulation processing is again omitted for simplicity. In Case 1, we have an incoherent transponder that merely heterodynes the received carrier with a local oscillator to generate the output carrier. In Case 2, the incoherent conversion is again present but now the oscillator signal is also transmitted as an additive unmodulated reference at a convenient frequency. In Case 3, the incoherent conversion generates a subcarrier that is phase-modulated on a carrier derived from the local oscillator (i.e., GRARR transponder). In Case 4, we have a coherent transponder based on phase-locked techniques.

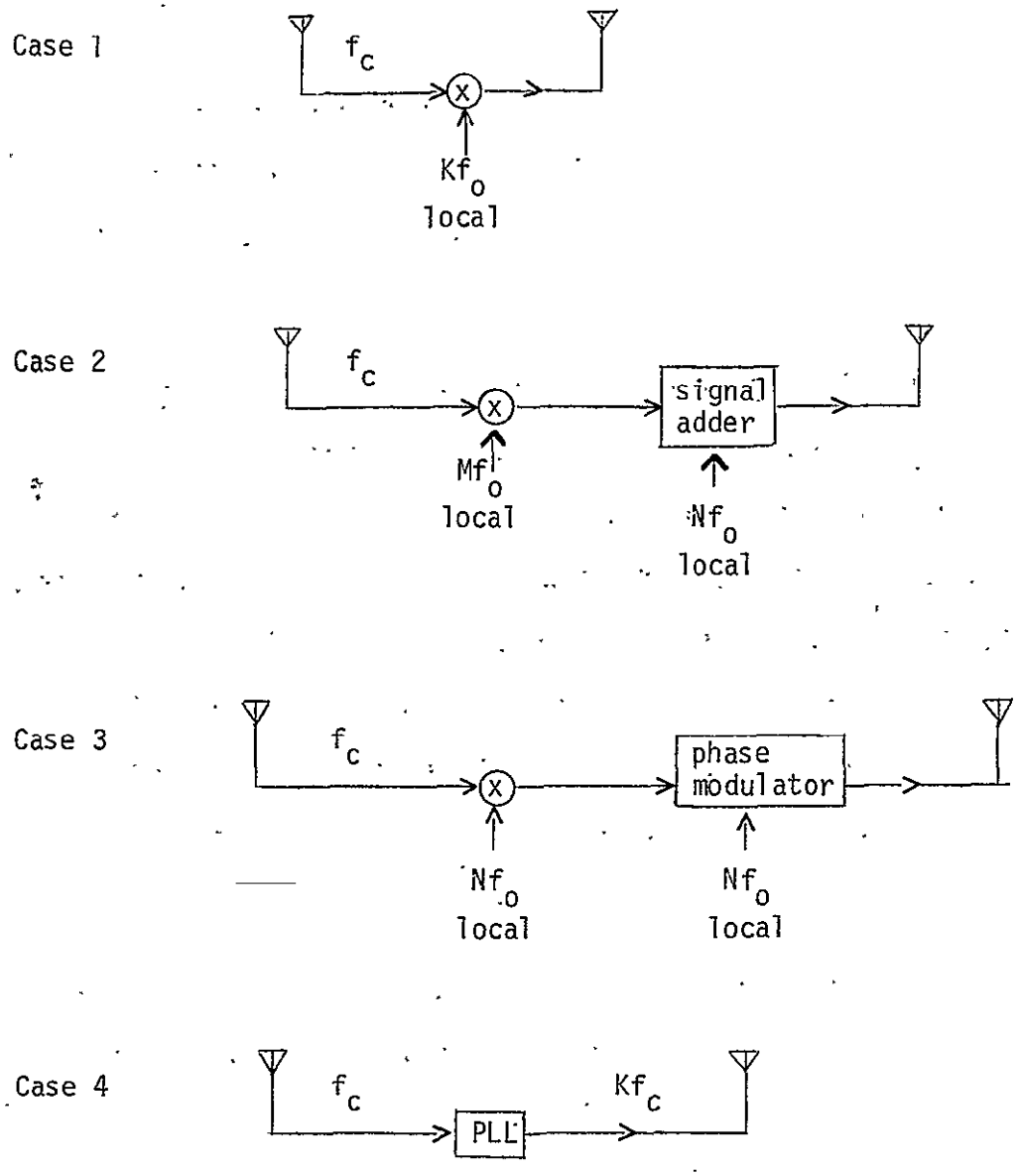

Figure 1.46 : Transponder Processing Alternatives

1.8.3.1 Doppler Extraction in Path P-I

We now consider the processing alternatives of Fig. 1.45 as the TDRS processing of the GS turn around signal in path P-I. The Case 1 does not permit a coherent two-way carrier reproduction, and is thus undesirable. The Cases 2-4 are permissible, and their respective doppler extractions are shown in Figs. 1.47-8-9 . The Cases 2 and 3 do not require acquisition and loss-of-lock search modes to be implemented at the TDRS; however, this need not be considered a crucial advantage over Case 4 since the small TDRS orbital dynamics and the corresponding small phase dynamics may permit a narrowband loop design and relax the acquisition-tracking vs. threshold performance compromise. However, remodulation of a PN ranging code in the coherently extracted and converted carrier will involve some additional signal processing in Case 4, but not in Cases 2-3. The path P-II signal processing exhibits more conceptual design constraints than that of path P-I, and it is thus better to postpone any path P-II discussion and recommendation until the path P-I alternatives are evaluated, in order to include interfacing considerations.

1.8.3.2 Doppler Extraction in Path P-II

We next consider the processing alternatives of Fig. 1.46, first as the TDRS processing of the GS-generated signal being retransmitted to the user, then as the user processing of the TDRS-retransmitted signal being turned around back to the TDRS, and finally as the TDRS processing of the user-generated signal being relayed back to GS. In all situations, we have to recognize certain restrictions that were absent in the previous discussion concerning the TDRS processing of the path P-I signal. These restrictions

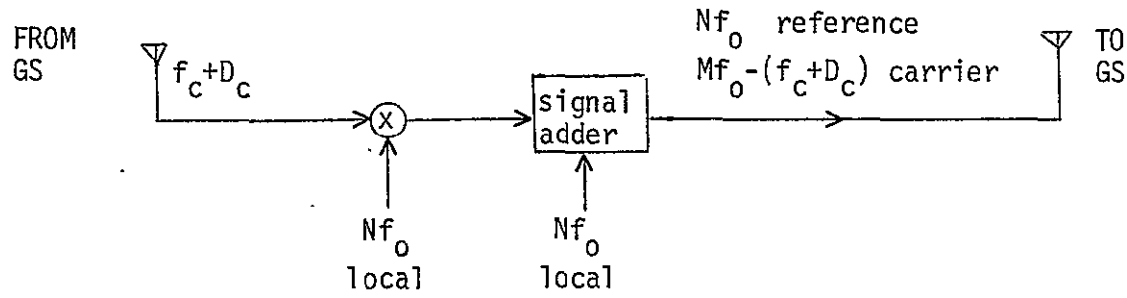

(a) TDRS-GS turnaround, Case 2

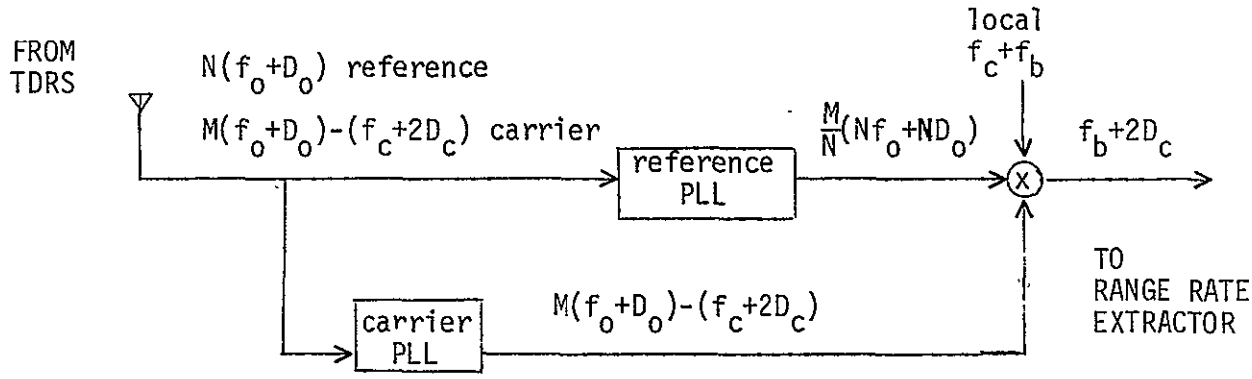

(b) GS receiver processing

Legend:
- f_c = GS - TDRS link carrier
- D_c = GS - TDRS link
- f_o = TDRS local oscillator
- D_o = GS - TDRS link doppler on f_o
- f_b = bias coherent to f_c

Figure 1.47: Two-Way Carrier Doppler Extraction:
Path P-I, Case-2 TDRS

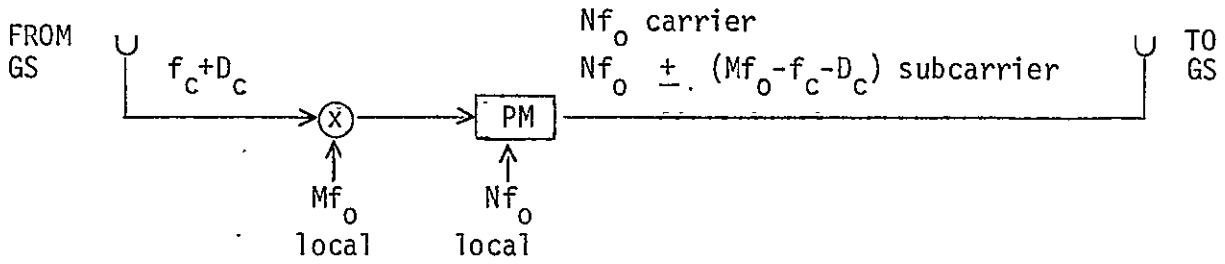

(a) TDRS-GS turnaround, Case 3

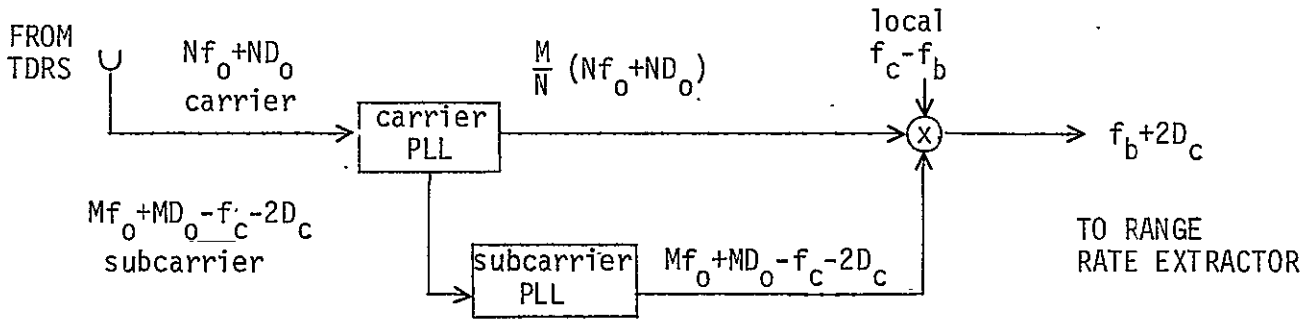

(b) GS receiver processing

Legend: f_c = GS-TDRS link carrier

D_c = GS-TDRS link doppler on f_c

f_o = TDRS local oscillator

D_o = GS-TDRS link doppler on f_o

f_b = bias coherent to f_c

Figure 1.48 : Two-Way Carrier Doppler Extraction: Path P-I, Case-3 TDRS

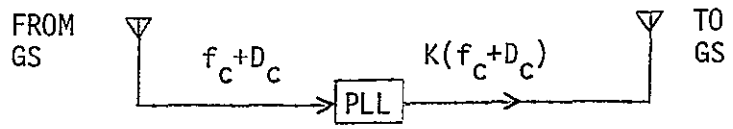

(a) TDRS-GS turnaround, Case 4

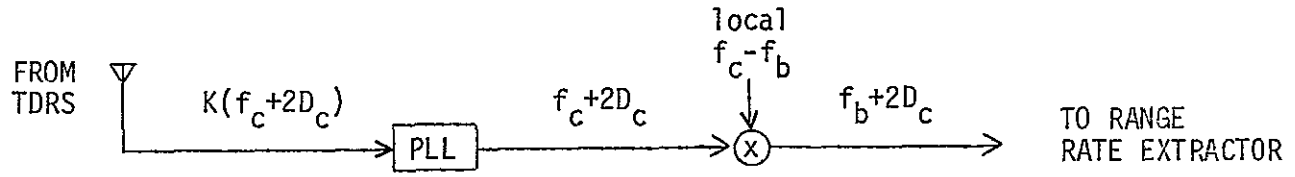

(b) GS receiver processing

Legend: f_c = GS-TDRS link carrier

D_c = GS-TDRS link doppler on f_c

f_b = bias coherent to f_c

Figure 1.49 : Two-Way Carrier Doppler Extraction:
Path P-I, Case-4 TDRS

involve the existence of channel multipath and interference in the TDRS-user and user-TDRS transmission links, the user demodulation of the TDRS-retransmitted carrier to extract its message, and the multiple-access capability of the user-TDRS-GS return link.

With reference to the TDRS processing of the GS signal for path P-II, Case 1 is permissible but neither Case 2 or 3 are desirable since the multipath or interference protection existing in the original signal (PN code) will be absent in the Nf_0 component, and the eventual extraction of the latter (whether taking place at the user, TDRS or GS) will be hindered by the aforesaid disturbances being added to its baseband. In Case 2 the Nf_0 reference may become undetectable and we might as well use Case 1. In Case 3 the picture is worse since now we have a protected subcarrier on an unprotected carrier, which is undesirable. The processing of Case 4 is permissible with the understanding that again the PN-code protection is remodulated on the carrier sent to the user, a somewhat more complex TDRS processing than in Case 1.

With reference to the user processing, again Case 1 is permissible, and again Cases 2 or 3 are undesirable since they respectively yield an unprotected reference and carrier. Also Case 4 is again permissible, except that now the phase-locked processing and signal remodulation are not a total extra burden as in the TDRS processing since carrier demodulation, message extraction, and PN-code synchronization and interchange is already taking place at the user.

With reference to the TDRS processing of the user-generated signal, Cases 1 and 2 are permissable and remain relatively simple in a multiple-access mode. In Case 3 the multiple-access introduces the problem of maintaining the modulation indices at a proper value regardless of the number of users, which could result in a complex format since variable loading is possible. In Case 4 the situation is worse since a multiple acquisition and loss-of-lock search mode must also be incorporated in the variable-loading, multiple-access format.

It should be understood that in the last three paragraphs we have evaluated the TDRS and user processing alternatives in path P-II only on the basis of their compatibility to a multiple-access operation in the multipath and interference environment, without any consideration to their potential to eventually yield a coherent carrier reproduction at the GS receiver. The results of this preliminary evaluation are summarized for reference purposes:

	TDRS processing of GS signal	user processing of TDRS signal	Processing of user signals
Case 1	OK minimum complexity	OK no complexity advantage since user processes modulation	OK minimum complexity
Case 2	NO- reference unprotected	NO reference unprotected	OK no complexity
Case 3	NO- carrier unprotected	NO carrier protected	OK-perhaps loading complexities
Case 4	OK some complexity to process modulation	OK compatible with user processing modulation	NO considerable complexity

Next, the interest is to consider which combinations of the permissible processings can indeed yield a two-way carrier doppler reproduction. It should be first noted that a non-phase-locked receiver (Cases 1-3) is to be used at the TDRS to process the user-generated signal. For the GS-generated signal, the TDRS processing is still open regarding the use of phase-locked techniques or not, and on this basis we will designate the TDRS as either an incoherent transponder (no PLL's either way) or a partially-coherent transponder (PLL for GS signal, no PLL for user signal). Insofar as the user is concerned, it is evident that a coherent transponder processing is the desired case, since a Case 1 transponder would suffer from the inability to eventually compensate for the user-TDRS subpath doppler of the user local oscillator.

Finally, one could also consider a variation of Cases 2 and 3 for the TDRS processing of the GS signal and the user processing of the TDRS signal, namely the locally-generated reference and carrier in question are assumed to be protected by a locally-generated PN code so that they become detectable. Some pertinent considerations result from these new alternatives and their discussion is postponed until the two-way carrier doppler reproduction is investigated for the four cases originally tabulated.

1.8.3.3 Case of an Incoherent TDRS

We first assume Case 1 for the TDRS processing of the GS signal, with a coherent user transponder. It was already illustrated in Fig. 1.44

that the use of Case 1 for the TDRS processing of the user signal will not permit compensation of the TDRS oscillator doppler by the GS receiver. Moreover, the use of Case 2 for the TDRS processing of the user signal will not accomplish the task either, since only the D_0 terms will be compensated while the predominant $2KD_0'$ doppler will remain. Finally, the use of Case 3 for the TDRS processing of the user signal is not acceptable either, as illustrated in Fig. 1.50, for the same reason.

1.8.3.4 Case of a Partially-Coherent TDRS

We now assume Case 4 for the TDRS processing of the GS signal, with a coherent user transponder. It is clear that the use of Case 1 for the TDRS processing of the user signal will not yield doppler compensation at the GS receiver, since the transmission will be characterized by a common coherent carrier in the GS-TDRS-user-TDRS link, plus an incoherent oscillator added in the last (TDRS-GS) link with its uncompensated doppler appearing on the received carrier. However, the use of Cases 2 or 3 for the TDRS processing of the user signal can provide the desired doppler compensation as illustrated in Figs. 1.51 and 1.52. The use of Case 2 has a complexity advantage over Case 3 since the latter could involve a complex TDRS format to handle a variable-loading, multiple-access, assignment of modulation indices. In any case, the path P-I two-way doppler extraction would be that indicated in Fig. 1.49, since a coherent TDRS transponder is processing the GS-generated signal.

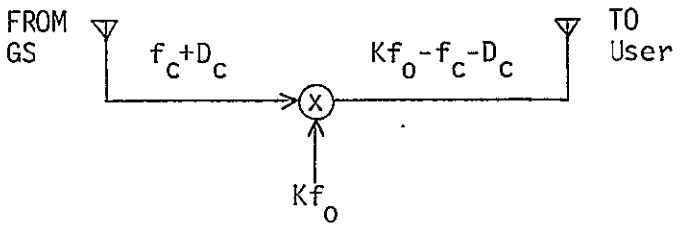

(a) TDRS Processing of GS signal, Case 1

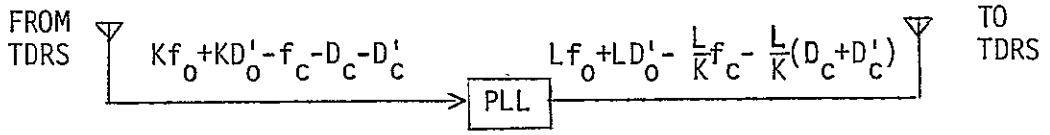

(b) User Coherent Processing of TDRS signal

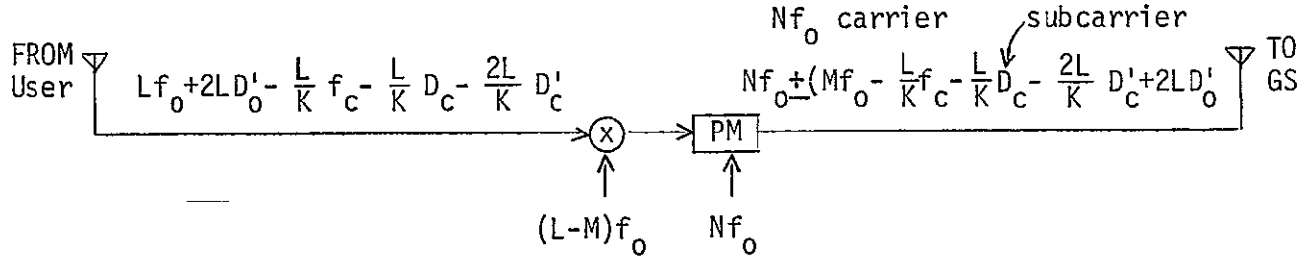

(c) TDRS Processing of GS signal, Case 3

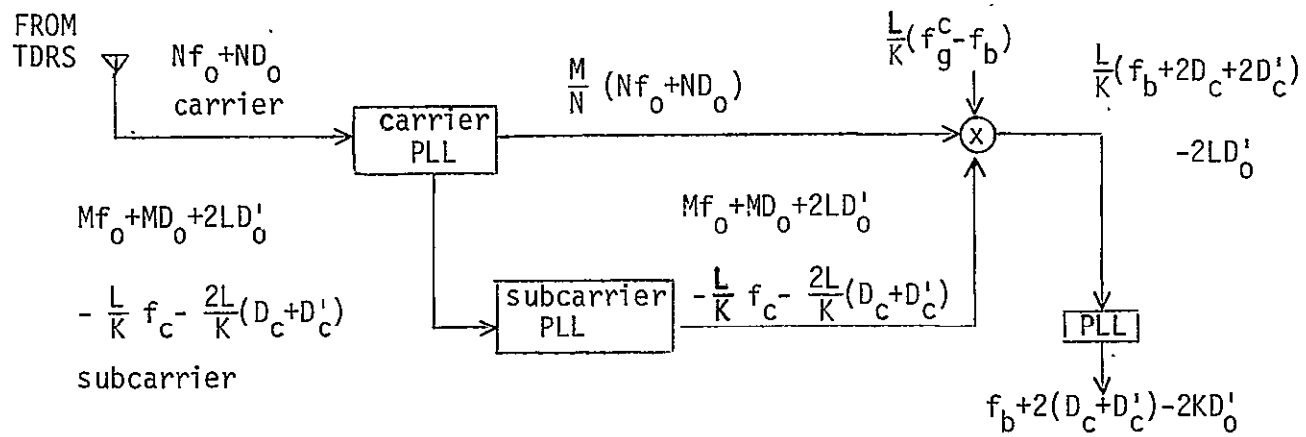

(d) GS receiver processing

Legend: f_c = GS-TDRS link carrier

D_c = GS-TDRS link doppler on f_c

D_c' = TDRS-User link doppler on f_c

f_o = TDRS local oscillator

D_o = GS-TDRS link doppler f_o

D_o' = TDRS-User link doppler on f_o

Figure 1.50 : Extension of GRARR Technique to the TDRS assuming a coherent User and an incoherent TDRS

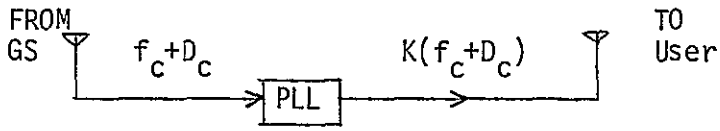

(a) TDRS processing of GS signal, Case 4

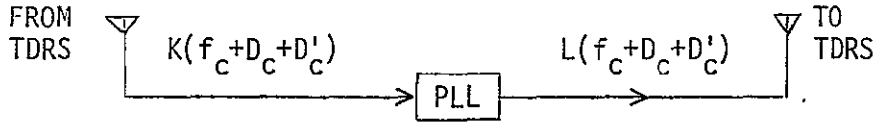

(b) User coherent processing of TDRS signal

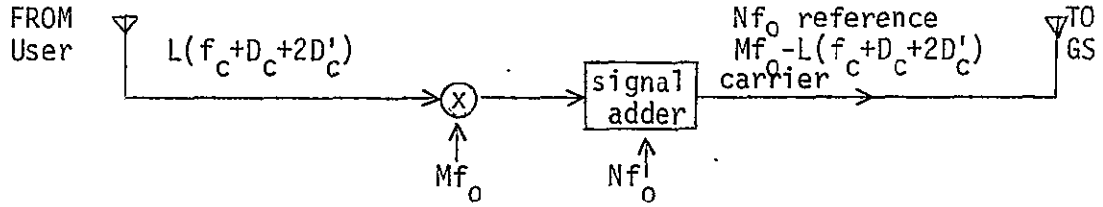

(c) TDRS processing of User signal, Case 2

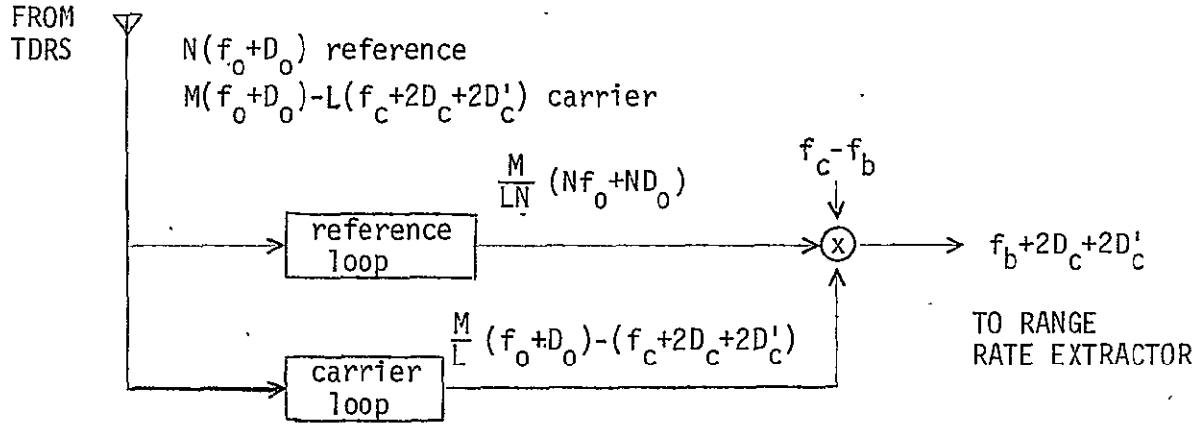

(d) GS receiver processing

Figure 1.51: Two-Way Carrier Doppler Extraction (path P-II) with a Partially-Coherent TDRS and a Coherent User: Independent-Reference Added in TDRS-GS Link

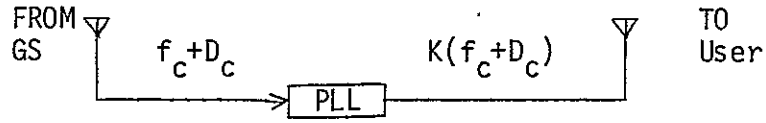

(a) TDRS processing of GS signal, Case 4

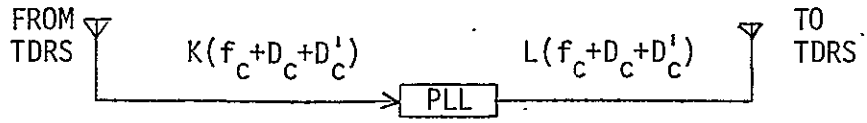

(b) User coherent processing of TDRS signal

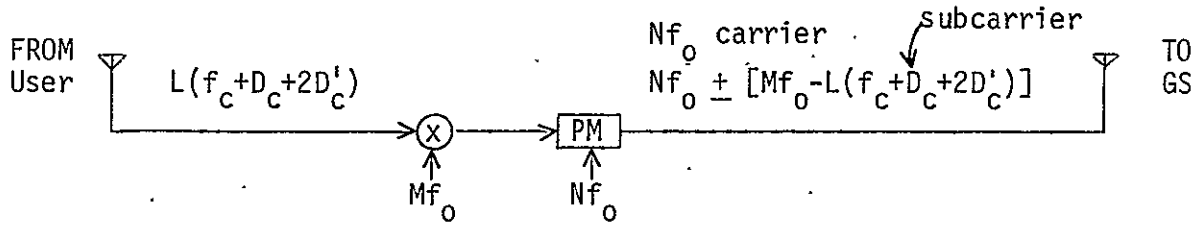

(c) TDRS processing of MSU signal, Case 3

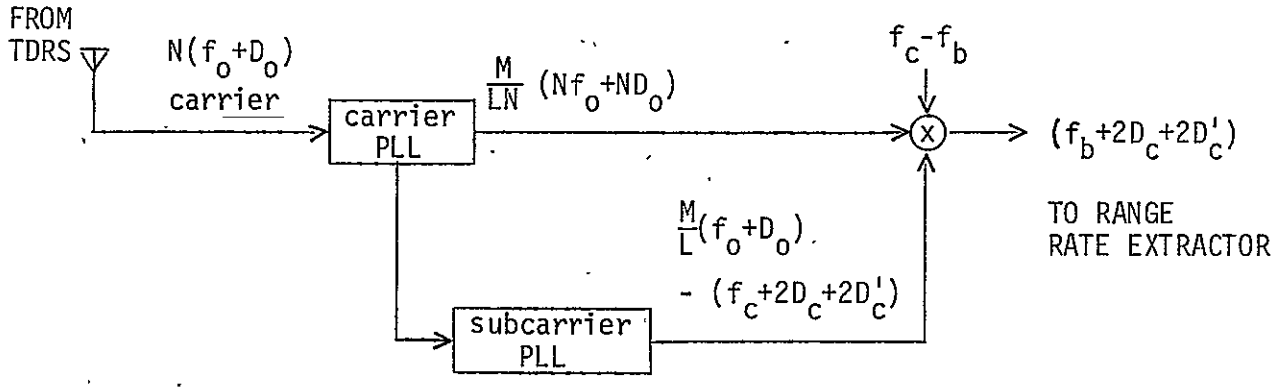

(d) GS receiver processing

Figure 1.52: Two-Way Carrier Doppler Extraction (path P-II) with a Partially-Coherent TDRS and a Coherent User: GRARR-Processing of User Signal by TDRS

1.8.3.5 Effect of Coded Reference and Carrier in Cases 2 and 3

We now consider the situation where Cases 2 and 3 are modified in the following way: the local reference or carrier now has a locally-generated PN code phase-modulated on it to provide detection immunity. In the TDRS, the transmission of an independent PN-protected reference to the user involves some system complexity to generate and modulate the local code, but the complexity is comparable to that of Case 4 (where re-modulation of the GS-generated code on the tracked carrier takes place), and Case 4 has been found to be the preferred method among those cases previously considered to be used to retransmit the GS signal to the user if two-way carrier doppler techniques are to be employed for range rate extractions. The protected reference generated at the TDRS can now be detected at the user in a multipath and interference environment, and it carries the TDRS-user link doppler of the TDRS local oscillator (which was the major uncompensated term hindering the two-way carrier doppler reproduction). This protected reference can be used to generate a coherent carrier with its proper doppler at the user for retransmission purposes, as indicated in Fig.1.53. Then Case 2 processing (unmodified) can take place at the TDRS for the retransmitted signal, and the doppler compensation taking place at the GS receiver now involves only the GS-TDRS link doppler of the local TDRS oscillator, as shown in Fig. 1.53.

The Case 3 can be analogously modified in the TDRS processing of the GS signal, and again the doppler compensation is derived between the user and the GS receivers, as illustrated in Fig. 1.54. The only difference

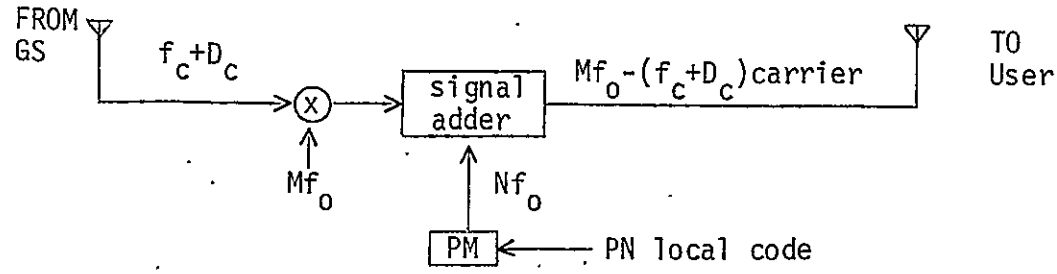

(a) TDRS processing of GS signal, Case 2 modified

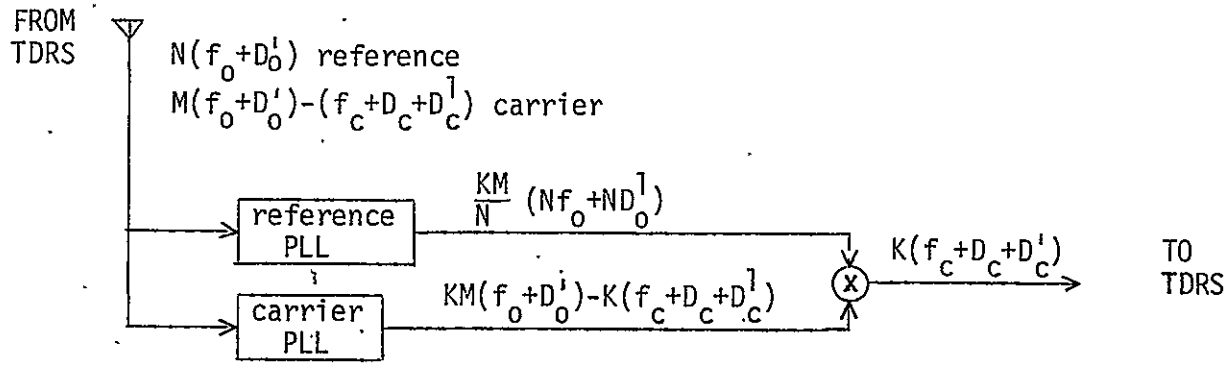

(b) User processing of TDRS signal

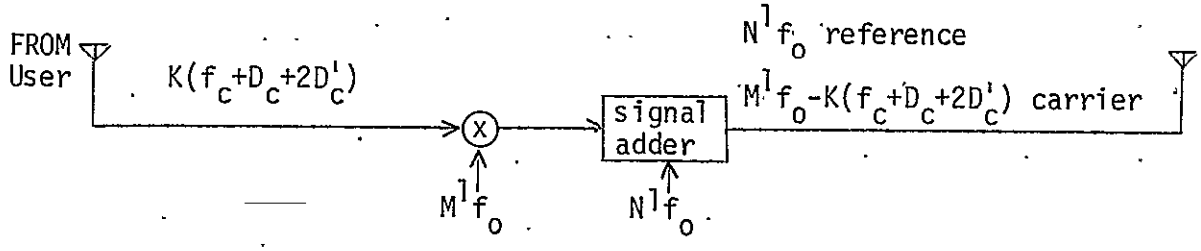

(c) TDRS processing of User signal, Case 2

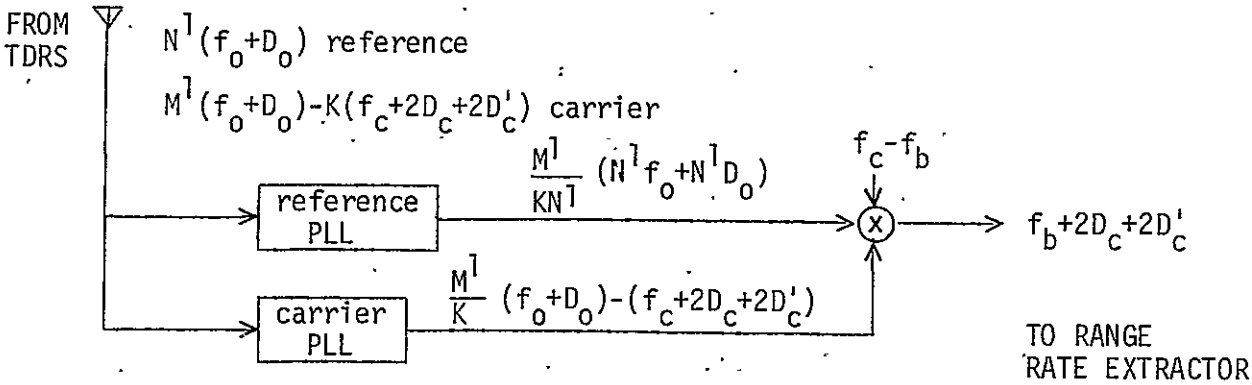

(d) GS receiver processing

Figure 1.53 Two-Way Carrier Doppler Extraction (path P-II) with an Incoherent TDRS and a Coherent User: Coded Reference Added in TDRS-MSU Link and Uncoded Reference Added in TDRS-GS Link

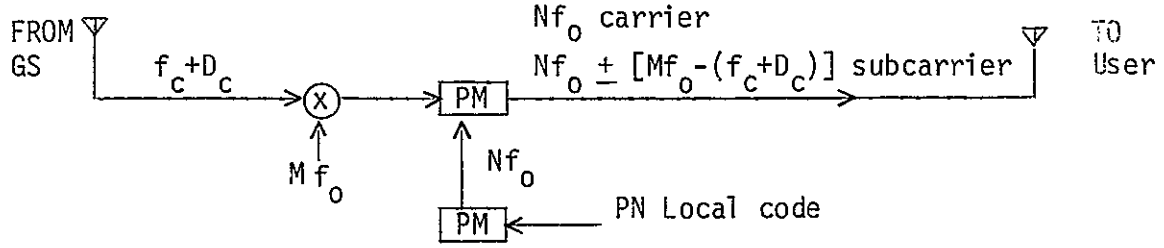

(a) TDRS processing of GS signal, Case 3 modified

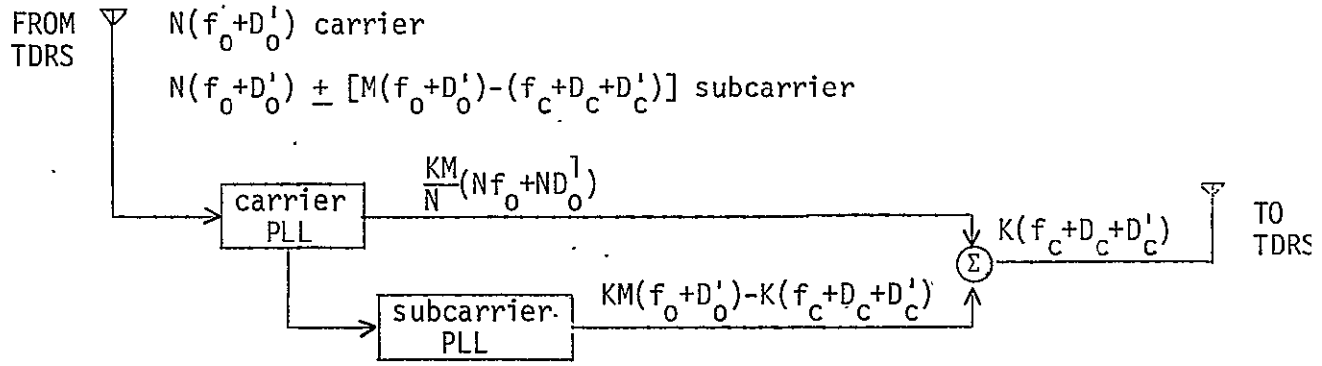

(b) User processing of TDRS signal

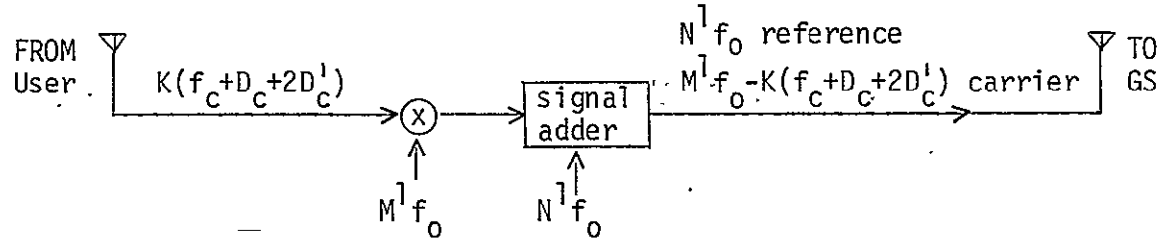

(c) TDRS processing of User signal, Case 2

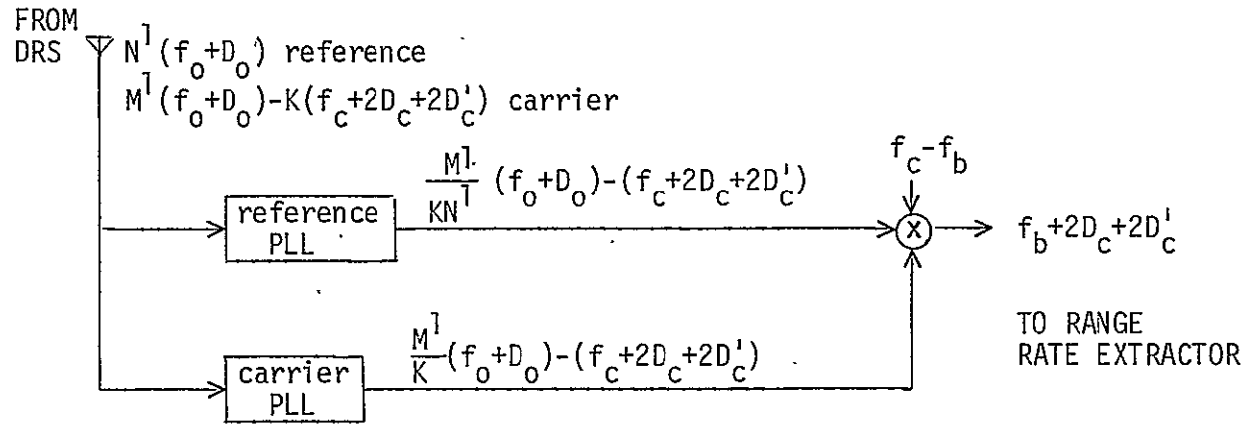

(d) GS receiver processing

Figure 1.54 : Two-Way Carrier Doppler Extraction (path P-II) using an Incoherent TDRS and a Coherent User: Coded-GRARR Processing of GS Signal by TDRS and Uncoded Reference Added in TDRS-GS Link

between the processings of Figs. 1.53 and 1.54 lies in reference modems vs. subcarrier modems. In the case of Fig.1.53 the path P-I processing would be that of Fig.1.47, while in the case of Fig.1.54 it would be that of Fig. 1.48.

It is not promising to consider the modified Cases 2 and 3 for the user processing from various considerations: (a) the multiple-access mode will produce 40 extra reference or carriers, (b) it is unnecessary in Figs.1.51-1.54, and (c) it cannot resolve the basic limitation of the uncompensated TDRS-user baseline doppler of an incoherent TDRS. It is also evident that the modified Cases 2 and 3 need not be considered for the TDRS processing of the user signals, since no special channel protection is required in the TDRS-GS link.

1.8.3.6 Summary and Comparative Evaluation of Two-Way Carrier Doppler Extraction Techniques

If two-way carrier doppler techniques are desired, the preliminary evaluation specified a coherent (phase-locked) user to process the TDRS signal, and a non-coherent (non-phase-locked) TDRS to process the user signals. A simple side-stepping TDRS processing of the GS and user signals was not capable of providing for local-oscillator doppler compensation at the GS receiver. Also, the inclusion of an uncoded local reference or GRARR-like carrier at the TDRS for doppler compensation purposes was restricted to the TDRS-GS transmission link, since the TDRS-user link is hindered by channel multipath and interference that would make such signals undetectable. The net effect was lack of compensation of the TDRS-user baseline doppler of the TDRS incoherent oscillator. In order to provide

the desired compensation in path P-II, the following four techniques resulted as potential TDRS-processing alternatives:

(a) Fig. 1.51 - Phase-locked conversion (Case 4) of the GS signal for transmission to the user, and side-stepping conversion of the user signals with inclusion of a local independent reference (Case 2) for transmission to the GS. The path P-I would use the processing of Fig. 1.49.

(b) Fig. 1.52 - Phase-locked conversion (Case 4) of the GS signal for transmission to the user, and GRARR-like conversion (Case 3) of the user signals for transmission to GS. The path P-I would use the processing of Fig.1.49.

(c) Fig. 1.53 - Side-stepping conversion of the GS signal with inclusion of an independent locally-generated coded reference (Case 2 - Modified) for transmission to the user, and side-stepping conversion of the user signals with inclusion of the independent uncoded reference (Case 2) for transmission to GS. The path P-I would use the processing of Fig. 1.47.

(d) Fig. 1.54 - GRARR-like conversion of the GS signal except that a coded carrier is used (Case 3 - Modified) for transmission to the user, and side-stepping conversion of the user signals with inclusion of the independent uncoded reference (Case 2) for transmission to GS. The path P-I would use the processing of Fig. 1.48.

The processing of Figs. 1.51 and 1.52 are identical in the GS-TDRS-user link, and essentially differ only in the TDRS processing of the user signals. The approach of Fig. 1.51 is preferred over that of Fig. 1.52 since the latter

could involve a complex format to adjust the modulation level in a variable-loading, multiple-access mode. In turn, the processings of Figs. 1.53 and 1.54are identical in the user-TDRS-GS link, where the multiple-access mode appears, and their relative merits lie in the complexity of independent-reference modems (Fig.1.53) vs. subcarrier modems (Fig.1.54).

With reference to Fig.1.51 vs. Figs.1.53-1.54, we note first that their processings are similar in the user-TDRS-GS subpath. Next, for the TDRS processing of the GS signal, Fig.1.51 exhibits a coherent conversion which is not required in Figs. 1.53-1.54. As previously mentioned, such coherent processing should not represent a fundamental limitation for Fig. 1.51 because of the small TDRS orbital dynamics. Also, the ranging-code remodulation required in the Fig. 1.51 b TDRS is comparable to the local PN-code modulation in Figs. 1.53 b - 1.54 b from complexity considerations. Note that in Figs. 1.53-1.54, the local PN-code inserted at the TDRS can be the same for all satellites since its purpose is to protect the local reference (Fig.1.53) or carrier (Fig.1.54) introduced for doppler compensation purposes. Hence, from a coding viewpoint, the use of Fig. 1.53 or 1.54 essentially means that we need one extra PN code besides the 40 codes already assumed to identify the users, which is not a major requirement. From the user processing viewpoint, the use of Figs. 1.53-1.54 implies the introduction of the extra tracking circuitry required to coherently detect the extra coded signal generated at the TDRS and to provide the doppler compensation in question. Such extra equipment (one per user) should not represent a major constraint from complexity considerations since the

users are already involved in the coherent interchange of PN-ranging codes and in the coherent processing of the carrier for range rate extraction purposes.

In summary, no fundamental relative advantages can be assigned to Fig.1.51 vs. Fig.1.53-1.54 regarding their respective signal processing considerations. Thus, they represent logical system alternatives to be considered if two-way, carrier-doppler, techniques are of interest for range rate extraction. In the case of Figs. 1.53-1.54, the available TDRS power for the GS-generated signal being retransmitted is divided between the ranging signal and the extra coded signal inserted for doppler compensation; this would involve a compromise between range vs. range rate error performance which must be verified to be satisfactory. Also, the separate coded protection of the GS and local signals in Figs. 1.53-1.54 represents a somewhat redundant approach to the anti-multipath and anti-interference problem. A slight edge may thus be assigned to the Fig. 1.51 system from a conceptual signaling efficiency viewpoint, as well as from user receiver complexity.

1.8.4 Range Rate System Selection Rationale

In section 1.8.2.1 we first presented the capabilities and limitations of a side-stepping TDRS repeater insofar as range rate extraction over path P-II is concerned. The main results were:

(a) Such a repeater is compatible with a range rate system based on the ranging PN-code doppler; the user need not process the carrier coherently since only coherent code interchange is required.

(b) Such a repeater is compatible with a range rate system based on carrier doppler if doppler aid data is available from the path P-I system; the user must maintain carrier coherence but its receiver can be doppler-aided so that it need only acquire the TDRS-user baseline doppler and not the GS-TDRS baseline doppler as well.

(c) Such a repeater is not compatible with a range rate system based on two-way carrier doppler over path P-II.

This last result then suggested an unrestricted consideration of various TDRS configurations capable of providing a two-way carrier doppler system over path P-II, and this was done in section 1.8.3. The resultant systems compatible with a multiple-access operation over the multipath and interference channel were then compared and the logical choices were narrowed to essentially two cases:

(1) The TDRS acts as a side-stepping repeater for the user signals but as a coherent transponder for the GS signal, plus transmits an extra locally-generated reference (coherent to the side-stepping oscillator) down to the GS; the user acts as a coherent carrier transponder.

(2) The TDRS acts as a side-stepping repeater for the user signals and also transmits the extra local reference back to the GS as before, but now the coherent processing of the GS signal is replaced by incoherent processing with inclusion of a locally-coded extra signal being sent to the user as an independent reference or as a new PM carrier (a la GRARR); the user again acts as a coherent carrier transponder plus provides doppler compensation of the incoherent TDRS oscillator effects prior to retransmission to the TDRS.

The first case has the carrier processing summarized in Fig. 1.51 and its main limitations are the increased TDRS complexity for processing the GS signal, since a carrier tracking loop (a Costas-like structure to extract the coded carrier) and PN-code remodulation circuitry will be required. The second case has the processings of either Fig. 1.53 or 1.54; it maintains the TDRS complexity since a locally-generated coded signal is now introduced and multiplexed along with the GS signal towards the user, plus also suffers from poor signaling efficiency since both the GS ranging signal and the TDRS local signal inserted for doppler compensation are separately coded for protection over the same channel. Both cases thus have a common drawback in TDRS complexity, plus other individual TDRS limitations such as the need for self-acquisition and loss-of-lock search modes in Fig. 1.51 (though path P-I doppler aid analogous to that of Fig. 1.44 can be considered) and the need for a locally-coded reference insertion in Figs. 1.53-1.54.

The simplicity and reliability of the simple side-stepping TDRS configuration represents a considerable advantage over the aforesaid two-way carrier doppler systems, and the use of such a repeater with either the PN-code doppler system or the doppler-aided carrier-doppler system seems to represent a preferred solution. The choice between a PN-code vs. a carrier doppler system for range rate extraction remains to be discussed.

In general, the advantages of carrier doppler systems are based on two issues: (a) the range rate resolution potential is greater than that of a system where the range rate data is obtained from the ranging

event itself, (b) the carrier doppler can be divided down to the ranging-signal frequency and used to rate-aid the ranging-signal tracking loop to improve the range measurement accuracy. The first issue refers to the doppler measurement occurring at the carrier frequency rather than at the ranging-signal frequency. The rms (single-measurement) range rate error is directly proportional to the square-root of the tracking loop bandwidth and inversely proportioned to the signal frequency whose doppler effect is being used. A lower bound on the loop bandwidth is introduced by dynamic tracking error considerations; e.g., phase acceleration errors are inversely proportioned to the loop bandwidth squared for conventional 2nd-order loop structures under certain regularity conditions. On this basis, a net degradation in rms range rate error when employing a 2 MHz signal rather than a 140 MHz carrier may be measured by the factor $(\frac{140}{2})^{1-\frac{1}{4}} \approx 24$. The second issue mentioned above involves the reduction of the input phase dynamics to be tracked by the ranging signal loop, which permits a narrower loop bandwidth design and a greater baseband phase-noise rejection with a corresponding improvement in the range error performance; the actual improvement dependent on the rate aid accuracy.

While both merit issues are representative of an independent carrier doppler system vs. an independent ranging-signal doppler system, it should be understood that our application in question requires the PN code to provide carrier extraction protection to the channel effects. In such a case there will exist a code-carrier loop interaction in the GS and user receivers to some extent, and any major improvement claims of a carrier doppler system vs. a code doppler system implicitly assumes that the code

contribution is secondary from the reproduced doppler viewpoint yet relevant from the carrier acquisition and protection viewpoints, which may or may not be mutually exclusive conditions for a particular code-carrier receiver realization and/or design. In any case, it should be emphasized that a coherent carrier retransmission at the user transponder (and coherent carrier detection at the GS receiver) should not represent a major system requirement since coherent extraction of its phase-modulated PN code is required for ranging purposes. Also, it should be noted that the GS-TDRS doppler compensation at the user receiver with the aid of the path P-I doppler measurement (see Fig.1.45) can be employed regardless of whether a carrier or code doppler system is used.

On this basis, it is thus recommended as a first choice that a side-stepping TDRS transponder be used for both GS and user signals in path P-II, that a coherent-carrier user transponder be used, that doppler aid from path P-I be employed to ease the user acquisition process, and that the detection-tracking subsystems of the user and GS receivers be designed so as to produce an optimum compromise that provides the necessary carrier protection by the code but simulates a carrier doppler system insofar as possible. As a second choice, we recommend a coherent TDRS transponder for the GS signal in path P-II, that a coherent-carrier user transponder be used, that a side-stepping TDRS transponder that inserts an additive reference be used for the user-TDRS-GS transmission, and that doppler aid from path P-I be used to ease the TDRS and user acquisition processes (in which case the processing of Fig.1.51 applies except that f_c is now received at the TDRS from the GS, so that the doppler extracted at the GS receiver is $D_c+2D'_c$

so that one-way doppler compensation is now required from the path P-I measurement to yield the TDRS-user two-way doppler). Finally, the range rate extraction in path P-I can be based on the incoherent systems of either Figs.1.47 or 1.48 for our first choice in path P-II, or on the coherent system of Fig.1.49 for our second choice in path P-II.

1.8.5 Unambiguous Ranging Considerations

In tracking systems, the unambiguous ranging requirement imposes a lower bound on the period of the ranging event. In sidetone ranging systems it specifies the lowest sidetone frequency, and in PN ranging systems it establishes the time duration of the PN code. In our application, a distinction must be made when considering the ranging operations over paths P-I and P-II, since the former provides direct ranging of a TDRS, but the latter only represents an intermediate step in the measurement of the TDRS-user baseline range. In either case, the available information concerning the possible GS-TDRS and GS-TDRS-user geometries should be exploited when establishing the required period of the ranging event.

The pertinent geometry for the TDRS ranging by a GS is illustrated in Fig.1.55. The minimum range is $r_{min} = h = 22375$ miles as established from the TDRS synchronous orbit. If one assumes a maximum station coverage of $\pm\,\theta$ degrees as indicated in the figure, the maximum range satisfies the equation

$$(R+h)^2 = R^2 + r_{max}^2 - 2Rr_{max}\cos(\pi-\theta) \qquad \text{eq. 1.95}$$

which has the solution

$$r_{max} = -R\cos\theta \pm \sqrt{(R+h)^2 - R^2\sin^2\theta} \qquad \text{eq. 1.96}$$

where the positive sign is the one of interest. The table that follows illustrates the dependence of the maximum range on the GS coverage angle.

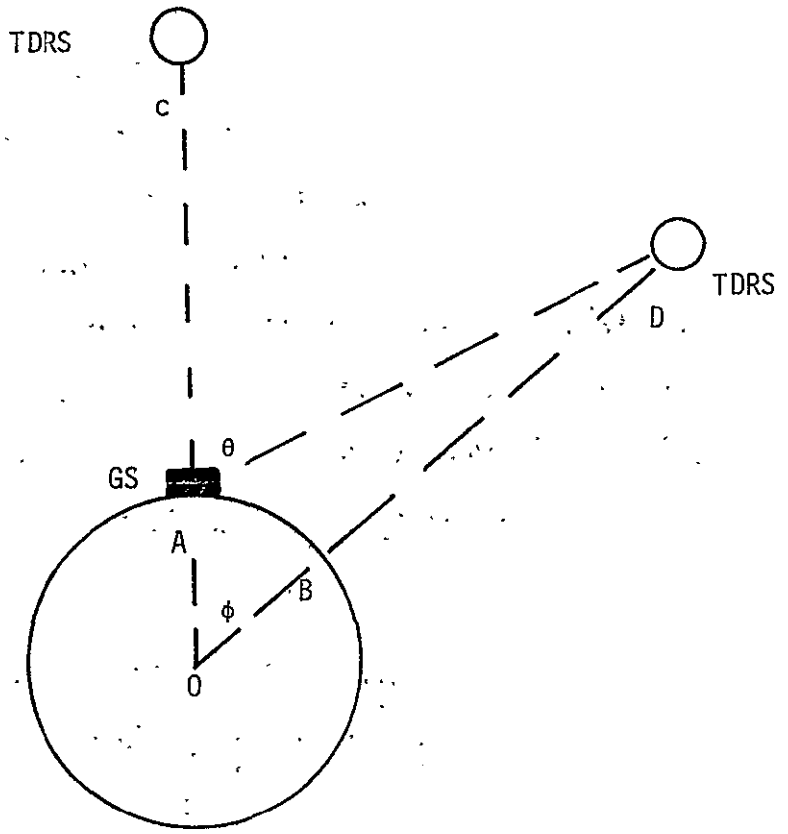

$R = OA = OB = 3985$ miles

$h = CA = DB = 22375$ miles

$r_{min} = CA = h$

$r_{max} = DA = [R^2 + (R+h)^2 - 2R(R+h)\cos\phi]^{1/2}$

Figure 1.55: Geometry for Station Coverage of TDRS

Since the minimum range is known, the ranging operation need only consider the difference $r_{max}-r_{min}$ for ambiguity-resolving purposes, and the table shows that this distance is within 3700 miles for a GS coverage up to $\pm$ 90°. The corresponding minimum period is also tabulated, and 0.04 sec is shown to be satisfactory for a GS coverage up to 90°.

θ	r_{max}	$r_{max}-r_{min}$	T_I
0°	22375 miles	0	0
30°	22835 miles	460 miles	0.00494 sec
45°	23390 miles	1015 miles	0.01089 sec
60°	24140 miles	1765 miles	0.01894 sec
90°	26060 miles	3685 miles	0.03954 sec

With reference to unambiguous ranging over path P-II, one could distinguish between two cases: (1) the user orbital determination procedure is based on separate unambiguous ranging over the P-I and P-II paths, (2) the procedure permits the use of the path P-I ranging operation to relax the ambiguity-resolving constraints over path P-II. If one denotes the GS-TDRS range by r and the TDRS-user range by r', then in the first case the distance of interest for ambiguity-resolving purposes is given by $(r+r')_{max}-(r+r')_{min}$, while in the second case it is given by $r'_{max}-r'_{min}$ since any one can permit range ambiguity over the $2(r+r')$ propagation path if it can be resolved from the 2r ranging operation. The principles of the second case are illustrated in Fig. 1.56: the ranging over path P-II is ambiguous since the received event R_2^1 may correspond to either the first or the second transmitted events $(x_1^1$ or $x_2^1)$, but the (synchronized) ranging over path P-I

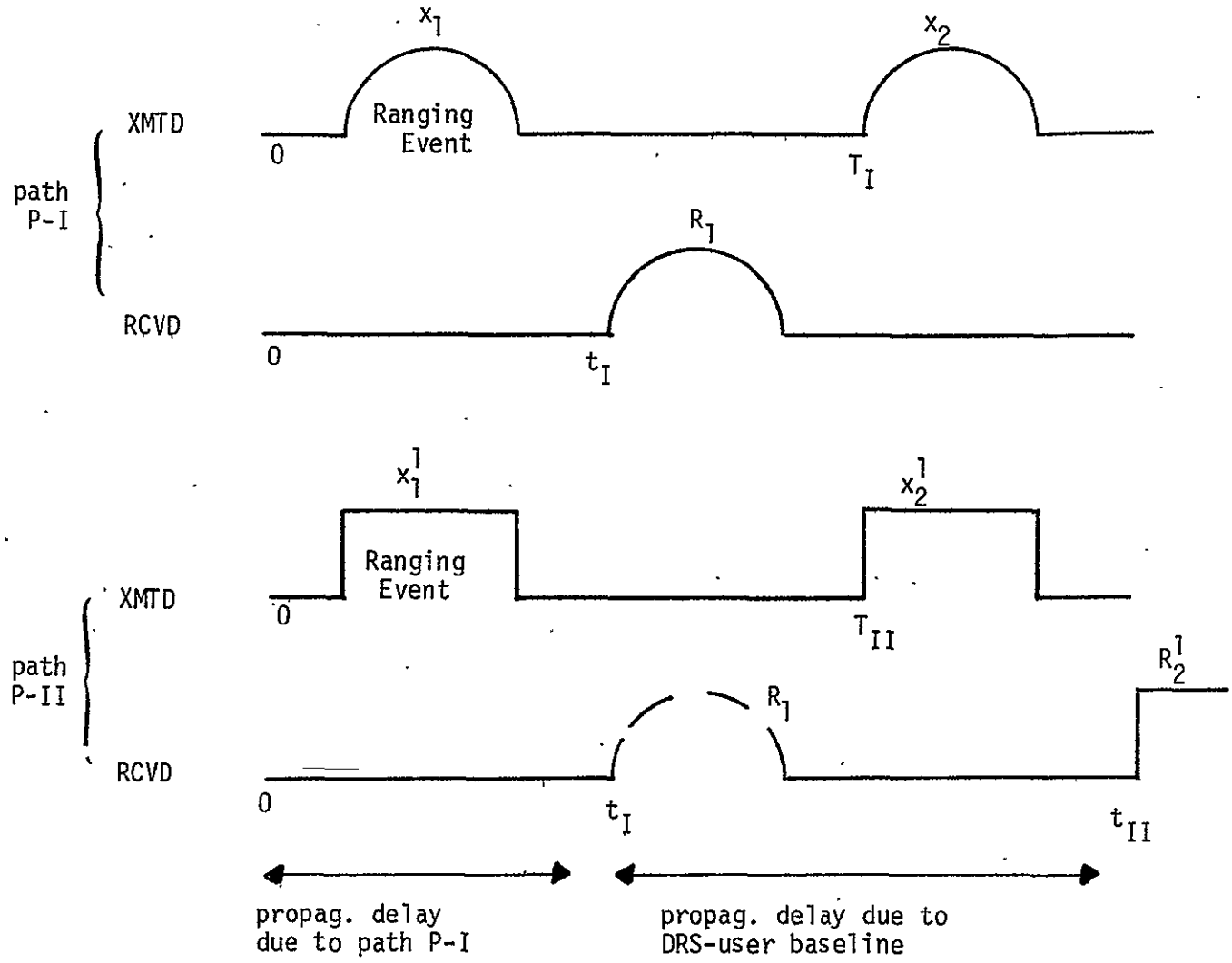

Figure 1.56: Unambiguous ranging over path P-II based on ambiguity-resolution aiding from the path P-I ranging operation

permits to identify x_1^1 as the transmitted event upon reception of R_1 prior to the occurrence of x_2^1. It should be understood that the ranging events over paths P-I and P-II need not be identical signal structures (e.g., one could have a sidetone in P-I and a PN code in P-II), and that the actual implementation of the ambiguity-aid principles of Fig. 1.56 depends on the range extraction sub-systems being used.

To establish maximum range conditions, we consider the system geometry with the aid of Fig. 1.57. The minimum TDRS-user baseline range is given by $r_{min}^1 = h-h^1$, and corresponds to the case when the TDRS and user are colinear with the center of the earth. This distance is 21375-22275 miles as established by the TDRS synchronous orbit and the specified user altitudes. The maximum TDRS-user range corresponds to the case illustrated in Fig. 1.57 where the TDRS and user form a rectangular triangle with the center of the earth, and is given by $r_{max}^1 = 26830$ miles (for $h^1 = 1000$ miles). Hence $r_{max}^1 - r_{min}^1 = 4500$ miles, and the minimum period for the ranging event over path P-II is $T_{II} = 0.0483$ sec if ambiguity-aid is provided from path P-I as previously discussed.

With reference to the case where independent unambigious ranging is required over path P-II, it is first evident from Fig. 1.57 that $(r+r^1)_{min} \approx 2[h+(h-h^1)] = 44950$ miles, when the GS, TDRS and user are (almost) colinear. In turn, the maximum range condition is essentially that illustrated in Fig. 1.57 and depends on the GS coverage angle θ. Notice that $(r+r^1)_{max} = r_{max} + r_{max}^1$ so we need only add 26830 miles to the values of $r_{max}(\theta)$ previously tabulated. The results of the table that follows indicates that the pertinent distance for ambiguity-resolving purposes in path P-II (when no aid is expected from the path P-I ranging)

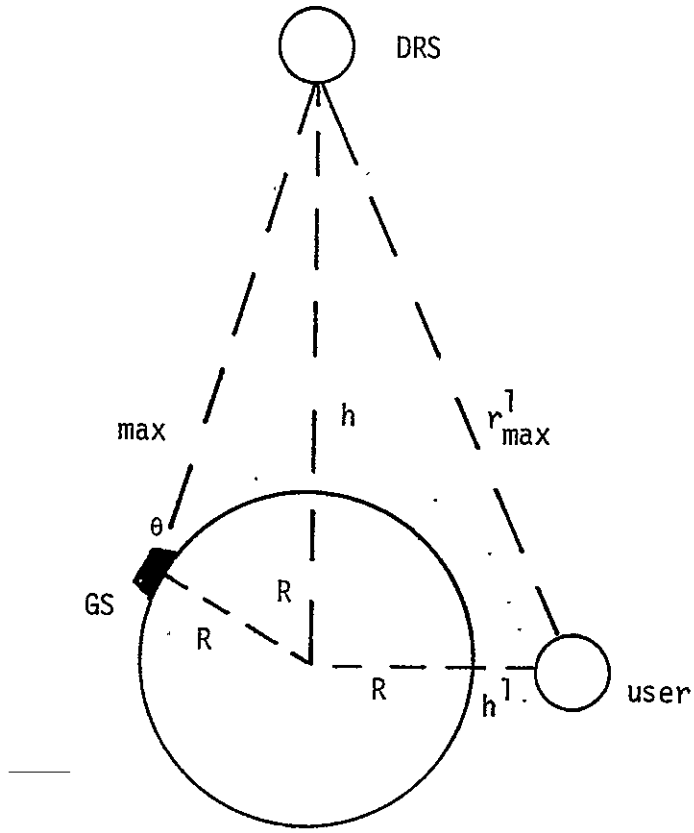

R = 3985 miles

h = 22375 miles

h^1 = 100-1000 miles

r^1_{max} = $[(R+h)^2 + (R+h^1)^2]^{1/2}$ = 26830 miles for h^1 = 1000 miles

r^1_{min} = $h = h^1$ = 21375-22275 miles for h^1 = 100-1000 miles

Figure 1.57 System Geometry for maximum propagation over path P-II

is within 8000 miles for a GS coverage up to 90°, with a corresponding period requirement of T_{II} 0.09 sec. This value is within a factor of two for the case where ambiguity-resolving aid is assumed. For most cases a value of T_{II} = .064 sec is adequate.

θ	$(r+r^1)_{max}$	$(r+r^1)_{max}-(r+r^1)_{min}$	T_{II}
0°	49205 miles	4255 miles	0.0457 sec
30°	49665 miles	4715 miles	0.0506 sec
45°	50220 miles	5270 miles	0.0566 sec
60°	50970 miles	6020 miles	0.0646 sec
90°	52890 miles	7940 miles	0.0852 sec

1.8.6 Range and Range Rate Accuracy for a TDRS PN Ranging System

In Appendix II, a one way range error analysis is presented for various realizations of a PN ranging system. There, it is shown, that one can expect (and has been verified by experimentation) a one way range error given by eq. 1.97.

$$\frac{C\,\pi\,T_c}{10\sqrt{\frac{S}{N_o B_L}}} \leq \Delta R_{rms} \leq \frac{\pi\,T_c\,C}{5\sqrt{\frac{S}{N_o B_L}}} \qquad \text{eq. 1.97}$$

$S/N_o B_1$ = SNR in one sided loop bandwidth B_L

C is the velocity of light and T_c = duration of the PN chip.

The above eq. 1.97 is valid for $S/N_o B_L$ > 10 db .

The upper bound occurs for bandlimited channels while the lower bound exists for an unlimited channel bandwidth.

The user to G.S. link through the TDRS is bandlimited to 2mhz at VHF while the G.S. to user link is limited to 1.9mhz at VHF.

The S/N_oB_L is determined by the user power (user to G.S. link) the ambient noise level, the multipath intensity and the sum of the other users signal power. T_c is dependent on the clock rate used to drive the PN coder on board the user craft. It has been shown that a 2mhz clock rate produces the maximum processing gain through the 2mhz TDRS channel (user to G.S.). Thus we can expect to obtain a range error contribution on this link given by

$$\Delta R = \frac{3\pi \times 10^{+2}}{10\sqrt{\frac{S}{N_oB_L}}} \sim \frac{10^2}{\sqrt{\frac{S}{N_oB_L}}} \quad \text{meters} \qquad \text{eq. 1.98}$$

where

$$\frac{S}{N_oB_L} = \frac{2 \quad P_u \quad (P.G.)_{loop}}{\underbrace{\frac{(K-1)Pu}{2}}_{\text{other users}} + \underbrace{KPu}_{\text{multipath}} + \underbrace{N_uW}_{\text{User to TDRS link noise}}}$$

P_u = user power at satellite

N_uW = -105 dbm

$(P.G.)_{loop}$ = processing gain of the code tracking loop

Interference is not considered in equation 1.98 but will be treated in section 1.1.2. The P.G. of the code tracking loop can be made very high, limited only by the orbital dynamics but from a practical standpoint the code loop tracking will be set at 10hz. Thus the expected on way range error for the user to G.S. link assuming worst case multipath and 39 other users is $\Delta R_{\substack{\text{user to} \\ \text{TDRS}}} \simeq 3$ meter. This is believed to be a conservative estimate for the assumed conditions and a user power level of 1 watt. An additional 6 dB of system margin would dictate a 4 watt user power to maintain 3 meter range error*.

The G.S. to user link 148-149.9 mhz while clobbered by interference, does not have to contend with other command signals and their multipath. It must contend with its own multipath however. Again the problem of interference on the 148-149.9mhz link will be analyzed later. Considering only noise and its own multipath, the command link signal path (TDRS to User) range error contribution is

$$\Delta R_{\substack{\text{TDRS to} \\ \text{User}}} = \frac{3\pi \times 10^{+2}}{10\sqrt{\frac{S}{N_o B_L}}} \qquad \text{for } T_c = 10^{-6} \qquad \text{eq. 1.99}$$

where

$$\frac{S}{N_o B_L} = \frac{2\ P_u\ (P.G.)}{P_u + N_u W} \longleftarrow \text{defined in eq. 1.98}$$

$$\therefore \quad \Delta R_{\substack{\text{TDRS to User}}} \sim \text{1.5 meter at VHF 148-149.9mhz for one watt out of TDRS}$$

*However, if the range error is relaxed to 6-8 meters then the 1 watt user power level is adequate for tracking.

It has been recommended in this report that instead of using the 148. to 149.9 band because of interference that the 400 to 402 band be considered for the command link. If this is accepted as a logical alternative the TDRS to user then an additional 10 dB of path loss is sustained and the range error increase to 4.5 meter for a one watt TDRS to user power level. As pointed out in the requirements section the TDRS to user link is expected to have a 10-20 watt power level. Thus a 10 watt power level TDRS to user would restore the 1.5 meter range error estimate at 400 MHz.

We realize that the above discussions have not included the effects of interference which will be treated later. However, based upon our analysis we are convinced that a PN coded signal between user and G.S. can provide a 10 to 15 meter 2 way range accuracy measurement at chip rates commensurate with the bandwidths of the VHF-TDRS channel while operating in the presence of 40 users and their multipath.

One way range rate errors for the VHF channel can be estimated by using eq.1.100.

$$\Delta\dot{R} = \frac{C}{2\sqrt{2}\,\pi\, f_c\, T_{obs.}\sqrt{\frac{S}{N_o B_L}}} \qquad \text{eq. 1.100}$$

$\Delta\dot{R} \sim 1$ cm/sec

for $B_L = 10$hz $\qquad f_c = 137$mhz $\qquad T_{obs.} = 1$ second

This estimate is valid for 40 users and their multipath. Thus the PN coded signal is expected to provide an acceptable 2-way $\dot{R}$ error at VHF for precise tracking of the user.

1.8.7 Ground Station Range Readout Instrumentation

To accomplish an accurate round trip range measurement from a G.S. to user to G.S. via a TDRS using a PN coded system, a code comparison is performed at the G.S. Assume for a moment that the range ambiguity problem has been resolved (this difficult problem is discussed in the Synchronization Section 1.9), the G.S. transmits to all users on code #1 and all users automatically search and synchronize to code #1. In turn each user transmits to the G.S. on unique codes which have excellent cross correlation properties (Gold Codes) and allows each user to be identified at the G.S. unequivocally. This infers that the G.S. receiver searches for a particular user by correlation techniques whereby the G.S. generates all the user codes and selects out the user signal by correlating the proper user code with the composite incoming signals. The common G.S. to user PN coded signal and the user code at the G.S. used to extract a particular user signal are derived from a common digital timing source and the round trip range is computed by precise code comparison at the G.S.

The actual instrumentation required to effect the precise range measurement has been developed by Magnavox and is referred to as Rapid and Precise Ranging Equipment (RAPRE). The equipment has the ability to readout (or compute) the roundtrip range measurement to an accuracy of 1/16-th of one PN chip. For TDRS applications, a two megachip/sec PN coded signal can be resolved by RAPRE to 31+ nano sec. The hardware required to realize RAPRE consists of four P.C. boards with logic speeds of 16-32 megabits/sec expected for TDRS applications.

1.8.8 Recommended Range and Range Rate Use Transponder

In keeping with the above conclusions, we illustrate in Fig. 1.58 the block diagram of the recommended PN coherent user transponder to accomplish accurate tracking of the user by the G.S. via precise range and range rate extraction. The transponder provides maximum range rate accuracy as well as a near optimum range tracking capability. The range accuracy of the PN transponder is summarized in section 1.8.6 and is thoroughly analyzed in Appendix II of this report. In addition to its ranging capabilities, the transponder thwarts multipath and interference while providing simultaneous multiple access of a TDRS satellite by 40 or more users at VHF. The exact code rates and code lengths employed in the transponder will be deferred to the section on synchronization, section 1.9. It is suggested that a similar transponder be employed in the G.S. to track the TDRS (for position location purposes) to allow the G.S. to extract the TDRS to G.S. range and doppler in order that the GS to user link can be doppler compensated to insure unbiased TDRS-user range rate measurements.

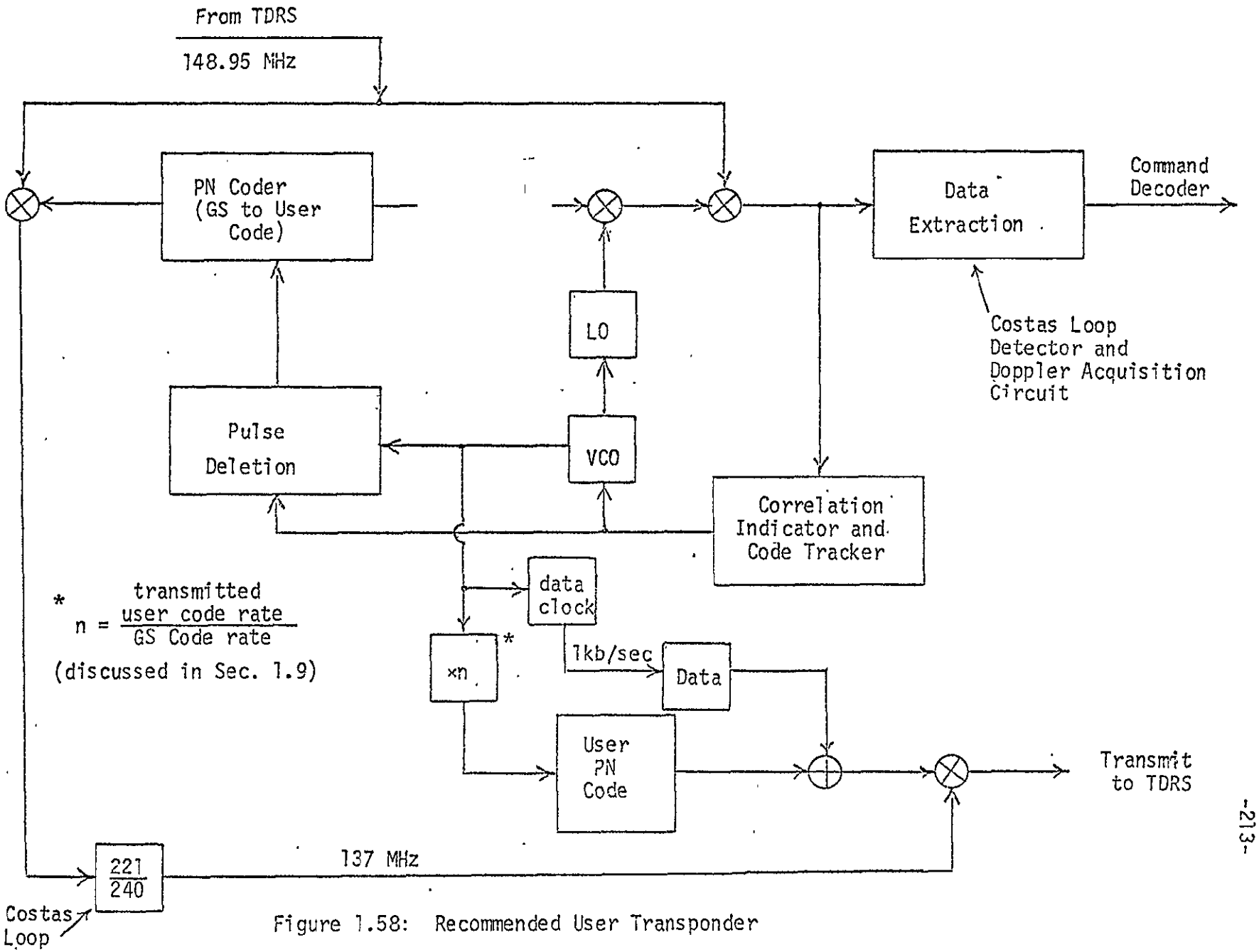

Figure 1.58: Recommended User Transponder

1.9 SYNCHRONIZATION OF WIDEBAND AND NARROWBAND SIGNALS FOR TDRS

In order to establish either voice or data communications through the TDRS between a user and ground station and in order to effect accurate range and range rate tracking of the user by the ground station, synchronization of the multiple access and anti-multipath signal used to convey data, voice, range and range rate must be accomplished by the user and the ground station.

Overall synchronization times are to be maintained at a minimum commensurate with proper sync reliability, false alarm probability and requirement to provide tracking within a realistic period of time after the onset of the mission.

Existing systems such as the Goddard Range and Range Rate System require various synchronization times from a few seconds to 10's of seconds depending upon the signal-to-noise ratio being experienced. We are led to conclude that maximum 2-way synchronization time on the order of 30 seconds is required and an average 2-way sync time of 15 seconds is desirable.

In this section we examine the synchronization performance of the wideband and narrowband signals which are under investigation for their multiple access and anti-multipath properties for application to the TDRS. We performed the analysis on the wideband system first under the assumption that noise and multipath are present and that no doppler exists on the VHF links. Using this optimistic initial approach, we are able to determine the best wideband system from the synchronization point of view. After determining the best wideband system, we concentrated our analysis on its synchronization performance

in the presence of doppler on both the ground station to user link and the user to ground station link at VHF.

Synchronization of the system at S-band presents no difficulty as a result of the absence of multipath and the large system margins which exist at S-band and K_u-band. In other words, if the synchronization problem is solved at VHF, synchronization at S- and K_u- bands is automatically resolved.

Prior to our analysis, we present some background material - the purpose of which is to assist in clarifying terminology and techniques which have been investigated for synchronization during this program.

1.9.1 Synchronization Techniques

In the synchronization of wideband communications systems, the synchronization mode need not be constrained by the modulation and demodulation techniques employed in the transmission mode, for the goals of the two modes are clearly separable. Therefore, the modulation and demodulation techniques by which synchronization is accomplished may differ from that employed in the data transmission mode, the acquisition time may be greatly reduced over that possible using the data transmission modem techniques.

Synchronization acquisition of a wideband signal such as PN, RADA or the PRTH involves searching the initial time uncertainty, ΔT, and the initial frequency uncertainty, ΔF. (This search through the uncertainty region will be defined as a pass.) The initial time uncertainty, ΔT, is due to the contributions of the possible drift of the system clock over the expected mission duration and the lack of knowledge of range between terminals. The inaccuracies of the frequency sources in the transmitter, the satellite and the receiver contribute to the initial frequency uncertainty, ΔF. The search model assumes quantization in time to Δt and in frequency to Δf; these depend on the specific modulation and demodulation processes. After synchronization has been accomplished and the search terminated, the magnitude of these initial uncertainties is a function of system parameters such as the degree to which ephemeris is used and amount of clock stabilization available, and the ability to correct for doppler.

While a classical search model considers moving the receiver's local reference signal in discrete jumps of Δt and Δf, practical implementation approximates a continuous linear sweep of the time and frequency variables. The final coherence of the search procedure is accomplished by automatic time and phase tracking loops in the receiver.

The problem now remains to relate these initial time and frequency uncertainties to the time required to synchronize as a function of a synchronization model.

1.9.1.1 Serial Search

Serial search is the generic term which covers all the sliding correlator forms of synchronization including the single mode, multimode and sequential detection. In general, however, to search the uncertainty aperture serially, one technique is to search the time uncertainty completely at each frequency (doppler) quantization level until the frequency uncertainty has been searched. In the following, synchronization time is given as a synchronization time - initial time uncertainty ratio, where the initial time uncertainty may be considered equal to the original time uncertainty multiplied by the number of times it must be searched to satisfy the frequency uncertainty. The factors that contribute to the time required for the location of the correct cell (a cell is the quantization in time and frequency) include search rate, procedures for testing cells, and the criteria for accepting and rejecting cells.

Synchronizers using a fixed sample size (FSS) detection system are most often encountered. It has the advantage of easy implementation, since each cell is tested for the same length of time. In contrast, a detection scheme using a variable test time for each cell, sequential detection, could be used. In sequential detection, the cell is tested until its likelihood of being the correct cell is greater than an upper threshold accepting the cells as a correct or less than a lower threshold rejecting the cells as incorrect. On the average, the sequential detection system is faster than the FSS system but occasionally a cell will be tested an extremely long time. In practice, the test is truncated to prevent excessive test periods.

The actual search process is compounded by the behavior of the tracking loops which have their own statistical acquisition properties, and must be handled analytically with a combination of statistical servo loop behavior and hypothesis testing. For example, the major effect on behavior noted experimentally is indicated by the acquisition probability, P_a, of the phase locked loop usually employed to obtain RF phase coherence in a sliding correlator search application.

1.9.1.2 Single-Mode Acquisition Model

This model gives an approximation to the maximum search time based on estimating the number of search cells multiplied by the average time (dwell time) spent in each cell. The required time in each cell is computed as a function of desired probability of correct detection, false alarm probabilities and output signal-to-noise ratios. The search time, assuming a uniform a priori distribution of the desired signal within the time frequency uncertainty region is approximated by:

T_s = number of search cells x dwell time per cell

$$= \frac{\Delta T}{\Delta t} \quad \frac{\Delta F}{\Delta t} \quad T$$

where $[X]$ = greatest integer less than x+1

and

T_s = Search (synchronization) time

ΔT = Total effective initial time uncertainty

ΔF = Total effective initial frequency uncertainty

Δf = Effective frequency error allowed by acquisition technique

Δt = Effective time error allowed by acquisition technique

T = Dwell time or time required for a decision at each Δf, Δt.

Typical coherent and noncoherent systems are analyzed with this model later in this section. In general, Δf for the phase locked loop in a coherent system has been measured to be 2.7b where b is the bandwidth related to the correlator integration time, T, by $T = \frac{1}{2b}$. Thus, the total probability of acquiring the signal when it is present, $P'_{SN}(A)$ is

$P'_{SN}(A) = P_a \times P_{SN}(A)$ = over synchronization probability

where

P_a and $P_{SN}(A)$ are the phase lock loop acquisition probabilities and the receiver acquisition probabilities respectively.

It should be noted that Δf in a noncoherent system is a function of the predetection bandwidths only. The allowable time uncertainty, Δt, for both coherent and noncoherent systems is determined from the transmitted signal structure and the particular detection techniques employed.

1.9.1.3 Multi-Mode Acquisition Model

While the simple acquisition model introduced above for a sliding correlator has wide application when the initial uncertainties ΔT and ΔF are relatively small, a saving in total synchronization time can result if the time and frequency uncertaintities are first broken up into cell sizes larger than the cell size required by the final coherent tracking circuits, then a sequence of synchronization modes is employed to reduce the cell size to the final required value. An example would be synchronizing a PN system between ground station and user where doppler ambiguity must first be resolved.

The multi-mode acquisition process basically follows the concept presented above. That is, the search starts out with coarse time-frequency cells and proceeds through a number of synchronization modes each successively refining the time-frequency cell size until the final cell is reached. Each mode has a search time, T_{si}, and the total search time is the sum for all modes.

Thus, the general form of the synchronization, or search, time for multi-mode operation is

$$T_s = \sum_{i=1}^{n} T_{s_i} = \sum_{i=1}^{n} \left[\frac{\Delta T_i}{s_i \Delta t_i}\right]\left[\frac{\Delta F_i}{r_i \Delta f}\right] T_i \left[(S/N)_o, L_i, P_{SN}'(A), P_N(A)_i\right] \qquad \text{eq. 1.101}$$

where

$[X]$ = greatest integer less than X + 1

T_{s_i} = search time for i^{th} mode

ΔT_i = total effective time uncertainty for i^{th} mode

ΔF_i = total effective frequency uncertainty for i^{th} mode

Δt_i = effective time error allowed by i^{th} mode acquisition technique

f_i = effective frequency error allowed by i^{th} mode acquisition technique

s_i = number of parallel processors in reducing time uncertainties in i^{th} mode

r_i = number of parallel processors in reducing frequency uncertainties in i^{th} mode

$L_i = L_s \times L_{r_i} \times L_{D_i} \times L_{I_i}$ is the total loss in the i^{th} mode

L_s = loss in parallel time processor

L_r = loss in parallel frequency processor

L_D = loss in non-coherent detectors

L_I = other non-ideal implementation losses

T_i = dwell time required at each $\Delta t_i \Delta f_i$ cell in i^{th} mode

$P'_{SN}(A) = P_a \times P_{SN}(A)$

P_a = probability of phase lock loop acquisition

$P_{SN}(A)$ = the conditional probability of detection in the last mode after phase locked loop acquisition

$P_N(A)_i$ = the conditional probability of false alarm in i^{th} mode

$(S/N)_o$ = the equivalent output signal-to-noise ratio.

The above model assumes the receiver buried in thermal noise, and a uniform a priori distribution of the signal over the total uncertainty region. Deviation from these assumptions are generally not critical and may be easily taken into account. In addition, it is assumed that $(S/N)_o$ is sufficiently high so that the synchronization time is not appreciably increased by the false alarm rate and the corresponding time required to verify the false alarm. Practice has indicated $(S/N)_o$ greater than 10 dB is sufficiently high to approximate the above assumptions and give an operationally usable system.

9.1.4 Example of Single-Mode, PN Coherent Search

One method of obtaining waveform acquisition is by active correlation detection techniques. In this single-mode PN coherent technique the time domain is searched by a sliding correlator while the frequency domain is searched with a phase locked loop following the correlation multiplier. The phase locked loop also serves as a significant part of the correlator integration process and, in fact, is a tracking filter. Although the phase locked loop might pessimistically be assumed to acquire only in its information bandwidth, $B_n = b$, further integration usually follows the phase locked loop so that the output signal-to-noise ratio at the threshold decision is related to the signal-to-noise ratio from the phase locked loop by

$$(S/N)_o = \frac{B_n}{b} (S/N)_{o_1} \qquad \text{eq. 1.102}$$

(S/N_o) is the signal-to-noise ratio or the correlator

B_n is the double-sided noise bandwidth of the phase-locked loop

b is the equivalent bandwidth of the synchronization correlator integrator

$(S/N)_{o_1}$ is the phase-locked loop output signal-to-noise ratio.

1.9.1.5 Two-Mode Technique with PN Noncoherent Search, Then PN Coherent Search

This technique uses a noncoherent search in the initial mode to reduce the time uncertainties while removing the requirement for a stringent frequency certainty. During the second mode the remaining frequency uncertainties are reduced by means of a coherent search. This method offers a slight improvement only if the frequency uncertainties are too large for coherent acquisition such as in the case of TDRS user.

The synchronization time is expressed by the multi-mode model with i = 2 so that the total time is the summation of synchronization times for each of two modes and is given by

$$T_S = \sum_{i=1}^{2} T_{S_i} = \sum_{i=1}^{2} \frac{\Delta T_i}{\Delta t_i} \left[\frac{\Delta F_i}{\Delta f_i}\right] \qquad \text{eq. 1.103}$$

where the parameters are again those defined in the previous models.

1.9.1.6 Short Code-Long Code Acquisition

This is a two step acquisition procedure. A short maximal length linear code is used for initial acquisition using the sliding correlator

technique. This step may be accomplished in either a single mode PN or multimode PN manner. The performance of this portion of the synchronization procedure has been covered in previous sections.

Once short code acquisition has been achieved, the system is synchronously switched to long code to provide unambiguous ranging between a user and ground station. At this point, a code tracking loop maintains synchronization by introducing a time dither or an equivalent early-late gate in the feedback loop.

.9.1.7 Sequential Detection

In the synchronization techniques presented to this point, the time to test an uncertainty cell or "dwell time" was constant for a given set of parameters. Sequential detection is a two-step synchronizer using a short primary test to eliminate the uncorrelated cells with low noise and a longer confirmation test to eliminate the uncorrelated cells with high noise. In sequential detection the length of the test on an uncorrelated cell is dependent on the amplitude of noise in the cell.

The output of the integrator, during integration, is sampled after each bit. This sample is compared against two thresholds. If it exceeds the upper threshold, the integration is stopped and the cell is accepted as the correlated cell. If it does not exceed the lower threshold, the integration is stopped and the cell is rejected as being an uncorrelated cell. If the sample exceeds the lower threshold but not the upper threshold, the integration is continued and another sample is taken. Thus, only the number of samples necessary for rejecting or accepting the cell are taken.

For systems requiring an extremely low probability of false alarm, the upper threshold can be eliminated which leads to a probability of false alarm approaching zero. With only a single threshold scheme, a cell is never really accepted, and the cell is either rejected or the cell continues to be tested. Thus the correlated cell will be continually tested. In a communication system using a preamble for synchronization, the length of time for synchronization is fixed. Hence, when the correlated cell is tested, the test continues until the end of the allowed time for synchronization. At this point, the tracking loop is engaged on the last cell being tested, the correlated cell.

1.9.1.8 Parallel Search

The use of parallel search can substantially reduce synchronization time. A parallel search can be used in the time uncertainty search, the frequency uncertainty, or both. A technique using parallel search for the time uncertainty is with multiple correlators. A parallel frequency search involves the use of doppler resolving filters, multiple use of PLL/s, or the use of swept PLL's for frequency acquisition. The use of n parallel correlators in time will usually serve to reduce the sync time by 1/n.

1.9.1.9 Matched Filter Techniques

In the active acquisition processes described for the PN and the frequency hopping, the time-frequency uncertainties were divided into cells which were searched sequentially. Matched filter acquisition techniques can reduce the serial search of a matched filter time of active acquisition by effectively utilizing parallel processing. The multiple taps or sections make the processing practically self-synchronizing.

Many possible schemes exist for utilizing large TW product matched filters to provide synchronization. In a typical matched filter system, when the transmitter desires to communicate with the receiver, a train of pulses is used to excite the transmitting half of the matched filter. After each pulse excites the filter, a pseudorandom sequence generator is advanced and a new pseudorandom number is utilized to switch the transmitting filter sections, so that by the time n pulses have been utilized to switch the transmitting filter sections, so that by the time n pulses have been utilized, the filter has produced noiselike waveforms of bandwidth W and a duration nxT.

At the receiver a gate will be opened (preferably at a time determined by the gross synchronization of the system and desirable operational procedures for a length of time equal to the time uncertainty). If the matched filter output threshold is exceeded during this time, the filter is switched to the sequence of possible numbers. The frequency uncertainties may then be searched; or the filter designed with sufficient numbers.

1.9.2 Synchronization of Wideband Systems

As discussed in section 1.4 there are a number of wideband techniques which are candidates for the TDRS. In the previous section 1.8 we argued that the PN signal appeared to be the best choice from a range and range rate requirement point of view. In this section we analyze the synchronization performance of the PRTH, RADA, and PN system in the presence of noise and multipath. Since doppler does not uniquely effect any of these approaches, we first select the best system without doppler considerations; that done we concentrate on the synchronization performance of the best technique with doppler included as a parameter.

Before beginning the analyses we should state the goals and tradeoffs involved in the synchronization of these digital systems.

a) overall two way sync time ∿15 second

b) sync reliability 90% for one sync pass

c) the G.S. to user signal occupies one channel <1.9 mhz and this single signal can be synchronized to by all the users in view of a particular TDRS.

Obviously for the wideband techniques range and range rate tracking and synchronization are inextricably entwined. That is, in order to meet the sync time requirement while still providing unambiguous ranging is a serious problem. Overall sync reliability can be improved with increased sync time and these requirements are in opposition.

All of the factors which effect synchronization will be discussed once the basic synchronization analyses have been performed to select the best wideband signal from a synchronization point of view.

1.9.3 Data Relay Satellite System Synchronization Performance

As a result of the studies presented in this report, three waveforms appear to have the multiple access properties required by the TDRS. These waveforms are Pseudo Random Time Hopping (PRTH), Random Access Discrete Address by frequency-time hop, (RADA), and PN Gold Coding (PN). The synchronization performance of these waveforms in the TDRS environment is evaluated in the analysis which follows below.

Synchronization performance is dependent on the signal to noise ratio of the received signal to which one is attempting to synchronize to. Consequently, the approach taken in the analysis has been to evaluate the signal to noise ratio, or more precisely, the signal energy to noise density ratio, of each of the waveforms after being relayed by TDRS. The ratios obtained reflect both the affects of thermal noise and multiple access intermodulation degradation.

Finally, the probability of acquisition, as based on the signal to noise ratios, is found. However, since the signal to noise ratios in general were low for the postulated transmitter power, a probability of acquisition was specified, and the required transmitter power solved for. The detection portion of the acquisition process was based on sequential detection, in light of the superior performance of this technique.

It is important to note that the analysis and the performance comparison of the three waveforms considers the severe TDRS multipath environment. The multipath environment was accounted for by considering each multipath signal to be another user.

1.9.3.1 PRTH-Synchronization

The pseudo random time hop (PRTH) modulation scheme utilizes low duty factor rf pulses emitted by the users transmitters. The pulses emanate at pseudo randomly selected times, known to the ground station, i.e., transmitter/receiver pairwise synchronization. However, the forty user transmitters all use independent time hopping programs. Thus, the pulses from the forty user transmitters overlap on a random basis, in accordance with the duty factor α . Each pulse is modulated with binary data, using biphase modulation, so that either RF phase coherence of user-ground station pairs of differential phase shift keying (DPSK) is utilized. In this scheme, each pulse represents a data bit, so that the average pulse rate from a user is equal to the data rate, 1000 bps. A block diagram of the transmitter and the receiver is shown respectively in figures 1.59 and 1.60 . The pseudo random code generators and the pulse position generators in the transmitter and receiver are identical. Due to the low duty factor of the pulses the code tracking loop and the carrier tracking loop are implemented as sampled data tracking loops. It should be noted that at the ground station there are forty such correlation receivers, one for each user.

The synchronization process is a serial search in which the local reference code is slewed until a threshold crossing indicating code coincidence occurs. This may be done either at a fixed search rate using a fixed interval search. Thus the synchronization performance of the PRTH waveform will be evaluated for a sequential detection synchronization procedure.

Since the sequential detection procedure (or any other sync detector for that matter) involves a threshold crossing detector, it is necessary to

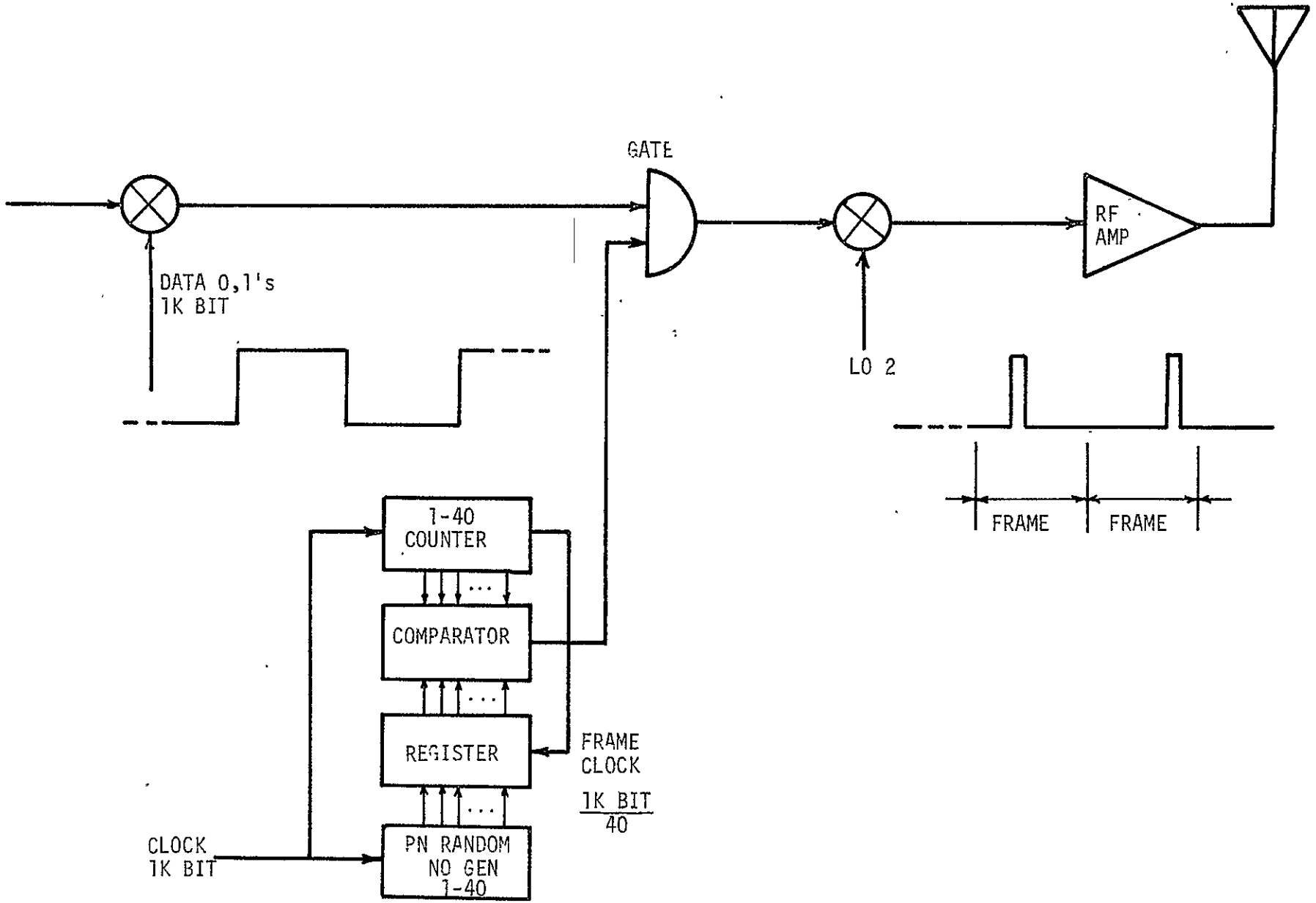

Figure 1.59 Pseudo Random Time Hop (PRTH) Transmitter

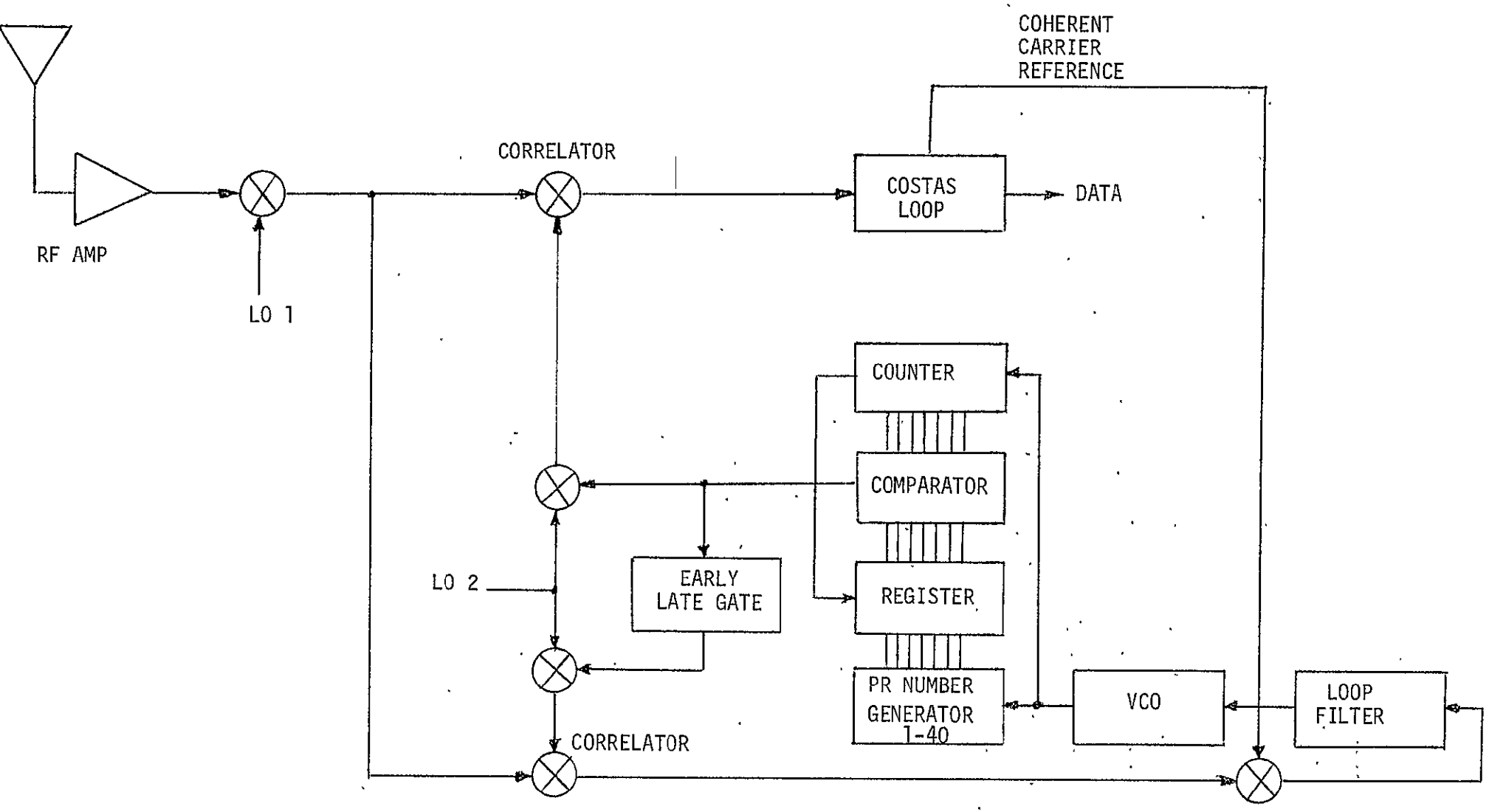

Figure 1.60 Pseudo Random Time Hop (PRTH) Receiver

determine the signal energy to total noise density ratio for the PRTH waveform. Since the bandwidth of the PRTH signal (2MHz) is equal to the reciprocal of the bit width the energy to noise density ratio at the output of the receiver correlator is equal to the ratio at the input to the correlator times the effective processing gain. This ratio, as developed by Cahn*, will be defined as the ratio of the mean to the variance of a chip (instant) at the ground receiver input. Each chip is taken to be statistically independent of the other chips received. In the expressions developed below, the following notation is used:

α - duty factor of user (same for all 40 users)

K - number of users (80, forty actual users plus forty multipath signals)

P_r - user transmitter power (peak referred to ground station)

N_o - noise spectral power density in the ground receiver

W - system RF bandwidth (1/pulsewidth)

E_b - received energy for one pulse (data bit)

The statistics for each chip are as follows:

1. With probability $(1-\alpha)^{K-1}$, the carrier amplitude is $\sqrt{2P_r}$ and the interference power is N_oW.

2. With probability $1-(1-\alpha)^{K-1}$, the carrier amplitude is zero and the interference power is $P_r + N_oW$.

Computing the mean of this distribution yields

*Op. Cit.

$$\text{Mean carrier amplitude} = (1-\alpha)^{K-1}\sqrt{2P_r} \qquad \text{eq. 1.104}$$

To compute the variance, we first obtain the total mean square value of a chip and then subtract the square of the mean, as follows

$$\text{Pre-correlator noise power} = (1-\alpha)^{K-1}[2P_r+N_oW] + [1-(1-\alpha)^{m-1}][P_r+N_oW] - [(1-\alpha)^{K-1}][\sqrt{2P_r}]^2$$

$$= N_oW + [1+(1-\alpha)^{K-1}-2(1-\alpha)^{2(K-1)}]\,P_r \qquad \text{eq. 1.105}$$

This computation is based on use of the chip amplitude after product detection with a coherent reference. In general, the result as developed below is somewhat approximate because the noise power due to the time gating is not really independent of the desired carrier component. However, making this assumption of independence, we may then write the signal energy to noise density ratio as

$$\frac{S}{N} = (P.G.)_{PRTH}\,\frac{\alpha(1-\alpha)^{2(K-1)}\,\frac{P_r}{N_oW}}{1+\frac{P_r}{N_oW}[1+(1-\alpha)^{K-1}-2(1-\alpha)^{2(K-1)}]} \qquad \text{eq. 1.106}$$

The processing gain, P.G., is defined for the purpose of synchronization as the ratio of RF bandwidth to search bandwidth

$$PG = \frac{W}{W_s} = WT$$

where T = time to search one PN bit. Thus upon substitution of the

appropriate values of K = 80 and $\alpha = 5\times10^{-4}$, as discussed in section 1.6.3, equation 1.106 reduces to

$$\left(\frac{S}{N}\right) = 2.3\ 10^{-4}\ \frac{P_R T_S}{N_o\left(1+.113\ \frac{P_R}{N_o W}\right)} \qquad \text{eq. 1.107}$$

1.9.3.2 RADA-Synchronization

The random access, discrete address system (RADA) differs from the pseudo random time hop (PRTH) system in that the low duty factor pulses are hopped both in carrier frequency and in time. In addition,the RADA system considered for the TDRS utilizes an m-ary alphabet to increase efficiency and thus reduce errors. Each character from the m-ary alphabet consists of a unique combination or address of K time - frequency slots chosen from the MN cell time - frequency plane shown in figure 1.13. This address is detected at the GS as a k-fold coincidence. The receiver for such a system is readily implemented as a digital matched filter as shown in figure 1.61. The overwhelming advantage of the digital matched filter is the elimination of the need for bit or slot synchronization. However, frame or m-ary character synchronization is required. The GS receiver must have m unique sets of taps (k taps per m-ary symbol) for each user. Since there are M users each having a unique m-ary alphabet, there are a total of KmM taps and mM coincidence gates.

The derivation of the signal energy to noise density ratio for the RADA signal is similar to that for the PRTH signal, with some exceptions.

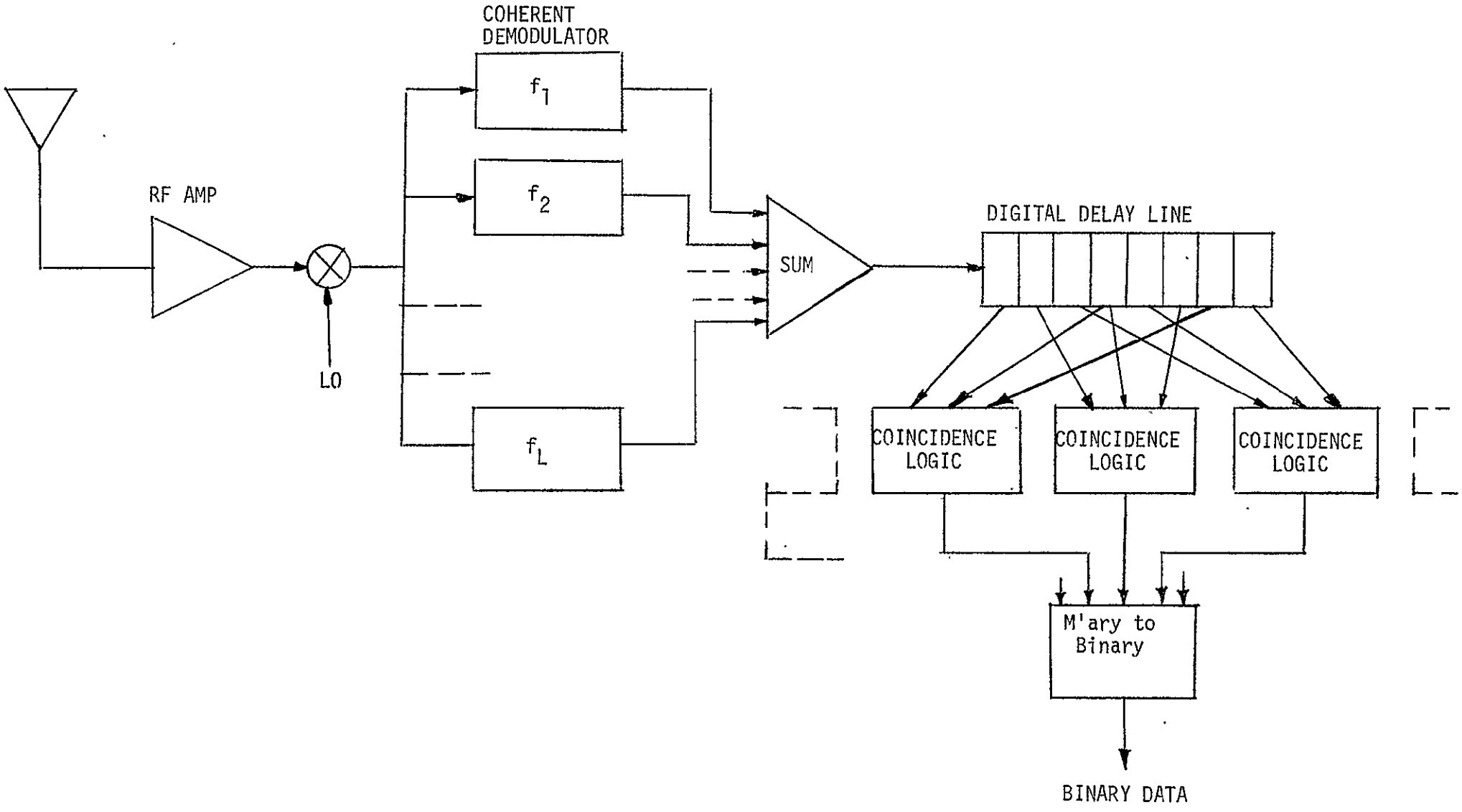

Figure 1.61 RADA Receiver Diagram

1. With probability $(1-\frac{1}{MN})^{K-1}$, the carrier amplitude is $\sqrt{2P_r}$ and the interference is N_oW.

2. With probability $1-(1-\frac{1}{MN})^{K-1}$, the carrier amplitude is P_r+N_oW, where K = number of users

M = number of frequency slots

N = number of time slots per frame

Thus, following the same reasoning as used for the PRTH signal, we can write for the RADA signal

$$\frac{S}{N} \doteq (P.G.)_{RADA} \frac{\frac{1}{MN}(1-\frac{1}{MN})^{2(K-1)} \frac{P_r}{N_oW}}{1+\frac{P_r}{N_oW}\left[1+(1-\frac{1}{MN})^{K-1}-2(1-\frac{1}{MN})^{2(K-1)}\right]} \qquad \text{eq. 1.108}$$

As with the PRTH waveform, the processing gain for synchronization is given by

$$PG = WT$$

where T = time to search one PN bit.

Upon substitution of the optimum value of MN = 100, section 1.6.4, equation

$$\frac{E}{N_o} = 1\times10^{-3} \frac{P_RT}{N_o(1+\frac{P_R}{N_oW})} \qquad \text{eq. 1.109}$$

1.9.3.3 PN-Synchronization

Pseudo random code modulation has been suggested as a means of achieving the multiple access communication for the forty TDRS users. This technique allows each user to transmit continuously, and depends on the orthogonality of the PN (pseudo noise) codes to discriminate between users. To determine the synchronization performance for the PN multiplex system it is first necessary to derive the signal to noise ratio (signal energy to noise density ratio) for the output of the correlation receiver which is used to receive the PN signal. A simplified block diagram of the PN transmitter is shown in figure 1.62 and a block diagram of the correlation receiver is shown in figure 1.63.

In the derivation of signal to noise ratio which follows below it will be assumed that a coherent carrier reference is available for coherent demodulation. This reference can take the form of a Costas loop which is shown in block diagram form in figure 1.64.

A diagram of the mathematical model used to derive the signal to noise ratio is shown in figure 1.65. The PN code of the desired signal is denoted by $S_1(t)$ and the PN code of the undesired or interfering signal is denoted by $S_i(t)$ so that the sum total of interfering PN codes and carriers is denoted by

$$\sum_{i=2}^{M} S_i(t)\cos(w_1 t+\theta_i) \qquad \text{eq. 1.110}$$

where θ_i is uniformly distributed between 0 and 2π. As usual there is

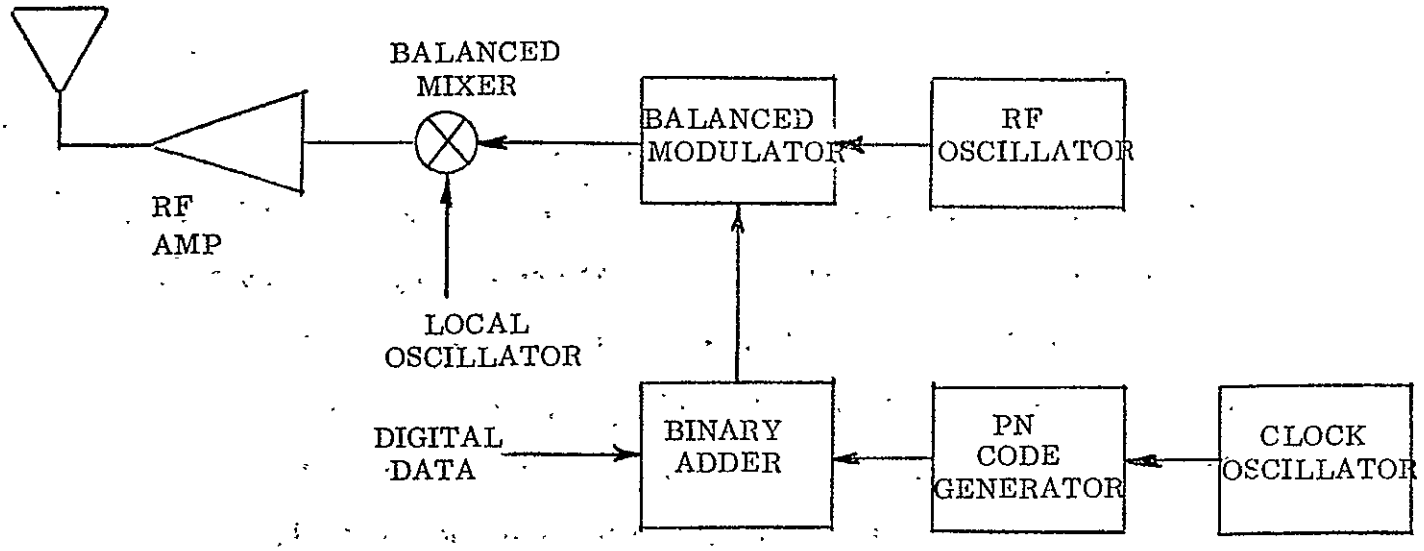

Figure 1.62 - Basis Pseudo Noise (PN) Transmitter

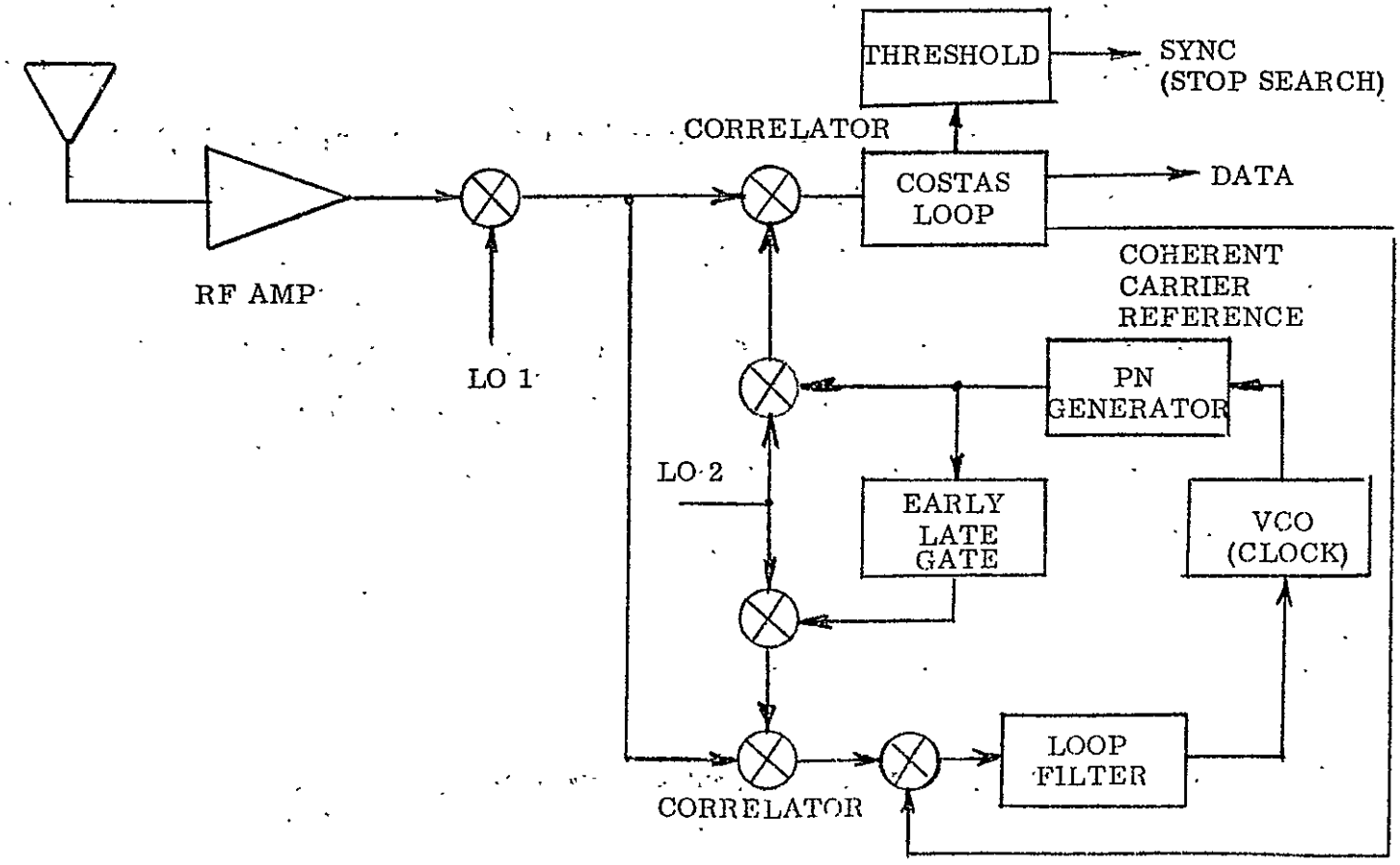

Figure 1.63 - Basic PN Receiver

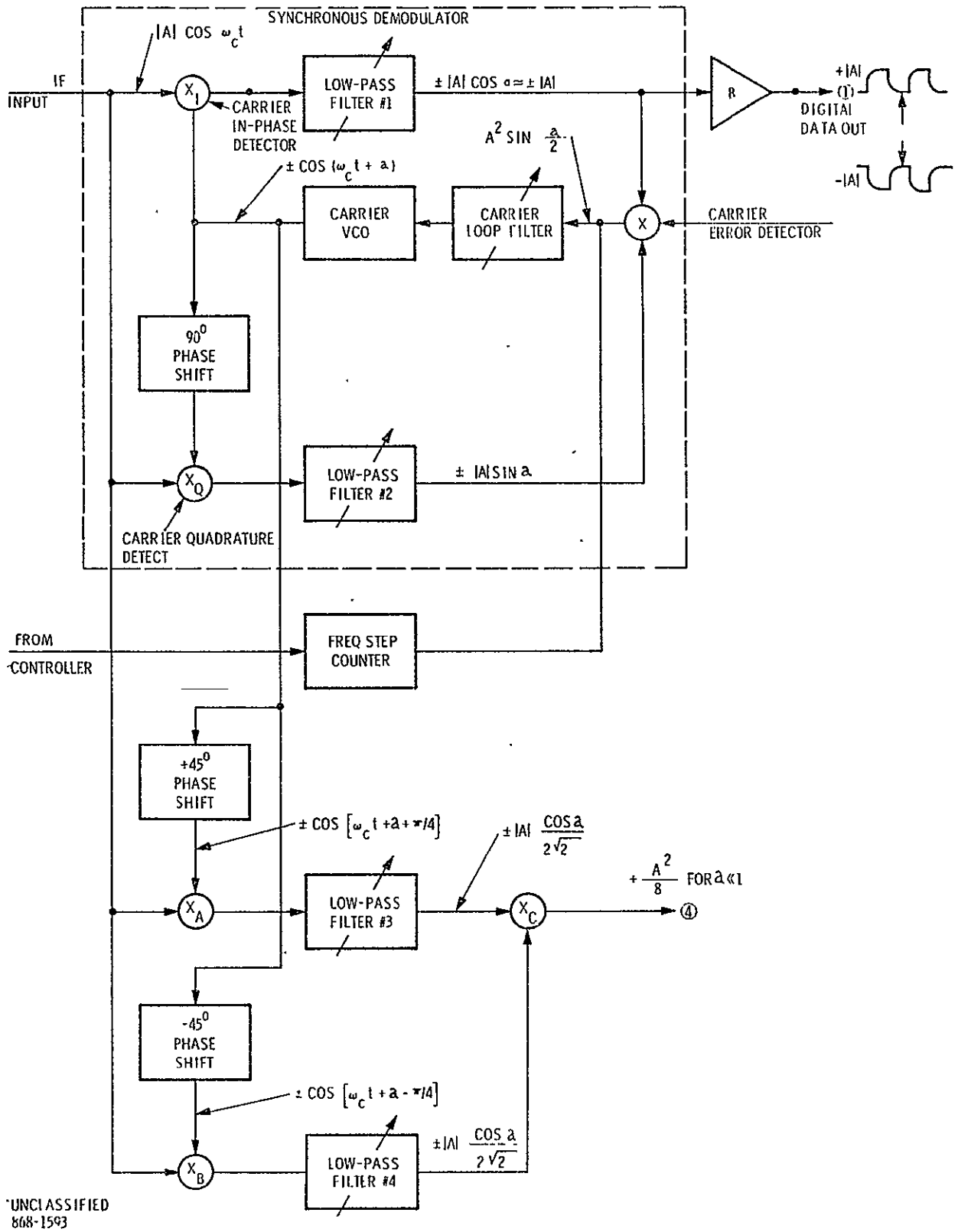

Figure 1.64 - Costas Loop Coherent Demodulator

also thermal noise of one side density N_o watts/hz to contend with. Thus, based on figure 165 , the output of the correlator is given by

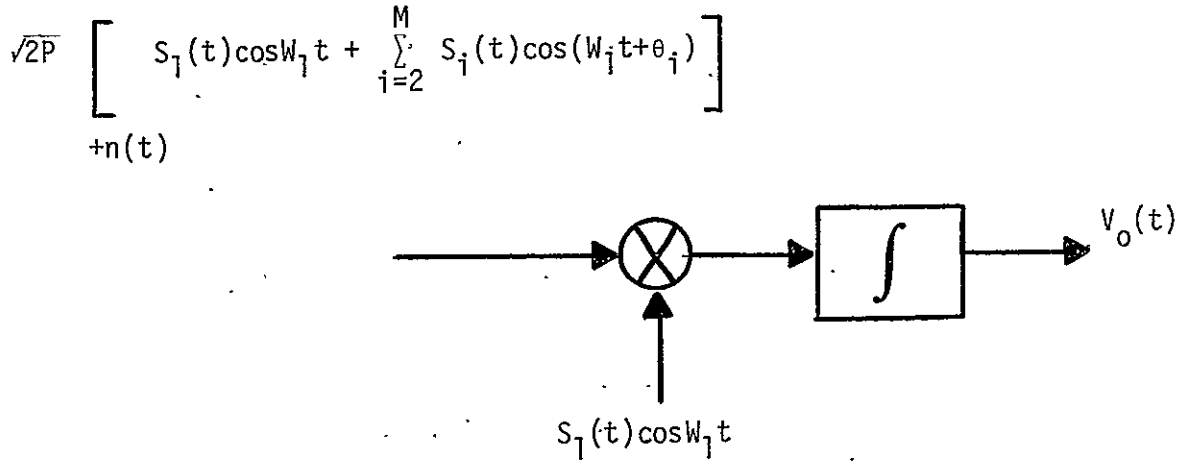

Figure 1.65 - Mathematical Model of Correlation Process

$$V_o(t) = \left[\sqrt{2P}\left(S_1(t)\cos w_1 t + \sum_{i=2}^{M} S_i(t)\cos(w_1 t+\theta_i)\right) + n(t)\right] \otimes$$

$$[S_1(t)\cos w_1 t]$$

$$= \frac{\sqrt{2P}}{2} S_1(t) \otimes S_1(t) + \sum_{i=2}^{M} \frac{\sqrt{2P}}{2} S_1(t) \otimes S_i(t)\cos\theta_i + n(t)$$

$$= \frac{\sqrt{2P}}{2}\left[C_{11} + \sum_{i=2}^{M} C_{1i}\cos\theta_i\right] + n(t) \qquad \text{eq. 1.111}$$

where $\otimes$ denotes correlation and

C_{11} = autocorrelation of $S_1(t)$

C_{1i} = cross correlation between $S_1(t)$ and $S_i(t)$

P = user transmitter power referenced to GS

It should be noted that C_{1i} is a random variable which is highly dependent on the particular code structure utilized, the relative phase between $S_1(t)$ and $S_i(t)$, and the correlation window or integration time. All of these parameters and their affects on synchronization performance will be discussed a bit later.

The signal to noise ratio at the output of the correlator is defined as

$$\frac{S}{N} = \frac{\overline{V_o(t)^2}}{\overline{V_o(t)^2} - \overline{V_o(t)^2}} = \frac{E}{N_o} \qquad \text{eq. 1.112}$$

In calculating the averages we find that

$$\overline{V_o(t)} = \frac{\sqrt{2P}}{2}\left[C_{11} + \sum_{i=2}^{K} \overline{C_{1i}}\ \overline{\cos\theta_i}\right] = \frac{\sqrt{2P}}{2} C_{11}$$

and

$$\overline{V_o(t)^2} = \frac{PC_{11}^2}{2} + \overline{\sum_{i=2}^{K} \frac{\sqrt{2P}}{2} C_{1i}\cos\theta_i}^{\,2} + N_p$$

$$= \frac{PC_{11}^2}{2} + \frac{P}{4} \sum_{i=2}^{K} \overline{C_{1i}^2} + N_p \qquad \text{eq. 1.113}$$

Thus

$$\frac{S}{N} = \frac{PC_{11}^2}{2N_p + \frac{P}{2}\sum_{i=2}^{K}\overline{C_{11}^2}} \qquad \text{eq. 1.113}$$

where

N_p = thermal noise power at output of correlator

$= N_o W$

where

$W = \frac{1}{T}$ = correlator bandwidth

and

T = correlator integration time

Since K is fairly large, i.e., 40, (actually 80 when we consider multi-path affects) we may apply the central limit theorem to the interference. Thus the affect of the large number of interfering signals is closely approximated by Gaussian distributed noise with zero mean and variance given by

$$\sigma^2 = \overline{C_{1i}^2},\ i = 2,3,\cdots,K$$

so that equation 1.113 reduces to

$$\frac{S}{N} = \frac{PC_{11}^2}{2N_p + \frac{P\sigma^2}{2}(K-1)} \qquad \text{eq. 1.114}$$

The term $\frac{P\sigma^2}{2}(K-1)$ may be referred to as the multiple access intermodulation degradation. When the incoming code $S_1(t)$ is lined up (in phase) with the receiver local reference code, C_{11} is equal to 1 (normalized). Furthermore, it is necessary to consider that the TDRS repeater output power is shared by each of the users and the noise and interference input to the repeater. It is shown in this report that the received power at the G.S. available for any one user is

$$P = P_S \frac{P_u}{KP_u + W_R N_u + I} \qquad \text{eq. 1.115}$$

where

P_S = total repeater output power referenced to the ground station

P_u = user uplink power referenced to repeater satellite

W_R = repeater noise bandwidth

N_u = uplink (user/repeater) noise density

I = total interference power

K = number of users

Similarly, the thermal noise power at the output of the repeater is given by

$$N_P = P_S \left(\frac{W_R N_u}{KP_u + W_R N_u + I} \right) \qquad \text{eq. 1.116}$$

Thus, substituting equations 1.116 and 1.115 into equation 1.114, we obtain

$$\frac{S}{N} = \frac{1}{2/\left(\frac{P_u}{W_R N_u} \right) PG + \frac{(K-1)^2}{2}} \qquad \text{eq. 1.117}$$

The term, $\frac{P_u}{W_R N_u}$ is the signal to thermal noise ratio for one user, $(S/N)_u$, at the repeater input, and PG is the correlator processing gain.

1.9.3.4 Comparison of Synchronization Performance for Wideband Signals

Thus far, we have derived the signal energy to noise density ratio for the PRTH, the RADA, and the PN waveforms for use with PRSS. This enables us to now quantitively determine the synchronization performance of these waveforms. Before doing this, a qualitative description of the synchronization process will be given to give perspective to the more analytical treatment.

The receivers which have been described for the respective waveforms in the previous paragraphs all fall into the category of matched filter receivers. In other words, they are the optimum receivers (in the stochastic theory sense) for their respective waveforms. Furthermore, the PRTH and PN-receivers are correlation receivers, i.e., a stored replica of the incoming waveform is multiplied times the incoming waveform and the product is integrated for an appropriate time interval.

The process of synchronizing the PRTH and PN waveforms may be considered to occur in two steps; 1) search over the range/time uncertainty, 2) detection of the correlation peak which indicates code synchronism. The search procedure involves slewing the replica code in phase with respect to incoming code. This is generally accomplished by running the clock which drives the replica coder at a slightly slower rate than the incoming code clock. The detection step consists of recognizing that no correlation peak exists for non synchronized positions and detecting the peaks and stopping

search for the synchronized position. This detection procedure may be implemented either as a fixed integration interval/constant search rate or as a sequential detection process. As the name implies, the fixed integration interval means that both the signal plus noise or noise alone is integrated for a fixed amount of time for each search position and then threshold sampled. The threshold value determines the probability of false sync and probability of sync. The sequential detection process integrates the signal plus noise or noise alone, until either a lower threshold indicating only noise or an upper threshold indicating signal plus noise is crossed. Crossing of the lower threshold causes the search to continue to the next position, while crossing of the upper threshold indicates sync and stops the search. A diagramatic comparison between the two types of detection is shown in figure 1.66 . It is statistically possible that integration could go on indefinitely without a crossing of either threshold, thereby drastically reducing the search rate. This condition is avoided by stopping or truncating the test after a fixed integration time and declaring sync. In the sequential detector the integration time T_S required for detection of the correlation peak is approximately equal to that required by the fixed integration time detector. The performance advantage of the sequential detector lies in the fact that on the average the decision "noise only is present," i.e., "incorrect sync position," is made in a much shorter time than that of the fixed integration time detector.

Synchronization of the RADA waveform is a slightly different procedure than that described already due to the utilization of the digital

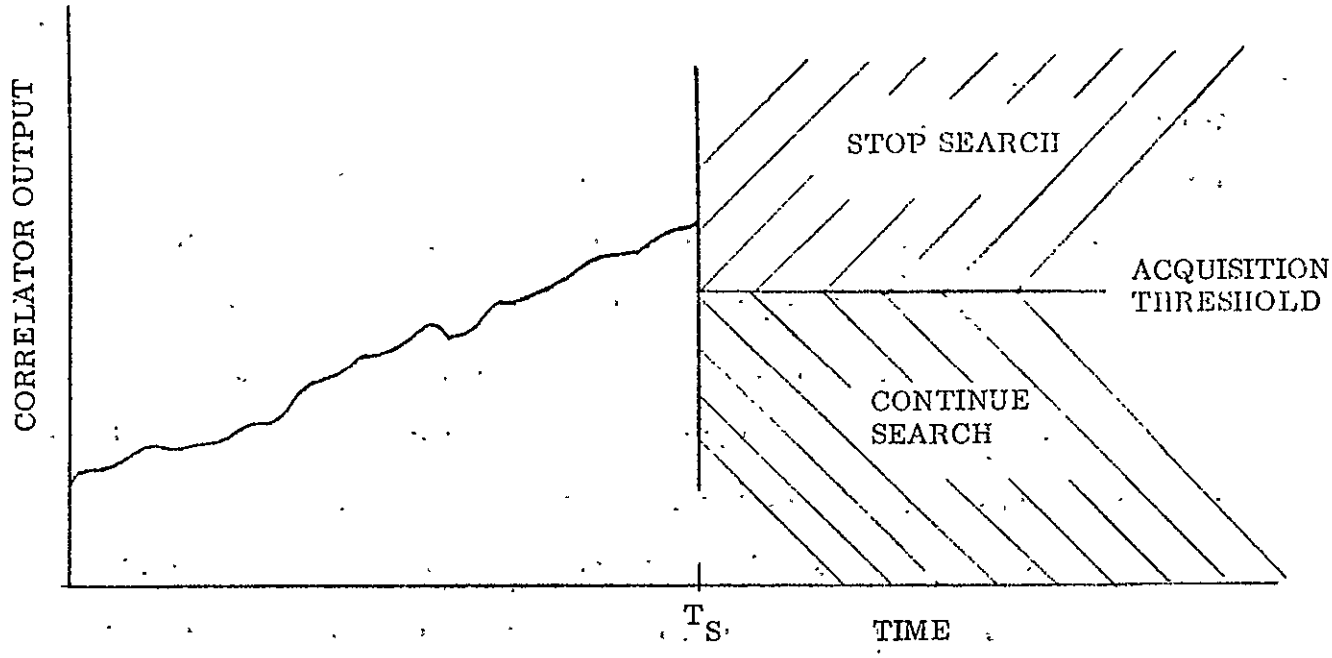

Fixed Integration Time Acquisition Detection

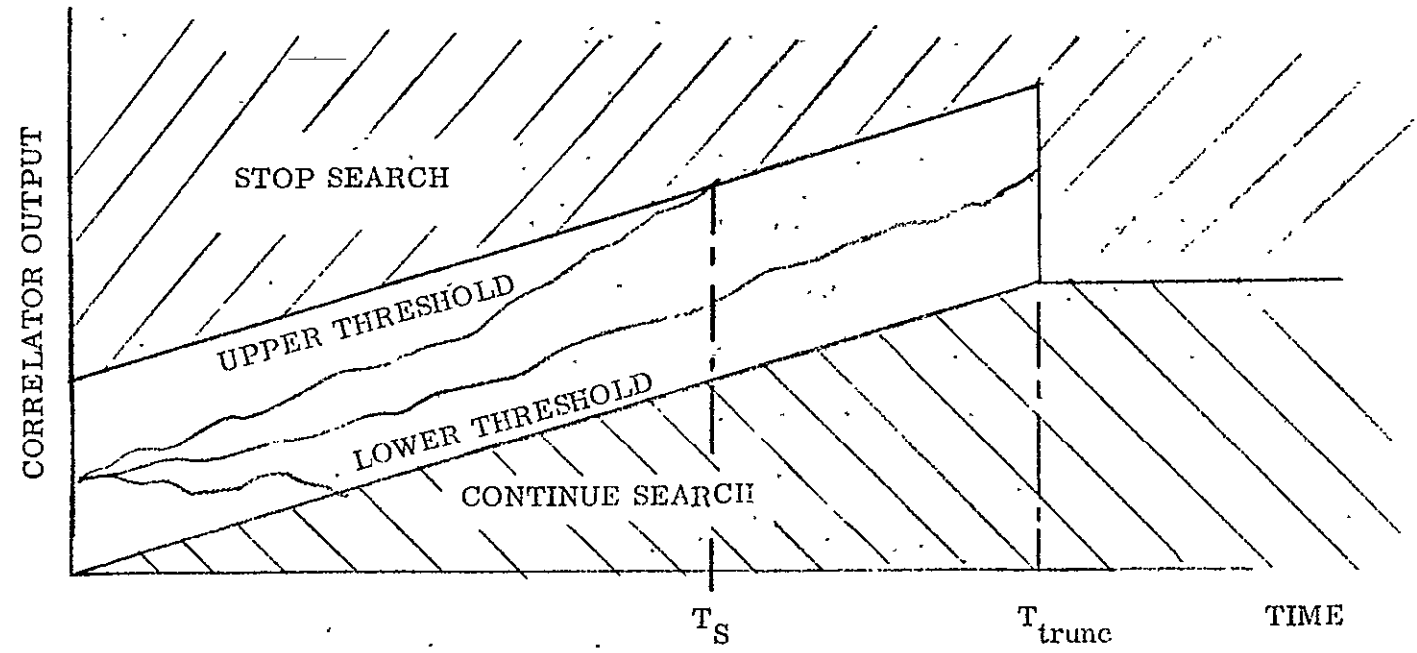

Sequential Detection Acquisition

Figure 1.66 - Comparison of fixed integration time and sequential detection acquisition

matched filter. Frame synchronization rather than bit synchronization is required. This means that the coincidence logic output is sampled for a maximum time equal to a frame time. Once again, however, it is expedient to utilize sequential detection procedures.

A detailed analytical study by Magnavox of the sequential detection process as applied to PN code synchronization has been recently concluded. In order to compare the synchronization performance of the three waveforms, the appropriate results of this study will be used.

The synchronization performance of the respective waveforms, PRTH, RADA, PN may be determined from the table 1.13. This table gives the probability of synchronization on one pass as a function of E/N_o . Before this table can be utilized to compare the three waveforms, it is necessary to evaluate the respective expressions for E/N_o which have been derived. These expressions are tabulated in table 1.11.

Waveform	$\frac{S}{N} = E/N_o$
PRTH	$2.3\times10^{-4} \quad \frac{P_R T}{N_o\left(1+.113 \frac{P_R}{N_o W}\right)}$
RADA	$1\times10^{-3} \quad \frac{P_R T}{N_o\left(1+ \frac{P_R}{N_o W}\right)}$
PN	$\frac{1}{4/\left(\frac{S}{N}\right)_u \; PG+(K-1)\sigma^2}$

Table 1.11 E/N_o for TDRS waveforms

The time to search one bit, T, is taken to be 10^{-3} seconds, in accordance with the data rate. This common search time T is not sacred but is representative for these three techniques. A RADA bit is ten times longer than either a PRTH or a PN bit because of the frequency hopping, consequently, T for RADA is ten times longer. Thus table 1.11 reduces to table 1.12.

The variance of the cross correlation σ^2 for the PN codes used must be calculated before the three waveforms may be further compared. As pointed out in section 1.6.6, a class of codes known as Gold codes possess the lowest values of σ^2. Gold has shown that the normalized variance of the cross correlation for a limited integration window is given by

$$\sigma^2 = \frac{1}{w}\left[1 - \frac{w-1}{N^2}\right] = \frac{1}{f_c T}\left[1 - \frac{w-1}{N^2}\right] \qquad \text{eq. 1.118}$$

where

w = integration window size (bits)

N = code length (bits)

f_c = code rate

If a code rate of 2 megabit and a 13 stage code generator (8191 bits) are used, an average integration time of $T = 10^{-3}$ gives a window size of $\sim$ 2000 bits. Thus the variance is found to be $\sigma^2 = -32$ dB.

Waveform	E/N_o
PRTH	$1.4\times10^{-7}\ \frac{P_R}{N_o}$
RADA	$.6\times10^{-5}\ \frac{P_R}{N_o}$
PN	$\sim\ \frac{1}{(M-1)\sigma^2}$

Table 1.12 E/N_o for Wideband TDRS waveforms

Thus, the following E/N_o ratios are obtained for the three waveforms:

$$\left.\begin{aligned} \frac{E}{N_o} &= -12.5 \text{ db} \quad (\text{PRTH}), \\ \frac{E}{N_o} &= -4 \text{ db} \quad (\text{RADA}), \\ \frac{E}{N_o} &= 11.5 \text{ db} \quad (\text{PN}). \end{aligned}\right\} \text{ 1 watt user}$$

We conclude that the PN system has the highest potential for reliability synchronization of the three systems considered.

There are a number of methods which can be employed to accomplish the serial synchronization and these techniques range from a uniform search (coherent) to adaptations of sequential testing using coherent, noncoherent, and costas loop implementations.

Table 1.13 Summary of Analyses and Simulations of Synchronization Performance

Probability of Synchronization = 0.9

	Uniform Search Rate Coherent No Data	Sequential Coherent No Data	Sequential Noncoherent No Data	Sequential Optimized Costas Loop		Sequential Differentially Coherent	
				No Data	Data	No Data	Data
E/N_o =	9.5	4.5	11.5	11.5	13.5	9.3 db	10.7 db

The above table 1.13 contains the required S/N needed to provide .9 probability for synchronizing a wideband digital system (PRTH, RADA, PN). This table results from a thorough study of serial search techniques performed by the Magnavox Research Labs. We have shown in this section (and in section 1.6.6.6) that the PN system will provide these required S/N at low user power levels (as little as $\sim$.5 watt) while PRTH and RADA required high peak powers (600-1200 watts) to attain the desired performance. From table 1.12 we see that the sequential differentially coherent (no data) approach requires a 9.3 db S/N to insure .9 sync probability for one pass. The best approach, sequential coherent (no data) is better however in practical for TDRS applications. Thus we conclude that the PN system can synchronize with a probability of .9 at user power levels of .5 watts, excluding the effects of doppler and no regard for system margins. In the next section we will include the effects of doppler and system margin on the PN system. We will also estimate sync times and sync reliability for both the G.S. to user link and the user to G.S. link for the PN system. We have taken the liberty to assume in the above discussions that no data will be transmitted during the synchronization process.

1.9.4 G.S. to User PN Synchronization and Commanding

In order to provide commands to individual TDRS users a dependable command channel must be provided between the G.S. and the user. Current TDRS concepts dictate the desirability of a command channel which operates on a single frequency and which can be easily synchronized to by those users in view of the TDRS.

The G.S. to User link is characterized by its 148-149.9 mhz bandwidth and the 10-20 watts of available power from the TDRS to the user. In order to command the users frequently, an overall data rate of 400 bit/sec is anticipated assuming that all 40 users are synchronized to the command channel, this data rate should provide commands every 10 sec to each user.

For the moment we neglect interference at the user from earth-based RFI. Thus the command channel must contend with noise and its own multipath.

A PN system conveying 400 bit/sec can easily contend with the ambient noise and worst case multipath. The (S/N) performance of such a system is given by

$$\left(\frac{S}{N}\right)_{\text{at user}} = \frac{(P.G.)S_c}{N_o W + S_c} \qquad \text{eq. 1.119}$$

$N_o W$ is the noise power at the user in a band W

P.G. is the processing gain, $\therefore \left(\frac{S}{N}\right)_{user} = \frac{2.5\times10^{-3} W\, S_c}{S_c + N_o W}$. Based on link calculation presented in Appendix IV, a 500K chip/sec rate insure 27 db output (S/N) in a 400 hz equivalent bandwidth.

The TDRS to user link is plagued with a peak doppler ∿4 khz , which serves to degrade the systems performance during synchronization. Doppler does not, in this case, degrade system performance (data detection) once synchronization has occurred, because of the relatively low doppler rate of change ∿4 hz/sec at VHF.

We now analyze a worst synchronization model for the G.S. to User. VHF link. This technique is the doppler filter synchronization (non-coherent) by serial search. This technique does not employ sequential detection because of the large (S/N) available at the user's correlator output.

First we assume the doppler filters are 1 khz wide so that eight filters are required at the user to resolve the signal into 1khz slots. The output from each filter is envelope detected on for each test period T 10^{-3} sec the outputs are compared, the largest filter compared to threshold and if the threshold is exceeded the search is stopped and the signal is identified with the filter which exceeded the threshold. The performance curve for this crude system is shown in fig. 1.67.

The false alarm number z is the maximum number of tests required to synchronize times the probability that one filter's envelope exceeds the threshold. It is obvious from fig.1.67 that at (S/N) ∿ 17 db will insure .99 probability of acquisition while insuring a false alarm number $z = 10^{10}$ which in turn guarantees a false alarm probability $< 10^{-6}$ for most practical PN sequence lengths. At the same time the (S/N) in the 1 khz doppler filter is 23 db (eq. 1.119) providing a 6 db system margin to insure this result.

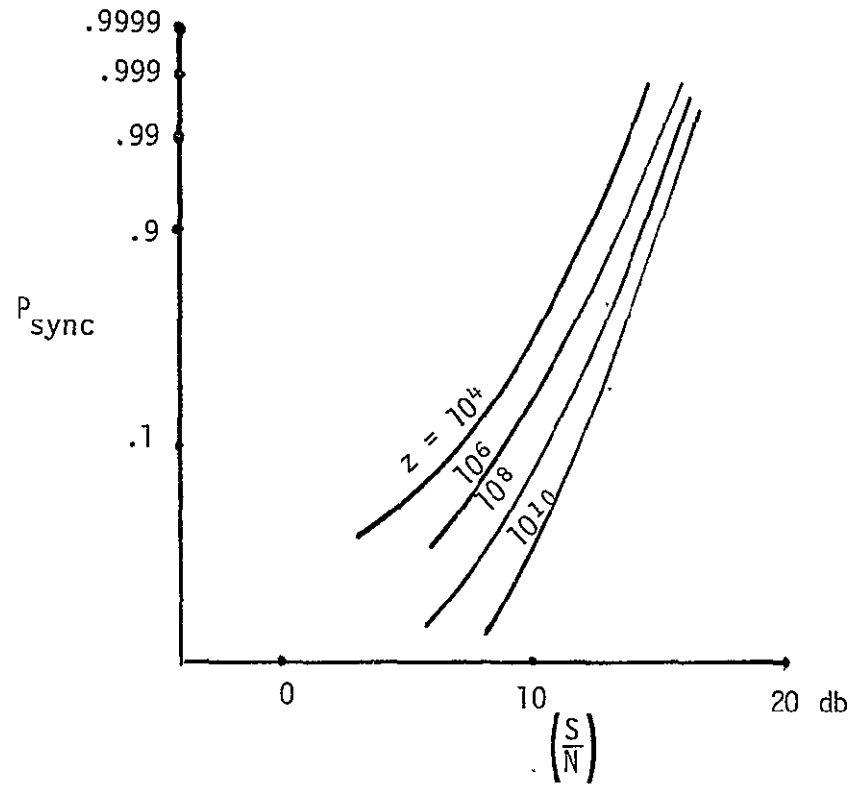

Figure 1.67: Probability of Sync versus $\left(\frac{S}{N}\right)$ in One Doppler Filter

The probability of synchronization is at least .99 for the GS to user link for the technique just analyzed. The time required to synchronize is another parameter of interest. The time to fully synchronize T_s is the sum of the code acquisition time T_{acq} plus the phase lock loop acquisition time required for frequency and phase lock. Since the G.S. to user doppler has been resolved to 1 khz, the time to acquire for a phase T_{PLL} lock loop is dependent on the frequency uncertainty $\pm\Delta w$ and, the loop natural bandwidth. Thus the total time to acquire

$$T_S = \underset{\text{code}}{T_{acq}} + T_{PLL}$$

$$T_S \simeq (2^n-1)T + T_{PLL} \qquad \text{worst case} \qquad \text{eq. 1.120}$$

where 2^n-1 = code length

If we assume that the test interval T is 1 msec and a code length of 8191 then the worst case $T_S \sim$ 8 sec since the T_{PLL} is approximately a millisec.

If a phase lock loop had been utilized instead of doppler filter the result would have been better. Thus we can conclude that the G.S. to user link is highly reliable and that the sync time is on the order of 8 seconds for the code length used in the example.

1.9.5 User to Ground Station Synchronization

The user to G.S. link is power starved and user limited dictating that more sophisticated synchronization techniques are required. We have shown in section 1.9.3.4 that synchronization can be accomplished at a

9.3 dB $(\frac{S}{N})_{out}$ at the G.S. in the presence of noise, 40 users, and their multipath. This result was obtained under the assumption that doppler was not present. The probability of acquisition was found to be .9 under the above conditions. This means that the user to G.S. link can be easily doppler compensated to insure this desirable condition. The doppler compensation is needed only during code acquisition. Doppler compensation information is available at the user and can be employed to compensate the user to G.S. link during the expected code acquisition interval.

Thus we recommend that the sequential differential coherent synchronization techniques be employed at the G.S. to insure the .9 sync probability for the user to G.S. link.

The overall sync probability for the 2 way link is essentially .9 since the G.S. to user link probability is virtually unity, only if doppler compensation is employed. If a link margin of 6 dB is factored into the power budget then a user power of 2 watts is required to meet the .9 sync probability.

The doppler problem is not unique to PN, it serves to degrade even the adaptive or programmed techniques outlined in section 1.6.7. Thus we would recommend that doppler compensation be employed on the user to G.S. link during the synchronization period to maintain low user power levels regardless of the modulation technique.

1.9.6 Choice of Code Lengths, Code Rates and Total Synchronization Time for the 2 Way PN Link

It has been shown in previous sections that;

a) the G.S. to user link can be synchronized with a very high sync probability >.99 for one pass

b) the user to G.S. can be synchronized with a probability of .9 for one pass with doppler compensation and a user power level of 2 watts which provides a 6 dB system margin.

c) the overall link can be synchronized with a probability of .9 for one pass.

d) to maximize the processing gain of the user to G.S. link one must use Gold Codes at code rates of 2 megachip/sec.

e) that we must provide unambiguous ranging of 10,000 mi. to track a user.

The unambiguous ranging requirement and the maximizing of the processing gain requirement are at odds since the 2 megachip/sec rate dictates that very long Gold sequences are required to insure unambiguous ranging. For example,

Code Rate	Code Length 2^n-1	Repitition Period	Required Ranging Time Unambiguous
2 megachip/sec	n=13	4 msec	60 msec
2 megachip/sec	n=15	16 msec	60 msec
2 megachip/sec ——	n=17	64 msec	60 msec

We see that a seventeen stage Gold sequence generator which produces a sequence of length ~128,000 chips is required to provide unambiguous ranging. If the chip rate is reduced to 500 K chip/sec the code length required to obtain unambiguous ranging is still 32,000 chips. Further reduction in the chip rate to 125K chips per/sec would allow the use of a 8191 length code and would satisfy the unambiguous ranging requirement. The G.S. to user link has an adequate link margin to insure the desired sync probability, bit error probability, etc., even at a chip rate of 125K chip/sec. However, the user to G.S. link requires a 2 megachip/sec rate to provide the maximum processing gain to allow for the forty users, their multipath and noise.

Let us assume that the 2 megachip/sec rate for the user to G.S. link is invariant, then it follows that there are two basic methods of providing simultaneously multiple access for 40 users, unambiguous ranging, sync time of approximately 15 sec, the desired uplink and down error probability of 10^{-5}, and an overall sync probability for the 2-way link of .9 for one pass. There are,

a) G.S. to user link at 125 K chip/sec and a linear maximal code of length 8191 chips. The user to G.S. link uses 2 megachip/sec and a Gold code length of 8191 for synchronization purposes. After synchronization has occured at the G.S., a command signal from the G.S. is sent to the user craft which switches the user code to a length ~128,000 bits to provide unambiguous ranging if it is desired. During non-ranging intervals, 2-way range rate is still available. Data can be conveyed from the user to the G.S. in either case. The overall sync time for the system is approximately 16 sec. The Gold Code of length 8191 from the user is synchronized to the 8191 code from the G.S. When unambiguous ranging is desired the 128,000 bit code is generated from 17 stage Gold generator but is truncated (an easy task for a finite state machine) so that the all one's condition of the 8191 G.S. to user code starts the 128,000^{+} chip sequence at the beginning of each repetition.

b) A second approach is a very simple concept. The G.S. to user PN link is a single signal as in case (a) and uses an 8191 length code but a high chip rate, e.g., 500 K chip/sec to increase the processing gain. With the additional processing gain range resolving data is interleaved with the user commands in a manner very similar to the way low

frequency ambiguity resolving tones are used in the GRARR side-tone system. These digital patterns are "turned around" at the user and returned to the G.S. under the protection of the PN sequence. The user to G.S. PN sequence is synchronized to the G.S. to user sequence as in case (a).

It is not clear which approach is optimal, however, both approaches appear to be quite feasible and meet all the basic requirements.

Since the user to G.S. link is power starved already approach (b) would burden the link with additional range resolving data if simultaneous data and ranging is required. This fact leads us to recommend approach (a) over (b) even though some slight range resolution in (a) may be incurred. (e.g., the TDRS to user range error would increase to 4.5 m at 10 watts from TDRS).

Both approaches are completely compatible with the emergency voice/data manned operation. Note that if further reduction in sync times are required then parallel correlator can be employed at a very small increase in hardware.

1.9.7 Synchronization of Narrowband Signals and User Commanding

In section 1.6.7 we presented several narrowband signaling techniques which completely avoid the multipath. In order to synchronize the user with the G.S. and vice versa both terminals should use the same timing format, gating, duty factor, etc. The full (S/N) ratio is not available for synchronizing, ranging, data transfer, etc., unless this mutual timing is observed.

This mutual timing requirement means that synchronizing, commanding, ranging are dedicated operations, i.e., if a user is to be commanded he must first be synchronized, then if another user is to receive a command

he must be synchronized separately and so on. Thus synchronizing ranging and commanding must be done sequentially and in a dedicated manner unless multiple G.S. to user channels are employed. Multiple channels of course remove the above criticisms.

The synchronization of the narrowband signals discussed in section 1.6.7 is greatly simplified if

a) the signals use fixed duty factors and spacecraft achieve the desired orbit

b) adaptive duty factors are employed, good ephemeris data will aid synchronization.

The worst synchronization problem that faces the narrowband systems occurs when the G.S. and the user have no a priori knowledge of each others timing, duty factor, etc. If the G.S. wishes to contact the user the G.S. must use a worst case duty factor that protects against the worst expected multipath and the user must perform a duty factor or timing search.

By and large the remarks made about acquisition in the presence of doppler for wideband signals hold for the narrowband signals.

Except for the worst case situations cited above, the narrowband signal should be capable of 2-way synchronization in a matter of a few seconds if proper procedures are to follow and ephemeris data is available.

We are concerned about the synchronization and commanding of the user at very low altitudes since the narrowband approaches offer little or no multipath protection at low altitudes during the launch phase.

1.10 PHASE LOCK LOOP TRACKING FOR EFFICIENT DETECTION OF DATA AND VOICE

In the previous section we have discussed the general problem of synchronization of wideband modulation systems which are under investigation for the TDRS. Once synchronization of the wideband system has been accomplished, data or voice must then be recovered in an efficient manner. This is usually achieved through the use of conventional phase lock loop techniques, and the tracking error must be small in order to approach performance predicted for the modulation coding structure.

In the absence of phase or frequency jitter on the received signal, the tracking loop could have a very narrow bandwidth. However, to accommodate such jitter, and in particular a changing Doppler in a moving terminal (e.g., a user), a lower bound is placed on the tracking loop bandwidth. It is the goal to maximize the allowable bandwidth, consistent with a specified overall system performance degradation. For example, the expected peak Doppler and peak for the TDRS Doppler rates are listed below.

	Doppler (peak)	Doppler Rate (peak)
VHF	3.75 KHz	4.0 Hz/sec
S Band	60 KHz	60 Hz/sec
K_u Band	420 KHz	420 Hz/sec

The problem is further complicated by the data modulation on the received signal. The tracking loop must be devised consistent with such modulation. For example, with PSK the carrier is completely suppressed by the data modulation and for such a signal, there are three basic methods for creating a carrier reference at the receiver. The first is to remove

the information and extract the carrier from the remaining signal. Loops which use this method are the squaring loop and the Costas loop. Essentially they square the received signal and track the double carrier frequency signal. Since the received signal is squared, the polarity of the carrier is lost, introducing a 180 degree ambiguity in the carrier recreated thereby. This ambiguity motivates consideration of the second method which is to inject a reference carrier into the transmitted information signal. Although ambiguity could have been resolved by using differential encoding, the performance of the system would have approached that of a coherent system only at high signal-to-noise ratios.

The third method ties decoding into the carrier tracking process. Essentially, when decoding is taking place correctly, the data modulation can be duplicated and removed from the received signal to recreate a carrier for tracking. This decision directed technique can potentially outperform a Costas loop; however, a practical restruction of importance is the decoding delay before the received modulation can be duplicated correctly.

With the additive reference system, the received signal, after the antimultipath/multiple access modulation has been removed, contains a reference signal component and a data signal component. The reference signal has power P_s, the data signal contains power S, and the total transmitted power, P_T, is constant such that $P_T = S + P_s$.

If the noise is assumed to be white and Gaussian with a single sided spectral density of N_0 (watts/Hz), then the signal-to-noise ratio of the data signal is

$$\frac{E}{N_0} = \frac{ST}{N_0}$$

where T = the digit interval, and the signal-to-noise ratio of the carrier tracking loop is

$$\alpha = \frac{P_s}{N_0 B_L} = \text{carrier loop SNR}$$

where B_L = one-sided noise bandwidth of the carrier tracking loop.

1.10.1 Performance of Binary PSK System with a Noisy Reference Carrier

The function of the carrier tracking loop for a PSK system is to estimate the phase of the received signal. The estimate is made by tracking the additive reference signal. Because of noise interference, the phase estimate will err by

$$\phi = \theta - \hat{\theta} \qquad \text{eq. 1.121}$$

where

θ = the transmitted phase angle

$\hat{\theta}$ = estimate of the transmitted phase angle

If the carrier tracking loop is assumed to be a first order loop, then the probability density function of the phase error is

$$p(\phi) = \frac{\exp(\alpha \cos \phi)}{2\pi I_0(\alpha)} \; ; \; |\phi| < \pi \qquad \text{eq. 1.122}$$

The assumption is valid since at signal-to-noise ratios where the PLL normally operates, experimental evidence has shown that the phase error distributions for first and second order loops are nearly equal.

Using the above assumption, Lindsey* has determined the probability of a hard decision error for PSK with an additive carrier versus E/N_0 with α as a parameter. The results are shown in Figure 1.68. Note that as E/N_0 increases, there is a point where the error rate no longer diminishes. This effect occurs because as more energy is placed into the information bearing signal, the ultimate performance of the system is governed by the signal-to-noise ratio in the carrier tracking loop. Thus, the effects on system performance caused by phase errors are clearly manifested. Note that as the loop SNR approaches infinity, the system performance approaches that of a coherent system.

Using a continuous additive carrier is not a particularly efficient or easily implemented method of generating a reference. The preceding results assumed that the data channel does not interfere with the sync channel. The gated reference system eliminates possible interference in the reference channel in a practical way. The system is implemented such that at predetermined times, a portion of the unmodulated carrier signal is diverted by means of a gate into the carrier tracking loop. The gated reference contains only carrier information and does not transmit any information. Thus there is the question of optimum allocation of power between the carrier reference signal and the information signal.

---

*Lindsey, W.C., "Phase-Shift-Keyed Signal Detection with Noisy Reference Signals," IEEE Trans. AES-2, No. 4, July 1966.

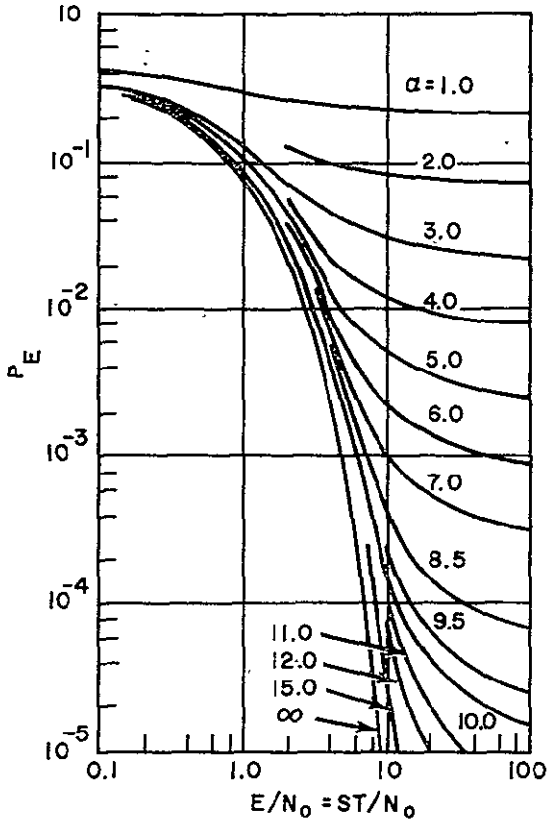

Fig. 1.68 ERROR PROBABILITY FOR PSK WITH AN ADDITIVE CARRIER

1.10.2 Suppressed Carrier Tracking Loop

The extraction of a carrier from a double sideband suppressed carrier signal by using a squaring loop is suggested by the form of the transmitted signal

$$y(t) = \sqrt{2S}\ m(t) \cos(\omega_0 t + \theta) \qquad \text{eq. 1.123}$$

where $m(t) = \pm 1$. Squaring the signal yields

$$y^2(t) = S\{1 - [\cos 2(\omega_0 t + \theta)]\} \qquad \text{eq. 1.24}$$

The carrier reference can then be extracted by a phase locked loop centered at the double carrier frequency. The squaring loop is mathematically equivalent to the Costas loop, a more practical implementation of extracting the carrier reference from a DSBC signal, so that the results that will be presented can be directly applied to analysis of the Costas loop.

Lindsey* has determined an expression for the probability of error based on the following assumptions:

- The distribution of the phase error is approximately given by the first order loop statistics.
- The input bandpass filter (BW = W) passes the signal y(t) undistorted.
- The ratio W/B_L is sufficiently large such that the output of the squaring device is very nearly Gaussian.
- The loop bandwidth, B_L, is small so that the spectrum within the loop is essentially flat.

*Lindsey, op. cit.

The results of the analysis are presented in Figure 1.69. The parameter δ is defined in the analysis as

$$\delta = \frac{1}{B_L T}\left[\left(1 + \frac{N_o W}{2S}\right)\right]^{-1} \qquad \text{eq. 1.125}$$

Note that the parameters of the loop should be adjusted so as to maximize δ for the loop to perform optimally. By observing Figure 1.69 it is seen that when $\delta \geq 5$ the loop operates within 1 dB of coherent at $P_E = 0.1$. A loop bandwidth $B_L \approx 0.1/T$ appears to be required in order to achieve this performance, in view of Equation 1.125 and the indicated loss of the squaring process.

Since the squaring loop operates on the total signal to generate the carrier reference, it appears at first look that the quality of the generated reference will be better than the reference generated by a carrier tracking loop which operates on a reference which is only a portion of the received signal. Yet because of the squaring operation a 180 degree phase ambiguity is introduced, which must be resolved with some loss. Furthermore, Equation 1.125 illustrates the fact that there is an inherent loss for carrier tracking by a Costas loop at low signal-to-noise ratio. Since there are lower practical limits to loop bandwidth, a tradeoff exists between the nonlinear S/N loss of Equation 1.125 and the power sharing loss of a transmitted reference system.

Usually the phase ambiguity in tracking a suppressed carrier signal is overcome by differentially coding the data. As discussed above, the loss of performance of such a system at low E/N_0 suggests investigation

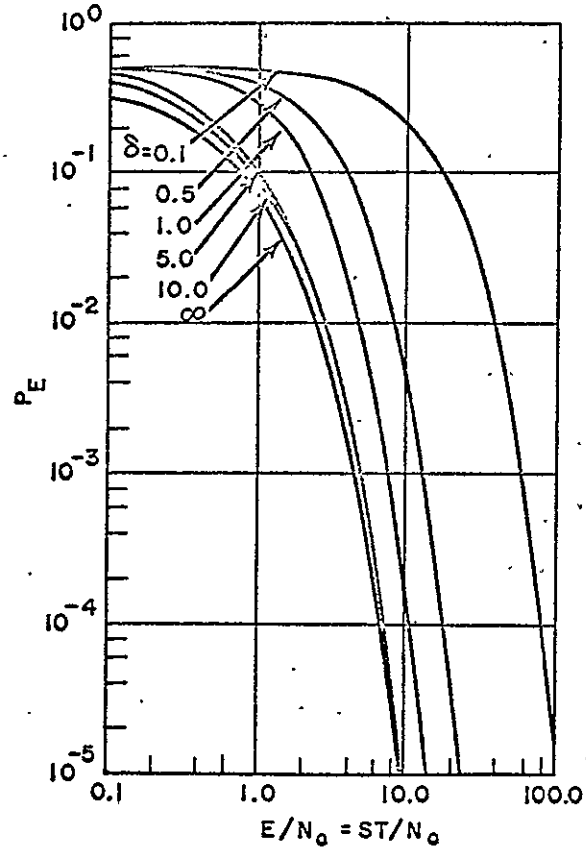

Fig.1.69 ERROR PROBABILITY FOR PSK USING A COSTAS OR SQUARING LOOP

of alternate techniques. A possible method of phase ambiguity resolution is accomplished by the injection of a phase reference bit among the data bits. The phase reference bit is compared with the squaring loop reference so that the phase ambiguity can be resolved. The question of optimization of the reference bit injection scheme arises, e.g., how many bits of information can be transmitted per synchronization bit. Note that this method superficially resembles the gated reference system discussed above, although the utilization of the reference is basically different.

The motivation for considering this scheme is qualitatively based on the argument that the Costas loop enables the carrier phase to be tracked using the entire received power. Then, reference bits need be inserted only commensurate with the probability of a loop flip (180 degree phase reversal due to noise). In principle, this technique offers promise of satisfactory operation with only a small fraction of power in the reference.

Another approach toward achieving carrier tracking on the entire signal and eliminating loss of a transmitted reference is to reconstitute phase using output data to remove the modulation. The phase of previous received digits is stored and employed in a finite averaging (after removal of modulation) to generate a reference for demodulation of the next digit. This has been studied by Gray* for its applicability to sequential decoding.

Since Gray's phase reconstruction method is based on a recursion relationship it is necessary to store the previous reference vectors. The most likely manner would be to store the orthogonal components with respect

*Gray, R.M., "Simulation of Sequential Decoding with Decision Directed Channel Measurement", M.S. Dissertation, MIT, June 1966.

to the reference vector into two digital registers. To store the vectors in the registers, they must be quantized. The smaller the intervals, the larger the register size.

1.10.3 Comparison of Methods for Carrier Tracking

To provide coherent detection in a practical communication link, the reference phase information must be extracted from the received signal by the receiver. Several means are available to circumvent this problem of an inherent phase ambiguity. For the following discussion, they can most easily be described in terms of systems that actually transmit an unmodulated phase reference, those that solve the ambiguity with data encoding, and those that tolerate the ambiguity through data encoding.

We are interested in providing the reference carrier for coherent demodulation schemes operating at very low ratios of energy per symbol to noise power spectral density (E/N_0).

Development of the performance of detection systems employing references derived from the received signal have shown that the performance is essentially equivalent to that of a coherent system if the signal-to-noise ratio in the tracking loop is greater than 10 to 13 dB. From this it can be seen that integration over a significant number of signaling elements is required. Several factors limit the maximum allowable integration time, however. These factors are manifested as phase modulation on the carrier; they determine coherence time of the carrier itself, exclusive of the information. Oscillator phase instabilities and propagation variations are common to all terminals. Moving terminals have a

further problem in that their relative motion produces effective carrier modulation (Doppler) that may limit the coherence time. For low data rates, these limitations on carrier coherence are extremely important.

When operating with low E/N_o with significant memory in the phase reference generator, the channel can no longer be adequately modeled as memoryless. When large phase errors occur their effect will extend over many bits so that a significant correlation will exist in the bit-to-bit error probability.

The transmitted reference technique involves essentially transmitting two signals - the information and the carrier phase reference. One mechanization of this is the gated reference. The phase information is multiplexed with the data stream and the phase locked loop input is gated to accept only the reference signals.

Another mechanism for transmitting the carrier phase is to leave a continuous carrier component in the transmitted information. This amounts to modulation by some angle less than $\pm\pi/2$. A drawback to this technique - and a consideration in all continuous reference techniques - is that the information power becomes a noise source, unless Manchester coding is employed. Furthermore, the reference information must be transmitted at the expense of the information power and this is a drawback. Another consideration is that since the reference power is low - to limit the effect on the information - the high signal-to-noise ratio desired in the tracking loop bandwidth must be achieved by extending the integration time in the phase locked loop.

An estimate of the tracking capability of the gated reference technique can be derived simply, assuming a second order phase locked loop. It can be assumed that it is desirable to have a signal-to-noise ratio (α) of 13 dB, given that α is

$$\alpha \triangleq \frac{P_r}{N_o B_L} \qquad \text{eq. 1.126}$$

where

P_r = the reference power

N_o = the one sided noise power spectral density

B_L = the loop noise bandwidth (one sided)

The average power in the reference is a fraction (ε) of the total power (P). Assuming $\alpha = 20$, then

$$B_L = \frac{\varepsilon P}{20 N_o} = \frac{\varepsilon}{20(1-\varepsilon)T} E/N_o \qquad \text{eq. 1.127}$$

where

$T = 1/R$

R = the basic signaling rate of symbols

E = the energy per symbol

From Viterbi's work, an optimum second order loop can track a maximum linear rate of change in frequency of (doppler change)

$$D = \frac{32}{9} B_L^2 \text{ radians/sec}^2 \qquad \text{eq. 1.128}$$

therefore the above tracking loop can track a maximum rate of change of frequency

$$D = \frac{32}{9} \left[\frac{\varepsilon}{20\ (1-\varepsilon)T} \ E/N_o \right]^2 \qquad \text{eq. 1.129}$$

Equation 1.129 is plotted in Fig. 1.70 using a normalized parameter DT^2. The family of curves is generated by employing various values of ε.

The problems associated with tracking on only a part of the power can be alleviated if a Costas loop or a squaring loop is employed. These loops track on the total power (only modulation is sent) but have an associated 180 degree ambiguity. There is an additional problem with these loops when operating in the region of interest, a signal-to-noise ratio suppression results from nonlinear operations.

From Rice's development of the output of a square law device with a sine wave plus noise input

$$N_0' = N_0{}^2W + 2SN_0 \qquad \text{eq. 1.130}$$

$$P = \frac{S^2}{2}$$

where

N_0' = the one-sided noise power spectral density at the second harmonid

W = the bandwidth of the noise input to the square law device

S = the input sine wave power

N_0 = the one-sided noise power spectral density

P = the output power in the second harmonic

As before, defining the signal-to-noise ratio in the tracking loop bandwidth as

$$\alpha = \frac{P}{N_0'B_L'} \qquad \text{eq. 1.131}$$

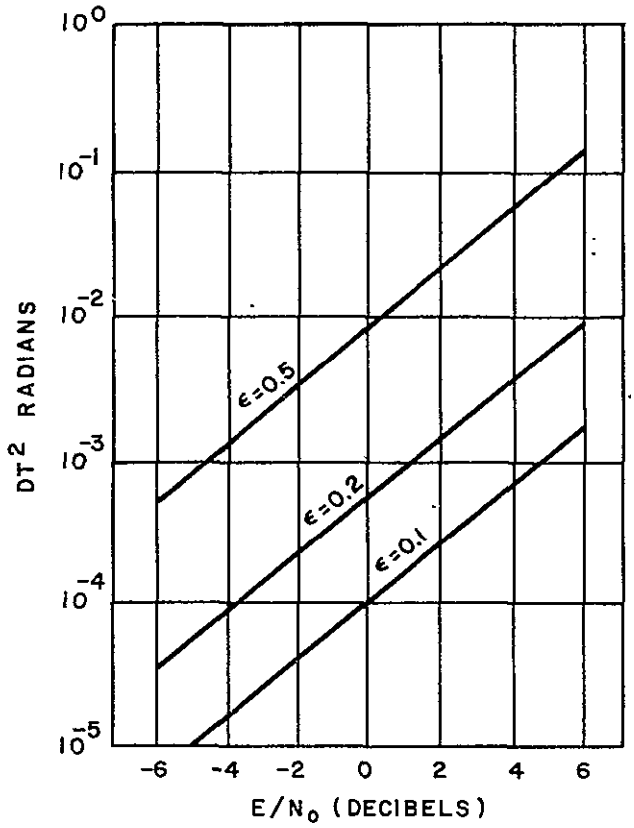

Fig. 1.70 PERFORMANCE OF GATED REFERENCE LOOP

the signal-to-noise ratio for the suppressed carrier tracking at the doubled frequency becomes

$$\alpha'_{2nd} = \frac{(S^2/2)}{(N_o{}^2W + 2SN_o)B'_L} = \frac{S}{4N_oB'_L}\left(\frac{1}{1 + N_oW/2S}\right) \qquad \text{eq. 1.132}$$

For high α' the phase jitter in the second harmonic tracking loop is $1/\alpha'$. At the carrier frequency, then, the rms phase jitter is one-fourth that of the second harmonic. Assuming an input filter having a bandwidth of $1/T_s$ where T_s is the digit length, the phase jitter at the carrier frequency becomes

$$\alpha' = \frac{1}{\alpha^2{}'_{rms}} = \frac{S}{N_oB'_L}\left(\frac{1}{(1 + N_o/2E)}\right) \qquad \text{eq. 1.133}$$

where E is the energy in a single symbol.

If, as before, a signal-to-noise ratio of 13 dB is desired, the required loop bandwidth (B'_L) and the maximum rate of change of frequency that can be tracked (D') become

$$B'_L = \frac{E}{20N_o(1-\varepsilon)T}\left(\frac{1}{1 + N_o/2E}\right) \qquad \text{eq. 1.134}$$

$$D' = \frac{32}{9}\left[\frac{1}{20(1-\varepsilon)T}\ E/N_o\left(\frac{1}{1 + N_o/2E}\right)\right]^2 \qquad \text{eq. 1.135}$$

Equation 1.135 is shown in Figure 1.71 along with some of the curves from Fig. 1.70 included as references.

Figure 1.71 shows that in the E/N_o regions of interest, the suppressed carrier tracking outperforms the gated reference technique even when very

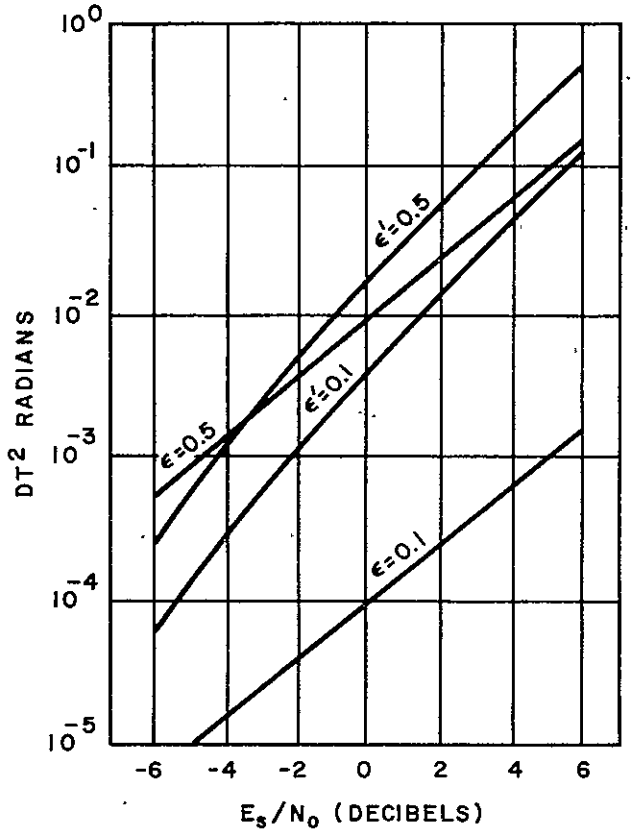

Fig. 1.71 COMPARATIVE TRACKING PERFORMANCE

large amounts of power are employed as references for both cases. It should be noted that the total received power at any given data rate is not constant in Figs. 1.70 and 1.71. Total power increases as ε is increased since the energy per symbol is being held constant.

Based upon the foregoing discussions we conclude that the Costas tracking loop is superior to that of the gated reference loop and may be regarded as a near optimum approach to carrier recovery for both digital and voice signals of the double sideband suppress carrier variety. Recently work has been carried out to further optimize the Costas loop or squaring loop for purpose of carrier recovery, the most notable of which is that due to Riter*. The basic difference in Riter's approach and that of the normal Costas loop is that a nonlinear hyperbolic tangent characteristic function is used in one of the Costas loop channels. The performance of the improved loop is essentially the same as a square law or Costas loop at low input signal-to-noise ratios but is 3 dB better than the normal Costas loop at high input signal-to-noise ratios. Fortunately, this improvement has little impact when the input signal-to-noise ratio is high and therefore the implementation due to Riter is of academic interest only in that the Costas loop performs in a near optimum manner when the input signal-to-noise ratios are at low values.

The Costas loop is easily implemented for either narrowband or wideband signaling techniques under investigation for the TDRS and we will not attempt to detail its implementation for each of the signaling methods although an implementation of the Costas loop is shown in Fig. 1.64 for PN/PSK.

---

*S. Riter and W. Hon, "Tactical Phase Reference Detectors for Fully Modulated PSK Signals", East Con 1968, Convention Record.

The basic or recommended approach for carrier recovery for both data and voice consists of a Costas loop detector which is a second order loop. Based upon a second order loop characteristic and the choice of the Costas configuration, we can now determine the ability of the carrier recovery loop to detect the data for the low data rate users in the TDRS, e.g., 400 - 1000 bps. These are the most critical data rates in that they are the lowest data rates used within the system and thus impose the narrowest restrictions on the Costas loop bandwidths. It has been stated that the Costas second order loop can track a linear changing doppler frequency or doppler rate of change given by $\frac{32}{9} B_L^2$ rad/sec^2.

We assume here that there is no difficulty in acquiring the signal through the use of phase lock loops which incorporate a saw-tooth search to search out the frequency uncertainty associated with the doppler. The primary difficulty involved in tracking wherein the maximum doppler rate of change varies from 4 Hz per second at VHF to as high as 420 Hz per second at K_u-band. Fortunately, at VHF the TDRS to user link which will require about 400 bits per second raw data rate can easily track the four Hz per second peak doppler rate of change utilizing a second order loop bandwidth which is 1/10 the lowest data rate.
In fact a loop bandwidth of 10 Hz will provide very adequately for the doppler rate of change at VHF for the unmanned user for both the 1000 bps user to G.S. link and the 400 bps G.S. to user link. At S-band and K_u-band for the manned user applications, a commensurately larger loop bandwidth can be utilized because the data rates of 4.8 kilobits to 50 kilobits per second are anticipated for these missions. Even at

K_u-band there is no difficulty forseen in using a Costas loop with a second order transfer function to provide accurate tracking capability for data rates of 4.8 kilobits through 50 kilobits and voice transmissions.

To substantiate our claim we show in Figure 1.72 the result of a computer program which shows the performance of the proposed Costas loop detector for various data rates, at a one g acceleration, and a carrier at 8 gHz, which is half way between the K_u-band and S-band frequencies. The maximum acceleration for a low orbit user is approximately one g. In Fig. 1.72 (a), (b), (c), B_L the loop bandwidth has been normalized to the data rate, e.g., at 300 bps, B_L = 1/6 corresponds to an actual PLL bandwidth of 50 Hz.

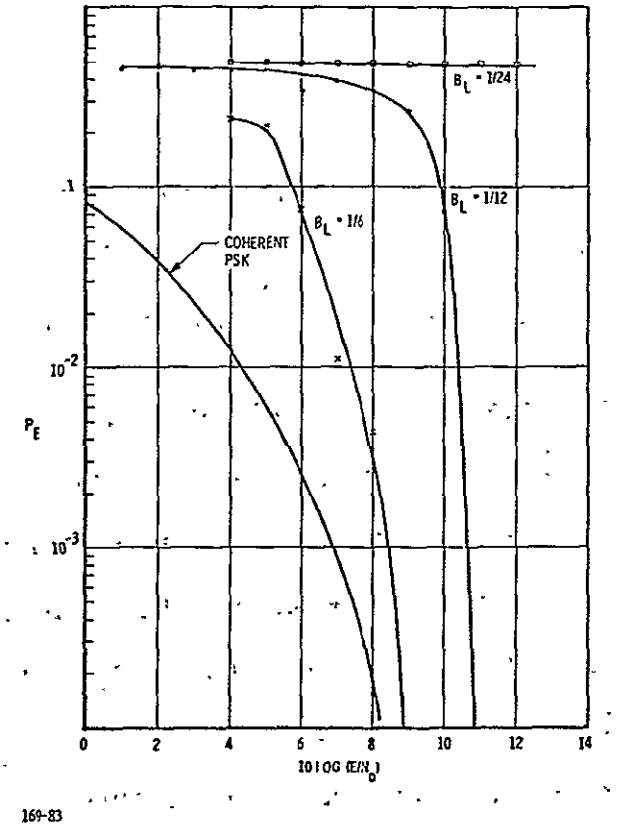

Figure 1.72(a) Bit Error with Doppler, Acceleration = 1 g
Digit Rate = 300

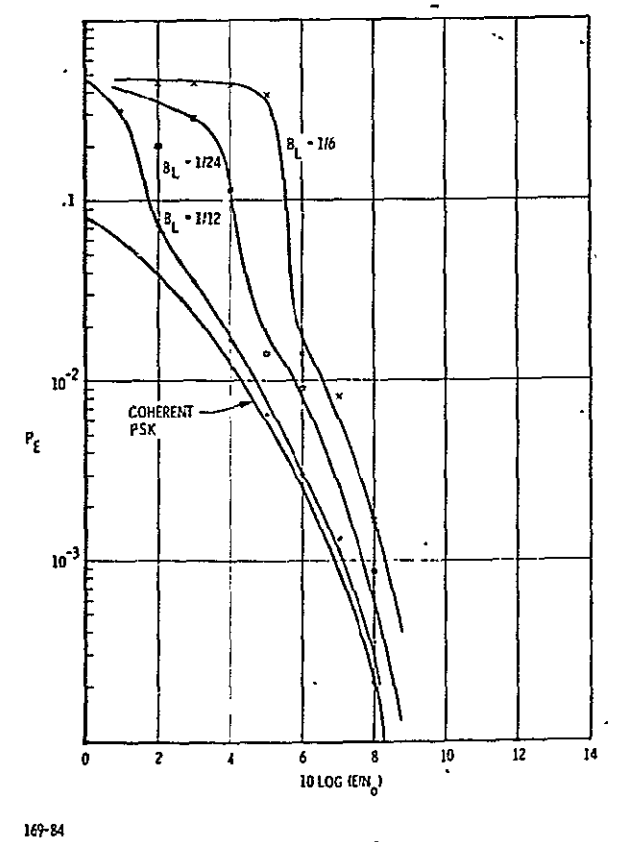

Figure 1.72(b) Bit Error with Doppler, Acceleration = 1 g
Digit Rate = 600

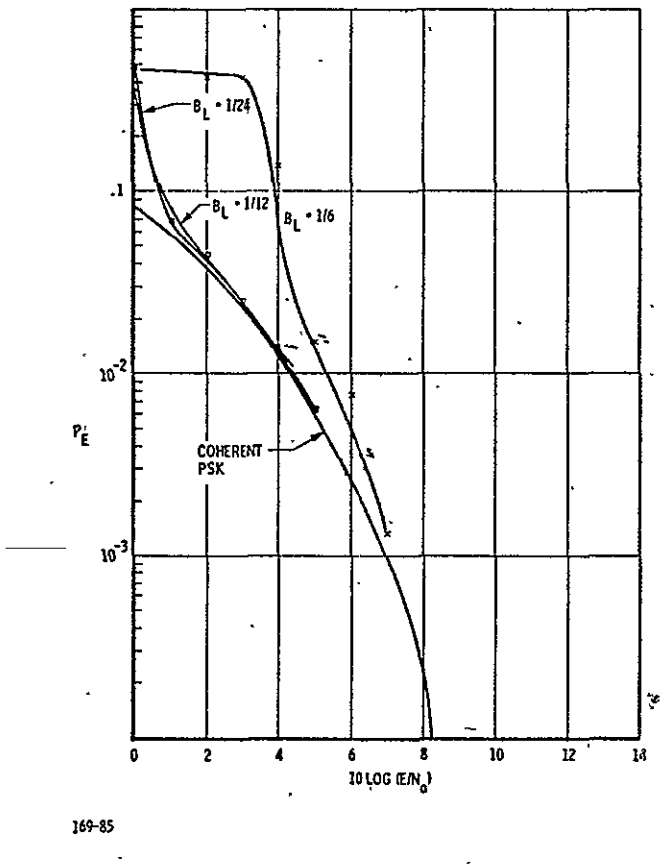

Figure 1.72(c) Bit Error with Doppler, Acceleration = 1 g
Digit Rate = 1200

1.11 VOICE CODING TECHNIQUES FOR THE TDRS

One of the primary requirements for the manned users of TDRS is to provide for normal mode and emergency mode voice from the manned spacecrafts. This requirement is in addition to the 50 kilobit/sec data requirement for the normal mode.

In the normal mode a full duplex voice channel is required between the ground station and the manned spacecraft. The manned user's voice signal will be multiplexed with the 50 kilobit/sec data and the composite signal will be transmitted between the manned spacecraft and the TDRS at either S-band or K_u-band, whereas the link between the TDRS and the ground station is exclusively at K_u-band.

The emergency mode is designed to provide communications between user and ground station when the manned spacecraft has lost stability, thus prohibiting the use of a directional antenna. The spacecraft would have to operate at VHF with essentially an omni-directional antenna. Fortunately the amount of power available at VHF for emergency voice and 4.8 kilobit simultaneous data is 100 watts continuous.

In the following paragraphs of this section we discuss various voice coding techniques, their implementations, and their relative merits with regard to cost, size, weight, performance, compatibility with wide and narrowband anti-multipath/multiple access systems, and their ability to be multiplexed with data. The voice coding techniques which have been considered in this study include normal PCM, linear delta mod, variable slope delta mod, predictive coding, pulse duration modulation coding, and various types of vocoders now in existence.

The basis for performance of any voice coding technique is the ultimate output signal-to-noise ratio available at the receiver to the listener. Shown in Fig. 1.73 is an intelligibility vs outputs signal-to-noise curve for continuous text and indicates that a 95% intelligibility score can be obtained for output signal-to-noise ratios on the order of 15 dB or greater. Throughout this section of the final report the intelligibility vs signal-to-noise curve will be used to rate the performance of the various voice coding techniques.

1.11.1 PCM Encoding

Under the restriction that the output signal-to-noise to the listener need be no greater than 15 to 20 dB in the presence of no digital errors, PCM coding offers a practical method of handling voice signals for TDRS manned space missions. It can be shown that the signal-to-quantizing noise for an arbitrary signal is given by

$$\frac{S}{N_q} = 3 \cdot 2^{2n} \left(\frac{\sigma}{A}\right)^2 \qquad \text{eq. 1.136}$$

where $\pm A$ represents the upper and lower coder limits, σ^2 is the signal power associated with the analog waveforms to be coded, and n is the number of the bits/sample used to describe the signal. It follows, then, that for sinewave loading of the PCM coder, we have a signal-to-quantizing noise given by

$$\left(\frac{S}{N_q}\right) = \frac{3}{2} 2^{2n} \qquad \text{eq. 1.137}$$

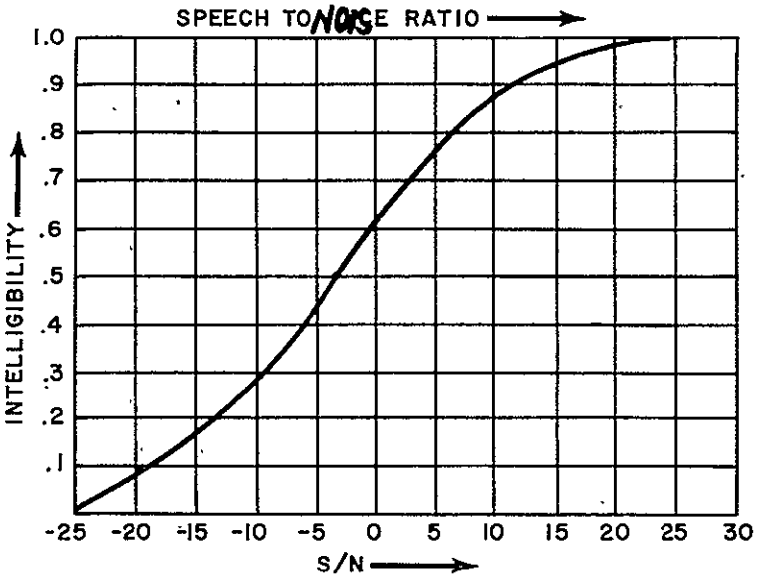

Fig. 1.73 INTELLIGIBILITY vs S/N FOR CONTINUOUS TEXT

Furthermore, if optimal speech companding is utilized, that is, the speech waveform is first compressed by a non-linear device having an appropriate transfer characteristic which transforms the probability density associated with speech signal into a uniformly distributed probability density, between the limits of the coder, then we have a signal-to-quantizing noise given by

$$\left(\frac{S}{N_q}\right) = 2^{2n} \qquad \text{eq. 1.138}$$

The latter condition is representative of optimal companded speech. Integrated circuit technology is such that a complete PCM encoder/decoder can be realized on 2 IC chips.

1.11.2 Linear Delta Mod Encoding

Another possible contender for handling voice signals in the TDRS is the linear delta mod coder. Linear delta mod is characterized by its inherent simplicity and lack of word sync, which is required in PCM coding. Present technology allows this type of system to be fabricated on one IC chip with negligible power consumption.

Abate* has shown through computer analysis that a speech signal-to-quantizing noise using linear delta mod coding can be calculated from

$$\left(\frac{S}{N_q}\right)_{LDM} = \frac{1}{\frac{\pi^2}{6}\left[\frac{\frac{\omega_3}{\omega_m}}{\tan\frac{\omega_m}{\omega_3}} - \frac{\omega_3}{\omega_m}\right]^2\left[\frac{(\ln B)^2 + 2.06\ \ln B + 1.17}{B^3}\right]} \qquad \text{eq. 1.139}$$

*Abate, Proc. I.E.E.E., March 1967

where B is the bandwidth expansion factor, ω_m is the highest radian frequency in the speech signal, ω_3 is the frequency at which the spectrum begins to roll off and $B = \frac{2f_s}{f_m}$, f_s is the sampling rate.

The ratio ω_3 to ω_m is equal to .23 for the speech signal. Using Abate's computerized results and the equations governing the output signal-to-quantizing noise companded PCM, we show in Fig. 1.74 a comparative set of curves for PCM and delta mod. The output speech signal-to-quantizing noise is plotted as a function of bit rate, i.e., bits per second. Note that for optimal companded speech the two systems cross over near 20 kilobits/second, and that a 20 kilobit LDM coder or a 3 bit PCM coder is required to obtain the desired 15-20 dB $(\frac{S}{N})_{out}$ for the TDRS.

1.11.3 Effect of Digital Errors on PCM and Linear Delta Mod Encoding Systems

In a recent paper by Whelan*, PCM encoding in the presence of digital errors is considered; that is, a resultant output signal-to-noise ratio $(S/N)_R$ consisting of contributions to the noise power due to quantizing as well as noise due to digital errors is considered. Whelan found that the signal-to-noise due to errors is given by

$$(\frac{S}{N})_E = \frac{(1 - 2P_E)^2}{4\,P_E(1 - P_E)} \quad \text{(PCM)} \qquad \text{eq. 1.140}$$

P_E = Probability of error

If one considers that the contribution to the total output signal-to-noise ratio is an additive process, that is, the noise due to errors and a noise due to quantizing are additive noises, we have

*Whelan, I.E.E.E. P.G.C.T., June 1966

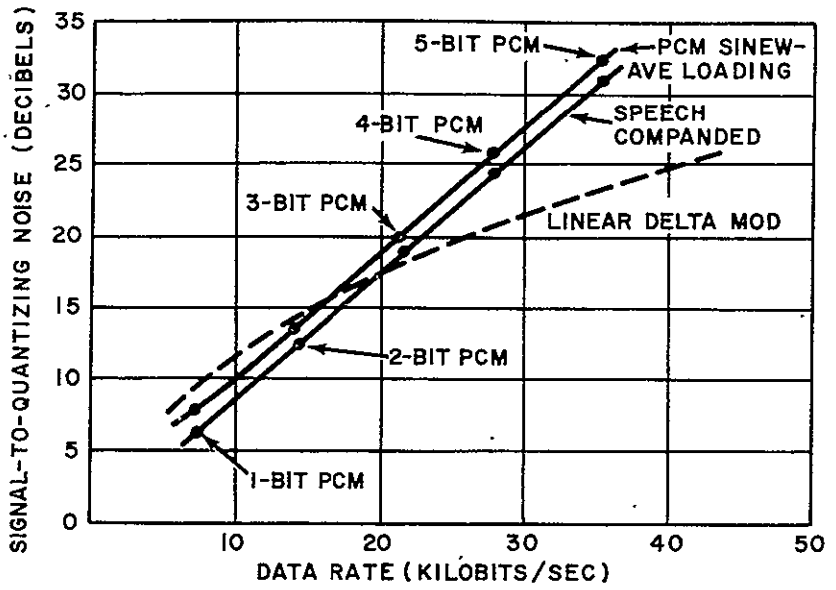

Fig.1.74 PCM AND LDM PERFORMANCE

$$\left(\frac{S}{N}\right)_R = \frac{1}{\left(\frac{N}{S}\right)_E + \left(\frac{N}{S}\right)_q} \qquad \text{eq. 1.141}$$

Fig. 1.75 illustrates the resultant or total signal-to-noise ratio for a PCM system as a function of the predetection signal-to-noise ratio, for various bits per sample or bits per PCM code word for both optimum PSK and differentially coded PSK modulation techniques. Also shown in Fig. 1.75 for reference is the $(S/N)_0$ for a sine wave modulated FM carrier with a mod index of 2. Note that the digital systems have a lower threshold. Furthermore, when speech is used to modulate the FM carrier instead of a sinewave, the threshold is further degraded.

Another paper by Wolf* considers the effect of digital errors on a linear delta mod system. Wolf's analysis results in an equation similar to that obtained by Whelan for PCM. Thus, for all practical purposes, Fig . 1.75 can be used for both PCM and delta mod.

From the preceding analysis, below 20 kilobits/sec, the linear delta mod system outperforms the PCM system in terms of signal-to-quantizing noise and is slightly less susceptible to digital errors from a purely subjective listening point of view.

1.11.4 Pulse Duration Modulated Voice

Like PCM and linear delta modulation the PDM voice modulation technique provides digitized voice which is compatible with the wideband and narrowband implementations considered for TDRS. A simplified block

*Wolf, I.E.E.E. P.G.C.T., February 1966

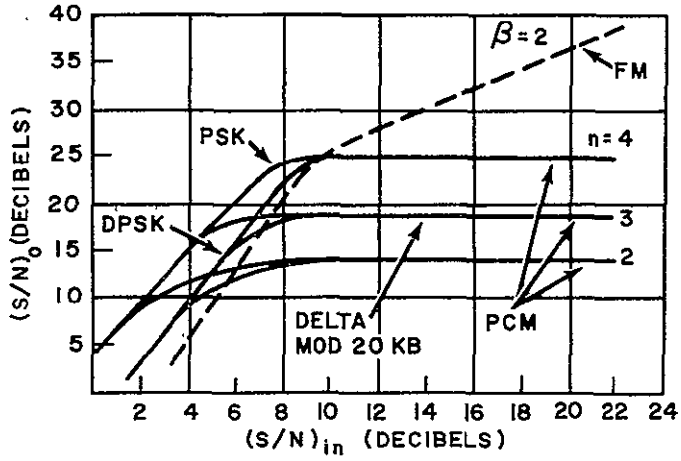

Fig. 1.75 COMPARATIVE VOICE CODING PERFORMANCE CURVES

diagram of the PDM modulator is shown in Fig. 1.76. The input signal from the microphone is amplified by the audio amplifier to a level suitable for processing by the PDM, then filtered to a 3 KHz bandwidth. The filtered audio signal is sampled at the clock rate and the sampled value is held until the next sample period. A sawtooth wave is generated by the ramp generator and the sampled audio and ramp levels compared in the differential comparator. The output of the comparator is a pulse train, the leading edge of which occurs at the fall of the sawtooth wave, and the positive duration of which is proportional to the voltage level stored in the sample and hold. Because the rise of the pulses contains no information (other than the clock), it is possible to reduce the average pulse repetition rate by using a stored clock at the receiver. This is what is actually done; thus, the falling edges of the PDM pulse train are applied to the clock input of a binary divider, causing the output of the divider to change state upon the fall of each PDM pulse. A timing diagram illustrating the modulation scheme is shown in Fig. 1.77. Since the PDM waveform is binary, it is completely compatible with PN and the narrowband modulation technique under investigation for TDRS anti-multipath and multiple access techniques.

In the receiver the output from a Costas loop synchronous demodulator is processed by the integrate and dump filter which is optimal in the presence of noise. The dc value of each integrated sample is held by the sample and hold circuit until the next sample time, thus producing at its output a quantized replica of the originally transmitted audio signal. The output of the sample and hold is low-pass filtered to a 3 KC bandwidth and then amplified to a suitable level for listening. The operation of

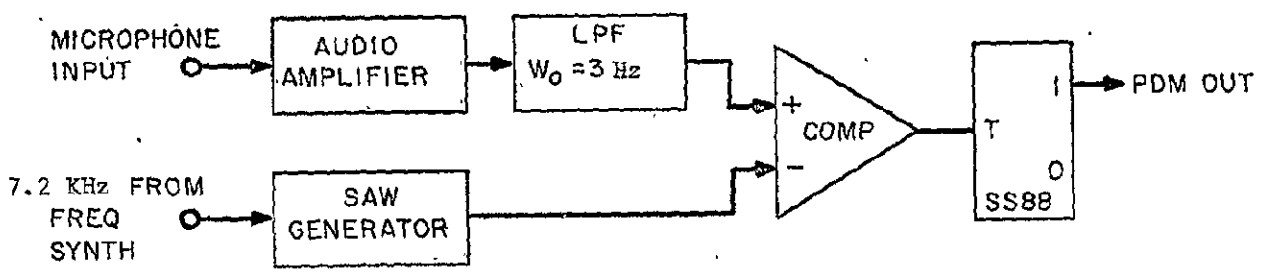

Fig. 1.76 PDM Modulator

the PDM demodulator shown functionally in Fig. 1.78 may be best understood by referring to the timing chart of Fig. 1.79. The chart is scaled to Fig. 1.79 and shows the waveform at various points in the demodulator. A stored 7.2 KC clock at the receiver which has been derived from the coder clock toggles the flip flop. The true output of the flip flop is AND gated with the recovered data while the complementary output is AND gated with the inverted data. The outputs of the two AND gates are combined in the OR gate producing the original PDM data as developed at the comparator in the modulator.

The output of the OR gate drives the integrate and discharge filter which produces the signal shown in the timing chart. The output of the I & D is examined by the sample and hold circuit just before the I & D is dumped, producing a stair-step version of the original input signal.

After filtering to the audio bandwidth and subsequent amplification, the audio is fed to a headset or loudspeaker.

Fig. 1.80 show the measured performance of PDM vs FM as a function of carrier to noise density C/KT or C/N_0. While FM out performs the PDM for high C/KT, the PDM does not exhibit a threshold at low C/KT. Also shown in Fig. 1.81 is a comparison of PDM (lower bound) with PCM. Note that PDM does not exhibit the threshold degradation associated with FM or PCM (also LDM). These curves show that PDM is superior to both FM and PCM (LDM) over the critical range of predetection carrier to noise ratios.

Modern circuit technology insures that the PDM system can be easily implemented on one or two IC chips.

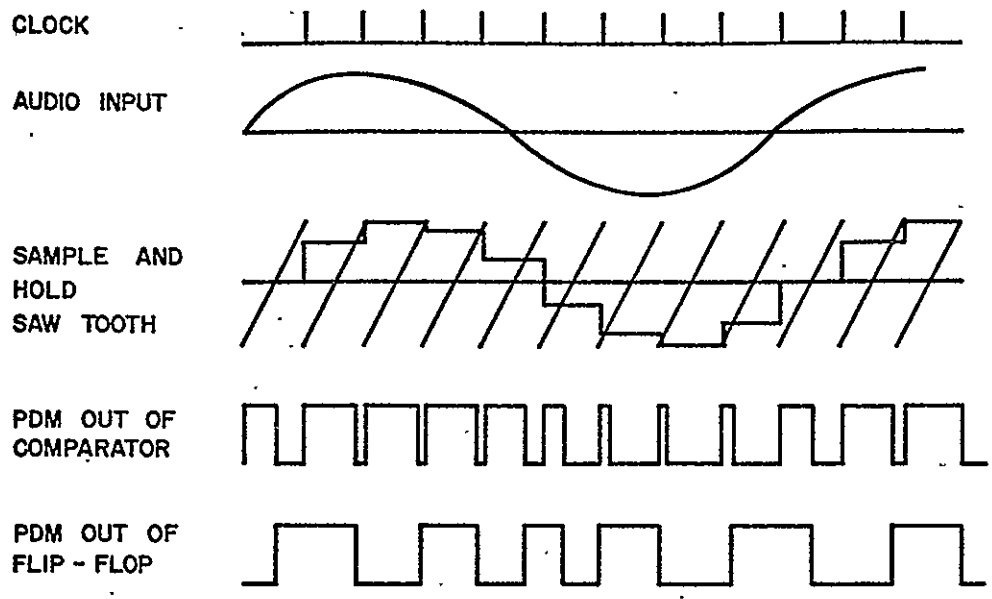

Fig. 1.77 PDM Modulator Waveforms

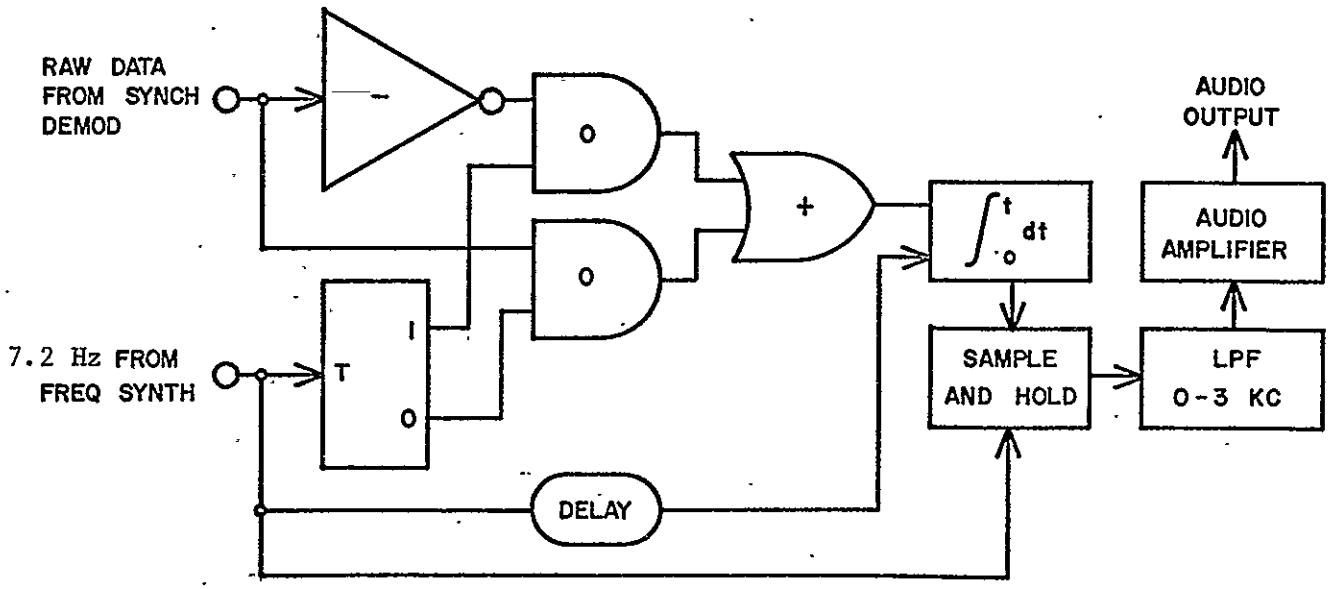

Fig. 1.78 PDM Demodulator

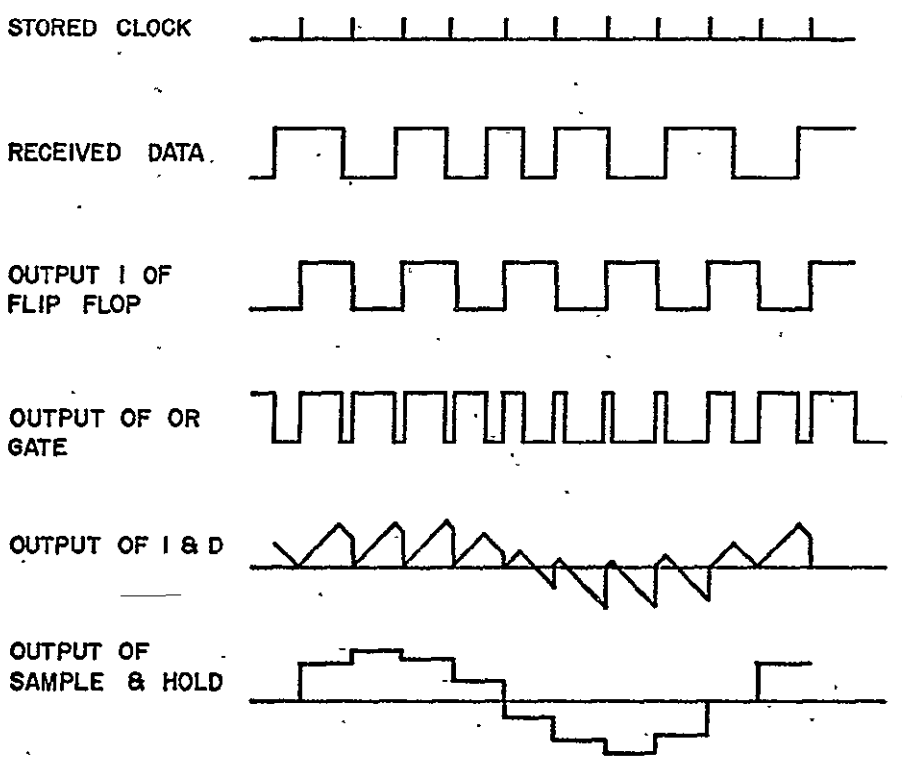

Fig. 1.79 PDM Demodulator Waveforms

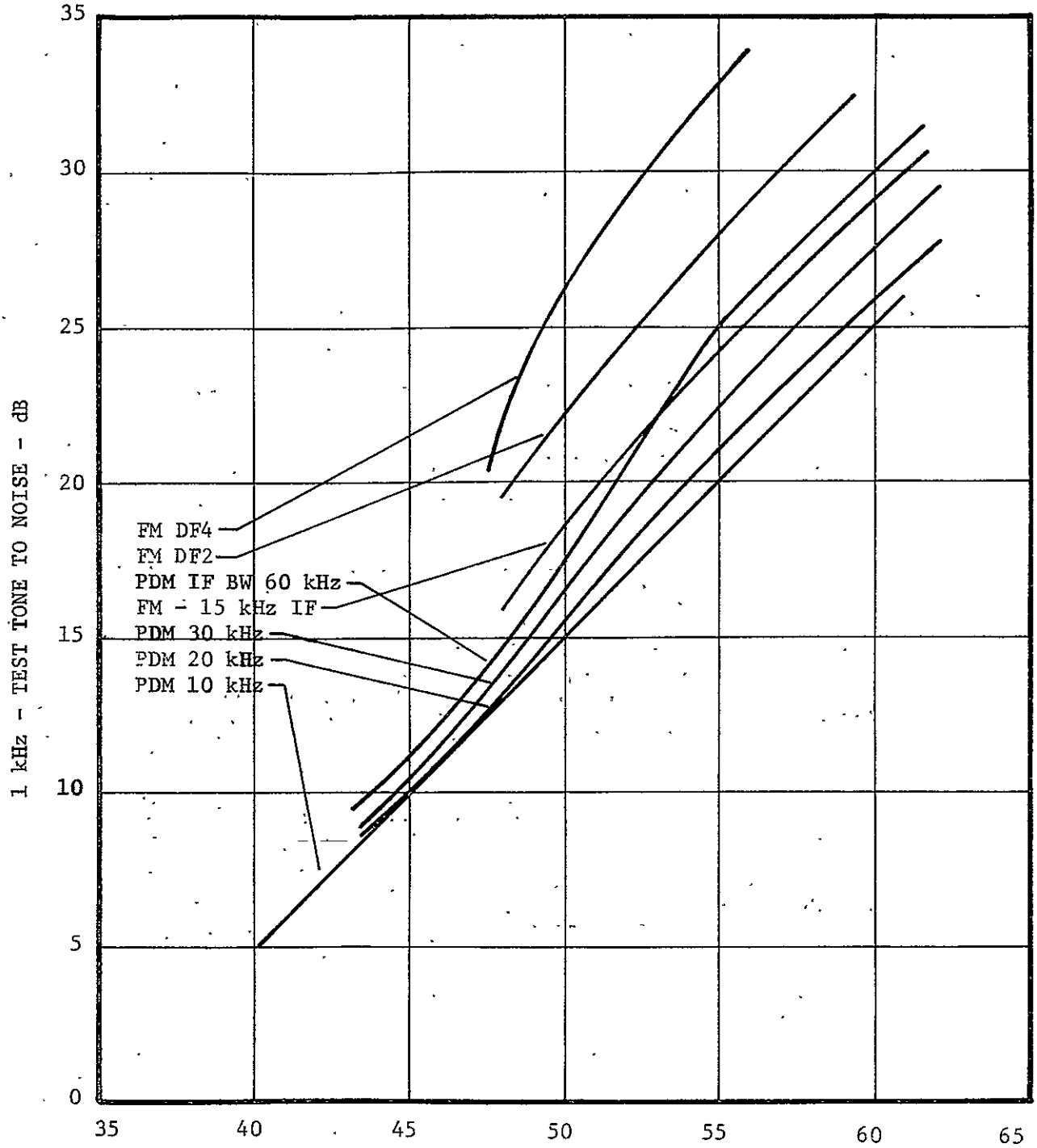

Figure 1.80 FM and PDM Performance Curves

Fig. 1.81 PDM versus PCM

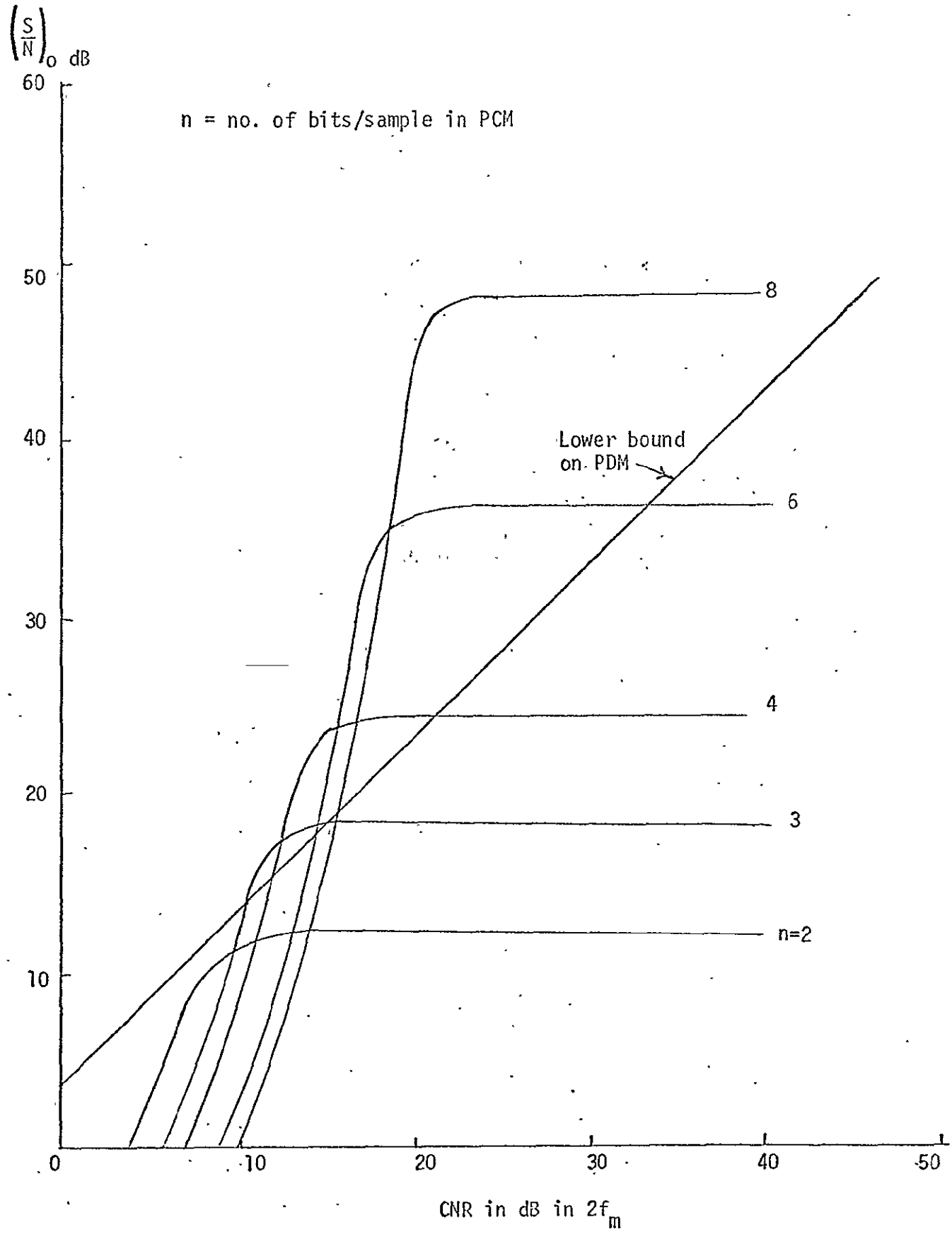

1.11.5 Variable Slope Delta Mod

Recently a voice coding technique referred to as a variable slope delta mod has been devised and shown to be superior in performance to PCM and linear delta mod, especially for data rates on the order of 20 kilobits/sec or higher. A simplified block diagram of the variable slope delta mod encoder/decoder is illustrated in Fig. 1.82. The unique feature of this system is that based upon the past history of the analog waveform the step size in the VSD system fed to the comparator circuit is controlled in an exponential manner. This provides an adaptive system which has the ability to follow rapid changes in the analog waveform thus preventing slope overload which is an inherent drawback of non-companded linear delta mods.

The variable slope delta mod technique has been implemented at data rates between 14.4 and 38.4 kilobits per second. At 14.4 kilobits per second the variable slope delta mod compares favorably with three bit PCM and 20 kilobit/sec linear delta mod encoders and outperforms three bit PCM and linear delta mod when rates are 20 kilobits or greater. The VSD like PCM and linear delta mod have been implemented using micro-circuit technology on one or two chips and for this reason is regarded as a simple system to implement.

1.11.6 Modern Vocoding Techniques

We have discussed a number of techniques for encoding voice signals into a digital form. The encoding processes have been inherently bandwidth expanding to one degree or another. PCM, delta mod, variable slope delta mod, PDM, etc., require greater bandwidths than the bandwidth

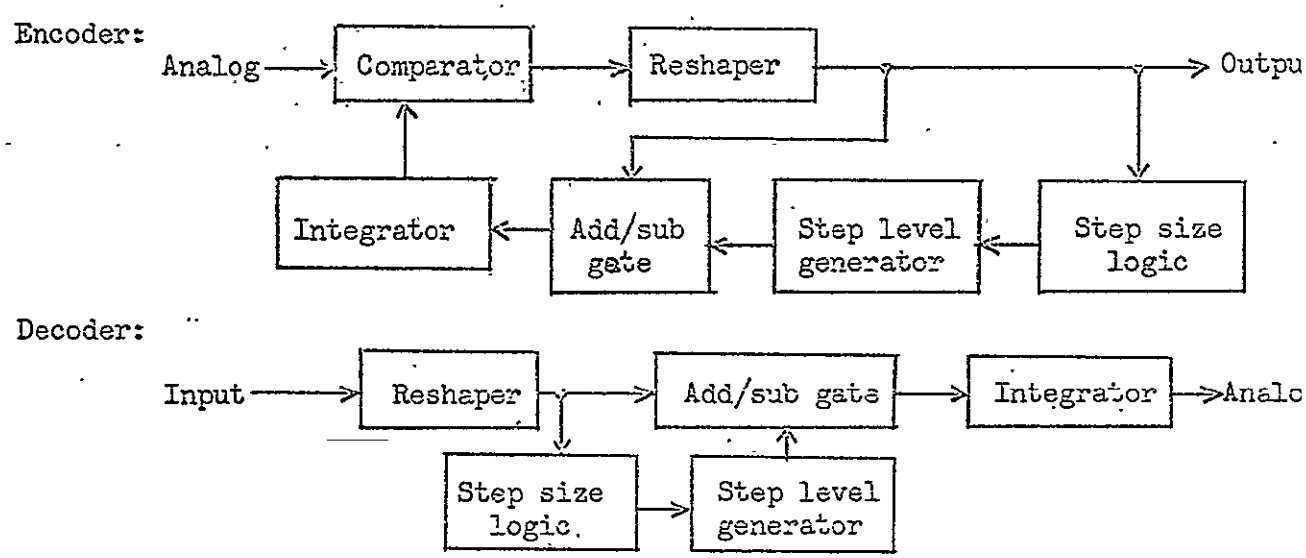

Fig. 1.82 Variable Slope Delta Mod Encoder/Decoder

required to transmit a normal voice signal with PDM requiring the least bandwidth of those techniques studied thus far. To circumvent this problem and to further reduce the bandwidth required to transmit the voice signal vocoders have been developed which perform a redundancy removal process prior to digital encoding.

The Dudley vocoder, or channel vocoder, has been developed by the Government and Bell Telephone Laboratories over the past 30 years. In its present form, the channel vocoder can faithfully reproduce speech at rates of 1,200 and 2,400 bits/sec. In the presence of no digital errors, intelligibility scores based on rhyme tests are as high as 92%. While the intelligibility scores indicate that the channel vocoder would be adequate for a manned space flight mission, the channel vocoder approach has several drawbacks. While the intelligibility can be high, the voice recognition associated with channel vocoders is quite low. Furthermore, using present day technology the channel vocoder is bulky and consumes a great deal of power when compared to PCM, PDM, delta mod, etc. Modern channel vocoders usually occupy one-half cubic foot of space and require 30-40 watts of power. The performance of channel vocoders in the presence of digital errors is inferior to that of the threshold performance of PCM, linear delta mod, VSD, and PDM. For example, modern channel vocoders rapidly deteriorate in performance when binary error probability exceeds .01 as compared to .1 for PCM, delta mod, etc. This fact negates some of the benefits one would hope to obtain through the ten-fold binary data rate reduction between PCM etc. and channel the vocoder. With the introduction of large-scale integration of microcircuits

we can expect significant reductions in size, weight, and power for the channel vocoder in coming years. 1975 projections for the channel vocoder are 150 cu. in. and 15 watts, with intelligibility scores maintained at 92%.

A newer version of the channel vocoder referred to as a voice excited vocoder has been developed recently by DOD and Bell Telephone Laboratories. While the data rates required for the voice excited vocoder are between 7,200 and 9,600 bits/sec, speaker recognition and overall quality of the device is far superior to that of the channel vocoder. Furthermore, its susceptibility to binary errors is closer to that of PCM and delta mod, the threshold being roughly 10% errors for the voice excited vocoder. Fundamentally there is no reason why the voice excited vocoder cannot fit in a package size approximately that of the channel vocoder.

Prior to developing the conclusions on the best voice coding technique we should mention that the use of more advanced predictive coding principles as outlined by Schroeder* have been considered by Magnavox for TDRS application. Unfortunately, it is premature to determine the extent of hardware required to actually implement the higher order predictive digital encoding technique, recently reported on. Suffice it to say that the data rates projected for this voice coding technique are on the order of 7.2 to 9.6 kilobits/sec with voice quality equal to or surpassing that of the voice excited vocoder.

---

*Wescon, '68

1.11.7 Multiplex of Voice with Data

PCM, LDM, VSD, the channel and voice excited vocoders, and PDM can all be efficiently multiplex with data. Since the voice encoding resulting in a binary stream in all cases, all of the techniques discussed thus far lend themselves to multiplexing with data. Because they are digital, the timing required for the voice encoder and the timing utilized for the data can be obtained from a common clock which in turn can be synchronized to the wideband modulation clock if a wideband technique is used to combat multipath, RFI, etc.

There are two efficient methods of multiplexing digital voice with data at 50 kilobit/sec or 4.8 kilobit/sec (emergency mode). These are time multiplexing and phase multiplexing. When bandwidth is at a premium phase multiplexing is the preferred technique while time multiplexing is the more efficient from a signal power economy or partitioning point of view. Time division multiplexing is well understood and perhaps an example of phase multiplexing would be in order. Specifically we have chosen the multiplexing of PDM voice with 4.8 kilobit data. It must be apparent however that any of the digital voice technique could be used in this example. A quadrature phase modulator is shown in Fig. 1.83. The demodulator, shown in Fig. 1.84 consists of a four phase demodulator which provide two outputs. Clock is recovered and divided by 6 to provide 1.2 kilobit clock which is in turn used to obtain 4.8 kilobits/sec data clock. The system effectively occupies the same bandwidth as the PDM voice modem.

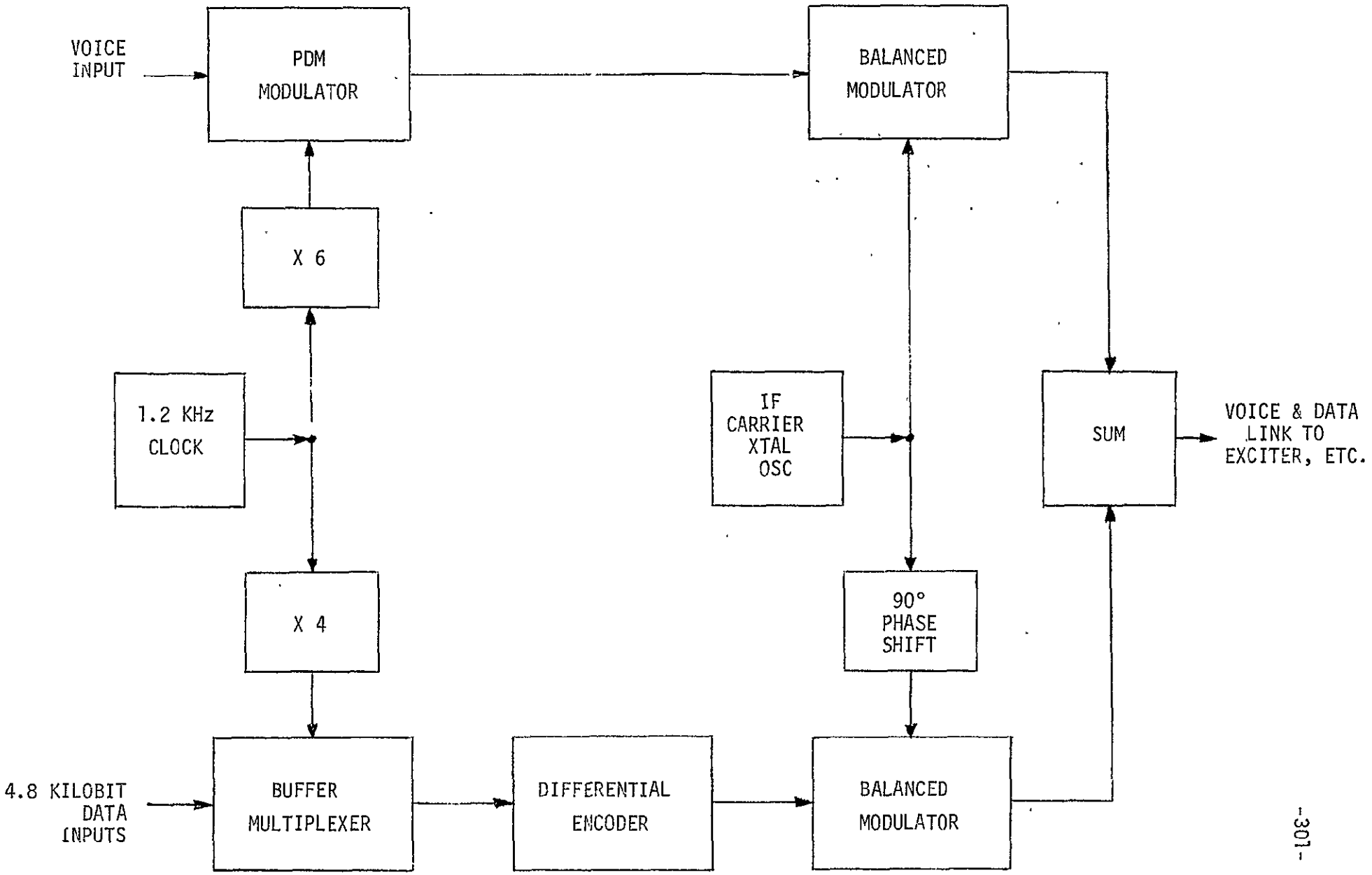

Fig. 1.83 Simultaneous PDM Voice and 4.8 Kbps Phase Multiplexer

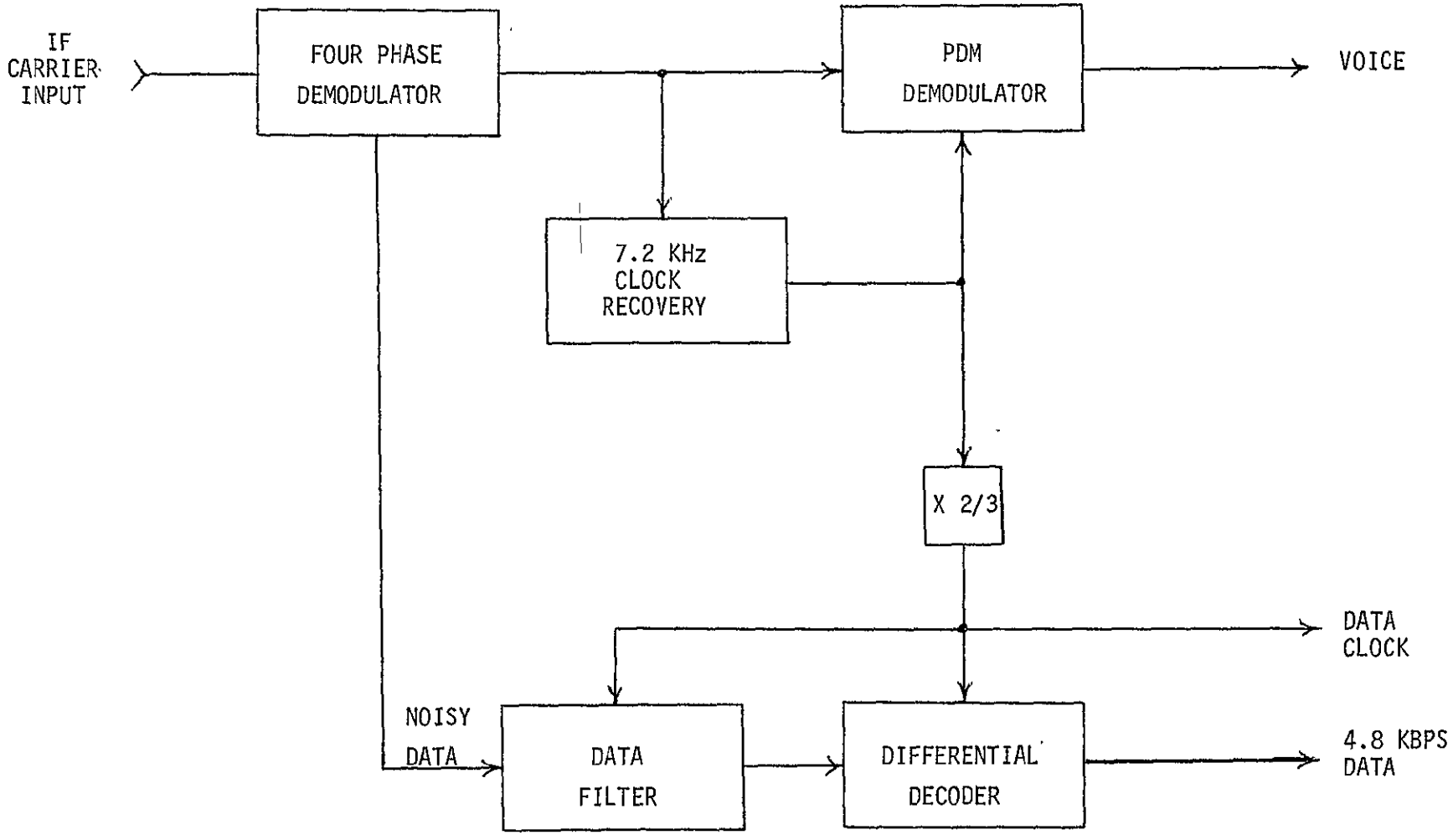

Fig. 1.84 Simultaneous PDM Voice and 4.8 Kbps Demodulator

To illustrate the performance of the phase multiplex technique just described we address the emergency voice link at VHF. We assume that the manned user's antenna is omni-directional and that the user power is 100 watts.

We consider only wideband pseudo-noise and the narrowband adaptive time hop or frequency/time hop since these approaches have been shown to be the leading potential solutions to the plethora of TDRS requirements.

We further assume that all unmanned users have access to the satellite at their normal low power levels and that in an emergency situation, the manned user must establish voice contact with GSFC via the G.S. without delays. In other words ideally the troubled MSF craft should have a reliable push-to-talk channel in the presence of the unmanned user signals at VHF. A less than ideal situation, but one that could be tolerated, is that when a MSF craft is in trouble he transmits an emergency signal (via various methods) which is detected by the G.S. and in turn the G.S. commands all the unmanned user to shut down, providing the MSF craft with a clear channel corrupted only by his multipath and RFI.

For the purpose of analysis we assume in this calculation that the channel is RFI free. This is justified since it is a mute point whether or not interference can be avoided by the narrowband system or removed at the receiver for the wideband system.

A conservative unmanned user power of 5 watts is assumed which totals to 200 watts for 40 users. The multipath is assumed equal to the user total power. Thus for a pseudo-noise system with a processing gain

of 24 dB (TDRS P.G. at VHF for 7.2 kilobits) the output $(\frac{S}{N})$ at the G.S. is from section 1.6.6.

$$(\frac{S}{N})_{PN} = \frac{1}{5} \text{ P.G.} = 17 \text{ dB}$$

which constitutes a 14 dB $(\frac{S}{N})$ for the PDM voice and 14 dB $(\frac{S}{N})$ for the 4.8 kilobits/sec data if the power is divided equally between data and voice. If the power is partitioned to insure a bit error probability of 10^{-5} for the 4.8 kilobits/sec data then the $(\frac{S}{N})$ for the emergency voice channel is 16 dB, or 95% plus intelligibility. Admittedly we have assumed rather severe conditions in this example.

When the adaptive time hopped signal is employed to transmit the voice/data multiplex under the same set of circumstances listed above, the resulting output $(\frac{S}{N})$ is obtained as follows. An unmanned user (operating in the same channel as the manned user) radiates 5 watts average power and uses a duty factor of d', while the manned user's duty factor is d. The manned user requires an R.F. bandwidth of approximately 45 KHz to transmit PDM and data when the user is in a 100 mi orbit. Since the adaptive time hop (ATH) maintains a 50% duty factor, the manned user radiates a 200 watt peak power signal for d = .5, while the unmanned user radiates 5/d' peak watts of power. The unmanned user's multipath signal is assumed equal to the unmanned user's direct signal thus increasing the interference as seen by the manned user by a factor of two. On the average then the manned user will operate at a signal to interference level of 10 dB, which is not acceptable. Admittedly an unmanned user power level of 1 watt is

probably more realistic than the conservative 5 watts predicated in the example for the adaptive time hopped system. When a one watt unmanned user is assumed, then the signal to interference level experienced by the manned user is improved to 17 dB which is the same as that obtained by the pseudo-noise system.

Note that if the channel vocoder had been used in the example, the 4.8 kilobit/sec data rate would have been the controlling rate as opposed to the voice signal.

The purpose of this example is to illustrate that simultaneous voice and data can be provided by either pseudo-noise or the narrowband adaptive time-hopped system.

The wideband pseudo-noise system however has a higher tolerance to the unmanned user interference level as shown in the following table.

Manned User Power	Unmanned User Power	$(\frac{S}{N})_{PN}$ Voice	$(\frac{S}{N})_{PN}$ Data	$(\frac{S}{N})_{ATH}$ Voice	$(\frac{S}{N})_{ATH}$ Data
100 watts	1 watt	20 dB	10 dB	16 dB	10 dB
100 watts	5 watts	16 dB	10 dB	7 dB	7 dB*

* note that 10 dB is required to insure a 10^{-5} error probability for uncoded data.

One way to improve the performance of the ATH system would be to provide 45 KHz dedicated or clear channels for the manned emergency voice mode. While this may be possible, simultaneous voice/data and tracking by an ATH system at VHF during emergencies appears difficult relative to the pseudo-noise approach.

Note that the other narrowband anti-multipath techniques investigated in section 1.6.7 require even larger bandwidth than the 45 KHz required of the ATH to transmit voice.

1.11.8 Conclusions and Recommendations for the Choice of Voice Coding Technique for Voice Coding and the TDRS System

Based upon the previous discussions we present in this subsection rationale for the choice of the voice coding technique for the TDRS. Perhaps the best way to illustrate all of the parameters which go into choosing the best techniques is to present our findings by means of a Table, wherein the various voice coding techniques have been listed along with the pertinent facts and parameters governing their performance, size, weight, etc. Thus, Table 1.14 reflects our current understanding of the state-of-the-art in voice coding techniques as it applys to TDRS.

Based upon the criteria which we have used in the selection of the voice encoding technique and the preceding analyses, it is apparent that the PDM approach is the best compromise system for voice encoding and data multiplexing.

Voice Coding System	Bit Rate for 15-20 dB (S/N)out	Size	Weight	Power	Cost	Subjective Performance Rating	Multiplexing Compatibility With Data	Susceptability to Noise, Minimum Acceptable
PCM	20 Kbps	1-2 IC chips	Negligible	Negligible	$30 @ in quantity	good	yes	10% errors
LDM	20 Kbps	1 IC chip	"	"	"	good	yes	"
VSD	14.4 to 20 Kbps	1-2 IC chips	"	"	"	very good	yes	"
PDM	7.2 Kbps	"	"	"	"	excellent	yes	exhibits graceful degradation & no threshold
Channel Vocoder	1.2 + 2.4 Kbps	1/2 cu. ft. 150 cu. in. by 75	40 lbs. 15 lbs. by 75	40 watts 15 watts	$5,000 in quantity	speaker recog. poor 92% intel-ligibility	yes	1% error
Voice Excited Vocoder	7.2 to 9.6 Kbps	"	"	"	"	excellent	yes	10% error*
High Order Predictive Coding	7.2 to 9.6 Kbps	?	?	?	?	excellent	yes	?
Narrowband FM	20 KHz	very small	negligible	negligible	negligible	excellent		exhibits sharp threshold at 10 dB CNR

* The voice excited vocoder has been shown to withstand a higher percentage of binary errors relative to channel vocoder, due primarily to the difference in the voice pitch extraction and synthesis.

Table 1.14 Comparison of Voice Coding Techniques

1.12 RFI CONSIDERATIONS FOR THE DATA RELAY SATELLITE SYSTEM

In addition to interference resulting from multipath, the user satellites and the TDRS will be confronted with unintentional interference from emitters which are located on the earth and in view of the user satellites and in view of the data relay satellite.

Modulation techniques which are designed to combat the effects of multipath must reject unintentional interference.

In order to evaluate the expected power levels experienced by the user and data relay satellite, The Magnavox Company, through the auspices of NASA, has collected printouts of various signal types and their power levels for Region II. This has been done for various frequency bands which have been allocated to space telemetry, command and control, and general exploration. The frequency bands covered in this analyses extend from 136 MC to as high as 33 GC and encompasses most of the available frequency bands allocated to space technology. Region II encompasses North and South America as shown in Fig. 1.85.

Table 1.15 we list the frequency bands investigated by Magnavox for their potential interference sources. We have also listed the known interference in Regions I and III of Fig. 1.85. This latter material was gathered from the International Telecommunication Union* publication. The data covering Regions I, II, and III collected from the I.T.U. is valid through 1965 and represents an approximation to the current R.F.I. statutes in these Regions. Table 1.16 contains the I.T.U. interference data of 136-138 MHz, 148-150 MHz, and 400-402 MHz, for Regions I, II, and III.

---

* I.T.U., Geneva Switzerland, 1965.

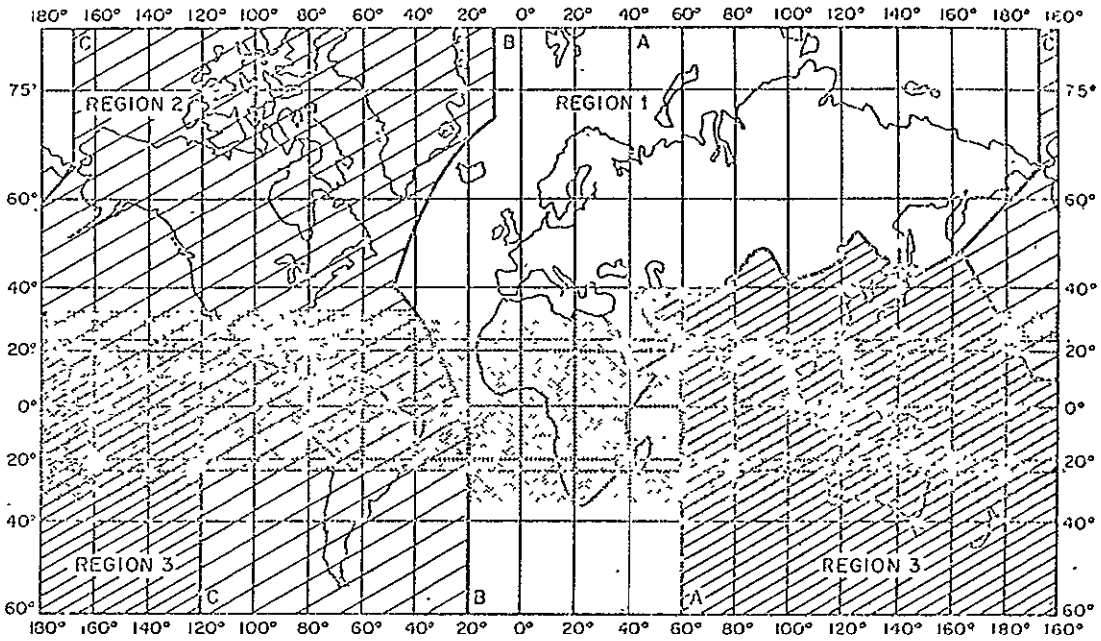

Fig. 1.85 RFI Regions

Table 1.15 Frequency Bands Covered By Interference Data for Region II

Frequency Band	Comment
136-138 MHz	72 emitters
148-154	looks bad
267-273	looks bad
401-402	possible replacement for 148-154 MHz
1427-1429	good
1525-1540	good
1700-1710	good
2290-2300	good
8.4-8.5 GHz	good
15.25-15.35	good
31-35	good

The above table is by no means exhaustive, but is felt to cover the primary frequency bands allocated to space technology in Region II.

Mr. John Bryan* of the NASA Goddard Center, Greenbelt, Maryland, has cataloged the potential interference sources confronting a data relay satellite located over the west coast of South America in view of North America and South America. Based upon the ECAC computer printout, Bryan counted approximately 72 emitters in the band from 136 to 138 MHz, with as many as 2633 emitters located in the band from 135 to 139. Emitters located just outside the 136 to 138 MHz band are allocated to the FAA and have on numerous occasions presented interference problems for the tracking facility at Rosman. There are over 1038 emitters assigned to the FAA for the frequency band 135.85 and 923 emitters at 135.95. These are typically 5 watt transmitters with essentially an omnidirectional antenna. Such a

* I.T.C., Washington, D.C. 1969, Vol. V, p. 287

136-138 MHz				148-150 MHz				400-402 MHz			
20	@ 100 w	Region I		7	@ 10 w	Region I		4	@ 2.5 w	Region I	
7	@ 50 w			3	@ 30 w			2	@ 10 w		
2	@ 10 w			2	@ 50 w			1	@ 20 w		
6	@ 20 w			1	@ 60 w			2	@ 50 w		
				20	@ 100 w			2	@ 200 w		
7	@ 10 w	Region II		9	@ 2.5 w	Region II		No Emitters		Region II	
3	@ 20 w			9	@ 10 w						
33	@ 30 w			6	@ 20 w						
3	@ 40 w			15	@ 30 w						
33	@ 50 w			4	@ 40 w						
1	@ 60 w			57	@ 50 w			1	@ 10 w	Region III	
5	@ 100 w			12	@ 60 w			22	@ 200 w		
				3	@ 100 w						
4	@ 10 w	Region III		3	@ 200 w						
5	@ 20 w			1	@ 150 w						
2	@ 30 w			3	@ 250 w						
3	@ 40 w										
18	@ 50 w										
1	@ 100 w			2	@ 2.5 w	Region III					
5	@ 200 w			5	@ 10 w						
1	@ 250 w			3	@ 20 w						
				3	@ 50 w						
				1	@ 100 w						
				1	@ 150 w						
				2	@ 200 w						
				1	@ 250 w						
				1	@ 2200 w						

Table 1.16(a) RFI Data for Regions I, II, III

Listing # of Emitters at Specific Power Level

136-138 MHz					148-150 MHz					401-402 MHz				
F3 -	4	@	75	kHz	F3 -	1	@	1.2	MHz	F3 -	3	@	3.6	MHz
A3 -	41	@	6	kHz	F3 -	2	@	200	kHz	F3 -	2	@	2.5	MHz
					F3 -	2	@	36	kHz	F3 -	5	@	36	kHz
					F3 -	1	@	16	kHz	A3 -	1	@	6	kHz
					F2 -	1	@	2	kHz					
					A3 -	26	@	6	kHz					
A1 -	14	@	3	kHz										
A3 -	30	@	6	kHz										
A3 -	2	@	8	kHz										
F3/A9 -	4	@	20	kHz										
F3/F13 -	4	@	30	kHz							0			
F3 -	4	@	36	kHz	A3 -	5	@	6	kHz					
F3 -	3	@	120	kHz	A3 -	4	@	10	kHz					
F9 -	2	@	150	kHz	F3 -	1	@	16	kHz					
F13 -	1	@	300	kHz	F3 -	41	@	20	kHz	A3 -	22	@	7	kHz
F9 -	1	@	340	kHz	F3 -	3	@	30	kHz	F3 -	1	@	36	kHz
F3 -	1	@	350	kHz	F3 -	44	@	36	kHz					
					F3 -	13	@	40	kHz					
					A3 -	1	@	100	kHz					
					F9 -	1	@	150	kHz					
					F13 -	2	@	300	kHz					
					F9 -	4	@	340	kHz					
					F3 -	2	@	356	kHz					
					F9 -	1	@	1000	kHz					
A3 -	33	@	6	kHz										
A3 -	2	@	10	kHz										
D0 -	1	@	1	kHz										
A3 -	1	@	5	kHz										
					A3 -	8	@	6	kHz					
					F3 -	4	@	36	kHz					
					F3 -	4	@	47	kHz					
					A3/F2 -	2	@	100	kHz					

Region I	F3 - 4 @ 75 kHz; A3 - 41 @ 6 kHz
Region II	A1 - 14 @ 3 kHz; A3 - 30 @ 6 kHz; A3 - 2 @ 8 kHz; F3/A9 - 4 @ 20 kHz; F3/F13 - 4 @ 30 kHz; F3 - 4 @ 36 kHz; F3 - 3 @ 120 kHz; F9 - 2 @ 150 kHz; F13 - 1 @ 300 kHz; F9 - 1 @ 340 kHz; F3 - 1 @ 350 kHz
Region III	A3 - 33 @ 6 kHz; A3 - 2 @ 10 kHz; D0 - 1 @ 1 kHz; A3 - 1 @ 5 kHz

Region I	F3 - 1 @ 1.2 MHz; F3 - 2 @ 200 kHz; F3 - 2 @ 36 kHz; F3 - 1 @ 16 kHz; F2 - 1 @ 2 kHz; A3 - 26 @ 6 kHz
Region II	A3 - 5 @ 6 kHz; A3 - 4 @ 10 kHz; F3 - 1 @ 16 kHz; F3 - 41 @ 20 kHz; F3 - 3 @ 30 kHz; F3 - 44 @ 36 kHz; F3 - 13 @ 40 kHz; A3 - 1 @ 100 kHz; F9 - 1 @ 150 kHz; F13 - 2 @ 300 kHz; F9 - 4 @ 340 kHz; F3 - 2 @ 356 kHz; F9 - 1 @ 1000 kHz
Region III	A3 - 8 @ 6 kHz; F3 - 4 @ 36 kHz; F3 - 4 @ 47 kHz; A3/F2 - 2 @ 100 kHz

Region I	F3 - 3 @ 3.6 MHz; F3 - 2 @ 2.5 MHz; F3 - 5 @ 36 kHz; A3 - 1 @ 6 kHz
Region II	0
Region III	A3 - 22 @ 7 kHz; F3 - 1 @ 36 kHz

Table 1.16(b) RFI Data for Regions I, II, III

Vs. Modulation Type (A3, F3, etc.),

# of Emitters, Bandwidth of Emitters

conglomeration of emitters at band edge requires that the pre-selection circuits in the TDRS and user equipments be such that these emitters can be effectively eliminated.

Heffernan and Bryan* have assumed that adequate pre-selection circuits can be designed to effectively eliminate all interference outside the 136 to 138 MC band and on the basis of the 72 catelogued in-band emitters have attempted to determine the amount of interference power as seen by the TDRS satellite. Heffernan** has shown that the mean squared summed RFI power, as seen at the data relay satellite, is approximately -92 dbm. This figure is arrived at by assuming essentially CW sources and neglects any duty factor weighting for the conglomeration of emitters. As such, this figure is conservative and must be regarded as an upper bound on the interference power as seen by the TDRS, over Region II in the band 136 to 138 MHz. Shown in Figure 1.86 is a plot of the power spectrum of the interference contained in the frequency band 136-138 MHz. This plot is based on data catalogued by John Bryan***, of NASA. It is apparent from the plot in Figure 1.86 that there are a number of relatively high power interference sources. Note that nearly all the individual interference bands are near to (-2 dB) or exceed the level of a one watt user measured at the TDRS.

---

* private communication from Heffernan and Bryan, NASA Goddard
** private communication
*** op cit

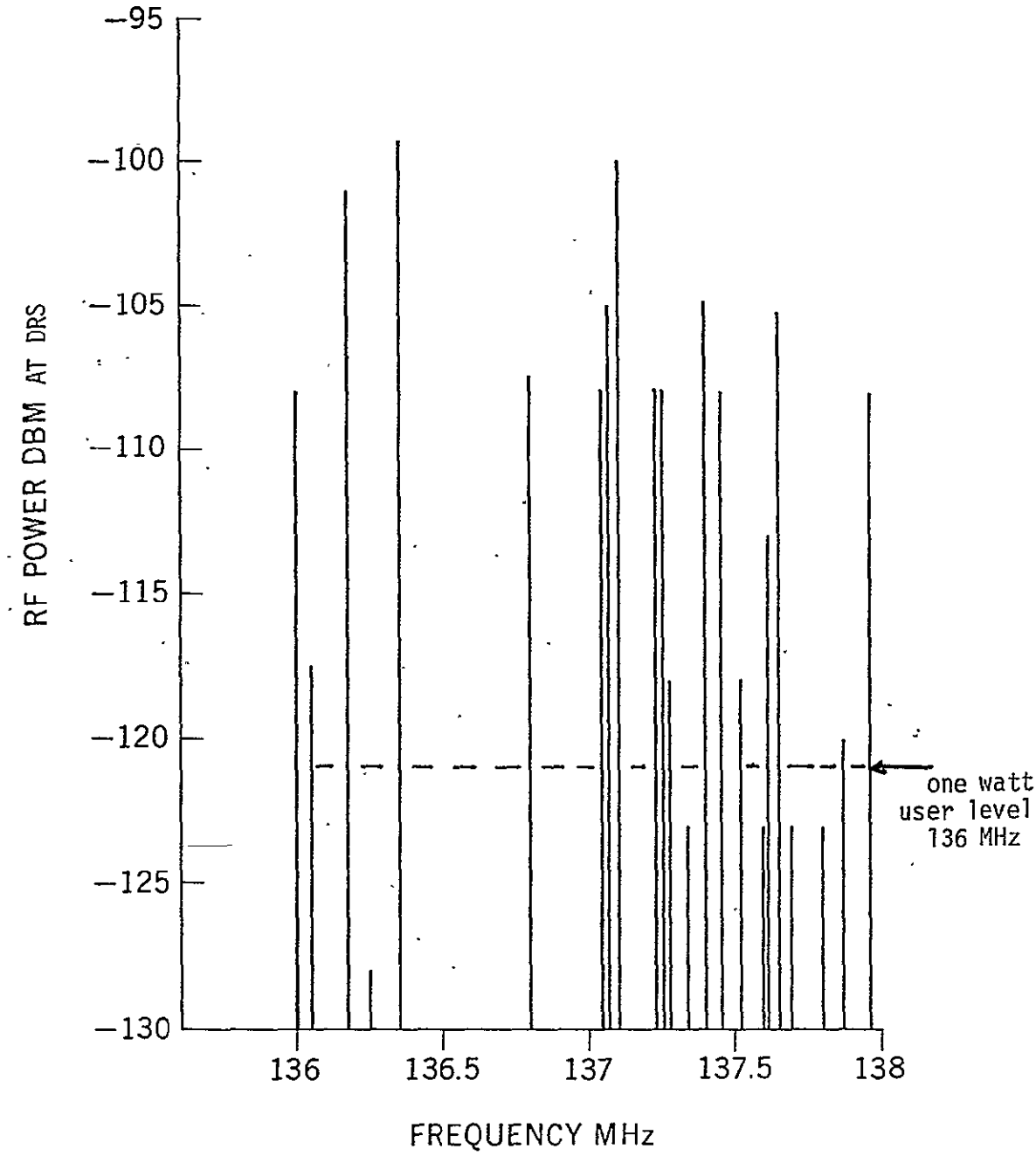

Fig. 1.86 THE EXPECTED INTERFERENCE SPECTRUM AS SEEN BY THE TDRS, 136-138 MHz Region II

The user satellites will receive command information and R and $\dot{R}$ in the frequency band 148 to 149.9 MC from the data relay satellite. In the receive mode the user will be confronted with two sources of interference, one resulting from multipath and a second source resulting from emitters located on the earth which occupy the band of 148 to 149.9. Again, Bryan* has compiled a rather thorough list of emitters which occupy this band for Region II, and this list is presented in Table 1.17. Note that while the ITU data agrees with Bryan's data for 136-138 MHz, Bryan predicts even a gloomier picture for the 148 to 149.9 MHz band.

It is obvious from the Tables 1.16 and 1.17 that there are a large number of relatively high power sources which a user satellite, because of its omni-directional antenna, will be able to see when passing over various parts of the world. Needless to say that there will be hot spots and cool spots as viewed by the user satellite.** Furthermore, these RFI sources will not be on continuously but will be governed by some duty factor. While not a uniform power distribution it would appear from Bryan's work there are few, if any, frequencies (of significant bandwidth) to be found in the 148 to 149.9 MHz band. This fact coupled with the limited ERP from the data relay satellite (30 dbw), the spreading loss advantage to the RFI sources, and recent OSO-IV experience, leads one to project a rather gloomy outlook for the use of the 148 to 149.9 MHz band for the downlink between the TDRS and the user spacecraft. From the data gathered by Bryan, the large majority of transmitters in 148-149.9 MHz are omni-directional and while many of the emitters are of a low duty factor the output powers can be as high as 25-100 watts.

---

*op cit

**[Intense interference has recently been observed in the 150 MHz command band by the OSO-IV Satellite. (ref: "Command Channel RFI and Its Effect on OSO-IV" X-154-68-413, April 69)]

Table 1.17

EFFECTIVE RADIATED POWER PER EMITTER IN WATTS

Frequency MHz	Total Emitters	1-9	10-19	20-29	30-39	40-49	50-59	60-69	80	Greater than 100 watts
148.20	6		5				1			
148.21	47		7	32		1	1	6		
148.215	4		3		1					
148.22	37	11		6	16	2	2			
148.23	28	1				12	13	2		
148.24	17				16			1		
148.25	56	4	8	29	11	1	1	1	1	
148.26	3									3
148.29	176	31	18	61	22	4	34	1	4	1
148.51	53	11		35				7		
148.515	18				17		1			
148.52	149	17	53	40	22	3	5	4	5	
148.54	88	21	59	1		1	2	1	3	
148.545	12		11					1		
148.55	316	50	222	8	15	5	11	4	1	
148.56	1									1
148.575	1									1
148.59	16	1				11	4			
148.93	1						1			
148.95	32	17		9			4	2		
148.988	1							1		
149.00	33		1	31				1		
149.01	285	13	32	159	52	3	22	2	1	1
149.47	40	18		22				1		

Table 1.17

Frequency MHz	Total Emitters	1-9	10-19	20-29	30-39	40-49	50-59	60-69	80	Greater than 100 watts
149.48	229	64	37	14	110	1	1	2		
149.49	15			9			5	1		
149.50	150	60	44	1	34	4	5	1	1	
149.51	347	83	8	77	183	2	1	3		
149.53	40	25	7			4	4			
149.54	39	28	6			3	2			
149.55	13						1	12		
149.56	70	40	5	11	3	3	4	8	1	
149.565	47			47						
149.57	100	23	35	7	9	3	7	8	9	1
154.19	3				1	1	1			

1) An equivalent mean square sum of these emitters is not meaningful since a user will not be exposed to all of them at one time.

2) The NASA command transmitters have been excluded from this listing.

In summary, we have presented interference data which tends to show the potential problem confronting the TDRS system in the 136-138, 148-149.9, 400-402 and other space frequency bands. The initial conclusions, after our short investigation, are:

1) Attempt to remove through government pressure the 72 emitters in the 136-138 MHz band. These are government owned emitters and can probably be relocated in frequency without difficulty.

2) Explore the use of 400-402 MHz space band for the TDRS to user link, since it has been shown that very little interference exists in this band.

3) Explore the use of electronic devices to remove interference in the 136-138 band and at

4) Clear a command channel in 148-149.9 MHz through government pressure.

5) Explore* the possibility of obtaining space bands in the government owned bands, i.e., 138-144 MHz, 173-174 MHz, 216-220 MHz, 225-328 MHz, 335-399 MHz, 406-420 MHz.

1.12.1 Interference Modulation Bandwidths and Projected Duty Factors

From Table 1.16 we see that a large number of the emitters in 136-138 MHz are of the AM telephony (A3) type (3-6 KHz bandwidth) and a moderate number of FM telephony (F3). In the 148-150 MHz band the F3 modulation dominates in Region II (U.S. and South America). Based on the I.T.U. data the F3 modulated carriers are licensed to be on 24 hrs/day while the A3 modulated carriers are governed by such statistical parameters as average usage $\bar{U}$ (as fraction of an hour channel is in use, averaged over 24 hours) average message length $\bar{\ell}$ (in seconds), and the standard deviation in message length σ_e (in seconds). We have attempted to estimate $\bar{U}$, $\bar{\ell}$, σ_e

*FREAVY - Federal Comm. Commission, PB-183614, May 1969

for the 136-138 band based on the assumption that A3 type modulation predominates in this band. Listed below are data extracted from the JTAC report of March 1968 on Spectrum Usage, for various typical A3 modulation users.

User No.	Mod.	Center freq., MHz	$\bar{U}$	$\bar{\ell}$	σ_e
1	AM	118.9	.37	14.8	12.2
2	AM	157.1	.11	32.5	27.7
3	AM	450	≈.27	58.6	51.3
4	AM	150	.31	≈25	≈6
average	-	-	.26	32.7	21.8

User Key

1. FAA Local Control, Los Angeles International Airport
2. U.S. Coast Guard Search and Rescue Operations, Long Beach, California
3. Special Industrial Radio, Los Angeles and Orange Counties, California
4. Los Angeles City Police Communications System

We conclude that an average duty factor of .25 is realistic for type A3 modulation. This duty factor would serve to diminish the average interference level by 6 dB.

1.12.2 Interference Reduction by Electronic Means

From what has been said in the previous section it is obvious that the data relay satellite system and its users are plagued by the presence of undesirable interference in the frequency bands 136-138 MHz

and 148-149.9 MHz. If these bands are to be used effectively it may be necessary to eliminate these interference sources at convenient points in the system by electronic means.

First let us consider the interference situation confronting the 136-138 MHz band. The interference is seen by the data relay satellite in addition to the user signals and their multipath. It is highly desirable to utilize interference removal techniques in the data relay satellite itself. The reason for this being that if the interference is effectively removed in the satellite the interference does not steal power from the user signals. It can be shown that onboard removal techniques can be complex and costly and may require a feedback channel to control the interference removal devices onboard the satellite. If onboard processing is not utilized, then the repeater must be designed to accommodate both the interference, the desired signals, and the multipath signals. Accommodate means that sufficient power is available to each user's signal on the TDRS to ground link so as to make this link noiseless while maintaining low intermod products between the various components at the input to the data relay satellite. In effect, interference and multipath serve to consume a portion of the data relay satellite power which could be utilized by the desired signals.

Heffernan* has shown that a linear repeater is feasible in terms of required spacecraft power when both a multiplicity of user signals and interference are present at the input to the data relay satellite in the 136-138 MHz band. This particular analysis further diminishes the desirability or need for onboard interference removal techniques.

---

* private communications, P. Heffernan, NASA Goddard

For the command and control link between the ground station and user craft it has been shown in Table 1.17 that there exists a multiplicity of high powered signals emanating from the ground. Since this interference enjoys a significant range advantage over the signals emitted from the data relay satellite to a user craft, the interference problem for this link is further enhanced and complicated. Furthermore, since the user equipment is to be kept at minimum complexity the use of the electronic interference reduction techniques onboard the user spacecraft in the 148-149.9 MHz link is questionable. One possible solution to the interference problem in the 148-149.9 MHz band would be to monitor via the data relay satellite system the signals in this band and to use a clear channel somewhere in the frequency band. This technique presupposes that the user craft can be told from the ground which are the usable bands within the 148-149.9 MHz region. This latter supposition seems to be erroneous and therefore it is recommended that a clear channel be created in the 148-149.9 band by government agreement. From the data accumulated on the interference sources frequency band 148-149.9 there appears to be very few, if any, narrow clear channels available for the command and control link. However, a clear channel bandwidth of the order of 200 KHz may be all that is required to insure adequate anti-multipath rejection and range and range rate accuracies, (see section 1.8). Thus it may be possible, with increased information concerning the 148-149.9 band, to select a narrow clear channel for the command and control link. It is recommended that this approach receive further investigation. Because of the intensity and density of the emitters in the 148-149.9 MHz band and the range advantage enjoyed by the earth based interference sources over signals radiated from the TDRS to the user

craft. calculations show that wideband anti-interference modulation techniques which utilize a large percentage of the band do not provide adequate system margins for reliable bit error probability of 10^{-5} at the power levels obtainable from the TDRS satellite, and for that matter none of the modulation techniques under investigation will function in this band. Furthermore, significant increases in the TDRS to user power levels would have to be provided in order to maintain an operational link of this type in the presence of interference found in the 148-149.9 MHz band.

It has been shown in Table 1.16 that a large percentage of interference in the 136-138 band is of the 6 KHz A3 modulation type, and is amenable to removal at the G.S. by tunable notch filters.

The above mentioned narrowband interference removal technique can be shown to be most effective when the signals utilized by the users in the TDRS are of a wideband nature. This is true since once interference has been removed from a narrowband the region within the notch filter must be regarded as unusable by a user's narrowband transmission. Thus, while the tunable notch filter can definitely eliminate interference they also reduce the effective usable bandwidths for the TDRS and therefore impact on the type of modulation system which can be most effectively used. In summary it can be shown that these narrowband interference removal techniques are most effective for the removal of co-channel interference when the user signals are of a wideband nature and are most effective for the removal of adjacent channel interference when the user signals are of a

narrowband nature. In a later section, 1.12.2, we show the potential benefits to the operation of the TDRS, for the 136-138 MHz band, when such narrowband interference removal techniques are employed on a selected number of interfering signal bands. This improved performance will be compared to a system without interference removal. The user signals are assumed to be pseudo-noise which occupies the entire 2 MHz bandwidth in the user to TDRS link.

1.12.3 Effects of Interference and Interference Removal on Pseudo-Noise Systems

To illustrate the effects of interference in the 136-138 MHz band we will now analyze the performance of a 2 MHz PN system. The performance of a PN system is accurately described in terms of the output signal to noise ratio, the input signal to noise or input signal to interference ratio, and the processing gain (P.G.) of the PN system. The time bandwidth product or the processing gain is defined here as the ratio of the pseudo-noise chip rate to the data rate. For example, if the pseudo-noise chip is 1 megabit per second and the data is 1 kilobit per second then the processing gain is 1,000 or 30 dB. The input-output signal to noise relationship for a conventional two-phase or four-phase PN system is given in equation 1.142 for a wideband PN system and a noiseless TDRS to G.S. link.

$$\left(\frac{S}{N}\right)_o \cong \frac{(P.G.)\,P_u}{\frac{3}{2}KP_u + I + N_u W_s} \qquad \text{eq. 1.142}$$

P.G. = 32 dB

$\frac{3}{2}K$ = number of user + equal multipath for Gold Coding

N_u = user to TDRS noise density

I = interference at the TDRS

W_s = spread bandwidth ~2 MHz

For all practical purposes the interference present at the input to a PN correlation receiver is spread over a bandwidth commensurate with the RF bandwidth of the PN system while at the same time through the same correlation process the received PN signal is collapsed into a spectrum width commensurate with the data.

Table 1.18(a) summarize the performance of a 2 MHz chip rate PN system, 40 users, equal multipath, and interference of -92 dbm as measured at the TDRS. The -92 dbm interference level is based on Bryan's data and no signal duty factor reduction has been included.

Table 1.18(a) Performance of 2 MHz PN System (136 MHz)

User Power (watts)	40 Users+Multipath	Interference	Noise	User Output S/N
1	-102 dbm	-92 dbm	-105 dbm	2 + dB
2	- 99 dbm	-92 dbm	-105 dbm	5 dB
5	- 95 dbm	-92 dbm	-105 dbm	9.5 dB
10	- 92 dbm	-92 dbm	-105 dbm	~10 dB

Table 1.18(b) summarizes the performance of the same wideband PN system when the six largest interference bands have been removed from the spectrum 136-138 MHz.

Table 1.18(b) PN Performance with Interference Removal

User Power (watts)	User Output S/N
1	9 dB
2	10 + dB
5	11.5 dB
10	12 dB

By removing the six largest interference bands with tunable notch filters, the overall interference is reduced by 10 dB. The reduction in available spectrum (i.e., P.G.) to the PN system is negligible.

Thus by applying interference removal at the G.S. to only six interference bands between 136-138 MHz, the wideband PN system's performance can be made acceptable. Note that a system margin of an additional 6 dB requires a user power level $\sim$ 4 watts, when six interference bands are eliminated. If ten bands are eliminated at the G.S. the interference can be further reduced by 10 dB or a total of 20 dB interference reduction. A 20 dB interference reduction makes the worst case interference in Region II of no consequence to the PN system performance.

1.12.4 Determination of the Effects of CW Interference Narrowband

PSK has served as the basic binary signaling method throughout most of our analysis. It is advisable to determine the effects of CW interference on this modulation technique. We do this for one reason, the adaptive and pre-programmed systems which utilize time hopping or FH techniques to avoid multipath but remain essentially narrowband transmissions can be interfered with.

We have taken some liberties in the following analysis in that it is assumed the interference is a constant amplitude CW signal. The reader is advised that if such interference is amplitude modulated then the results of the following analyses must be averaged over the amplitude modulation statistics. When the interfering signals are constant envelope such as narrowband FM or PM transmissions, then the results contained in this section are considered quite valid.

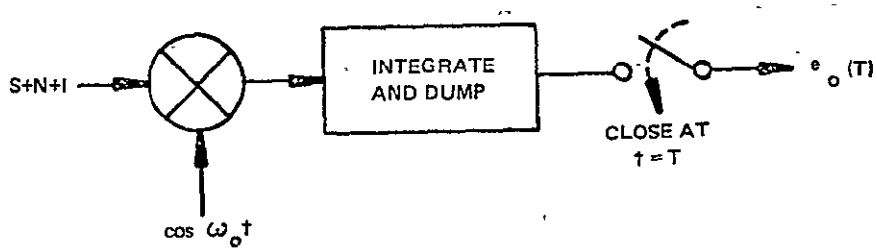

$S = A \cos \omega_o t$ (signal)

$N = x_c \cos \omega_o t + x_s \sin \omega_o t$ (noise)

$I = B \cos (\omega_o + \omega\Delta)\, t + \theta$

Figure 1.87 Coherent Detector

The input to the coherent detector is a phase-reversal-keyed signal (which has been coded) in the presence of an interfering tone and an associated bandpass Gaussian noise. It is assumed that the reference in the receiver is phase-aligned with the desired signal, and that the reference is unaffectived by the presence of the interference. It follows that the output from the integrate and dump at the sampling instant is given by:

$$e_0(T) = AT + \int_0^T \left[x_c(t) + B \cos(\Delta\omega t + \theta)\right] dt \qquad \text{eq. 1.143}$$

This results in a conditional binary error probability given by:

$$P_e(\theta) = \frac{1}{2} \operatorname{erfc}\left[\frac{A}{\sqrt{2}\sigma}\left(1 + \frac{B}{A}\left|\frac{\sin\frac{\Delta\omega T}{2}}{\frac{\Delta\omega T}{2}}\right| \cos\psi\right)\right] \qquad \text{eq. 1.144}$$

where:

$$\psi = \theta - \frac{\Delta\omega T}{2}$$

$$\frac{A}{\sqrt{2}\sigma} = \frac{E}{\sqrt{N_0}}$$

$$\frac{E}{N_0} = \text{energy to noise density.}$$

Equation 1.144 assumes that the probabilities of 1 and 0 are equal. Under the assumption that the phase angle θ is a random variable, we are free to determine the average binary error probability by averaging the conditional density over a uniform density in θ or ψ:

$$\overline{P}_e = \frac{1}{2\pi} \int_{-\pi}^{\pi} \frac{1}{2} \operatorname{erfc} \left[\frac{A}{\sqrt{2}\sigma} (1 + K \cos \psi) \right] d\psi \qquad \text{eq.1.145}$$

Equation 1.145has been programmed on a digital computer and the results are shown in Figure 1.88 for various values of K as a function of the signal-to-noise ratio. K is not to be confused with the number of users.

The value of K is seen to be the ratio of the interference to the signal level times a weighting factor which is a function of frequency and duration of the binary symbol. Interference which is well inside the bandwidth occupied by the data transmission is unaffected by the frequency weighting of the integrate and dump filter. The binary error probability for $\Delta PSK \simeq 2\ P_{PSK}(1-P_{PSK})$ or $\simeq 2P_{PSK}$.

We see from Figure 1.88 that an interference to signal ratio of -3 dB will cause a 8 dB degradation in system performance at 10^{-5} bit error probability. Interference to signal ratios -20dB are of little concern.

The primary result of the analysis is to point out small amounts of narrowband interference can serve to dramatically degrade the performance of narrowband signals or in effect require more power from the user craft to maintain a desired bit error probability.

Note that adjacent channel interference (other users) and TDRS repeater intermodulation products will have similar effects on narrowband antimultipath signals.

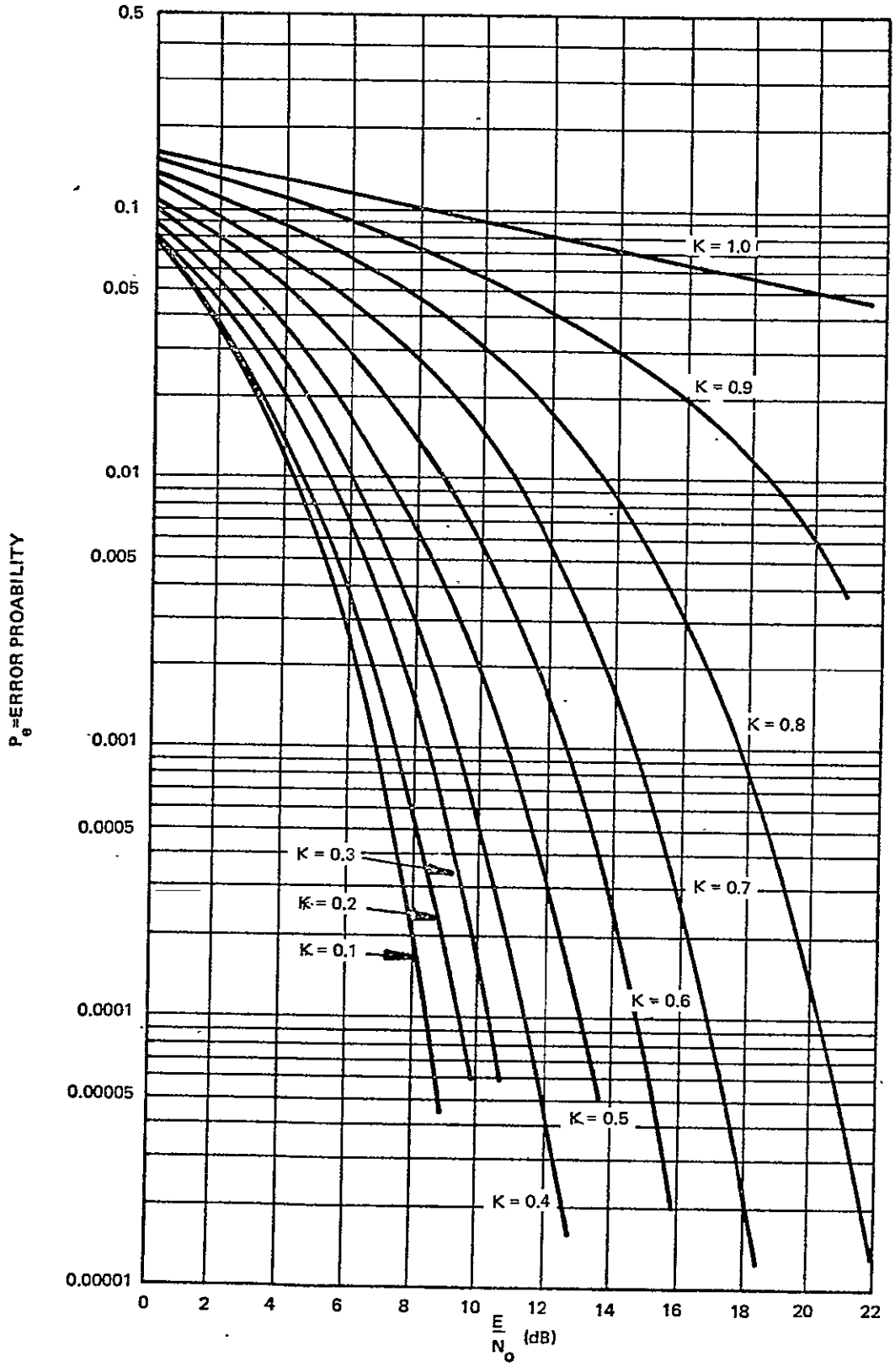

Figure 1.88 Average Binary Error Probability For Coherent PSK In The Presence of CW Interference and Gaussian Noise

It is evident from Fig. 1.86 (for Region II) that a narrowband signal with a one watt user power level is over shadowed by most of the interference and the remaining interference is close (-2 dB) to the user level at one watt. This leads us to conclude that

a) interference removal using narrow tunable notch filters is a good idea even for narrowband user signals since removal of very large interference reduces the possibility for generating inter-mod products in the receiver. Interference removal, however, does not make the filtered channel available for use by a narrowband user signal.

b) a high dynamic range receiver should be employed at the G.S.

c) adjacent channel interference problem can be quite severe for a low power user signal (Fig. 1.86). Even though the majority of the signals 136-138 MHz are narrowband their sidebands extend beyond the normal limit of their bandwidth and thus sideband energy can appear in a so-called "clear channel" and degrade the narrowband user performance.

d) to avoid the interference a narrowband user should be equipped with a number of alternate channels which can be directed from the ground to use in the event that interference exists on the primary channel. This requirement complicates the user's receiver, transmitter, and range and range rate instrumentation.

1.12.5 Recommendation Concerning RFI in the Space Band

We have made several recommendations in Section 1.12 already with regard to steps that should be taken to alleviate the projected RFI problem. We reaffirm here those recommendations and state that we have only scratched

the surface in our efforts to determine the true RFI picture in the bands of interest. Thus we recommend that further study and measurements are required before the effects of RFI can be really evaluated.

It is true, as we have pointed out in Section 1.12.1, that the RFI is probably not as severe as projected as a result of the application of signal duty factors, however, we are not sure to what degree this is true.

We could postulate a variety of interference models and show that the wideband system will not function under one model or that the narrowband signal will be functional under yet another model. Thus we hesitate to conclude at this time the effects of interference on any of the approaches. We have presented calculations and best data which tend to confirm that the interference can be effectively "handled" in the 136-138 MHz band, but there may be a real problem in the 148-149.9 band.

1.13 HARDWARE DESIGNS OF THE TDRS CANDIDATE SYSTEMS

A very important consideration leading to the final choice of a system for the users of the TDRS is the relative hardware complexity of the various approaches.

While one system may show a slight advantage in performance over a second system, the first system may require such complex instrumentation that the performance advantage is overshadowed by the hardware complexity requirement. Conversely simplicity of design is no substitute for outstanding performance.

We have been directed to assess the hardware complexity needed to implement the various anti-multipath systems under consideration. We approach this problem with a view of the entire system and do not restrict the assessment to the anti-multipath portions of the instrumentation alone.

It is evident that such circuitry as doppler acquisition, doppler tracking, data recovery, carrier synthesizers, transmitters, r-f receiver front ends, and forward error control circuitry are not restricted to any one system but are required for all of the implementations. Therefore we assume that these circuits are common to all implementations. What must be determined is the relative complexity of the equipments after all the common (necessary) circuits have been accounted for, leaving unique hardware required for the particular approach.

In order to carry out this relative hardware complexity evaluation we show in Fig. 1.89 through Fig. 1.93 the basic transmitter block diagrams

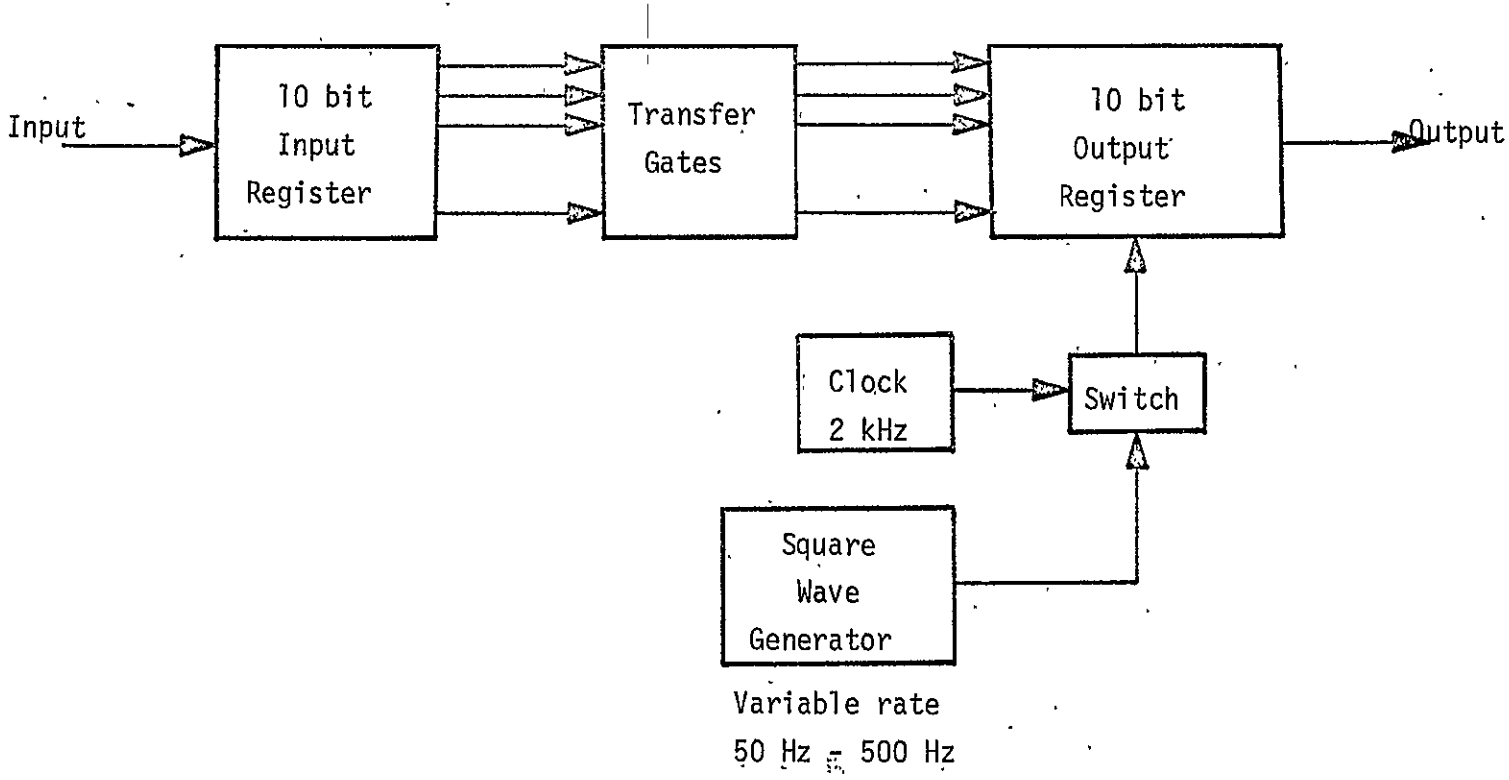

Fig. 1.89 Functional Block Diagram for Generation of Adaptive TH

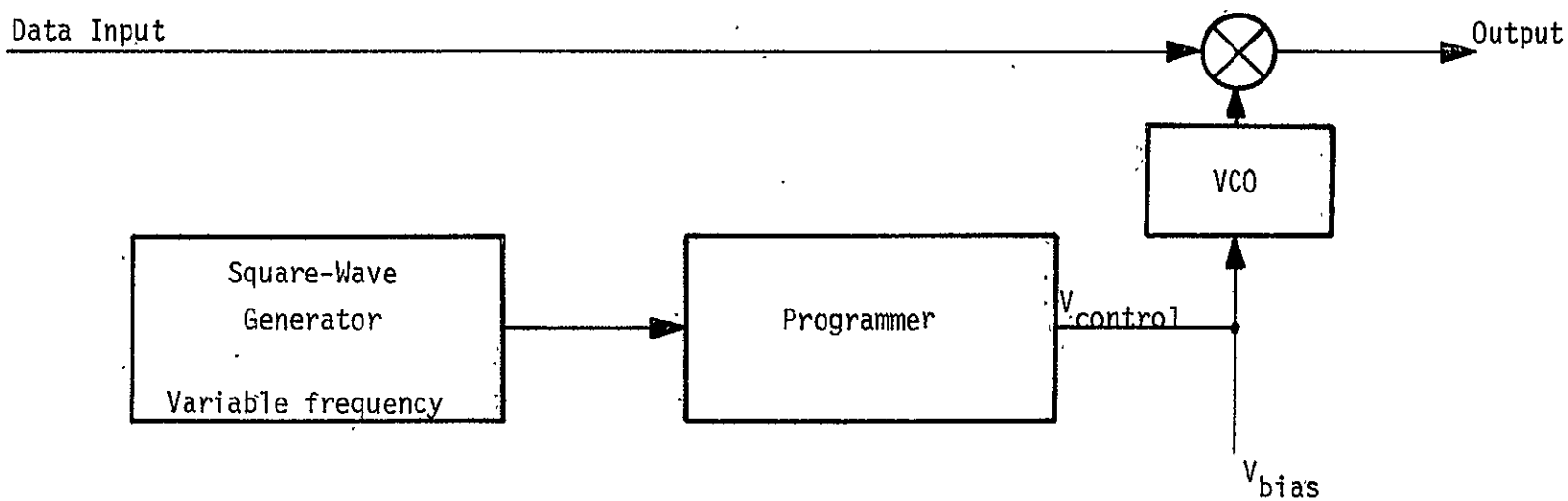

Fig. 1.90 Functional Block Diagram for Generation of Adaptive FH

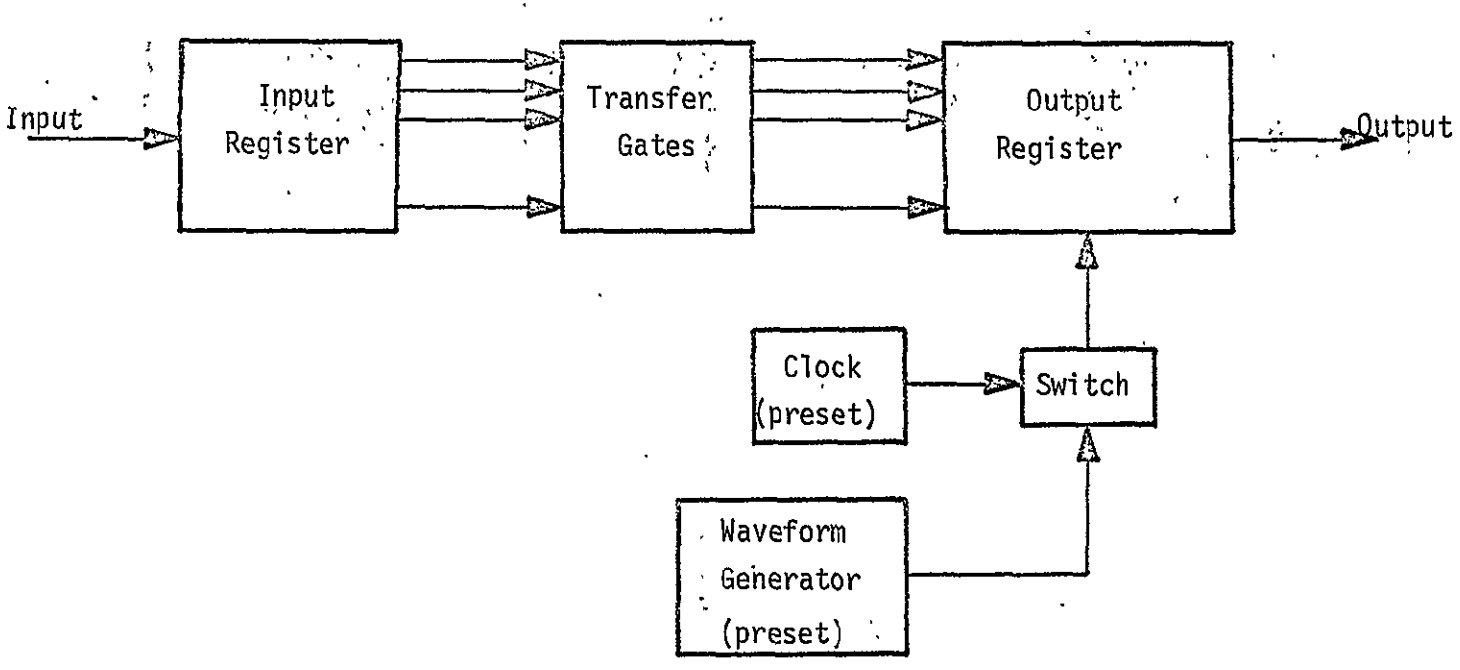

Fig. 1.91 Functional Block Diagram for Generation of Programmed TH

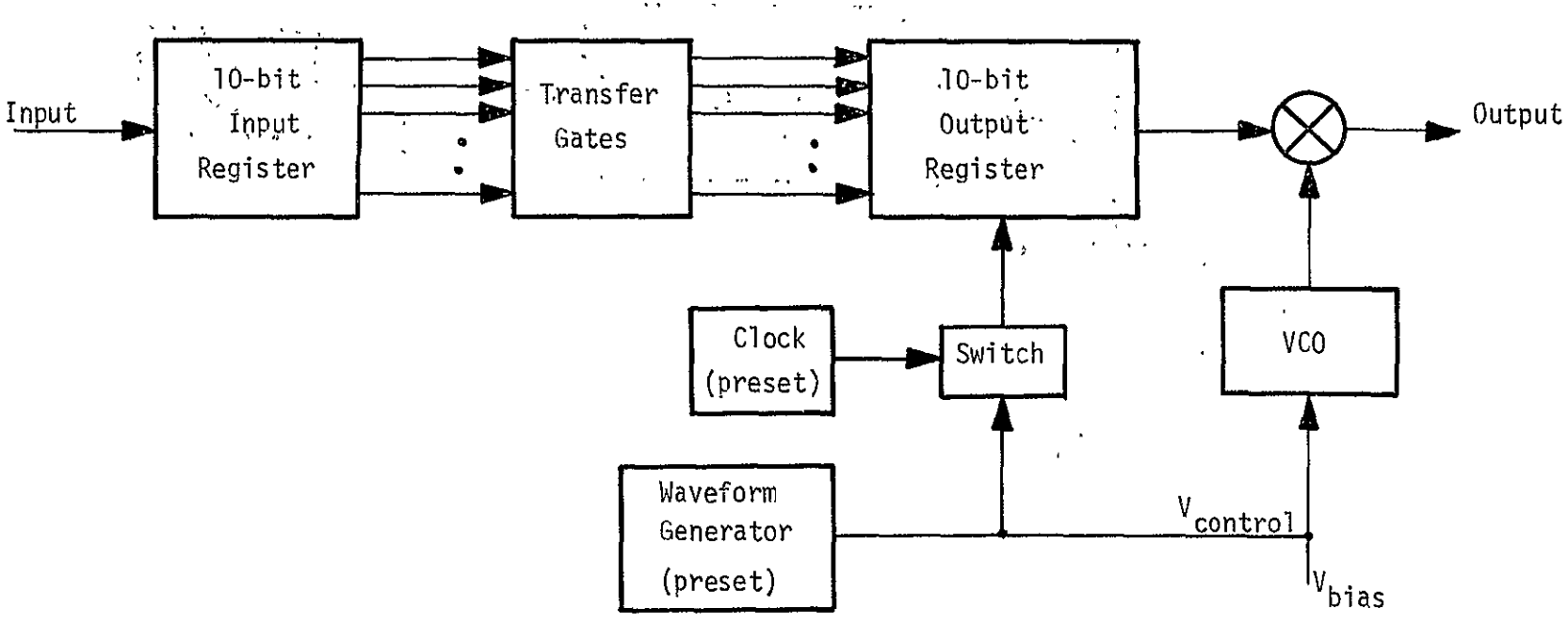

Fig. 1.92 Programmed FH Functional Block Diagram

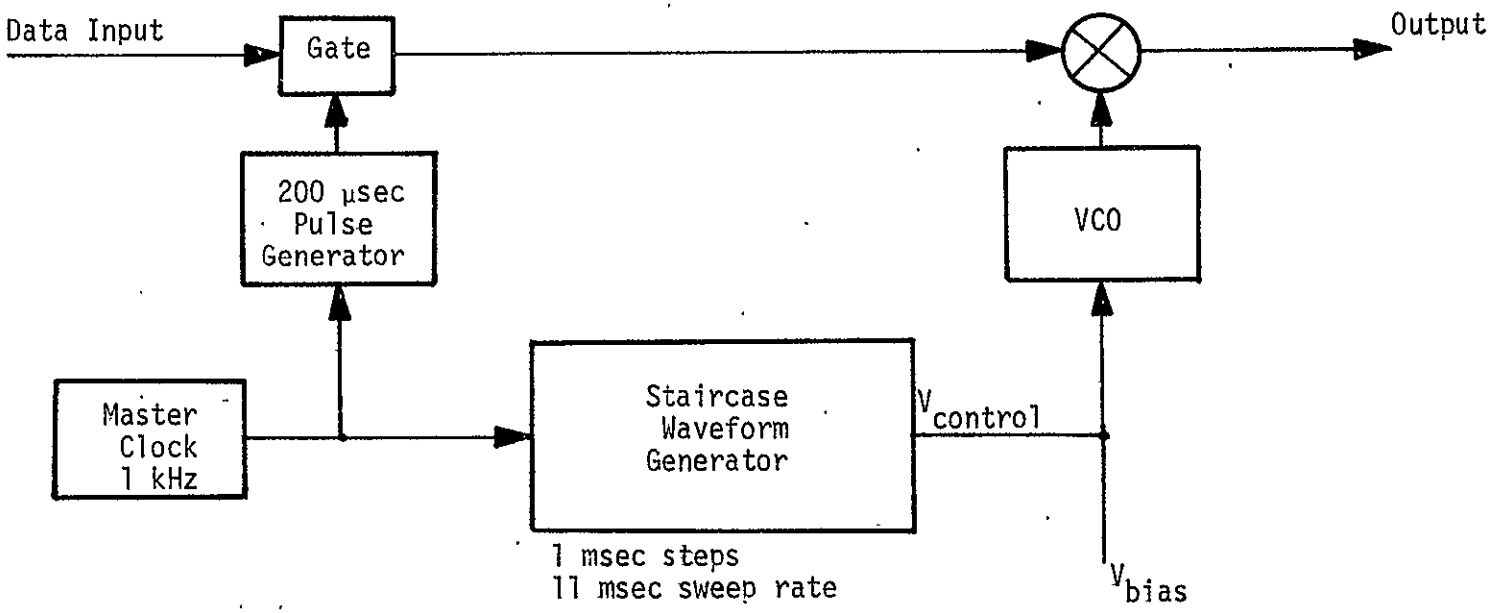

Fig. 1.93 Functional Block Diagram for Generation of TH/FH Patterns

of the Adaptive FH, Adaptive TH, TH/FH, Programmed TH, and Programmed FH systems described in Section 1.6.7. The receivers compatible with these transmitters are of the same order of complexity. We conclude from Fig. 1.89 through 1.92 that these systems are of low relative complexity. We have shown only the anti-multipath instrumentation in these figures and have not included range and range rate instrumentation.

Shown in Figures 1.94 and 1.95 is the transmitter and receiver of the pseudo-random time hop (PRTH) system, and shown in Figures 1.96 and 1.97 are the transmitter and receiver block diagrams of the Random Access Discrete Address (RADA) system. Of these two approaches the PRTH is the simpler, with RADA regarded as a relatively complex system owing to the frequency synthesizer requirement and multi-filter requirement in the receiver.

Shown in Figures 1.98 and 1.99 are block diagrams of a basic PN transmitter and user transponder. The PN transmitter is very simple, while the receiver is more complex. The PN system is an integrated system in many respects in that the circuitry required to realize a working receiver also provide a number of "fall-outs" such as code tracking for range, carrier acquisition for efficient data recovery, and doppler tracking. A single integrated waveform provides communication, positive identification, and precise ranging in the PN implementation. Thus in order to compare the PN system with an apparently less complex implementation, one must compre on the basis of total number of functions being satisfied or accomplished by the circuitry. For example, the systems shown in Figures 1.89 to 1.93 have less complex receiver implementations

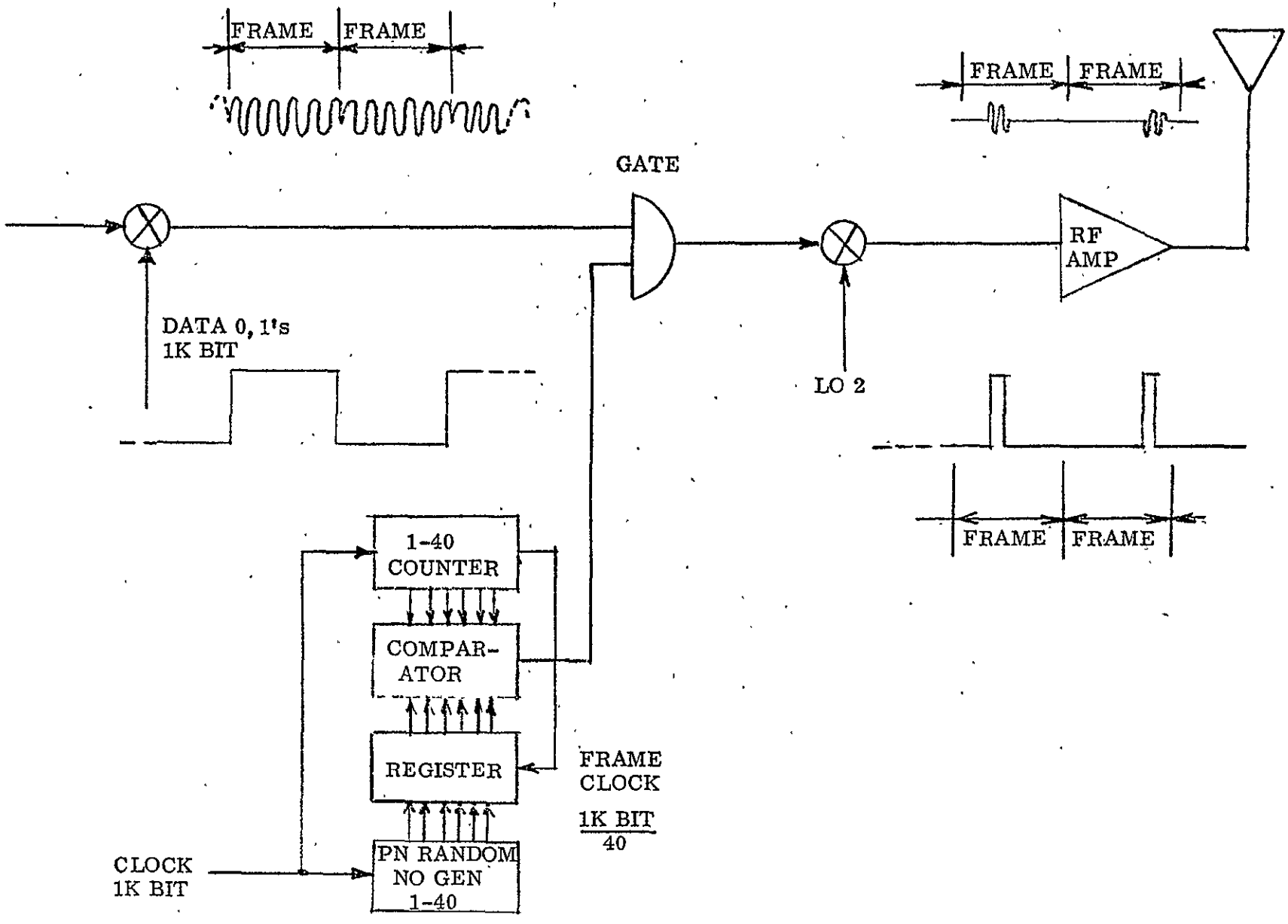

Figure 1.94 - Pseudo Random Time Hop (PRTH) Transmitter

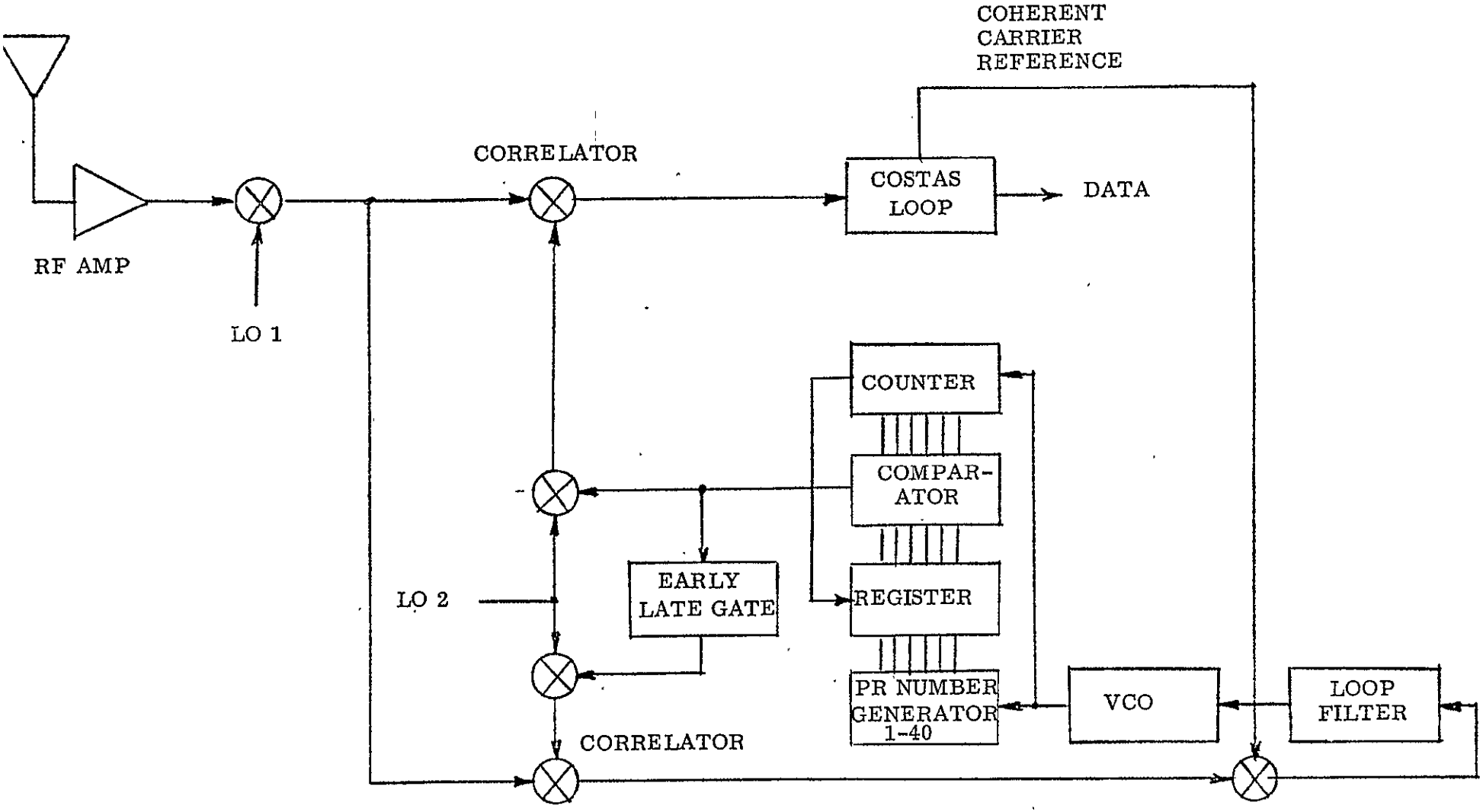

Figure 1.95 Pseudo Random Time Hop (PRTH) Receiver

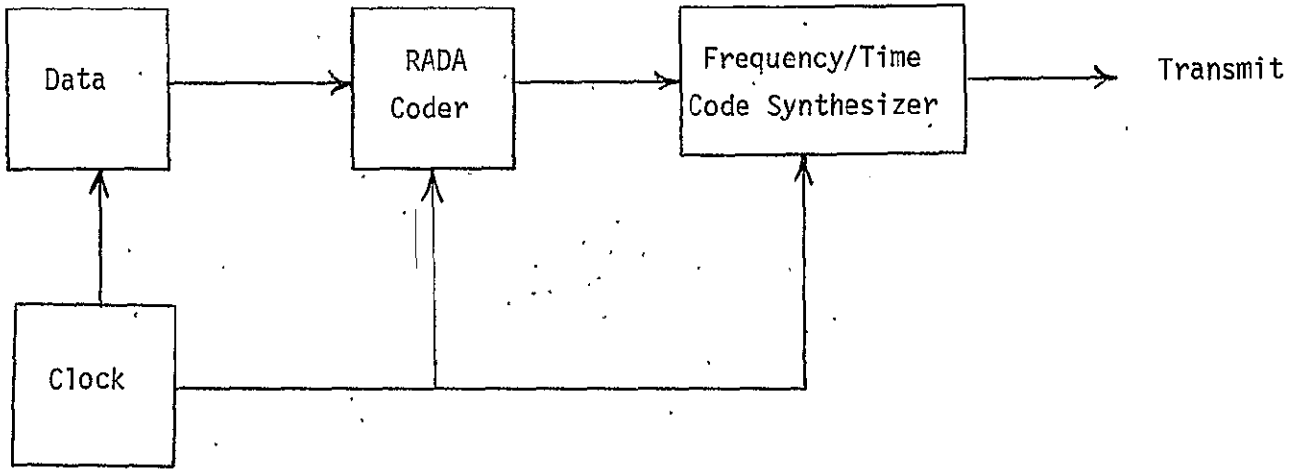

Fig. 1.96 RADA Transmitter

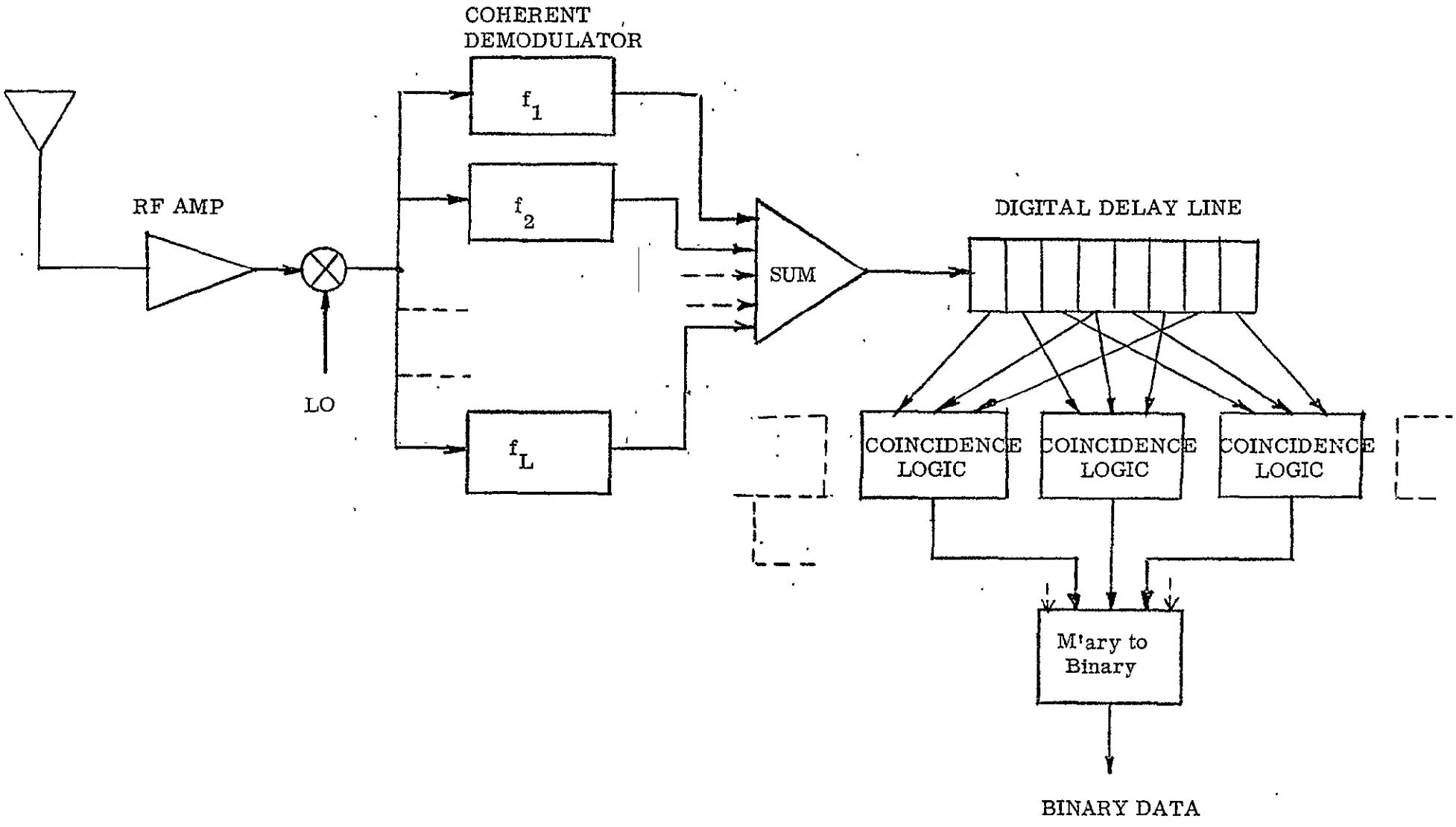

Figure 1.97 - RADA Receiver Diagram

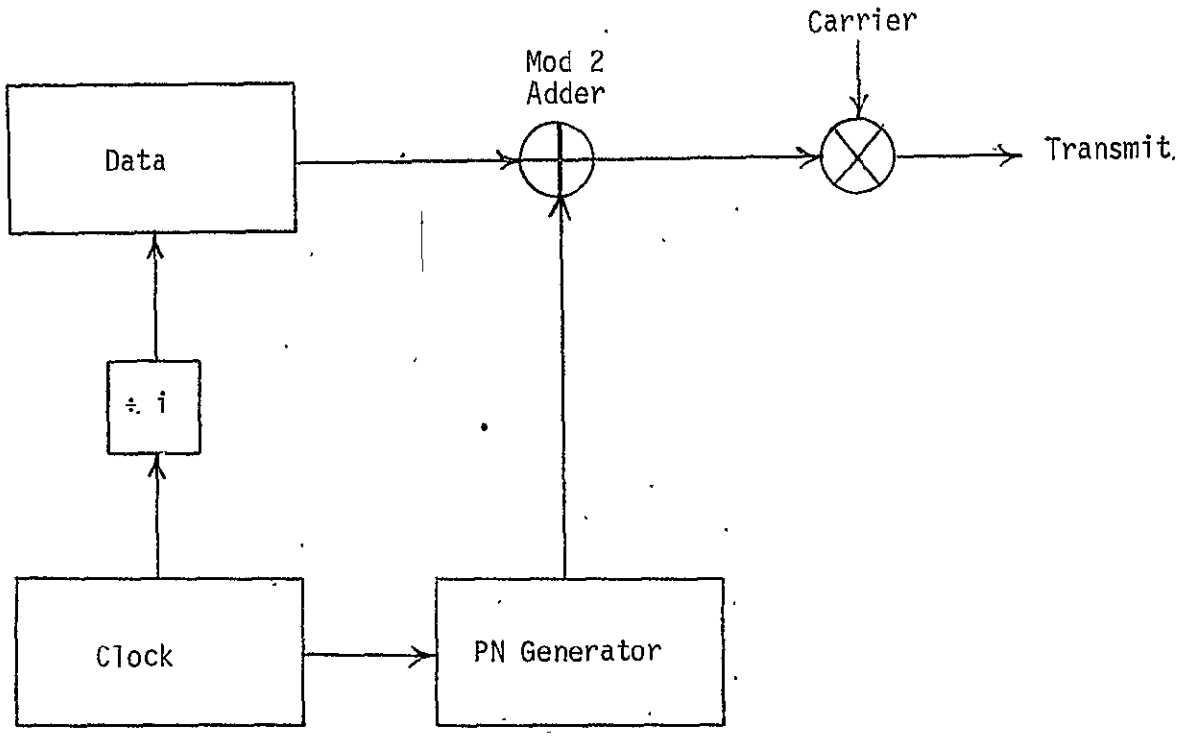

i = ratio of PN Code to Data Rate

Fig. 1.98 PN Transmitter

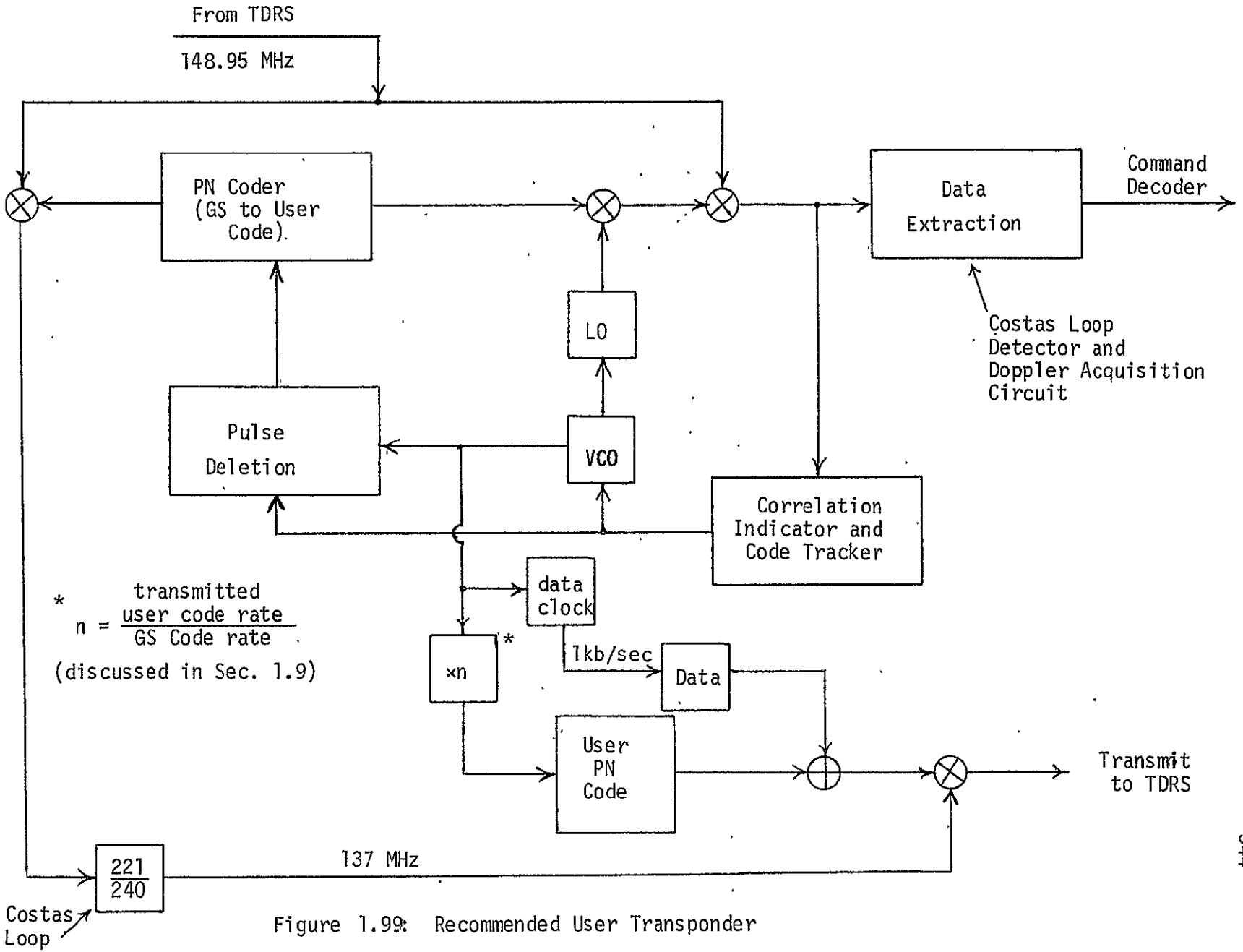

Figure 1.99: Recommended User Transponder

compared to PN but when circuitry is added to these implementations to provide ranging, carrier acquisition, doppler tracking, etc. Then for all practical purposes the PN system and the "apparently less complex" approaches are equal in complexity. In fact since the PN system is an integrated approach, those techniques which require changes in their signal format to provide range and range rate measurements may in practice be more complex than the PN modem when all the circuitry is properly counted.

We conclude that of the systems we have investigated thus far the PN, PRTH, and Adaptive and Programmed Techniques will require about the same order of complexity while the RADA system is far more complex than any of the above.

Recently, Magnavox concluded an in-house study to determine reduction size estimates for a PN system. Using existing IC technology we conclude that a complete user transponder can be comfortably fabricated in a 12 cu. inch volume. This figure excludes power supply but includes the VHF r-f receiver stages.

1.14 DESCRIPTION OF THE RECOMMENDED SYSTEM

The preceding discussions and analyses lead us to recommend a pseudo-noise PN approach for the users of the TDRS. We arrive at this firm conclusion based on comparative analyses covering multipath performance, multiple access performance, resistance to interference, ranging capabilities, synchronization performance, efficient handling of data and voice, and hardware complexity.

Shown in Figure 1.100 is a functional block diagram of the overall system, illustrating both ground station and user transponder equipment. Included in 1.100 are estimates of the number of equipment types at each end of the terminal. Note that the TDRS is a simple "bent pipe" non-coherent repeater.

The advantages obtained by using PN as the basic approach are listed below.

a) immunity to worst case multipath on both VHF links
b) resistance to interference
c) support of 40 simultaneous users through a common TDRS repeater
d) simple TDRS "bent pipe" non-coherent linear repeater
e) precise range and range rate for tracking
f) coherent user transponding
g) compatibility with forward error control
h) capacity to handle all desired data rates and voice
i) precise tracking of the TDRS by ground station

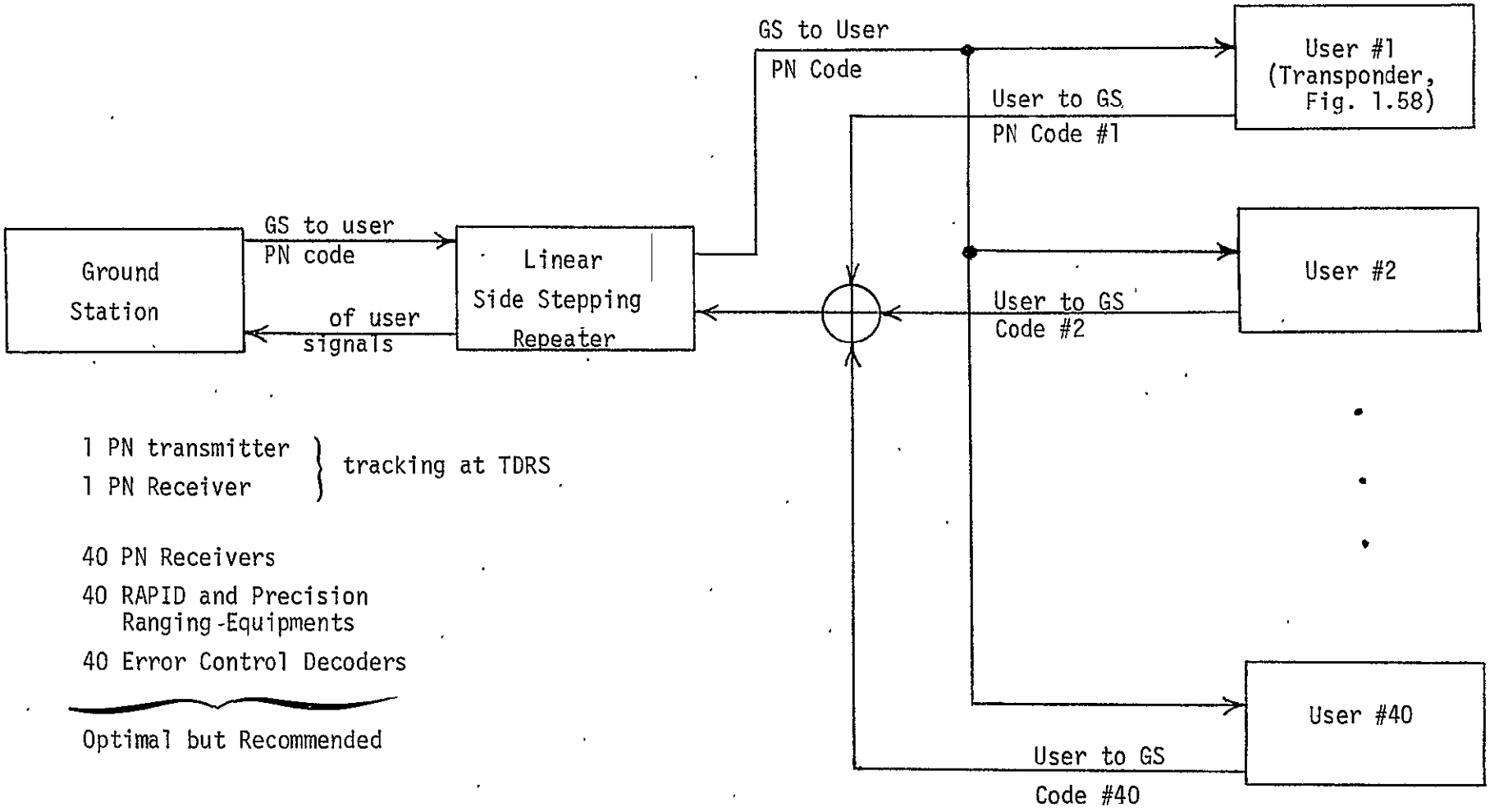

Fig. 1.100 Functional Block Diagram of Overall Recommended PN System

j) positive identification of each user at the ground station as a result of unique PN Gold Coding

k) single ground station to user command carrier does not require multiple command channels

l) compatible with PCM, tone, and tone digital command formats

m) allows tracking of user throughout entire mission by one or more TDRS's

n) simultaneous tracking of a large number of users

o) utilizes proven digital techniques such as those currently used in unified S-band.

1.15 THE IMPACT OF THE PROPOSED TDRS INSTRUMENTATION ON EXISTING NASA TECHNOLOGY

It is instructive to review existing NASA instrumentation to determine the proposed PN system approach is compatible with any existing NASA instrumentation. The word "compatible" means that some portions of the system can be used, e.g., receiver, antenna, etc. We do not mean that the entire system can be used in a wholesale sense, rather, only portions can be used. This survey is intended to identify equipment designs already in NASA's inventory to determine if parts of the inventory can be used with the proposed TDRS modulation.

What follows in this section is a brief survey of the existing STADAN system as outlined in the NASA-Goddard Space Flight Center Document X53067304, entitled "Space Tracking and Data Acquisition Network Manual," dated July 1967. We also comment on the Manned Space Flight Network instrumentation.

1.15.1 STADAN

The primary functions of the existing STADAN system is to provide acquisition and recording of spacecraft data, the tracking of spacecraft, the commanding of spacecraft, the handling of telemetry data from spacecraft, and the transfer of this data to the Goddard Space Flight Center in Greenbelt. The STADAN system is also required to perform operational control of spacecraft and to provide communication with all related activities. The STADAN system is connected to the Goddard Space Flight Center through NASA-Goddard's NASCOM facility.

To accomplish the telemetry or data acquisition activity in the STADAN system, a station within STADAN may be equipped with large antennas such as 85-foot dishes or 40-foot dishes. Associated with the large antennas are the satellite automatic tracking antenna network SATAN receive antenna and a 9 element yagi antenna. However, all stations are not equipped with the full complement of antennas.

For the purpose of tracking a STADAN station can be equipped with three separate subsystems: 1. the mini-track optical tracking system; 2. the mini-track interferometer system; and 3. the Goddard Range and Range Rate System. As in the case of telemetry acquisition all stations are not equipped with a full complement of tracking equipment.

Since the STADAN stations are required to command and also control the operation of the scientific satellites they are outfitted with a complement of commanding antennas. These include dual yagi antenna systems, single yagi antenna systems, disk-on-rod antenna command systems, and satellite automatic tracking network command antenna, SATAN.

For the purpose of data handling, recording, and transferring of data to the NASA-Goddard Space Flight Center some of the STADAN stations are equipped with various types of receiving and demodulating equipment for the purpose of extracting specified telemetry subcarriers to perform a multiplexing function, to demodulate and decommutate the telemetry signals, and to record or reformat the information for retransmission to the Goddard Space Flight Center.

The information collected at the STADAN sites is conveyed to the Goddard Space Flight Center through NASCOM which consists of a grid of land lines, undersea cables, microwave and radio links of various types of capacities.

1.15.2 Receiving and Transmitting Antennas

The 85-foot dish is a parabolic reflector with associated feeds, autotrack receivers and axis measuring and positioning of encoders, etc. The antenna telemetry feeds provide the capability for receiving 136 MHz, 400 MHz, and 1700 MHz frequency bands. It is also equipped with a dipole for reception of 235 MHz. The 40-foot dish antenna is very similar in function to that of the 85-foot dish and similarly equipped. The SATAN receiving antenna is designed to receive signals from 136-137 MHz and consists of a 16-array yagi structure. In addition to the VHF SATAN receive antenna a 9-element yagi array also can exist at a STADAN site.

The basic receiving and demodulating equipment at the STADAN sites consists of dual channel telemetry receivers with associated phase lock demodulators and diversity combiners. The subreceivers usually operate as a two-channel unit between 130 and 140 MHz. Signals received at a STADAN site at 400 MHz or at 1700 MHz are down-converted to 130-140 MHz for further processing and demodulation. The actual signal demodulation is accomplished through phase-locked demodulators which provide both AM or PM signal demodulation using synchronous detection techniques. Diversity combining is also provided at 500 KHz IF. The actual bandwidth modulator function, etc., are obtained through switching functions on the front panel of the receiving equipment. The receiving equipment at STADAN sites for

the collection of data from unmanned spacecraft consists of receivers at 130-140 MHz front ends. Signals received at this frequency, of course, are directly processed through dual-channel demodulators. Signals received at 400 or 1700 MHz are translated to 130-140 MHz for final demodulation. The bandwidth of the 140-130 MHz front end is several MHz wide and the primary band limitations are imposed by subsequent channelizing prior to final demodulation in the receiver. The IF bandwidths of the receivers are selectable from 10 KHz to 3 MHz.

The STADAN stations can be equipped with data buffering instrumentation for the purpose of synchronizing incoming data which can be at various rates reformating the data and transmitting the data at 600, 1200, 2400 bits per second to the Goddard Space Flight Center over conventional 3 KHz voice channels.

The STADAN station has the capability of commanding or transmitting to the unmanned user craft at frequencies between 120 MHz to 150 MHz. The ground station to user commands are transmitted on the uplink from ground stations at 2.5 or 5 KW power levels and normally at either 123 MHz or at 140 MHz.

Regarding the tracking instrumentation, the Goddard Range and Range Rate System is of primary interest. The Goddard Range and Range Rate System has receivers at both VHF and S-band and is an inherently wideband receiving system. The GRARR transmits at both VHF and S-band at power levels of 1 or 10 KW. The Goddard Range and Range Rate System is equipped with its separate antennas at both VHF and S-band.

In addition to the primary instrumentation associated with STADAN, there are other application areas, e.g., the ATS system which has been installed at such sites as Mojave and Rosman and Cobie Creek. Note that Mojave and Rosman are CONUS stations and might in fact be utilized as CONUS tracking stations for the TDRS. Of particular importance in the ATS system is the interfacing in both the transmitter and receive at a wideband 70 MHz IF. The 70 MHz interface is in conformance with existing standards of 70 MHz IF interfaces for most of the communication systems which have been generated in the past five years. Both wideband and narrowband systems considered for TDRS could very easily interface with the ATS system at 70 MHz point. Note further that the ATS system operates at transmit and receive frequencies of 6 and 4 GHz.

1.15.3 Spacecraft Telemetry Signal and Command Standards

The purpose of this section is to describe existing telemetry signals for the unmanned user spacecraft to ground station and the command signals from the ground station to the unmanned user. An adequate understanding of these signals is required in order to determine the impact of proposed TDRS changes on the instrumentation of the existing system.

In the existing system information is conveyed to the ground from the user spacecraft by primarily two modulation methods:

1) PCM
2) PFM

The user to ground station data rate for the unmanned spacecraft has been specified for this study at one kilobit per second and therefore the user

to ground station telemetry signals such as PCM and PFM will not be discussed in this report but are adequately described in NASA X56063-2 Aerospace Data Systems Standards, 1 April 1968.

The commands from ground station to user can be one of three types: tone command, tone digital command, and the PCM command. The tone command uses frequencies or subcarriers located between 2,000 and 7,000 Hz for the purpose of addressing the unmanned user spacecraft and to provide up to 3 executions. There are a total of 22 execute address tones in the tone command system. The tone command system is used primarily for on-off commands to the spacecraft. The subcarrier tone duration lasts between .5 and 3.5 seconds with sub-intervals of 1/2 second.

In addition to the tone command signal format a tone digital command can be used to control spacecraft from the ground station. The tone digital command utilizes a pulse duration/AM/AM broadcast technique or modulation technique in the present system. A pulse period is defined as 72 cycles of the encoder clock. Sync preamble and 1's and 0's are a fraction of the 72 cycles of the encoder clock. Namely, 18, 36, 54 and 72. Presently the PDM pulses modulate subcarriers which can be selected between 7,000 Hz and 11,000 Hz. In the spacecraft the receiver consists of narrow filters having a bandwidth in the order of 6% of the center frequency at the 6 dB point.

The tone digital system is used primarily for real time on-off commanding a spacecraft. The basic tone digital system provides for direct addressing, synchronization, and execute commands.

The final command signal in use and expected to increase in usage is the standard PCM command technique. The present system utilizes PCM, FSK, prior to the AM modulation of the primary carrier. The two frequencies which have been assigned for the FSK operation are at 7 and 9 KHz. The PCM word link is fixed at 64 bits per second with a maximum number of these attributed to data at 46 bits. The current bit rate is at 128 bits per second with 1,000 bits per second being taken under consideration for the command standard or up to 1,000 bits per second for the command standard. The PCM word provides for bit synchronization, spacecraft addressing, execution and varification of receipt and execution at the ground station.

1.15.4 Compatibility Conclusion

To determine the compatibility of the proposed PN approach for TDRS instrumentation with the STADAN system we list the current frequencies proposed for TDRS below.

User to TDRS	VHF, S, K-band
TDRS to User	VHF, S, K-band
TDRS to G.S.	K-band
G.S. to TDRS	K-band

Note that the TDRS to user is at VHF, S-band, or K-band, while TDRS to ground station frequencies are at K-band exclusively. Thus we can conclude that the existing STADAN transmitting and receiving equipment which is at 136, 400, 1700 megacycles and at 4 gc for the Goddard Range and Range Rate System will have to be modified in order to function with the proposed TDRS

to ground station frequencies. It is beyond the scope of this study to recommend exactly how the STADAN receiving equipment could be modified to accommodate the new K-band TDRS to G.S. frequency. However, we can conjecture that by translating the K-band frequencies to either L-band or directly to 136 MHz, a portion of the existing ground station receiving equipment could be utilized. We cannot state at this time whether the antenna systems associated with present STADAN could be modified to incorporate K-band feeds. It may require a special design K-band antenna. Similar comments could be made about ATS or Goddard Range and Range Rate System; that is, suitable translation from K-band to either S-band or VHF could be accomplished allowing both portions of the Goddard Range and Range Rate System receiver portions and of the ATS instrumentation to be utilized on the TDRS to ground station link. We conclude that bandwidths on the order of 3 to 10 MHz are available from the instrumentation surveyed; that is, if suitable translation is provided, the existing STADAN, Goddard Range and Range Rate, and ATS systems could be utilized as receivers for the wideband signals proposed for TDRS.

The ground station to TDRS link at K-band probably cannot utilize much of the instrumentation now in existence without major redesign to provide a K-band source and a K-band antenna and/or feed system.

We conclude that the PN approach for TDRS can use a great deal of the existing technology already in NASA's inventory. Wideband receiver and transmitters appear to exist in both the STADAN and MSFN* which with modification could be used with the wideband PN system. Furthermore, we conclude that the PN system (using PDM) can be configured to handle the PCM, tone, or tone digital type commands.

---

*Unified S-band Tech. Conf. - Edited by K.E. Peltzer, NASA, July 1965

1.16 FACTORS WHICH INFLUENCE THE OPERATIONAL PERFORMANCE OF THE TDRS

There are three factors which we feel need mentioning which can serve to improve the operation performance of the TDRS.

a) We have assumed throughout our analyses that worst case multipath conditions exist. Actually, Habib* has projected the satellite population through 1980 and the distribution of this population shows an average user altitude close to 500-1000 miles depending upon the exact year. We can conclude that the multipath from users 500 to 1000 miles above the earth should be 6 to 9 dB below the worst case conditions assumed in the report, i.e., direct signal to multipath of unity. This fact should alleviate the multipath problem somewhat (see comment on antenna pattern effects to follow).

b) We have shown in Section 1.12 that the RFI contained in the VHF space bands will probably have some average duty factor associated with it, thus reducing the worst case RFI. We have attempted to estimate this average duty factor and we conclude that .25 is representative of the type of signals contained in the VHF bands. This duty factor would reduce the RFI on the average by 6 dB.

c) In addition to the above factors, the natural shielding of the earth will on the average reduce the number of users in view of a TDRS by a factor of .43. While this factor cannot be relied upon to prevent all 40 users from crowding together, it will on the average serve to reduce the loading on a TDRS.

---

*op cit

We have pointed out in the Requirements Section of this report that the user antenna pattern were not perfectly omni-directional at VHF. To combat deep nulls in the patterns, polarization diversity or clever antenna array designs must be employed on the user craft at VHF. The residual variations in antenna gain (3 dB ripple seems feasible) can decrease the desired signal while increasing the multipath signal or vice versa. Assuming a 3 dB ripple in the pattern exists, a 3 dB increase in the ratio of multipath to desired signal can be sustained. Modulation techniques described thus far to combat multipath react to these antenna pattern anamolies in differing ways. For example,

a) The diversity system is further degraded by 3 dB.

b) The wideband signals are not materially affected since the large number of users tends to keep the average multipath constant. A single wideband signal however can sustain a 1.5 dB loss.

c) The narrowband PN system can be degraded by 3 dB.

d) The adaptive or programmed narrowband technique avoid the multipath, thus the antenna pattern variations only set a lower bound on the duty factors, and contribute to a 1.5 dB user signal loss.

During the actual operation of the TDRS system care must be taken to avoid supporting very high altitude users, particularly at VHF. The reason for this is that a high altitude user, 30,000 Km near a TDRS, can capture the TDRS repeater or cause a severe division of power imbalance at the output of the repeater.

1.17 RECOMMENDATIONS

Our primary recommendation is to continue studying the impact of RFI on the TDRS system. Actual measurements of the RFI by a properly instrumented spacecraft represents the ultimate in resolving the RFI question. This measurement can be supplemented by a more thorough analysis of available RFI data from government sources and the International Telecommunications Union.

The problem of handover of a user from one TDRS to another should receive more study. We have not addressed this problem in this report; however, we have considered several ways to accomplish this. The use of 4 PN codes, one assigned to each TDRS for the G.S. to user command link is one approach which appears quite feasible.

APPENDIX I

THE EFFECTS OF SPECULAR AND DIFFUSE MULTIPATH ON OPTIMUM BINARY MODULATION

It is the purpose of this appendix to document the effects of both diffuse and specular multipath on optimum binary communications systems such as binary delta phase shift key (ΔPSK). In this section we will not perform an exhaustive analysis on other types of binary systems such as differential PSK or FSK since the results appears in the open literature*. We have chosen for analysis the optimum binary ΔPSK system, since this system represents an upper bound on the performance of binary communication systems in the presence of multipath. From this analysis we will be able to determine the need for forward error control and the ability of diversity systems to operate in the presence of multipath.

In this analysis we have considered the combined effects of specular and diffuse multipath and ever present Gaussian noise on the performance of a ΔPSK transmission. When forward error control is utilized a minimum acceptable bit error probability of .05 must be obtained in order that effective convolutional coding sequential decoding can be utilized to drop or reduce this raw bit error probability to 10^{-5}. The above criteria assumes a rate ½ coder for the forward error control technique.

It has been shown** that the conditional bit error probability for a coherent reference PSK transmission can be expressed in the following form.

---

* J. J. Jones, IEEE Comm. Tech. Dec. 68

** J. N. Birch, Magnavox Tech. Paper

$$P_\varepsilon(K,4) = \frac{1}{2}\,\mathrm{erfc}\ \sqrt{E/N_o}\ (1 + K\cos\psi) \qquad \text{eq. 1}$$

coh PSK

$$K = \sqrt{\frac{S_{ind}}{S_{dir}}}\ \left|\ \frac{\sin\frac{\Delta\omega T}{2}}{\frac{\Delta\omega T}{2}}\ \right|$$

$\Delta\omega$ = differential Doppler

ψ is a uniform random phase angle

The value of K in the above equation represents the instantaneous ratio of the multipath signal to the desired signal. In practice the multipath signal can consist of a specular component which is essentially a delayed replica of the direct path signal and a diffuse component which occupies a bandwidth equal to the fading bandwidth plus the original data bandwidth. The envelope statistics associated with the indirect signal will follow a Rician probability density. Thus we could argue that K itself will follow a Rician density which is normalized to the power in the direct path. The average bit error probability using the above equation 1 can be calculated from following equation 2.

$$\overline{P}_\varepsilon = \int_0^\infty \left[\frac{1}{\pi}\int_0^\pi P_\varepsilon(K,\psi)\ d\psi\right] P(K)dK \qquad \text{eq. 2}$$

The above equation can be simplified by considering the diffuse component as Gaussian noise and by considering the specular component as narrowband constant envelope interference; that is, we assume that these components are separable. Under the validity of such assumptions which are in general true we may restate the above average bit error probability in the following terms.

$$\overline{P_\varepsilon} = \frac{1}{\pi} \int_0^\infty \frac{1}{2} \operatorname{erfc}\left[\sqrt{\frac{S_{dir}}{N_g+N_{diff}}} \left(1 + \sqrt{\frac{S_{spec}}{S_{dir}}} \cos \psi\right)\right] d\psi \qquad \text{eq. 3}$$

S_{dir} = direct power

S_{spec} = specular power

N_{diff} = diffuse power

We have considered the diffuse component as noise and the specular component as constant envelope interference with a uniform phase angle.

The results of equation 3 have been computerized or obtained from computer programs and are listed for convenience at the end of this appendix. Note that the effects of differential Doppler between the direct and the indirect path have been embedded in the value of K. Furthermore, the frequency weighting effects of the integrate and dump circuit have not been utilized in calculating the noise power due to the diffuse component, thus the results obtained from equation 3 can be considered worse case, meaning when low differential Doppler exists and the fading bandwidth is well within the limits of the data bandwidths.

There are several conclusions which can be drawn from the above analysis.

(1) Diffuse multipath creates a irreducible bit error probability at high desired signal to Gaussian noise ratios whereas specular multipath can be overcome by sufficiently high desired signal to Gaussian noise ratios.

(2) At low desired signal to Gaussian noise ratios both specular and diffuse multipath serve to create essentially equal bit error probabilities.

The actual bit error probability for ΔPSK is $2\ P_\varepsilon(1-P_\varepsilon)$ where P_ε is the bit error probability associated with the PSK transmission. For bit error probabilities on the order of .1 and less the above equation for the bit error probability associated with the ΔPSK system is given as $2\ P_\varepsilon$.

In the attached printout. P_ε is tabulated for coherent PSK. To convert to ΔPSK multiply by approx 2. K2 is the ratio of direct power to total multipath and spec/diff is the ratio of specular to diffuse multipath power.

Fig. 1 is a plot of optimum binary PSK vs E/N_0 and ΔPSK vs E/N_0 for comparison. Fig. 2 is a plot of optimum PSK in the presence of specular or diffuse multipath.

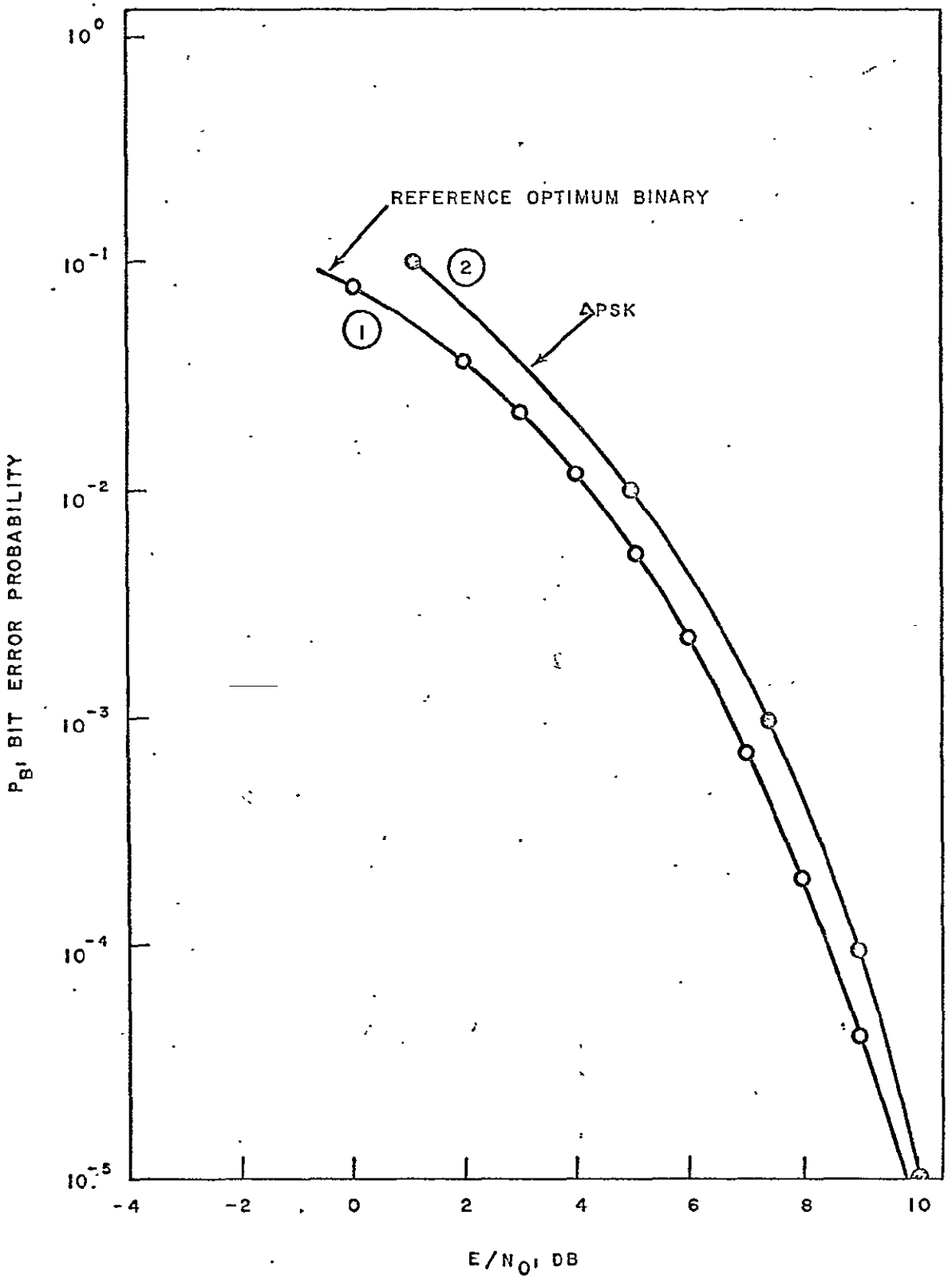

Fig. 1 OPTIMUM BINARY PSK AND ΔPSK VS E/N_0

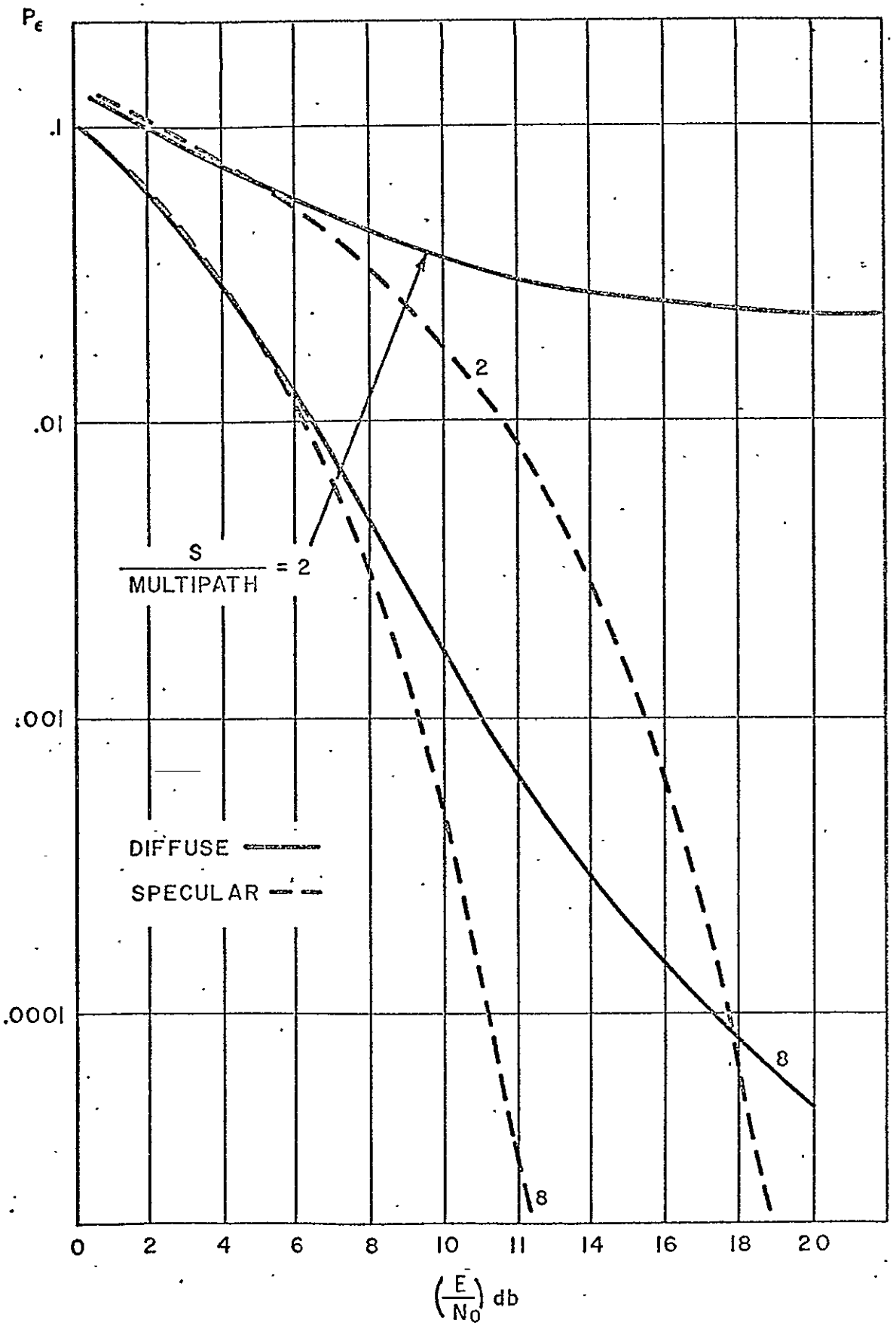

Fig. 2 OPTIMUM PSK IN THE PRESENCE OF SPECULAR OR DIFFUSE MULTIPATH

SPEC/DIFF= 0

PE	S/N
.160362	1
.125433	2
.104049	4
9.21817 E-2	8
8.59379 E-2	16
8.27378 E-2	32
8.11183 E-2	64
8.03037 E-2	128

SPEC/DIFF= .25

PE	S/N
.160841	1
.126103	2
.104807	4
9.29558 E-2	8
8.67029 E-2	16
8.34918 E-2	32
8.18649 E-2	64
8.10461 E-2	128

SPEC/DIFF= .666667

PE	S/N
.162082	1
.127836	2
.106666	4
9.47038 E-2	8
8.82997 E-2	16
8.49777 E-2	32
8.32844 E-2	64
8.24294 E-2	128

SPEC/DIFF= 1.5

PE	S/N
.164237	1
.130763	2
.109499	4
9.69318 E-2	8
8.99247 E-2	16
8.61886 E-2	32
8.42536 E-2	64
8.32681 E-2	128

SPEC/DIFF= 4.

PE	S/N
.167483	1
.134974	2
.112933	4
9.85627 E-2	8
8.98025 E-2	16
8.48247 E-2	32
8.21434 E-2	64
8.07473 E-2	128

SPEC/DIFF= 107374 1823

PE	S/N
.160916	1
.129523	2
.105562	4
8.63878 E-2	8
7.07379 E-2	16
5.78294 E-2	32
4.71138 E-2	64

UNDERFLOW IN 601

PE	S/N
.125433	1
7.94859 E-2	2
5.17826 E-2	4
3.72165 E-2	8
2.99965 E-2	16
2.64596 E-2	32
2.47191 E-2	64
2.38573 E-2	128

SPEC/DIFF= .25

PE	S/N
.125645	1
7.97384 E-2	2
5.19484 E-2	4
3.72322 E-2	8
.029885	16
2.62672 E-2	32
2.44815 E-2	64
2.35958 E-2	128

SPEC/DIFF= .666667

PE	S/N
.126103	1
8.02236 E-2	2
5.20191 E-2	4
3.66864 E-2	8
.028842	16
2.49186 E-2	32
.022966	64
2.19936 E-2	128

SPEC/DIFF= 1.5

PE	S/N
.126827	1
8.08732 E-2	2
5.16366 E-2	4
3.48683 E-2	8
2.59162 E-2	16
2.13418 E-2	32
1.90469 E-2	64
1.79011 E-2	128

SPEC/DIFF= 4.

PE	S/N
.127836	1
8.15688 E-2	2
5.02333 E-2	4
3.06271 E-2	8
1.95497 E-2	16
1.38201 E-2	32
1.09839 E-2	64
9.59318 E-3	128

SPEC/DIFF= 107374 1823

PE	S/N
.129144	1
8.21254 E-2	2
4.68614 E-2	4
2.16161 E-2	8
6.72768 E-3	16
1.00304 E-3	32

UNDERFLOW IN 601

3.64049 E-5	64

UNDERFLOW IN 601

K2= 4
SPEC/DIFF= 0

PE	S/N
.104049	1
5.17826 E-2	2
2.30016 E-2	4
1.05831 E-2	8
5.77662 E-3	16
3.87969 E-3	32
.003075	64
2.71011 E-3	128

SPEC/DIFF= .25

PE	S/N
.104136	1
5.18611 E-2	2
2.29756 E-2	4
1.04341 E-2	8
5.56084 E-3	16
3.64142 E-3	32
2.83140 E-3	64
2.46584 E-3	128

SPEC/DIFF= .666667

PE	S/N
.104291	1
5.19484 E-2	2
2.27155 E-2	4
9.81307 E-3	8
4.79670 E-3	16
2.86996 E-3	32
2.08424 E-3	64
1.73931 E-3	128

SPEC/DIFF= 1.5

PE	S/N
.104514	1
5.20141 E-2	2
2.21094 E-2	4
8.60223 E-3	8
3.48003 E-3	16
1.68286 E-3	32
1.02819 E-3	64
7.66035 E-4	128

SPEC/DIFF= 4.

PE	S/N
.104807	1
5.20191 E-2	2
2.10246 E-2	4
6.72169 E-3	8
1.78659 E-3	16
4.79340 E-4	32
1.63245 E-4	64
7.80157 E-5	128

SPEC/DIFF= 107 37 41823

PE	S/N
.105169	1
.051914	2
1.93043 E-2	4
4.19845 E-3	8
3.22473 E-4	16
3.24875 E-6	32
5.89810 E-10	64

UNDERFLOW IN 601

3.58368 E-17	128

K2= 8
SPEC/DIFF= 0

PE	S/N
9.21817 E-2	1
3.72165 E-2	2
1.05831 E-2	4
2.37056 E-3	8
5.54043 E-4	16
1.76392 E-4	32
8.27755 E-5	64
5.31459 E-5	128

SPEC/DIFF= .25

PE	S/N
9.22192 E-2	1
3.72449 E-2	2
1.05596 E-2	4
2.31393 E-3	8
5.07753 E-4	16
1.46857 E-4	32
6.28050 E-5	64
3.77107 E-5	128

SPEC/DIFF= .666667

PE	S/N
9.22738 E-2	1
3.72615 E-2	2
1.04341 E-2	4
2.12714 E-3	8
3.85616 E-4	16
8.41449 E-5	32
2.73939 E-5	64
1.34774 E-5	128

SPEC/DIFF= 1.5

PE	S/N
9.23455 E-2	1
3.72597 E-2	2
1.01905 E-2	4
1.82306 E-3	8
2.32045 E-4	16
2.86446 E-5	32
5.04403 E-6	64
1.51917 E-6	128

SPEC/DIFF= 4.

PE	S/N
9.24342 E-2	1
3.72322 E-2	2
9.81307 E-3	4
1.42735 E-3	8
9.64957 E-5	16
3.34865 E-6	32
1.02192 E-7	64
5.43950 E-9	128

SPEC/DIFF= 107 37 41823

PE	S/N
9.25398 E-2	1
.037171	2
9.28771 E-3	4
9.81677 E-4	8
1.90005 E-5	16
1.27600 E-8	32
1.06338 E-14	64
1.38477 E-26	128

K2= 16
SPEC/DIFF= 0
PE S/N
8.59379 E-2 1
2.99965 E-2 2
5.77662 E-3 4
5.54043 E-4 8
3.23324 E-5 16
1.98018 E-6 32
2.16365 E-7 64
4.97987 E-8 128
SPEC/DIFF= .25
PE S/N
8.59549 E-2 1
3.00097 E-2 2
5.77015 E-3 4
5.42781 E-4 8
2.88794 E-5 16
1.41729 E-6 32
1.14323 E-7 64
1.99554 E-8 128
SPEC/DIFF= .666667
PE S/N
8.59762 E-2 1
3.00174 E-2 2
5.73305 E-3 4
5.07753 E-4 8
2.10232 E-5 16
5.90709 E-7 32
2.24036 E-8 64
1.93714 E-9 128
SPEC/DIFF= 1.5
PE S/N
8.60018 E-2 1
3.00185 E-2 2
5.66372 E-3 4
4.53595 E-4 8
1.24960 E-5 16
1.34123 E-7 32
1.16581 E-9 64
2.11989 E-11 128
SPEC/DIFF= 4.
PE S/N
8.60315 E-2 1
.030012 2
5.56084 E-3 4
3.85616 E-4 8
5.77027 E-6 16
1.13311 E-8 32
3.58344 E-12 64
7.00000 E-16 128
SPEC/DIFF= 10737 41823
PE S/N
8.60655 E-2 1
2.99966 E-2 2
5.42329 E-3 4
3.09685 E-4 8
1.84541 E-6 16
1.21160 E-10 32
9.81373 E-19 64

UNDERFLOW IN 601
1.21485 E-34 128

K2= 32
SPEC/DIFF= 0
PE S/N
8.27378 E-2 1
2.64596 E-2 2
3.87969 E-3 4
1.76392 E-4 8
1.98018 E-6 16
7.98724 E-9 32
3.39239 E-11 64
4.38747 E-13 128
SPEC/DIFF= .25
PE S/N
8.27459 E-2 1
2.64663 E-2 2
3.87903 E-3 4
1.74537 E-4 8
1.80870 E-6 16
5.34239 E-9 32
1.17985 E-11 64
6.67345 E-14 128
SPEC/DIFF= .666667
PE S/N
.082755 1
2.64713 E-2 2
3.87025 E-3 4
1.68537 E-4 8
1.41729 E-6 16
2.06165 E-9 32
1.11254 E-12 64
1.02378 E-15 128
SPEC/DIFF= 1.5
PE S/N
8.27653 E-2 1
2.64744 E-2 2
3.85322 E-3 4
1.59078 E-4 8
9.76453 E-7 16
4.88669 E-10 32
2.52639 E-14 64
7.04302 E-19 128
SPEC/DIFF= 4.
PE S/N
8.27765 E-2 1
2.64755 E-2 2
3.82784 E-3 4
1.46857 E-4 8
5.90709 E-7 16
6.24733 E-11 32
5.20284 E-17 64
5.27819 E-25 128
SPEC/DIFF= 10737 41823
PE S/N
8.27888 E-2 1
2.64743 E-2 2
3.79401 E-3 4
1.32574 E-4 8
3.08273 E-7 16
3.17529 E-12 32
6.41234 E-22 64

UNDERFLOW IN 601

K2=	64
SPEC/DIFF=	0
PE	S/N
8.11183 E-2	1
2.47191 E-2	2
.003075	4
8.27755 E-5	8
2.16365 E-7	16
3.39239 E-11	32
6.59984 E-16	64
1.35334 E-20	128
SPEC/DIFF=	.25
PE	S/N
8.11222 E-2	1
2.47226 E-2	2
3.07544 E-3	4
8.24754 E-5	8
2.06198 E-7	16
2.45849 E-11	32
1.93540 E-16	64
7.20916 E-22	128
SPEC/DIFF=	.666667
PE	S/N
8.11264 E-2	1
2.47256 E-2	2
3.07381 E-3	4
8.13792 E-5	8
1.80607 E-7	16
1.17985 E-11	32
1.60155 E-17	64
2.26380 E-24	128
SPEC/DIFF=	1.5
PE	S/N
8.11309 E-2	1
2.47281 E-2	2
3.07011 E-3	4
7.95727 E-5	8
1.48002 E-7	16
4.20541 E-12	32
4.53054 E-19	64
3.02472 E-28	128
SPEC/DIFF=	4.
PE	S/N
8.11356 E-2	1
.02473	2
3.06432 E-3	4
7.71405 E-5	8
1.14323 E-7	16
1.11254 E-12	32
3.12827 E-21	64
1.68830 E-34	128
SPEC/DIFF=	107374823
PE	S/N
8.11406 E-2	1
2.47315 E-2	2
3.05643 E-3	4
7.41664 E-5	8
8.34165 E-8	16
2.08315 E-13	32
2.50946 E-24	64
6.96880 E-46	128

K2=	128
SPEC/DIFF=	0
PE	S/N
8.03037 E-2	1
2.38573 E-2	2
2.71011 E-3	4
5.31459 E-5	8
4.97987 E-8	16
4.38747 E-13	32
1.35334 E-20	64
6.13867 E-30	128
SPEC/DIFF=	.25
PE	S/N
8.03057 E-2	1
.023859	2
2.71054 E-3	4
5.31029 E-5	8
4.88931 E-8	16
3.66938 E-13	32
5.00824 E-21	64
2.18830 E-31	128
SPEC/DIFF=	.666667
PE	S/N
8.03077 E-2	1
2.38607 E-2	2
2.71044 E-3	4
5.28903 E-5	8
4.63052 E-8	16
2.41279 E-13	32
7.20916 E-22	64
5.60420 E-34	128
SPEC/DIFF=	1.5
PE	S/N
8.03098 E-2	1
2.38622 E-2	2
2.70982 E-3	4
5.25186 E-5	8
4.25898 E-8	16
1.35551 E-13	32
5.57262 E-23	64
1.48177 E-37	128
SPEC/DIFF=	4.
PE	S/N
8.03119 E-2	1
2.38636 E-2	2
2.70868 E-3	4
5.19981 E-5	8
3.81996 E-8	16
6.67345 E-14	32
2.26380 E-24	64
1.78446 E-42	128
SPEC/DIFF=	107374823
PE	S/N
8.03141 E-2	1
2.38649 E-2	2
2.70702 E-3	4
5.13389 E-5	8
3.34957 E-8	16
2.89510 E-14	32
4.27210 E-26	64
1.79481 E-49	128

APPENDIX II

RANGING PERFORMANCE OF A PSEUDO-NOISE SYSTEM

by

P. Nilsen (Magnavox Research Labs)

1.0 INTRODUCTION

In a PN system, the range measurement is made by comparing the phase between clocks which are synchronized to the respective received PN codes. Thus, the range measurement accuracy is limited by the time jitter error of the clock tracking loops. In the PN system it will be assumed that a separate implementation performs a coherent demodulation to extract the pseudo-random code, and the clock tracking loop operates on the low-pass demodulated signal.

2.0 THEORETICAL BASIS

The phase comparison measurement between receiver clocks is actually a relative time of arrival measurement of the signal. Measurement of the time of arrival of a signal in the presence of background interference may be interpreted as a problem in the estimation of an unknown signal parameter. To examine the basic case, assume reception of a pulse waveform $s(t-\tau)$, where τ is the unknown time of arrival, in the presence of white noise of spectral density (one-sided) N_0. The received signal is observed over some interval - T/2 to T/2 such that edge effects are eliminated; i.e., we write

$$r(t) = s(t - \tau) + n(t) \quad -T/2<t<T/2 \qquad (1)$$

The estimation of the parameter τ is obtained through the log likelihood function, given by[1]

$$\log \Lambda \left[r(t), \tau\right] = \frac{2}{N_o} \int_{-T/2}^{T/2} r(t)\, s(t-\tau)\, dt - \frac{1}{N_o} \int_{-T/2}^{T/2} s^2 (t-\tau)\, dt \qquad (2)$$

The maximum likelihood estimation is the value of τ which maximizes Equation (2). If the maximum is interior, it may be found by differentiation

$$\begin{aligned} \frac{\partial \log \Lambda}{\partial \tau} &= \frac{2}{N_o} \int_{-T/2}^{T/2} \left[r(t) - s(t-\tau)\right] \frac{\partial s(t-\tau)}{\partial \tau}\, dt \\ &= -\frac{2}{N_o} \int_{-T/2}^{T/2} r(t)\, s'(t-\tau)\, dt \end{aligned} \qquad (3)$$

where it is noted that the last term in Equation (2) is independent of the parameter τ. The value of τ which sets Equation (3) equal to zero is the maximum likelihood estimator $\hat{\tau}_{m\ell}$. That is,

$$\int_{-T/2}^{T/2} r(t)\, s'(t - \hat{\tau}_{m\ell})\, dt = 0 \qquad (4)$$

Equation (4) is the theoretical basis for the time of arrival measurement. It leads to the concept of a tracking loop which correlates the received signal, with noise, against the derivative of the known waveform, driving the correlation to a null.

A lower bound on the variance of the maximum likelihood estimator (or on any unbiased estimator) can be stated.[2] Ignoring edge effects and letting the true value be zero for convenience

$$E\left[\hat{\tau}^2\right] \geq \frac{N_o}{2 \int_{-T/2}^{T/2} \left[s'(t)\right]^2 dt} \qquad (5)$$

A case of importance here uses a signal of average power S, biphase modulated by a pseudorandom code with clock period T_c. After coherent demodulation, not of concern here, the desired signal may be written

$$r(t) = \sqrt{S}\, a(t) + n(t) \tag{6}$$

where a(t) is a repetitive pulse shape of energy T_c (for normalization to unit power) and whose polarity changes pseudorandomly at each clock period. The in-phase component of interference is denoted as n(t). The normalization is such that n(t) has density N_o if the received interference has density N_o. Then Equation (5) simplifies to

$$E\left[\hat{\tau}^2\right] \geq \frac{N_o/S}{(2T/T_c)\int_{-\infty}^{\infty} [a'(t)]^2\, dt} \tag{7}$$

Letting $A(\omega)$ be the Fourier transform of a(t), Equation (7) can be written as

$$E\left[\hat{\tau}^2\right] \geq \frac{N_o/S}{(2T/T_c)\frac{1}{2\pi}\int_{-\infty}^{\infty} |A(\omega)|^2\, \omega^2\, d\omega} = \frac{N_o}{2TS(2\pi\beta)^2} \tag{8}$$

In Equation (8), β is defined as an rms bandwidth, in Hz, as follows:[3]

$$(2\pi\beta)^2 = \frac{\frac{1}{2\pi}\int_{-\infty}^{\infty} |A(\omega)|^2\, \omega^2\, d\omega}{\frac{1}{2\pi}\int_{-\infty}^{\infty} |A(\omega)|^2\, d\omega} = \frac{\int_{-\infty}^{\infty} [a'(t)]^2\, dt}{\int_{-\infty}^{\infty} [a(t)]^2\, dt} \tag{9}$$

It may be observed that assumption of a rectangular pulse shape yields an infinite bandwidth, according to Equation (9).

3.0 LOOP ANALYSIS

The clock tracking loop is usually implemented as a delay lock loop or a τ jitter loop or some variation of either such as the early late gate. A step by step analysis of the performance of both the delay lock loop and the τ jitter loop follows below. The results obtained for the delay lock loop also apply for practical implementations of an early late gate tracking loop.

The analysis considers the received signal and noise to be bandlimited by an IF filter. The noise itself is assumed to be white, Gaussian noise. The rms tracking errors for the delay lock and τ jitter loops are derived and presented by Equations (34) and (51), respectively. The tracking performance described by these equations is plotted in Figures 4 and 8, respectively. In addition, the effects of varying the jitter time displacement on tracking performance is shown in Figures 5 and 9.

The most significant result of this analysis is that the delay lock loop has better tracking performance than the τ jitter loop, as shown in Figure 10. In addition, as the time jitter displacement is made smaller, the delay lock loop tracking performance improves whereas the τ jitter loop tracking performance degrades.

Finally, in light of the superior performance of the delay lock loop, some consideration is given to channel gains and time delay differentials. It is shown that for reasonably well designed channels the tracking error does not increase very much with reasonable channel unbalances.

3.1 ANALYSIS OF THE DELAY LOCK LOOP

A block diagram of the delay lock tracking loop is shown in Figure 1. Coherent demodulation to baseband will be assumed as it is more convenient to analyze a baseband loop and the results apply directly to an IF loop. The receiver filter will be assumed to be an ideal bandpass filter which represents the bandlimiting accomplished by the IF filtering. The loop can be modeled mathematically as shown in Figure 2, if the tracking error is $< 1/2$ radian. In the analysis which follows, the variance of the tracking error $\Delta\tau$ and thus the rms tracking error will be found.

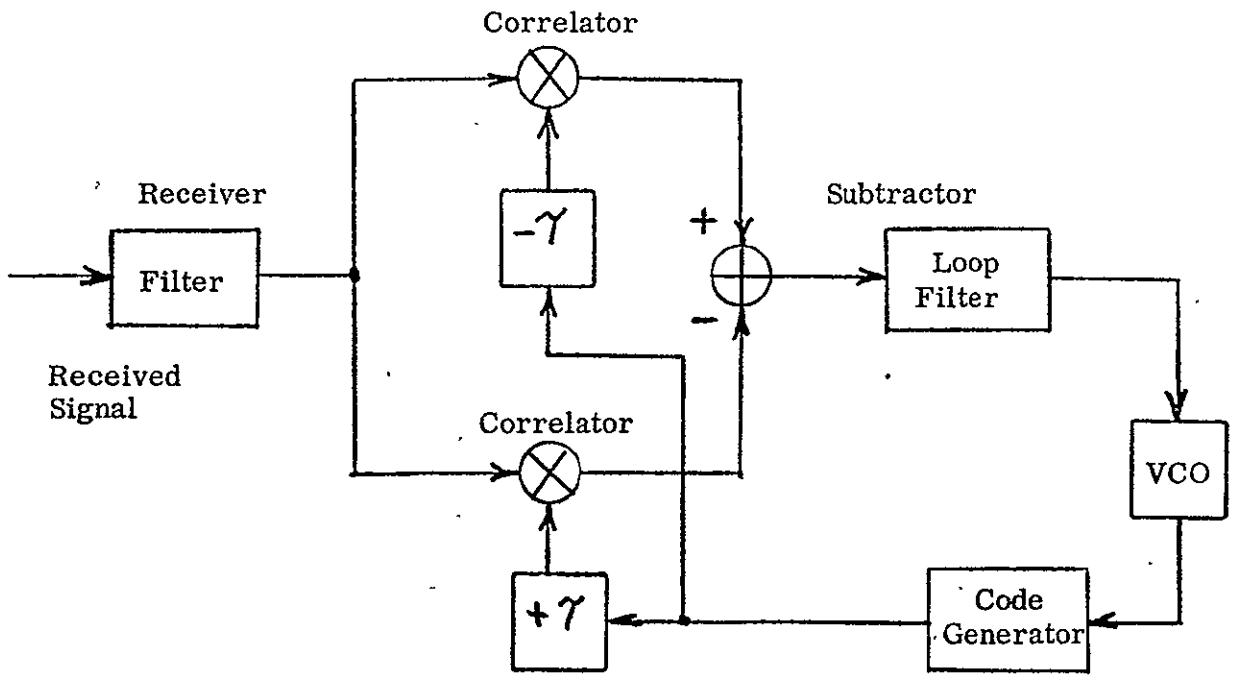

Figure 1 - Block Diagram of Delay
Lock Tracking Loop

From Figure 2 it can be seen that by superposition

$$\tau_2 = \Delta\tau \left[AKF(p) \frac{1}{p} \right] + n'(t) \left[KF(p) \frac{1}{p} \right] \tag{10}$$

where p is operator notation for $\frac{d}{dt}$. Furthermore, in response to noise alone,

$$\Delta\tau = -\tau_2 \tag{11}$$

so that by combining Equations (10) and (11) we obtain

$$\Delta\tau = -\frac{KF(p)/p}{1 + AKF(p)/p} \quad n'(t) \tag{12}$$

Since it is more convenient to work with power spectral densities, Equation (12) is written as

$$S_{\Delta\tau}(\omega) = \left| \frac{KF(j\omega)/j\omega}{1 + AKF(j\omega)/j\omega} \right|^2 S_{n'}(\omega) \tag{13}$$

where

$S_{n'}(\omega)$ is the power spectral density of the noise

and

$S_{\Delta\tau}(\omega)$ is the power spectral density of the loop tracking error.

The noise density can be found from consideration of the process taking place in the loop "discriminator," shown in Figure 3.

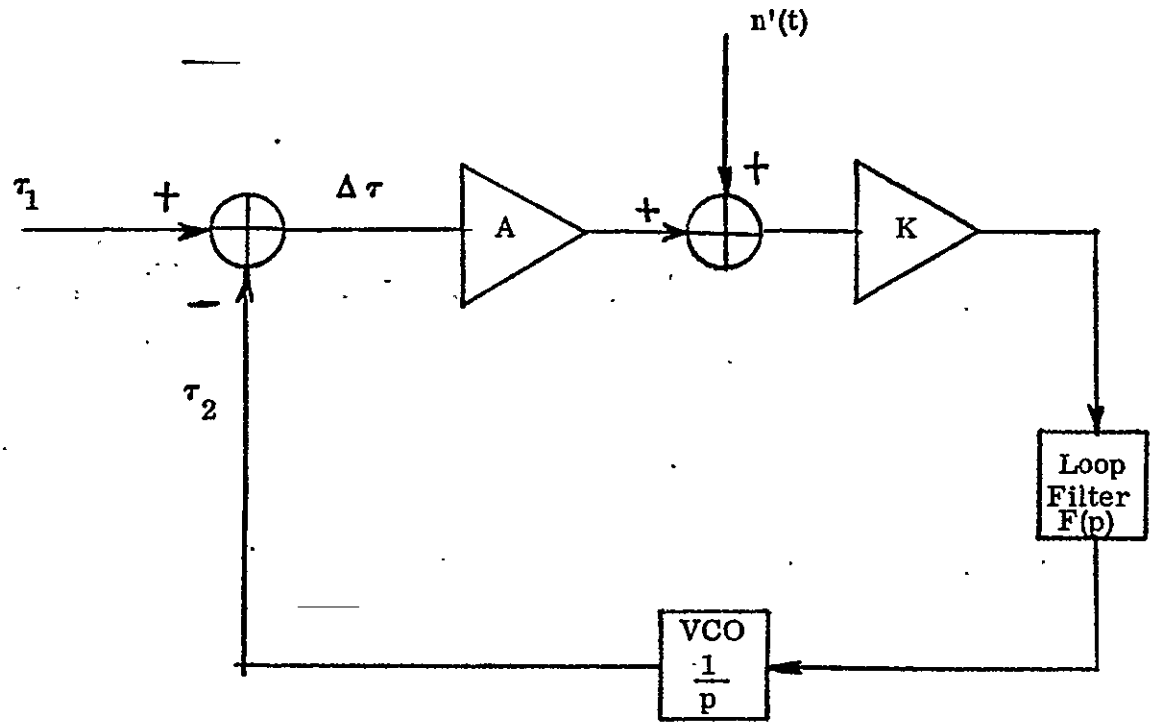

τ_1 = time delay of received PN code

τ_2 = time delay of reference PN code (loop estimate of τ_1).

$\Delta\tau$ = loop tracking error

A = error voltage gain

K = loop gain constant

n'(t) = equalent noise voltage

Figure 2 - Mathematical Model of Delay Lock Tracking Loop

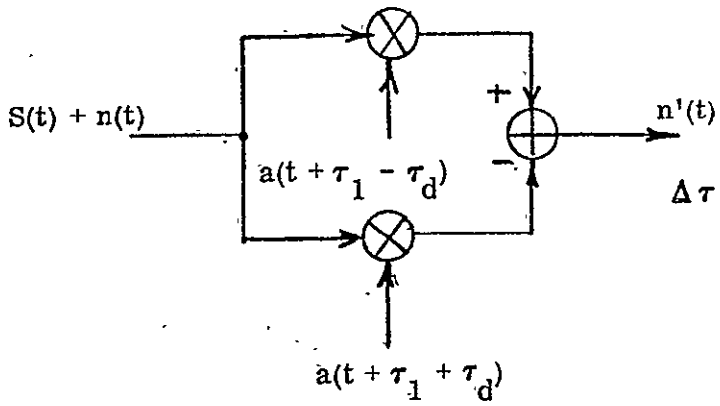

Figure 3 - Delay Lock Loop
Error Discriminator

From examination of Figure 3, it is seen that the equivalent noise, n'(t), for the math model is related to the actual input noise by

$$n'(t) = n(t)\, a\,(t - \tau_d) - n(t)a(t + \tau_d) \tag{14}$$

$$= n(t)\left[a\,(t - \tau_d) - a\,(t + \tau_d)\right]$$

where

n(t) = the actual input noise N(t) filtered by the receiver filter

$a(t - \tau_d)$ = reference PN code advanced by τ_d bits

$a(t + \tau_d)$ = reference PN code delayed by τ_d bits

Since multiplication in the time domain is equivalent to convolution in the frequency domain, the power spectral density of the noise n'(t) is given by

$$S_{n'}(\omega) = S_n(\omega) \otimes A\,(\omega) \tag{15}$$

where

$A\,(\omega)$ = power spectral density of $a(t - \tau_d) - a(t + \tau_d)$

and $\otimes$ indicates convolution.

The power spectrum of $A\,(\omega)$ is given by

$$A\,(\omega) = a\,(\omega)\;\; a\,(\omega)^* \tag{16}$$

where

$a(\omega)$ = voltage spectrum for $a(t - \tau_d) - a(t + \tau_d)$

$$a(\omega) = a_o(\omega) \left[e^{-j\omega\tau_d} - e^{+j\omega\tau_d} \right] \tag{17}$$

so that

$$A(\omega) = -A_o(\omega) \left[e^{-j2\omega\tau_d} + e^{j2\omega\tau_d} - 2 \right] \tag{18}$$

where

$A_o(\omega)$ = power spectrum of reference PN code with zero delay and the exponential terms account for the advance of the reference code by τ_d. The noise spectral density $S_n(\omega)$ will be assumed to be white of value N_o watts/Hz and limited to f_R, the bandwidth of the receiver filter.* Thus, from Equations (18) and (15), the power spectral density of the equivalent noise is given by

$$S_{n'}(\omega) = S_n(\omega) \otimes A(\omega)$$

$$= \frac{N_o}{2\pi} \int_0^{2\pi f_R} A_o(\omega) \left[2 - e^{-j2\omega\tau_d} - e^{j2\omega\tau_d} \right] d\omega$$

$$= \frac{N_o}{2\pi} \left[2\int_0^{2\pi f_R} A_o(\omega)\, d\omega - \int_0^{2\pi f_R} A_o(\omega) e^{-j2\omega\tau_d} d\omega - \int_0^{2\pi f_R} A_o \omega e^{+j2\omega\tau_d} \right]$$

$$= N_o \left[2R(0)_{BL} - R(+2\tau_d)_{BL} - R(-2\tau_d)_{BL} \right] \tag{19}$$

$$= 2N_o \left[R(0)_{BL} - R(2\tau_d)_{BL} \right]$$

*f_R = low pass equivalent bandwidth

where

$R(X)_{BL} \equiv$ the bandlimited autocorrelation function for the PN code evaluated at X

The equivalent noise spectral density given by Equation (19) may now be substituted into Equation (12) to obtain the tracking error power spectral density, $S_{\Delta\tau}(\omega)$. Thus,

$$S_{\Delta\tau}(\omega) = \left| \frac{KF(j\omega)/j\omega}{1 + AKF(j\omega)/j\omega} \right|^2 2N_o \left[R(0)_{BL} - R(2\tau_d)_{BL} \right] \tag{20}$$

Before proceeding further, it will be helpful to consider the term in the absolute value signs in hopes of simplifying Equation (20). First, by examining the math model block diagram, Figure 2, it is seen that the voltage transfer function may be written as

$$\frac{\tau_2}{\tau_1} = \frac{AKF(S)\frac{1}{S}}{1 + AKF(S)\frac{1}{S}} \tag{21}$$

and the power transfer function is given by

$$\left| H(j\omega) \right|^2 = \left| \frac{AKF(j\omega)\frac{1}{j\omega}}{1 + AKF(j\omega)\frac{1}{j\omega}} \right|^2 \tag{22}$$

Since the error signal gain A is independent of ω, Equation (22) may be written as

$$\frac{\left| H(j\omega) \right|^2}{A^2} = \left| \frac{KF(j\omega)\frac{1}{j\omega}}{1 + AKF(j\omega)\frac{1}{j\omega}} \right|^2 \tag{23}$$

The quantity in the absolute value sign on the right side of the equation is recognized as being the same quantity in the absolute value signs in Equation (20). Thus, substituting Equation (23) into Equation (20), we obtain

$$S_{\Delta\tau}(\omega) = \frac{\left| H(j\omega) \right|^2}{A^2} 2N_o \left[R(0)_{BL} - R(2\tau_d)_{BL} \right] \tag{24}$$

Each term in Equation (24) has been well defined with the exception of A. So far, A has been called the error signal gain. Referring again to the math model block diagram, Figure 2, and to the loop "discriminator," Figure 3, it is seen that A:

1. Must convert a time displacement, $\Delta\tau$, between the incoming code and the reference code to an error voltage.

2. Is solely a function of signal and not noise; i.e., is really the loop "discriminator" function for signal.

3. Has an output which is also proportional to the signal level $\sqrt{S}$.

4. Being a discriminator, has a transfer function given by the slope of the discriminator characteristic.

Thus, based on the above considerations,

$$A = \sqrt{S}\,\frac{d}{d\tau}\left\langle a(t+\tau_1)\,a(t-\tau_2-\tau_d) - a(t+\tau_1)\,a(t+\tau_2+\tau_d)\right\rangle_{\Delta\tau=0} \tag{25}$$

where

$\langle X\rangle \equiv$ average value of X

S = signal power

By making a simple change of variables, Equation (25) may be written as

$$A = \sqrt{S}\,\frac{d}{d\tau}\left\langle a(t)\,a(t+\Delta\tau-\tau_d) - a(t)\,a(t+\Delta\tau+\tau_d)\right\rangle_{\Delta\tau=0} \tag{26}$$

$$= \sqrt{S}\,\frac{d}{d\tau}\left[R(\Delta\tau-\tau_d)_{BL} - R(\Delta\tau+\tau_d)_{BL}\right]_{\Delta\tau=0} \tag{27}$$

where the quantity $R(\Delta\tau - \tau_d) - R(\Delta\tau + \tau_d)$ is the discriminator characteristic for the delay lock tracking loop. Thus

$$A = \sqrt{S}\left[R'(\Delta\tau-\tau_d)_{BL} - R'(\Delta\tau+\tau_d)_{BL}\right]_{\Delta\tau=0}$$
$$= \sqrt{S}\;2R'(\tau_d)_{BL} \tag{28}$$

where the bandlimited autocorrelation function is used since the signal is first filtered by the receiver filter. By substituting Equation (28) into (24), we obtain

$$S_{\Delta\tau}(\omega) = \left|H(j\omega)\right|^2 \frac{2N_o\left[R(0)_{BL} - R(2\tau_d)_{BL}\right]}{S\left[2R'(\tau_d)_{BL}\right]^2} \tag{29}$$

From noise theory,

$$\sigma_n^2 = \int_0^\infty S_n(\omega) \frac{d\omega}{2\pi} \tag{30}$$

so that by substituting Equation (29) into (30) we obtain

$$\begin{aligned}\sigma_{\Delta\tau}^2 &= \int_0^\infty \left|H(j\omega)\right|^2 \frac{2N_o\left[R(0)_{BL} - R(2\tau_d)_{BL}\right]}{S\left[2R'(\tau_d)_{BL}\right]^2} \frac{d\omega}{2\pi} \\ &= \frac{2N_o}{S} \frac{R(0)_{BL} - R(2\tau_d)_{BL}}{\left[2R'(\tau_d)_{BL}\right]^2} \int_0^\infty \left|H(j\omega)\right|^2 \frac{d\omega}{2\pi}\end{aligned} \tag{31}$$

A system's noise bandwidth is defined as

$$B_L \equiv \int_0^\infty \left|H(j\omega)\right|^2 \frac{d\omega}{2\pi} \tag{32}$$

so that Equation (31) reduces to

$$\sigma_{\Delta\tau}^2 = \frac{2N_o B_L}{S} \frac{R(0)_{BL} - R(2\tau_d)_{BL}}{\left[2R'(\tau_d)_{BL}\right]^2} \tag{33}$$

Thus, the delay lock loop rms tracking error may be written as

$$\Delta\tau_{rms} = \frac{1}{\sqrt{\frac{S}{2N_o B_L}}} \cdot \frac{\sqrt{R(0)_{BL} - R(2\tau_d)_{BL}}}{2R'(\tau_d)_{BL}} \tag{34}$$

where

B_L = one sided loop noise bandwidth
N_o = one side noise power density
S = average signal power

3.2 DELAY LOCK LOOP TRACKING PERFORMANCE

It is desireable to plot the rms tracking error, $\Delta\tau_{rms}$, as a function of $\frac{S}{N_o B_L}$, the loop signal-to-noise ratio, and several values of bandlimiting and displacement τ_d.

The bandlimited autocorrelation functions used in Equation (34) can be shown to be given by

$$R(X) = \frac{1}{\pi}\left[\frac{2}{B}\cos BX\,(\cos B - 1) - 2X\,\mathrm{si}\,[BX] + (1+X)\,\mathrm{si}\,[B(1+X)] + (1-X)\,\mathrm{si}\,[B(1-X)]\right] \tag{35}$$

where $B = 2\pi f_R T$

f_R = one sided bandwidth of receiver filter

T = PN code bit width

X = time displacement in bits

and

$$\mathrm{si}\,[X] \equiv \int_0^X \frac{\sin y}{y}\,dy \tag{36}$$

The rms tracking error (Equation (34)) is plotted in Figure 4 as a function of $\frac{S}{N_o B_L}$ and several values of B and τ_d. It is obvious that the larger B is, the smaller $\Delta\tau_{rms}$, and the smaller τ_d, the smaller $\Delta\tau_{rms}$. However, because of data transmission requirements and limited available spectrum, B is typically limited to 1.5π in a spread spectrum system. Thus, a plot of $\Delta\tau_{rms}$ vs. τ_d for $B = 1.5\pi$, 3π, and ∞, as shown in Figure 5, shows that for no bandlimiting the tracking error may be made infinitesimally small by making τ_d infinitesimally small. However, for practical values of bandlimiting; i.e., $B = 1.5\pi$, $\Delta\tau_{rms}$ changes very little as a function of τ_d.

3.3 ANALYSIS OF THE τ JITTER LOOP

A block diagram of a τ jitter tracking loop is shown in Figure 6. For analysis purposes, the equivalent math model for the τ jitter tracking loop is the same as that for the delay lock loop, with the exception of the error discriminator. Essentially, the error voltage is generated by correlating the received code with a reference code which is alternately advanced and delayed (jittered) by τ_d bits and phase detecting the resultant signal with the square wave voltage which jittered the reference code. This error discriminator is modeled as shown in Figure 7. By calculating the error signal gain, A, and the output noise power for this discriminator, some of the results of the delay lock loop analysis based on Figure 2 may be used.

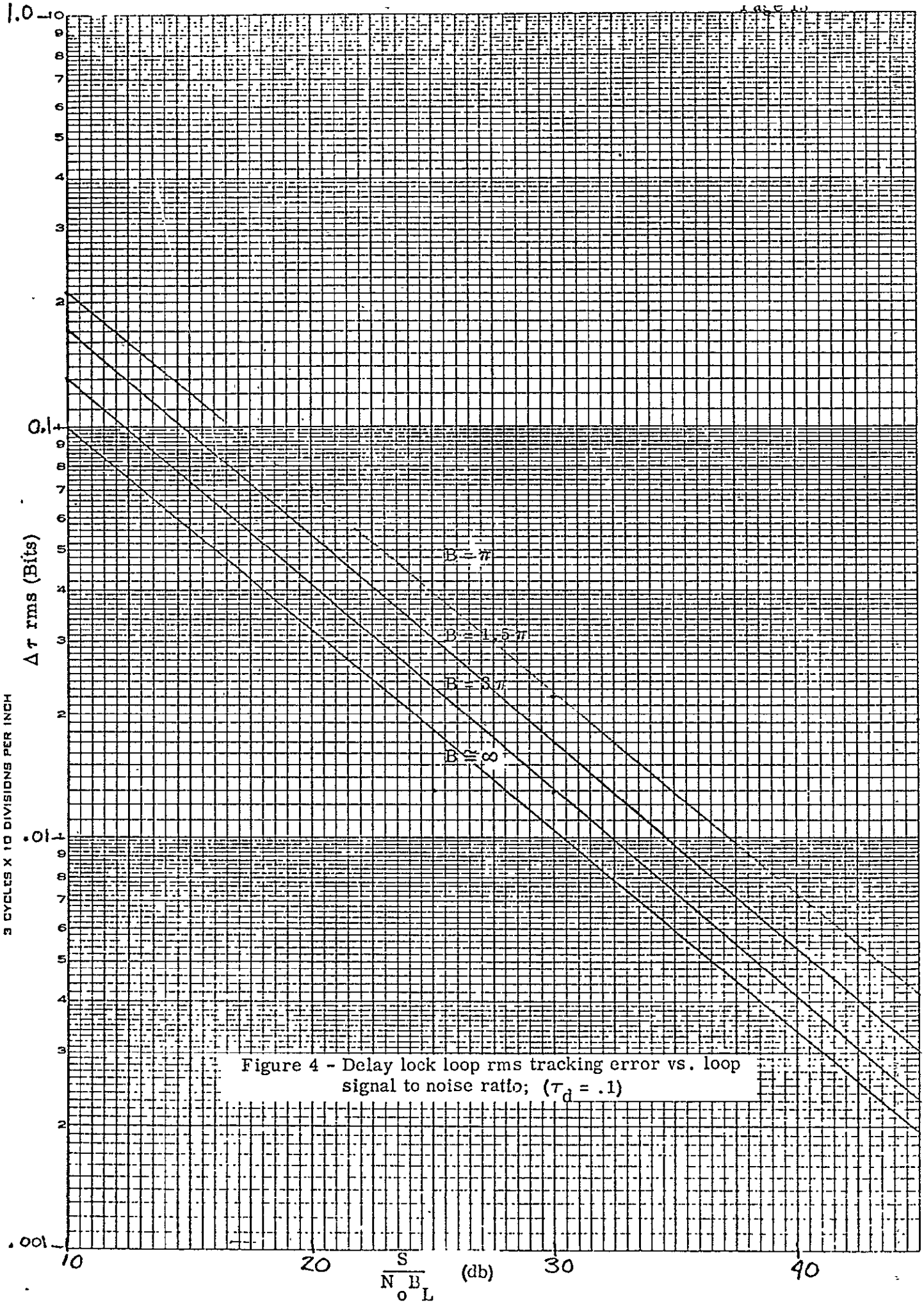

Figure 4 - Delay lock loop rms tracking error vs. loop signal to noise ratio; ($\tau_d = .1$)

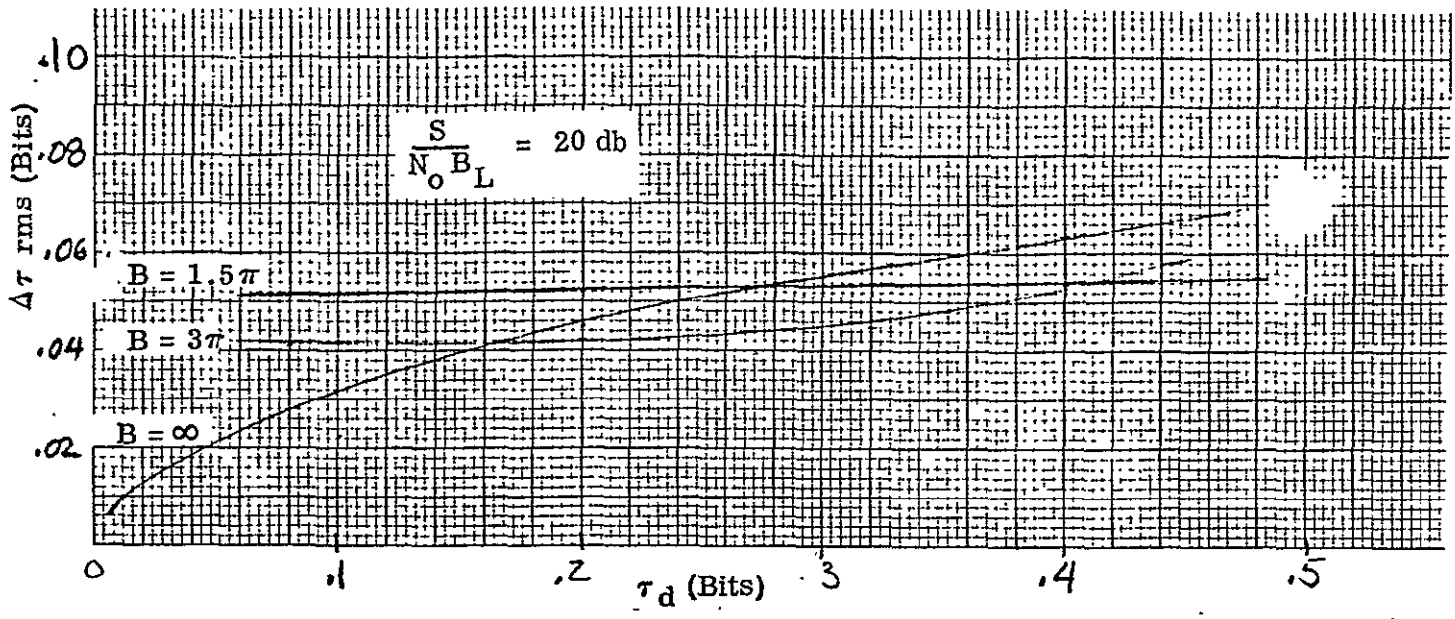

Figure 5 - Delay Lock Loop rms Tracking Error as a Function of Displacement τ_d

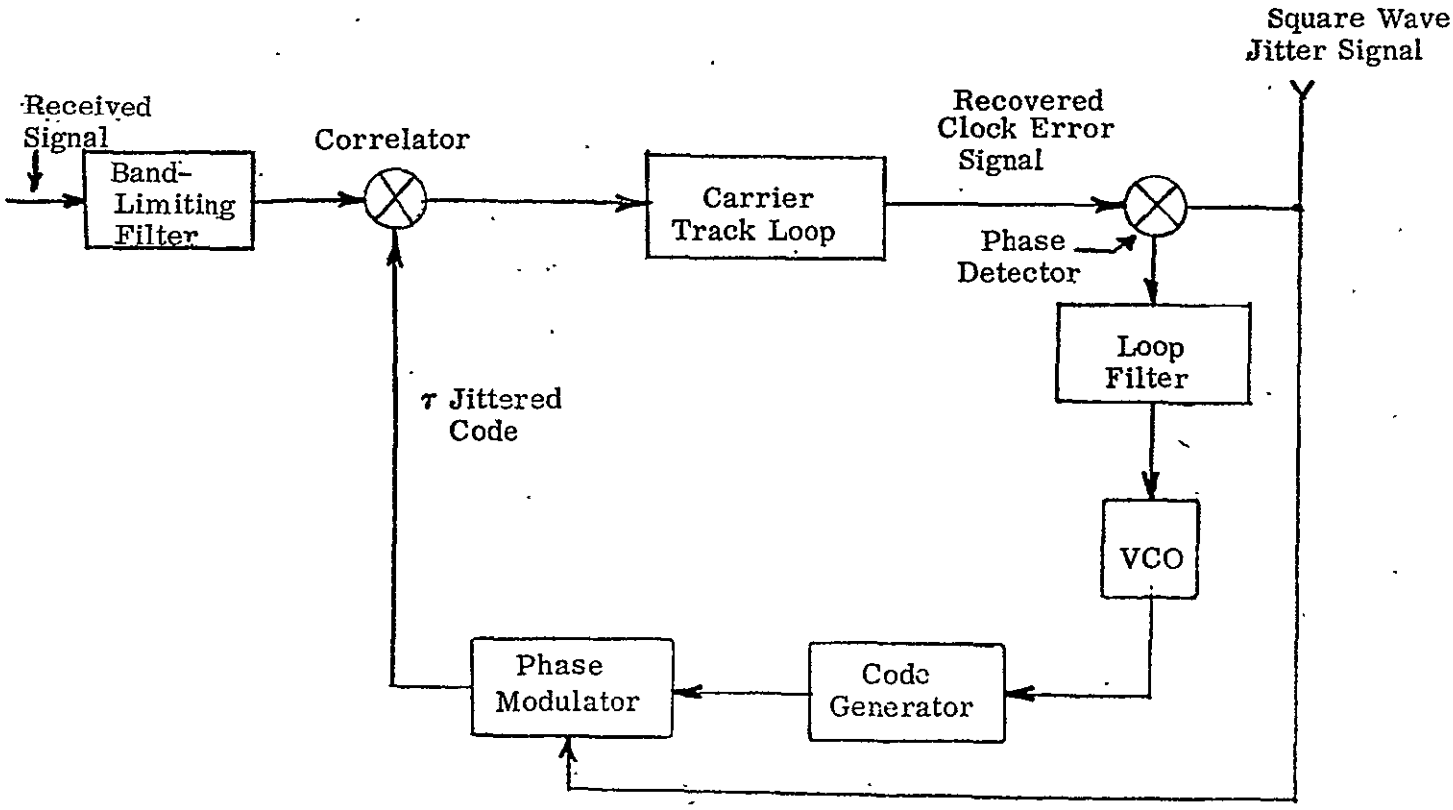

Figure 6 - τ Jitter Tracking Loop

For the purpose of analysis, the jittering of the reference code is accomplished by means of a switching function U(t), which has the following properties:

1. $U(t) \equiv$ 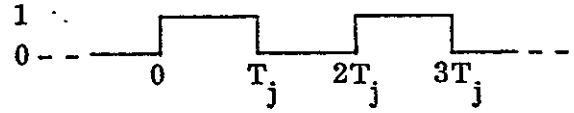

2. $\widehat{U(t)} \equiv 1 - U(t)$

3. $\langle U(t) \rangle = \langle \widehat{U(t)} \rangle = \frac{1}{2}$

4. $U(t)^N = U(t), \ \widehat{U(t)}^N = \widehat{U(t)}, \ N = 0, 1, 2, \ldots$

5. $U(t)\,\widehat{U(t)} = 0$

The jittered reference PN code is denoted by

$$V_0(t) = a(t + \tau_2 - \tau_d)\, U(t) - a(t + \tau_2 + \tau_d)\, \widehat{U(t)} \tag{37}$$

so that the correlator output is given by

$$V_1(t) = \left[\sqrt{S}\, a(t + \tau_1) + n(t)\right] \left[a(t + \tau_2 - \tau_d)\, U(t) - a(t + \tau_2 + \tau_d)\, \widehat{U(t)}\right] \tag{38}$$

The reference for the phase detector is the jittering signal and is denoted by

$$V_2(t) = U(t) - \widehat{U(t)} \tag{39}$$

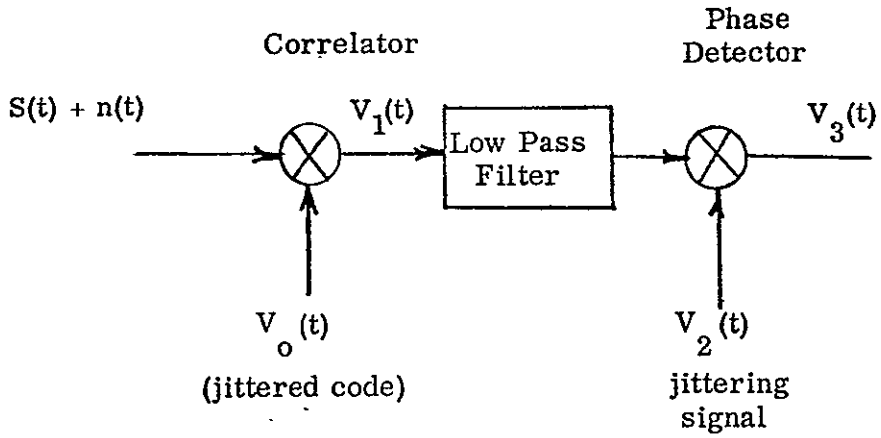

Figure 7 - τ Jitter Error Discriminator Model

The output of the phase detector is given by

$$V_3(t) = V_1(t)\, V_2(t)$$

$$= \left[\sqrt{S}\, a(t+\tau_1) + n(t)\right] \left[a(t+\tau_2-\tau_d)\, U(t) - a(t+\tau_2+\tau_d)\, \widehat{U(t)}\right] \cdot$$

$$\left[U(t) - \widehat{U(t)}\right]$$

$$= \sqrt{S}\, a(t+\tau_1)\left[a(t+\tau_2-\tau_d)\, U(t)^2 - a(t+\tau_2+\tau_d)\, \widehat{U(t)}^2\right]$$

$$+ n(t)\left[a(t+\tau_2-\tau_d)\, U(t)^2 - a(t+\tau_2+\tau_d)\, \widehat{U(t)}^2\right] \qquad (40)$$

The average value of the phase detector output, $V_3(t)$, is the discrimator error voltage,

$$V_3(t) = \left\langle \sqrt{S}\, a(t+\tau_1)\left[a(t+\tau_2-\tau_d)\, U(t)^2 - a(t+\tau_2+\tau_d)\, \widehat{U(t)}^2\right] \right\rangle$$

$$= \frac{\sqrt{S}}{2}\left[R(\Delta\tau-\tau_d)_{BL} - R(\Delta\tau+\tau_d)_{BL}\right] \qquad (41)$$

The quantity inside the square brackets is recognized as being the same discriminator characteristic as the delay lock loop. Thus, as before, the error signal gain, A, for the math equivalent model is given by

$$\overline{A} = \frac{d}{d\tau}\ \frac{\sqrt{S}}{2}\ \left[R(\Delta\tau-\tau_d)_{B_L} - R(\Delta\tau+\tau_d)_{BL}\right]_{\Delta\tau\,=\,0}$$

$$= \sqrt{S}\, R'(\tau_d)_{BL} \qquad (42)$$

Since the discriminator shown in Figure 7 is a linear system, it is possible to find the relationship between the noise density at its input and at its output by finding the relationship between the input and output noise power. The noise power in the output is found by squaring $V_3(t)$ and averaging. Thus,

$$P_{N_{out}} = \left\langle V_3(t)_n^2 \right\rangle \qquad \text{(subscript n indicates noise component of } V_3(t)\text{)}$$

$$= \Big\langle n(t)^2 \Big[a(t+\tau_2-\tau_d)^2\, U(t)^2 + a(t+\tau_2+\tau_d)^2\, \widehat{U(t)}^2$$

$$+ 2\, a(t+\tau_2-\tau_d)\, a(t+\tau_2+\tau_d)\, U(t)\, U(t) \Big] \Big\rangle$$

$$= \Big\langle n(t)^2 \Big[a(t+\tau_2-\tau_d)^2\, U(t) + a(t+\tau_2+\tau_d)^2\, \widehat{U(t)}^2 \Big] \Big\rangle$$

$$= \left\langle n(t)^2 \right\rangle \Big[\left\langle a(t+\tau_2-\tau_d)^2 \right\rangle \left\langle U(t) \right\rangle + \left\langle a(t+\tau_2+\tau_d)^2 \right\rangle \left\langle U(t) \right\rangle \Big] \qquad (43)$$

Since the noise is bandlimited by the receiver filter;

$$\left\langle a(t+\tau_2-\tau_d)^2 \right\rangle = \left\langle a(t+\tau_2+\tau_d)^2 \right\rangle = R(0)_{BL}$$

and Equation (43) reduces to

$$P_{N_{out}} = \left\langle n(t)^2 \right\rangle R(0)_{BL} \qquad (44)$$

Since,

$$P_{N_{in}} = \left\langle n(t)^2 \right\rangle$$

We find that the noise power out of the τ jitter discriminator is related to the noise power in by

$$P_{N_{out}} = P_{N_{in}} R(0)_{BL}$$

so that by considering the noise in the same bandwidth

$$S_{n'}(\omega) = N_o R(0)_{BL} \tag{45}$$

where N_o is the input noise power spectral density. Thus, from Equation (13),

$$S_{\Delta\tau}(\omega) = \left| \frac{KF(j\omega)/j\omega}{1 + AKF(j\omega)/j\omega} \right|^2 S_{n'}(\omega), \tag{46}$$

the spectral density for the tracking error for the τ jitter tracking loop is given by

$$S_{\Delta\tau}(\omega) = \left| \frac{KF(j\omega)/j\omega}{1 + AKF(j\omega)/j\omega} \right|^2 N_o R(0)_{BL} \tag{47}$$

Upon substituting Equation (23) into Equation (47), the tracking error spectral density is found to be

$$S_{\Delta\tau}(\omega) = \frac{\left|H(j\omega)\right|^2}{A^2} N_o R(0)_{BL} \tag{48}$$

and since A for the τ jitter loop is given by Equation (42), Equation (48) reduces to

$$S_{\Delta\tau}(\omega) = \frac{N_o R(0)_{BL}}{SR'(\tau_d)_{BL}} \left| H(j\omega) \right|^2 \tag{49}$$

Thus, the variance of the tracking error is found to be

$$\begin{aligned} &= \int_0^\infty S_{\Delta\tau}(\omega) \frac{d\omega}{2\pi} \\ &= \frac{N_o}{SR'(\tau_d)_{BL}} \int_0^\infty \left| H(j\omega) \right|^2 \frac{d\omega}{2\pi} \\ &= \frac{N_o B_L R(0)_{BL}}{SR'(\tau_d)_{BL}} \end{aligned} \tag{50}$$

so that the rms tracking error for the τ jitter loop is given by

$$\Delta\tau_{rms} = \frac{1}{\sqrt{\frac{S}{N_o B_L}}} \frac{\sqrt{R(0)_{BL}}}{R'(\tau_d)_{BL}} \tag{51}$$

3.4 τ JITTER TRACKING LOOP PERFORMANCE AND COMPARISON WITH DELAY LOCK LOOP PERFORMANCE

The rms tracking error for the τ jitter tracking loop, Equation (51), is shown plotted in Figure 8. A bandlimiting factor of $B = 1.5\pi$ was used since that value is typically used in our PN systems. As can be seen, the error increases as τ_d, the jitter displacement, decreases. The dependence of $\Delta\tau_{rms}$ on τ_d is better illustrated by the plot of $\Delta\tau_{rms}$ vs. τ_d shown in Figure 9. This inverse relationship between τ_d and $\Delta\tau_{rms}$ is opposite of the relationship for the delay lock loop, where $\Delta\tau_{rms}$ decreases for decreasing τ_d. This performance difference is obvious from comparing Equations (34) and (51). However, a better understanding of the performance difference between the two loops is obtained from comparing what happens to the input noise in each of the "discriminators". In the delay lock loop, as τ_d becomes smaller, the noise at the output of each correlator becomes more correlated with the other channel's noise. Thus, as $\tau_d \rightarrow 0$ the noise in each channel becomes the same so that the subtractor is subtracting the noise from itself and the noise output becomes zero. If the noise approaches zero, it is obvious that the tracking error also approaches zero. However, due to bandlimiting and practical considerations, this does not actually happen in hardware loops. The τ jitter loop, on the other hand, does not subtract noise from itself since it time shares (time multiplexes) a common channel between the advanced and delayed signals. Furthermore, as τ_d becomes smaller, the slope of the bandlimited autocorrelation curve decreases and since the error signal gain is given by this slope, the performance of the loop decreases. The error signal gain for the delay lock loop also decreases as τ_d gets smaller, however, this is offset by the decrease in effective loop noise.

The degradation of tracking performance for a τ jitter loop relative to a delay lock loop and a conventional phase locked loop is shown plotted in Figure 10. The plot is a function of τ_d, with $B = 1.5\,\pi$. Since it is common to make τ_d small (around .1 bit) so that the correlator output may be used for data demodulation, it is obvious that better tracking performance may be obtained from the delay lock loop. This is especially important for navigation and position location systems where range measurement from PN code delay determination is the primary concern.

3.5 EFFECTS OF CHANNEL UNBALANCES ON DELAY LOCK LOOP PERFORMANCE

In view of the superior tracking performance of the delay lock loop, it is worthwhile considering the effects of channel gain and time delay differentials on tracking error.

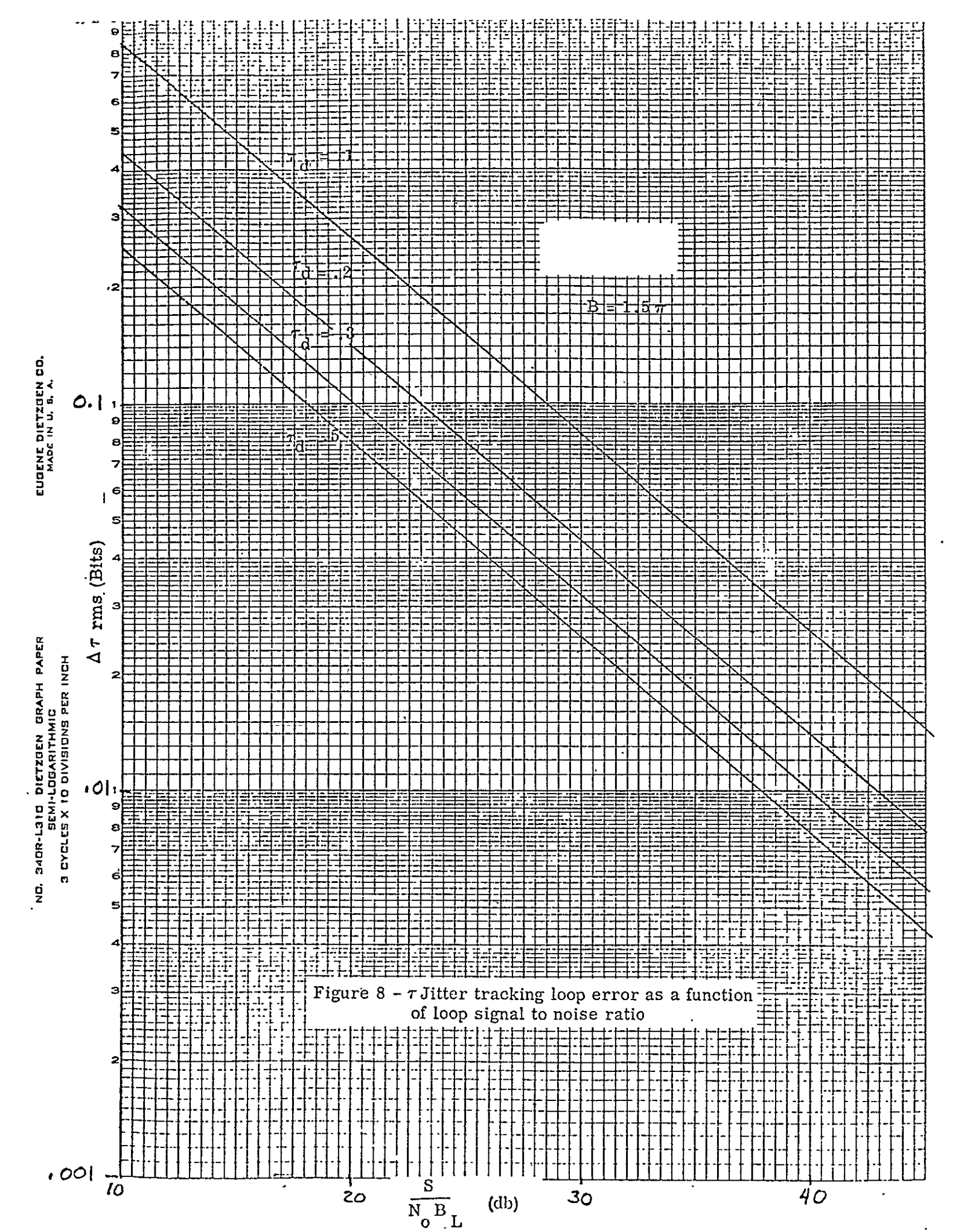

Figure 8 – τ Jitter tracking loop error as a function of loop signal to noise ratio

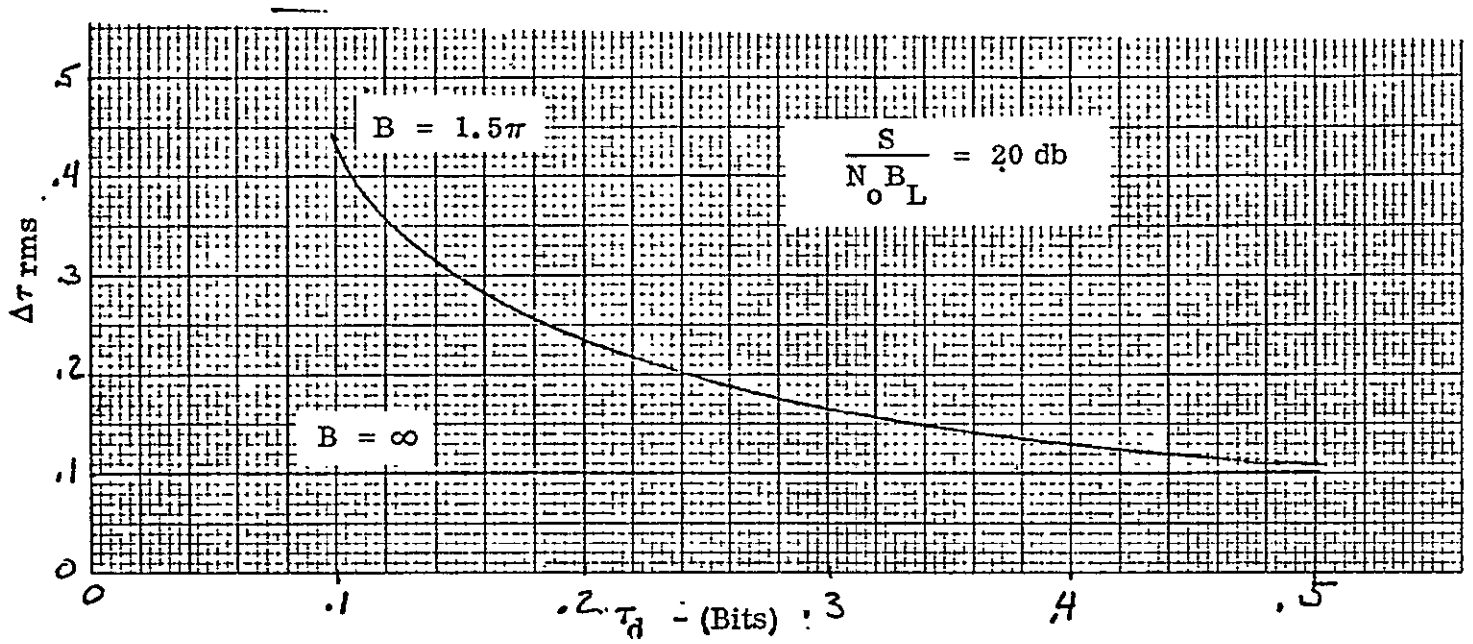

Figure 9 - τ jitter tracking loop error as a function of jitter displacement τ_d

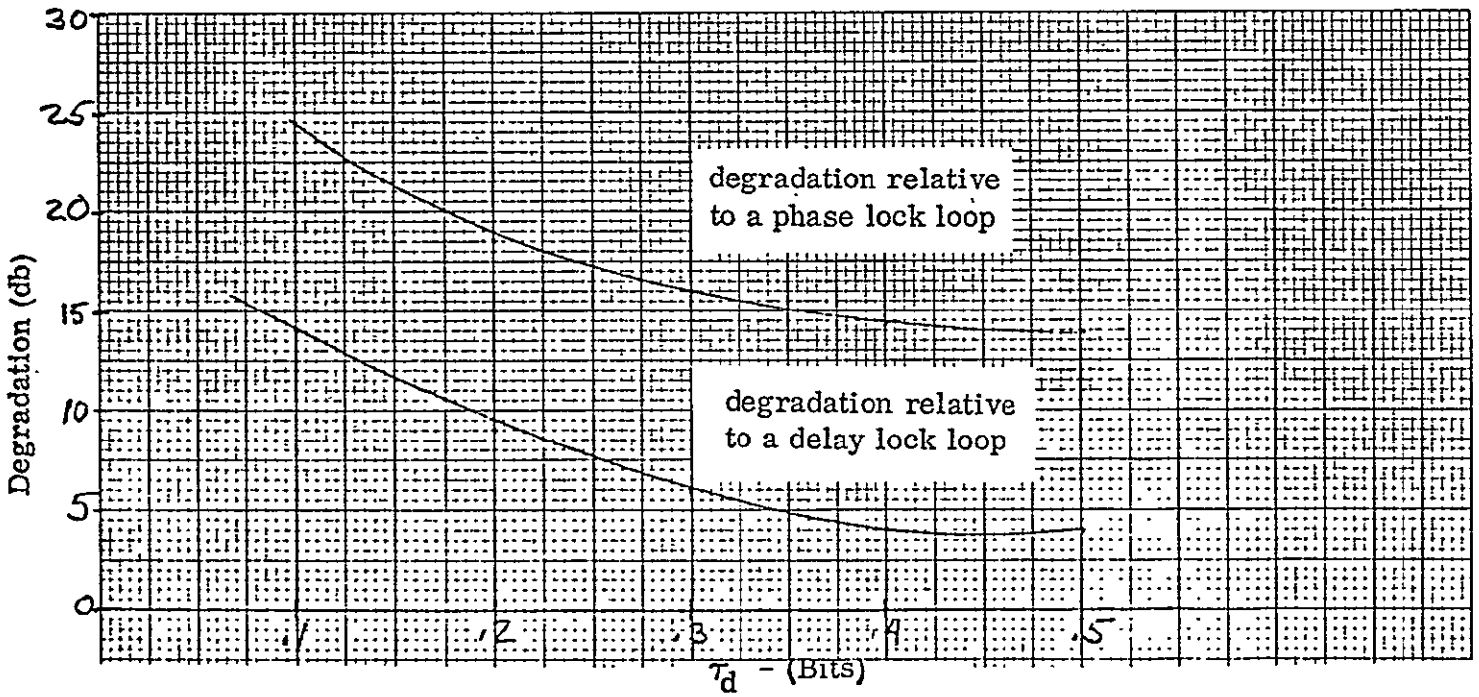

Figure 10 - τ jitter tracking degradation as a function of τ_d

Figure 11 shows a delay lock discriminator model having a differential time delay of Δ in one channel and a differential amplitude gain of K in the other channel.

This is merely the general case of the delay lock loop analysis given in Section 2.0, where $\Delta = 0$ and $K = 1$. Thus, it is easy to show that the rms tracking error for the loop having the discriminator shown in Figure 11 is given by

$$\Delta\tau_{rms} = \frac{1}{\sqrt{\frac{S}{N_o B_L}}} \cdot \frac{\sqrt{(1+k^2)R(0)_{BL} - 2kR(2\tau+\Delta)_{BL}}}{kR'(\tau)_{BL} - R(-\tau+\Delta)_{BL}} \qquad (52)$$

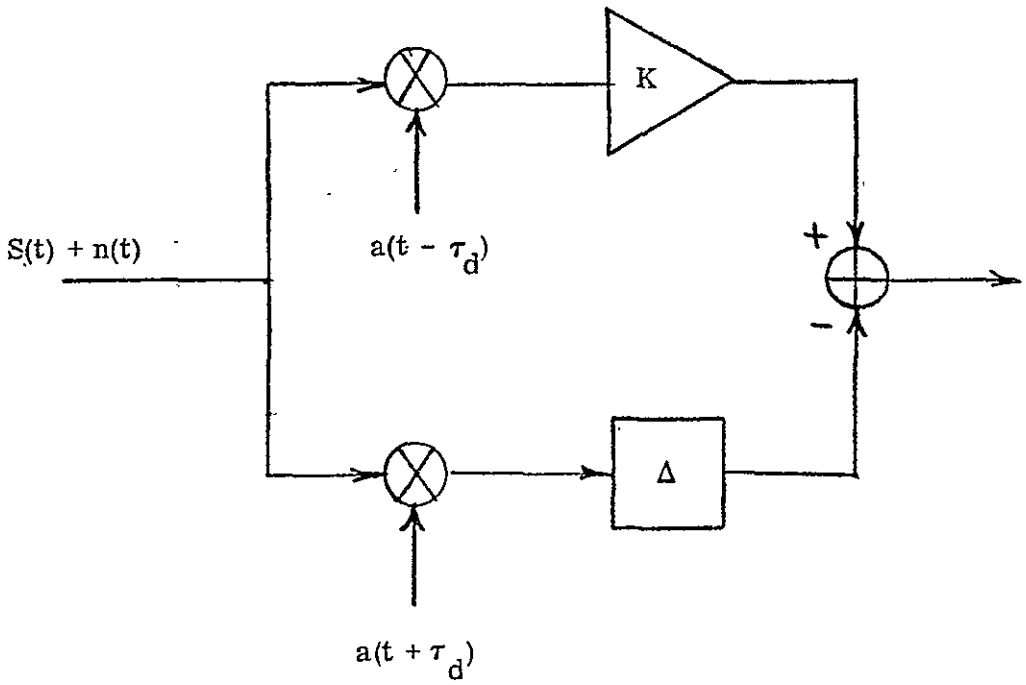

Figure 11 - Delay Lock Loop Discriminator With Gain and Time Delay Unbalances

By comparing the performance specified by Equation (51) with that specified by Equation (52), the effects of Δ and k may be evaluated. These effects are shown tabulated in Table I. It seems reasonable that through good engineering design the gain differential should be no greater than 1 db and the time delay differential should be no greater than 10% of the time displacement of the reference code, τ_d. From Table I it can be seen that this results in a 15% increase in the rms tracking error or approximately 1 db performance degradation.

Table I - Effect of Gain and Delay Differentials on Delay Lock Loop Tracking Error

K(db)	Δ(bits)	Δ/τ_d(%)	% Change of $\Delta\tau_{rms}$
.1	.01	10	12
.1	.05	50	65
1.0	.01	10	15
1.0	.05	50	71

3.6 EARLY LATE GATE TRACKER IMPLEMENTATION

A slight variation of the delay lock tracking scheme results in the so-called early late gate tracker. If the advanced and retarded reference codes are first subtracted and then the resulting difference multiplied times the received code, the early late gate tracker is obtained. It is easily seen that the same mathematical error discriminator model is obtained as for the delay lock tracker and, therefore, the tracking performance will be the same. Consideration of the subtraction process as $\Delta\tau \longrightarrow 0$ reveals that the difference really approaches the derivative of the reference code; i.e.,

$$\frac{da(t)}{dt} = \lim_{\tau \longrightarrow 0} \frac{a(t-\tau) - a(t+\tau)}{\tau} \tag{53}$$

where the $\frac{1}{\tau}$ factor may be interpreted as merely a gain factor. Furthermore, the early late gate process may be more accurately implemented digitally, as opposed to the analog subtraction delay lock process implementation. The early late gate implementation is shown in Figure 12.

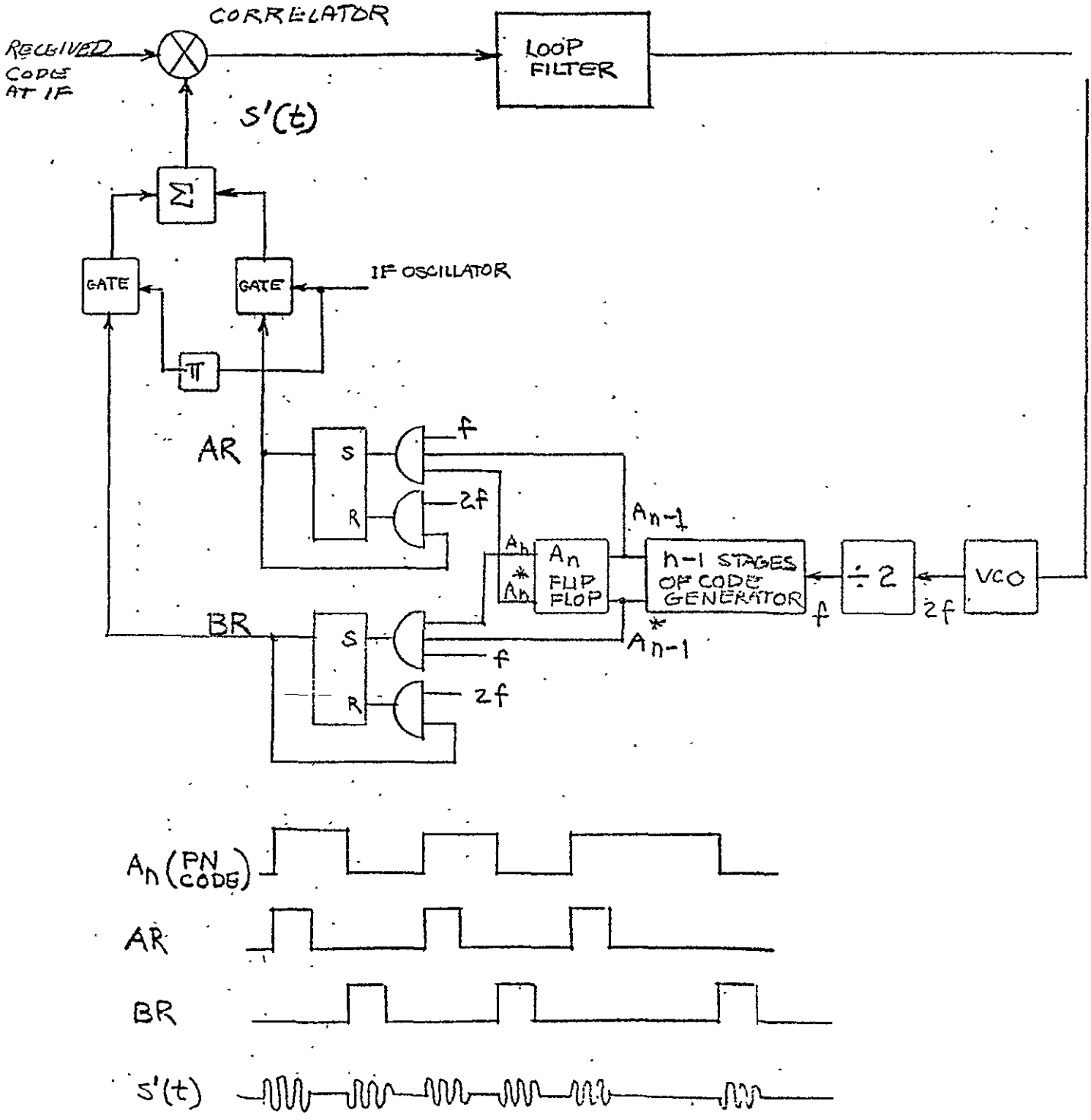

Figure 12 - Digital Early Late Gate Tracker

APPENDIX III

USING THE NAVY NAVIGATION SATELLITE SYSTEM

By

Thomas A. Stansell, Jr.
Magnavox Research Laboratories
Torrance, California

Presented at

The Institute of Navigation
National Marine Navigation Meeting
Second Symposium
On
Manned Deep Submergence Vehicles

4 November 1969

USING THE NAVY NAVIGATION SATELLITE SYSTEM

by

Thomas A. Stansell, Jr.
Magnavox Research Laboratories
Torrance, California

ABSTRACT

Installation and operation of satellite navigation equipment is described, including what the user should expect during a satellite pass. Characteristics of the new short Doppler computer program which promote better and more consistent accuracy are given, including documentation of 150 ft. RMS fix results. Approaches to an integrated navigation system are reviewed.

INTRODUCTION

Application of the Navy Navigation Satellite System has not been limited to the Navy, nor even to shipboard navigation. The number of commercial and non-military Government applications has been growing rapidly, as indicated by Reference 1. For example, the Magnavox 702 satellite navigation equipment has been used to support oceanographic research, a land survey mission to the north pole, commercial offshore oil exploration, transatlantic telephone cable laying, and submarine activities. Specific examples of support for submarines and submersibles are: its use on the White Sands in support of the Trieste II, use on the undersea oceanographic submarine Baya, and the installation aboard the Mizar.

For the potential user interested in learning more about the system, the literature abounds in descriptive material. This writer has seen one fairly good description translated from a Russian book on navigation. The system configuration, its theory of operation, various error sensitivities, etc., have all been well covered.

In an attempt to complement rather than to paraphrase the existing literature, this paper describes the installation and operation of satellite navigation equipment, including use of the new short Doppler navigation program. Improvement in accuracy to 150 ft. RMS through use of the short Doppler program is detailed, and a review of approaches to an integrated navigation system is given.

EQUIPMENT INSTALLATION

A complete satellite navigation system, the Magnavox MX/702/hp, is pictured in Figure 1. The equipment consists of a 43 pound antenna-preamplifier assembly, 200 ft. of armored coaxial cable, the Magnavox satellite navigation receiver, a Hewlett-Packard 2114 computer with 8,192 words of memory, and an ASR-33 Teleprinter for input/output. All but the antenna and cable are mounted in a welded rack with forced ventilation. The high speed photoelectric tape reader is often provided as an option.

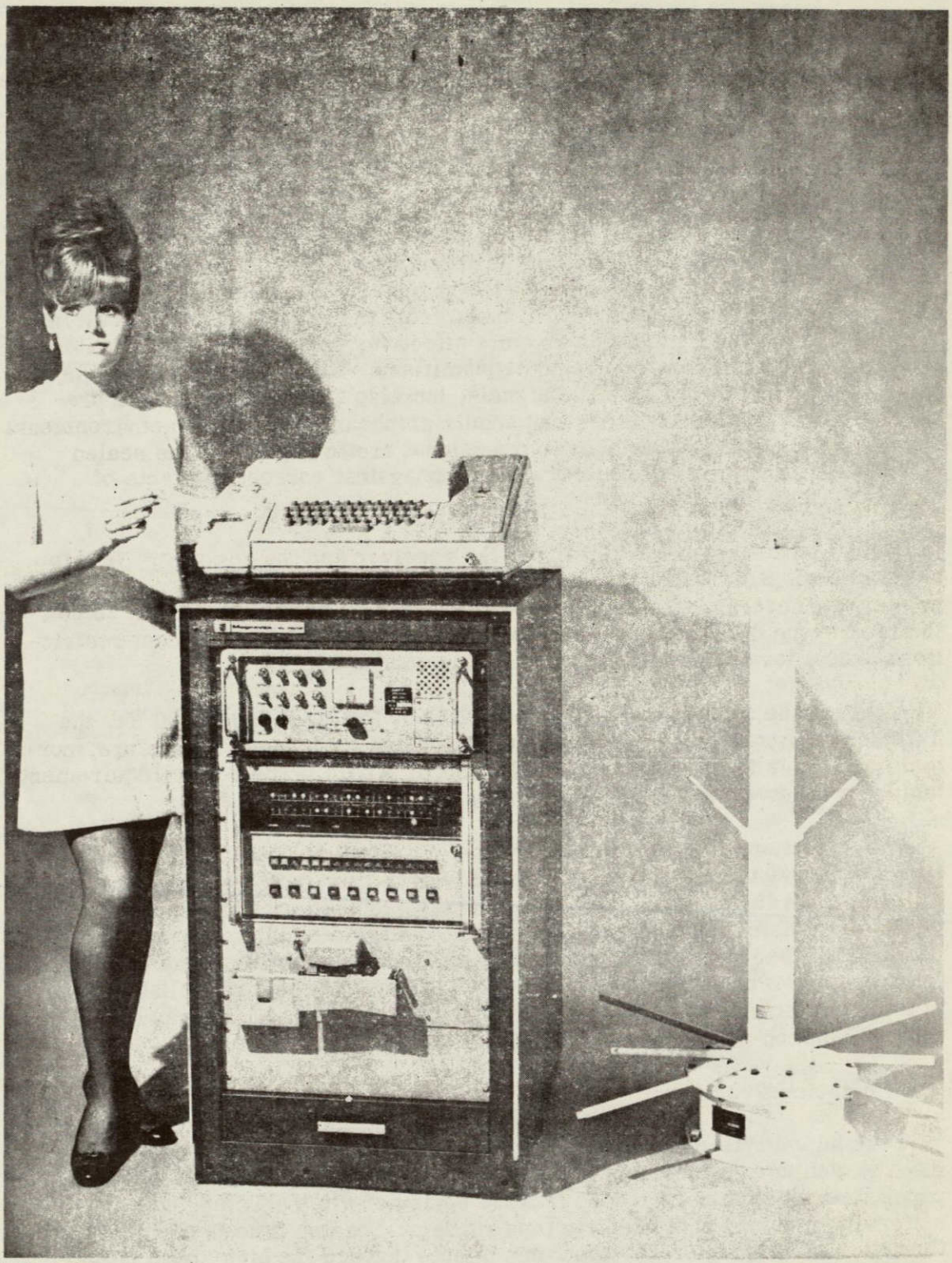

1069-2701
UNCLASSIFIED

Figure 1. The Magnavox MX/702/hp Satellite Navigation System with Optional Photoelectric Tape Reader. Rack Dimensions Are 41.3" High, 23" Wide, and 35.5" Deep. Girl's Dimensions Remain Classified.

Figure 2 shows a typical installation of the antenna-preamplifier unit. The antenna should be placed so as to minimize obstruction of its field of view. The equipment is fairly tolerant of antenna installation compromises, but considering that the satellites transmit only about one watt of RF power over distances up to 2000 miles, it is clear that a good antenna location is quite desirable.

The single antenna receives both the 150 MHz and the 400 MHz satellite signals. In the preamplifier enclosure, these signals are separated, passed through preselect filters, amplified, filtered again, re-combined, and sent via the single RG-116/U coaxial cable to the receiver. The filters are designed to eliminate interfering signals, e.g., those from the radar antennas shown in Figure 2. They have proved to be quite effective, permitting operation even on Navy ships with million-watt radar transmitters. The single coaxial cable carries not only the two satellite signals, but also the DC power to the preamplifiers. The electrical design permits shipboard operation in environments ranging from the hottest tropics to the coldest arctic regions. The sealed antenna and preamplifier enclosures protect against corrosive effects of moisture, salt, and stack gas.

Figure 3 illustrates installation of the receiver and the computer, in this case on the U.S.S. New Jersey. Because the receiver, computer, and Teleprinter are securely fastened in the welded rack, it is necessary only to bolt the rack to the deck at the desired location. There are no placement restrictions except for normal operation and maintenance access.

Although the receiver will operate on 115 or 230 VAC, 50 to 400 Hz, the Teleprinter motor requires a fairly constant line frequency. Therefore, normal practice is to use 115 VAC ±10% at 60 Hz ±1 Hz. The power requirement, including receiver, computer, and blowers, is about 1100 watts.

The equipment is shipped with the internal reference oscillator and the standby battery turned off. After power is connected (and the rear panel battery switch is turned on), about 24 hours are required for the oscillator to reach acceptable stability. As the oscillator warms up, fix accuracy will change from bad to poor to good. The standby battery protects the oscillator from prime power interruptions of up to 8 hours. Whenever oscillator power is totally removed for more than a few minutes, several hours may be required before acceptable stability is reached again.

The Computer Program.

The equipment is normally shipped with the navigation program already loaded into the computer's memory. The program is also supplied on a roll of punched paper tape which may be loaded into the computer via the Teleprinter or via the optional high speed photoelectric tape reader. Loading time is about 30 minutes through the Teleprinter and about one minute through the high speed reader. Current programs have instructions which provide protection when power is turned on or off, so it is seldom necessary to reload the program.

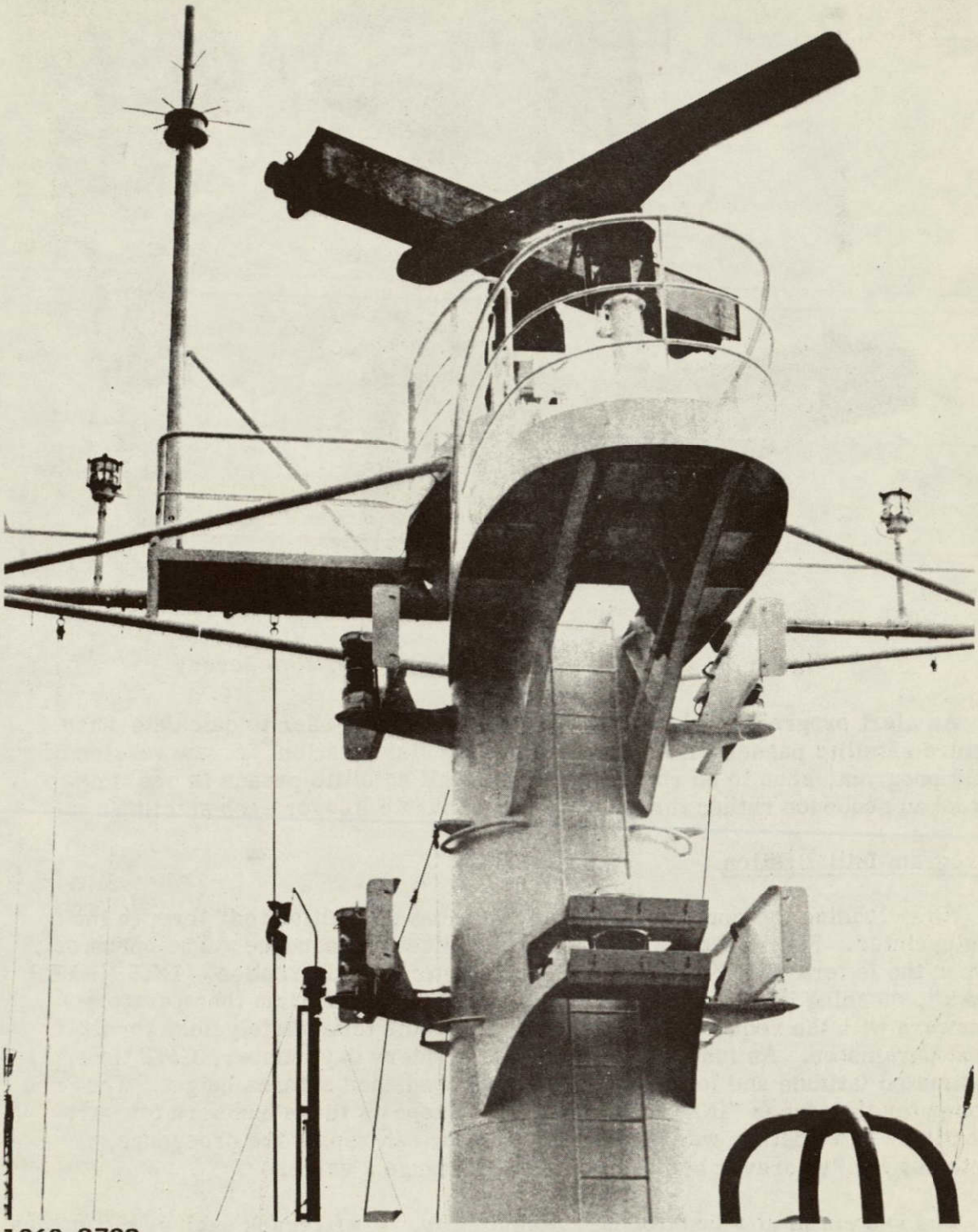

1069-2702
UNCLASSIFIED

Figure 2. Typical Antenna-Preamplifier Installation

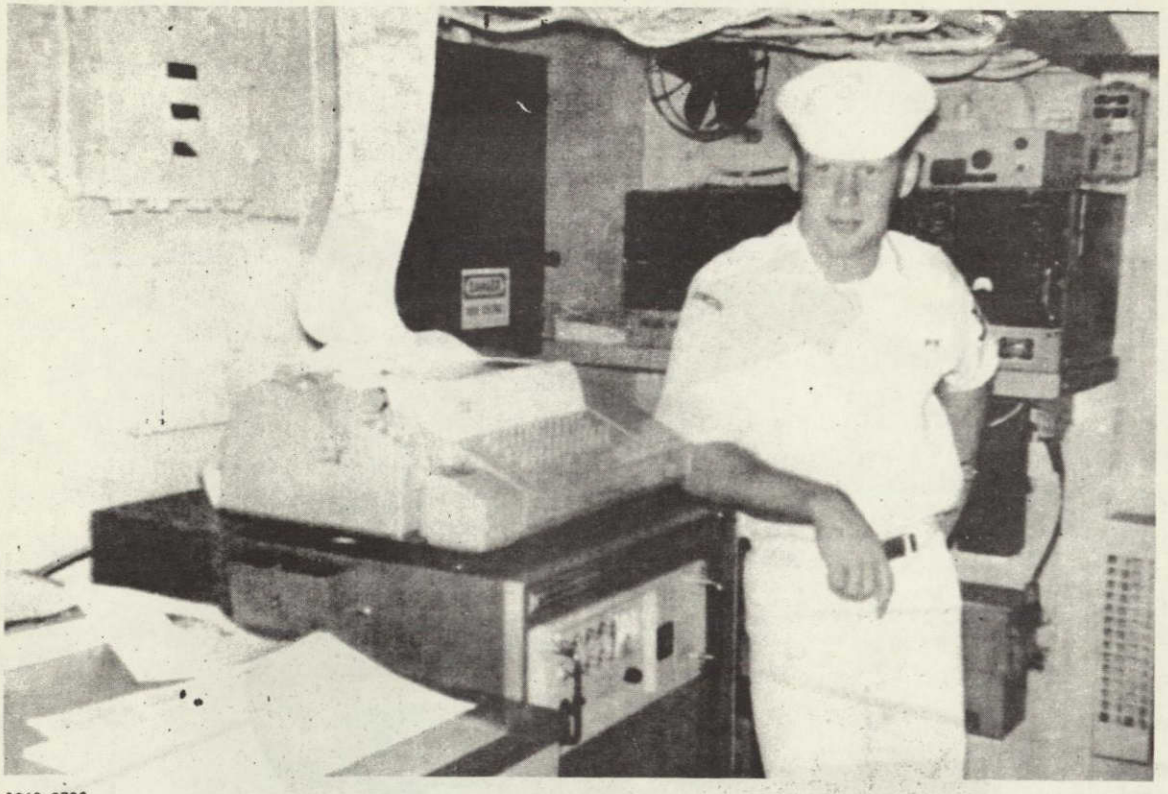

1069-2703
UNCLASSIFIED

Figure 3. Installation Aboard the U.S.S. New Jersey

An alert program is also available, permitting the user to calculate when future satellite passes will occur at his particular location. A new version of this program, soon to be released, will list all satellite passes in one time-ordered sequence rather than providing a separate list for each satellite.

Program Initialization

After loading the computer program, it must be "initialized" through the Teleprinter. Figure 4 shows a typical initialization sequence. The operator types the letters "NNSS", to which the computer quickly replies, "INIT ENTER DAY", meaning initialization, enter day number. Each time the operator answers with the requested number, the computer immediately asks for the next parameter. As indicated, the operator enters day number, GMT time, estimated latitude and longitude, heading, speed, and antenna height. The computer then types *INITIALIZATION* and repeats these numbers for verification. If a mistake was made, the operator can repeat the procedure, entering "no"wherever he does not wish to change a value.

The system is now functioning automatically. It will track each satellite pass and produce a position fix without further operator intervention, if desired. This automatic capability depends on having a clock programmed into the computer. The clock is started at the time of initialization, and it runs by counting transfers from the satellite receiver. Thus, the computer can process each

```
NNSS
INIT
ENTR
DAY
290
TIME
0710
LAT
033 50.000 N
LONG
118 20.000 W
HDG
000.00
SPD
000.00
ANTH
+0013.
*INITIALIZATION*

DAY   TIME  LATITUDE       LONGITUDE
290   0710  033 50.000 N   118 20.000 W

HDG    SPD     ANT
000.0  000.0   +0013.
```

1069-2704

Figure 4. Program Initialization Format. The Operator Types Only the Lines Indicated.

satellite pass automatically without requiring manual entry of time. The fix computation will correct for clock errors up to ±15 minutes, so the time initialization does not have to be extremely accurate.

Antenna Height

Antenna height means height above a reference ellipsoid, which is the consistent, world-wide datum used by the satellite navigation system. Its shape is defined by a semi-major axis of 6378.144 Km and a flattening coefficient of 1/298.23.

To obtain antenna height, one must know height of the antenna above mean sea level plus the deviation of mean sea level from the reference ellipsoid at that location. The term "geoid" means a world-wide model of mean sea level, so the term geoidal height means the deviation of mean sea level from the reference ellipsoid. Maps showing contours of geoidal height are provided with each satellite navigation system. Therefore, the antenna height entered during initialization is obtained by adding height above sea level to the local geoidal height read from the contour map. All dimensions are in meters. Figure 6 of Reference 2 is a geoidal height map.

DURING A SATELLITE PASS

Signal Acquisition

Figure 5 illustrates the receiver's front panel frequency meter in two different situations. On the left, the shaded region shows the frequency range over which the receiver automatically searches for a satellite signal. This is where the signal will be during the first few minutes after the satellite appears above the horizon. The narrow search region promotes fast signal acquisition by searching only the area where the signal must first appear.

When the receiver tunes across a satellite signal, it automatically acquires lock, as indicated by two front panel lights, one for each satellite channel. The frequency meter also stops the search pattern and begins to track the slowly changing satellite frequency.

Navigation satellites transmit two very stable frequencies, one at 150 MHz and the other at 400 MHz. The received frequency changes slowly throughout a satellite pass; this Doppler frequency shift is caused by motion of the satellite relative to the receiver, and vice versa. The receiver displays an inverted Doppler frequency, i.e., the frequency meter moves from low values on the left to higher values on the right during a pass. The center is marked 32 kHz, which is known as the satellite's offset frequency.

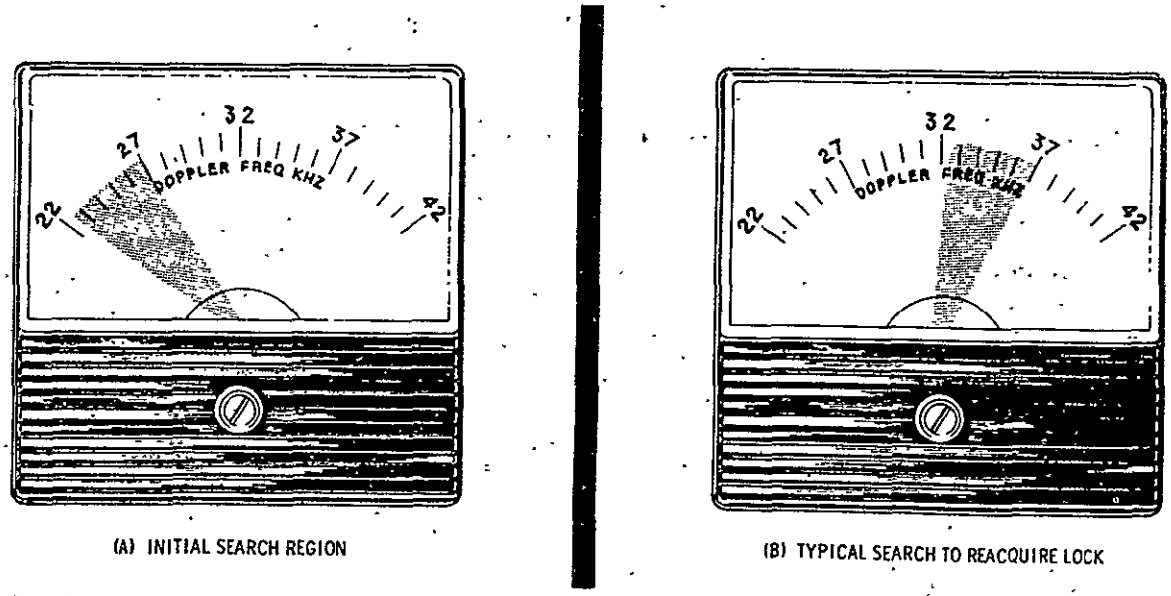

Figure 5. Receiver Frequency Meter
(a) Initial Search Region
(b) Typical Search to Reacquire Lock

Before the computer begins to process satellite data, two steps of synchronization must occur. Each step is denoted by a light on the receiver front panel. The first, called bit synchronization, occurs within a few seconds after signal acquisition. The second is message synchronization, which occurs at the next satellite time mark. These are transmitted every two minutes on the even minute.

Short Doppler Counts

When message synchronization occurs, the computer begins to receive information from the receiver. This consists of the demodulated satellite's navigation message plus Doppler counts, which are measurements made by the receiver of the changing Doppler frequency. (See Reference 2 for a detailed description.) If the operator wishes, he can set a computer switch which causes this data to be listed on the Teleprinter, as shown in Figure 6.

All data above the word "PAUSE" is printed during the satellite pass. It consists of Doppler counts from each of the two receiver channels, labeled 400-CH and 150-CH, plus a refraction corrected combination labeled "count". The 150 MHz and 400 MHz counts differ slightly from each other because of refraction error introduced as the signals pass through the ionosphere. This ionospheric refraction error must be removed to achieve the best fix accuracy. Fortunately, the difference between the two counts provides a measure of the error, and the third column is the result of removing that error, i.e., they are the refraction corrected Doppler counts.

The Doppler printout of Figure 6 illustrates a very significant step forward in commercially-available satellite navigation. All other navigation programs make use of two-minute Doppler counts only, i.e., each count is accumulated over a period of two minutes. Typically there will be six to eight of these per satellite pass. A brief loss of lock on the satellite signal invalidates at least one of these two-minute counts, which is a large fraction of the total Doppler data available. In Figure 6, the counts numbered 05, 10, 15, 20, 25, 30, and 35 are the two-minute Doppler counts. All the others are subtotals of the accumulating two-minute counts taken approximately every 23 seconds. The point is that every one of these provides the computer with an independent, refraction-corrected Doppler count. A brief loss of lock now invalidates only a few of the 23-second counts, rather than one or more of the long two-minute counts. By this means, plus others not so obvious, the short Doppler program provides more position fixes, more reliable position fixes, and substantially better accuracy. These attributes are discussed later in this paper as well as in Reference 3.

Loss of Lock

Suppose the receiver were to lose lock on the satellite signal as shown at count number 08 in Figure 6. One or both of the channel lock lights would blink off, indicating loss of lock. The bit and message synchronization lights would remain on, however. Bit and message synchronization can be maintained in what is called the coast mode for well over a minute. This permits Doppler and message data to be processed immediately after regaining lock without having to wait for the next even-minute time mark.

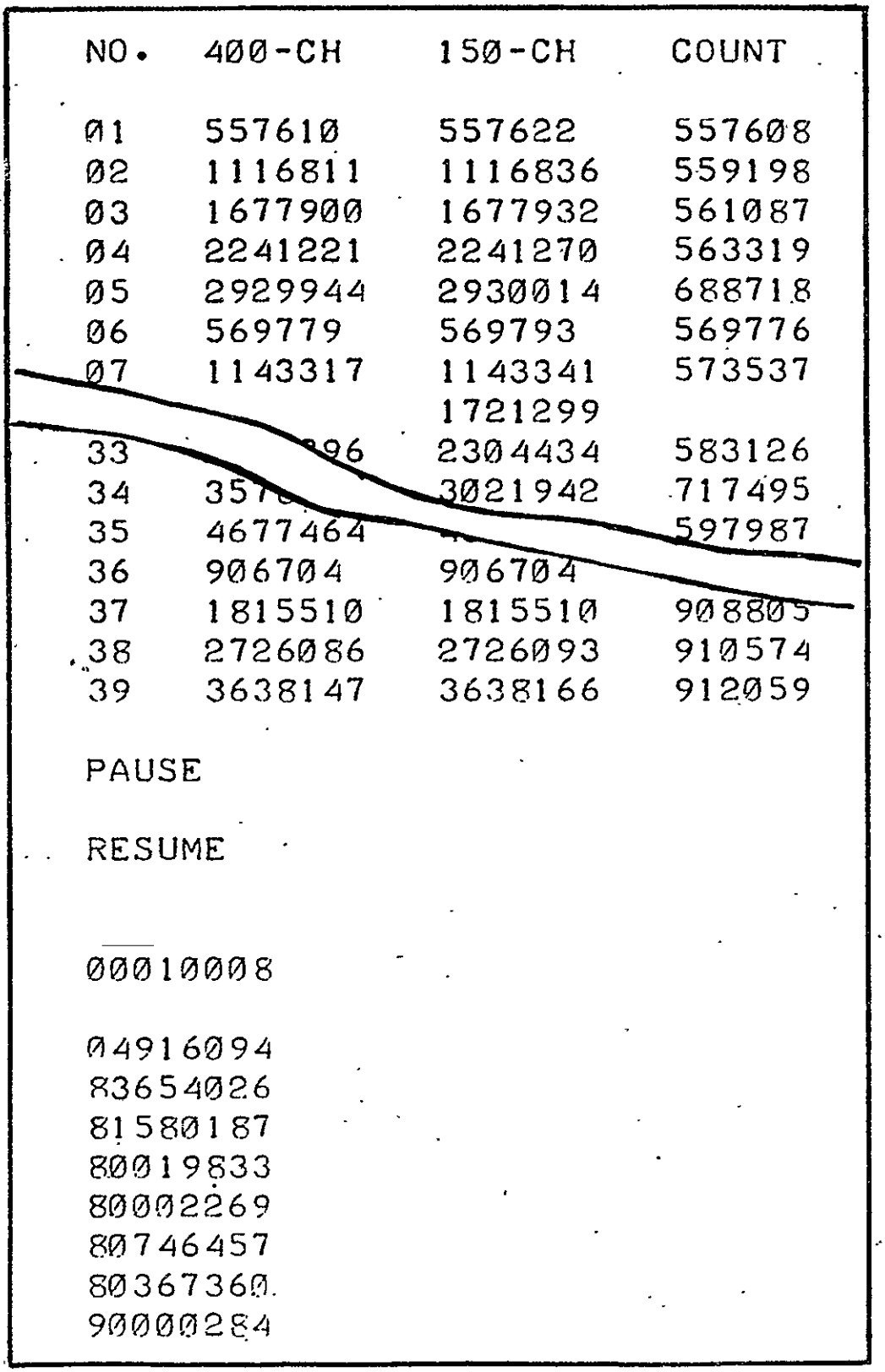

NO.	400-CH	150-CH	COUNT
01	557610	557622	557608
02	1116811	1116836	559198
03	1677900	1677932	561087
04	2241221	2241270	563319
05	2929944	2930014	688718
06	569779	569793	569776
07	1143317	1143341	573537
		1721299	
33	[illegible]96	2304434	583126
34	357[illegible]	3021942	717495
35	4677464	[illegible]	597987
36	906704	906704	
37	1815510	1815510	908805
38	2726086	2726093	910574
39	3638147	3638166	912059

PAUSE

RESUME

00010008

04916094
83654026
81580187
80019833
80002269
80746457
80367360
90000284

1069-2706

Figure 6. Optional Output of Satellite Doppler and Navigation Message Data

For a few seconds the receiver will dwell at the last locked frequency. If the signal appears during this dwell interval, lock will be instantaneous. After the dwell interval, the receiver begins to search over a frequency band centered on the last known frequency, as illustrated by Figure 5b. This search region is moved slowly upward to anticipate the continuing Doppler shift. The narrow search region promotes rapid signal reacquisition, and it also reduces the chance of tuning to some other available signal, such as another satellite.

If loss of lock was because the satellite pass was over, then the frequency search will return to the rise frequency region of Figure 5a after about 90 seconds. The computer automatically will begin the position fix process as soon as this occurs or as soon as it has sufficient data, whichever occurs first.

The Position Fix

As soon as the computer recognizes that the satellite pass is over, it types the word PAUSE and does just that for 30 seconds. This gives the operator an opportunity to re-initialize the computer if he wants to adjust values of estimated latitude, longitude, heading, speed, or antenna height. Initialization is started by hitting the Teleprinter "line feed" key. The computer then asks for each initialization parameter, and the operator supplies the value or answers "no" if no change is required. If an initialization is not required, the operator may hit any other key or simply wait 30 seconds; in either case the computer will then type RESUME and do just that.

If the operator requested the Doppler printout, the data shown in Figure 6 after RESUME are also provided. These are the verified satellite message parameters. The satellite message is transmitted a number of times during a satellite pass. If an error occurs during reception, it can be detected and eliminated by comparison with the same data received several other times. This process is called verification or majority voting.

Figure 7 shows the remainder of the position fix printout. The first two lines are optional and show the result of each iteration of the fix computation. The computer must solve for three parameters: latitude, longitude, and offset frequency. Each numbered line shows the computed value of frequency, followed by the changes in frequency, latitude, and longitude produced by that iteration. The computation is repeated, or iterated, until these changes are less than a preset criterion. At that point the fix is said to have converged, and the final result is printed.

The line of zeros and ones with two arrows underneath is a very useful fix quality index. Each character represents one of the short Doppler counts. A "one" shows that it was used in the fix computation and a "zero" shows that it was not. A "zero" indicates either that a particular Doppler count was not available or that the program deleted that count as part of its low elevation Doppler editing routine. If a low elevation count must be used because there are too few counts to permit further editing, a question mark will be printed, indicating a less than desirable count.

```
01      31967.082    -32.927694      0.0000011     -0.0000010
02      31967.082     0.0009201     -0.0000001     -0.0000005

000111101111111111111111111111111110000
                      ↑↑

SAT FIX   MAPS-69227

DAY   TIME  LATITUDE       LONGITUDE
290   0918  033 50.459 N   118 20.272 W

HDG    SPD     ANT      ITER  ELEV
000.0  000.0   +0013.    02    40

SAT ID = 7464.57
```

1069-2707

Figure 7. Position Fix Printout

The two arrows mark the satellite pass center, i.e., the time of closest approach. Accuracy is very dependent on having enough Doppler data and on that data being reasonably symmetrical about the pass center. Therefore, this Doppler spread printout is a very effective indicator of fix quality. One should tend to discount a pass in which the Doppler data has many long gaps or is badly unsymmetrical. Short Doppler counts help prevent these conditions by reducing data loss and by permitting a more symmetrical Doppler edit.

The satellite fix printout is essentially self-explanatory. MAPS-69227 is the program "model number", showing that it was compiled on day 227 of year 1969. The fix time is hours and minutes GMT. The heading, speed, and antenna height are the initialization parameters used for that fix computation. Speed is expressed in knots and antenna height in meters above the reference ellipsoid. The number of iterations required to converge and the maximum elevation angle of the satellite pass are useful in evaluating fix quality. Too many iterations or too low or too high an elevation angle warrants caution. The satellite ID, or identification, is the semi-major axis of its orbit in kilometers. The fix computation requires about 30 seconds per iteration.

Fix Re-Computation

After the fix computation is complete, the operator may realize that one or more of the initialization parameters were incorrect. All too often he may

have forgotten to tell the computer of a change in speed or heading. To recover, he types RCMP, meaning recompute, and the computer again requests the initialization parameters. As soon as the new initialization is complete, the position fix is re-computed with the revised parameters.

FREQUENCY OF SATELLITE FIXES

Figure 8 shows the navigation satellite passes for San Diego during the 48 hours of 3-4 November 1969. It is clear that the distribution is not uniform. At times there are relatively long gaps, and at other times passes may occur almost simultaneously. A few more satellites would do much to reduce the average time between fixes and sharply reduce the incidence of long gaps.

Simultaneous passes can be troublesome. For instance, at 0602 a 75° pass begins which will not yield a reliable fix. However, it will have captured the receiver during the 28° pass which begins a few minutes later. Only if one were aware of this interference and manually tuned the receiver to the preferred signal would a desirable fix be obtained. At other times, it is possible for the receiver to switch from one satellite signal to another during simultaneous passes. This situation is one reason why a narrow re-acquisition frequency searoh is desirable, to minimize the possibility of locking to the second satellite signal.

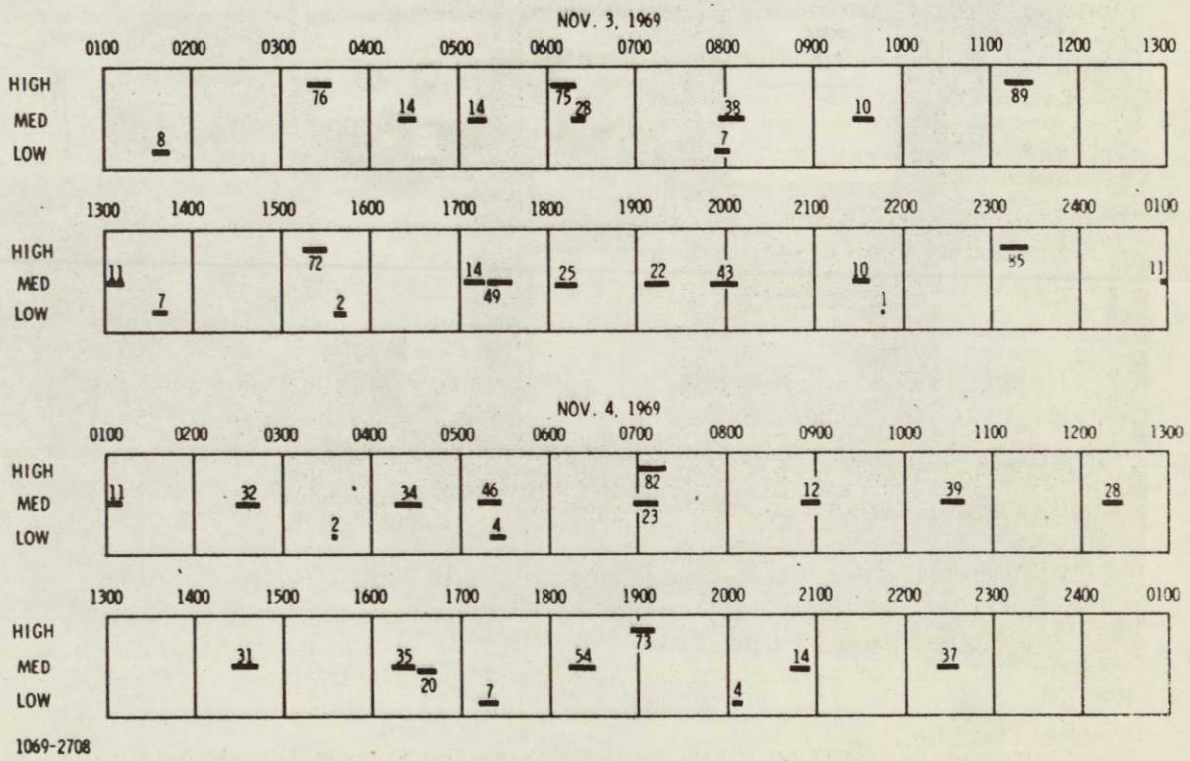

Figure 8. Satellite Passes for San Diego During 3–4 November 1969

It is likely that during the 48 hours shown, 24 or 25 acceptable satellite fixes would be obtained. This is an average of one fix every two hours. The longest gap with no acceptable fix would be either 4 hours or 4.35 hours, depending on whether the 7° pass at 0753 blocked the 38° pass at 0758. The receiver's narrow search region helps to ignore low elevation passes, but 7° is a marginal case.

SYSTEM INTEGRATION

Of all the navigation systems now in use, only certain inertial systems and the TRANSIT Navigation Satellite System have required a digital computer. However, once a digital computer is introduced into the realm of navigation, it becomes obvious that better results can be obtained by tying all the primary navigation sensors into the computer. The result is commonly called an Integrated Navigation System. Reference 3 discusses one such system.

Most users configure the system for their own navigation requirements and for their particular operational constraints. Two examples are given in Figures 9 and 10. The first shows one of the GEO NAV Systems now in operation by the GSI Division of Texas Instruments. From left to right the major components of this system are: 1) VLF receivers for radio navigation, 2) an

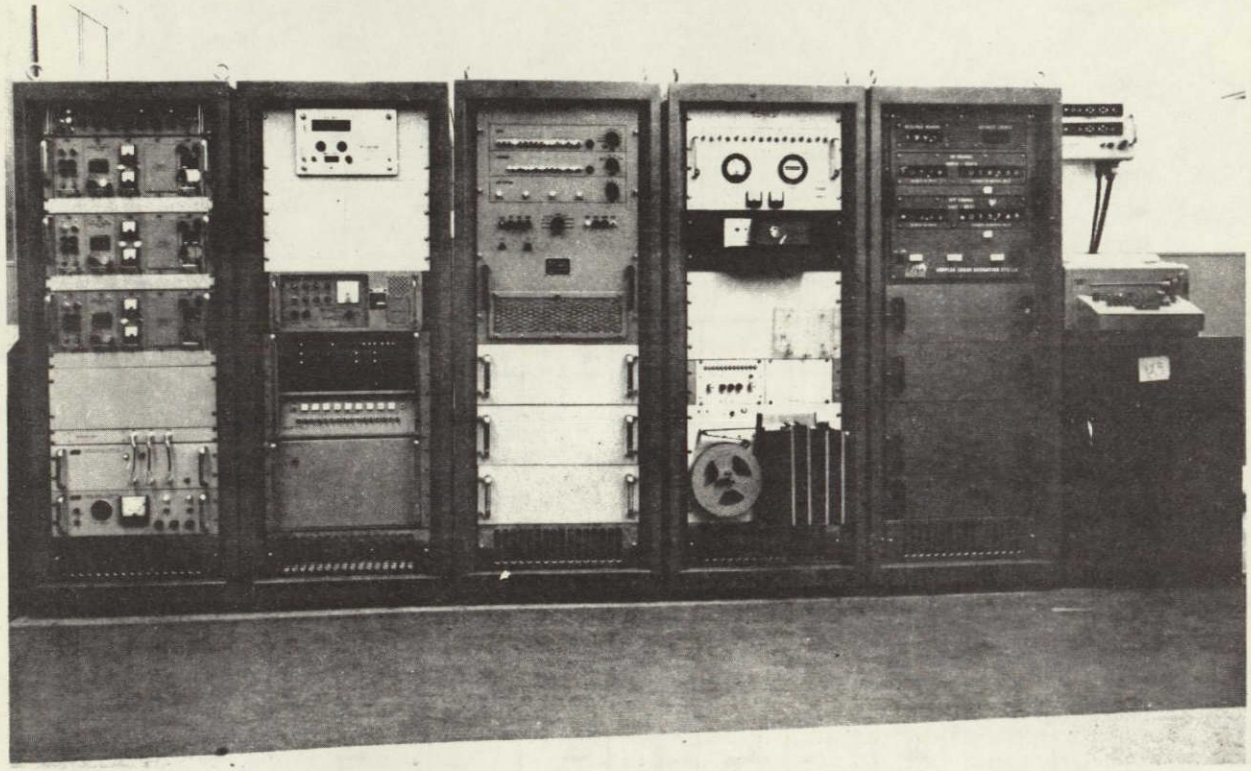

1069-2709
UNCLASSIFIED

Figure 9. GEO NAV Integrated Navigation System Developed by the GSI Division of Texas Instruments (Photograph courtesy of GSI Division of Texas Instruments)

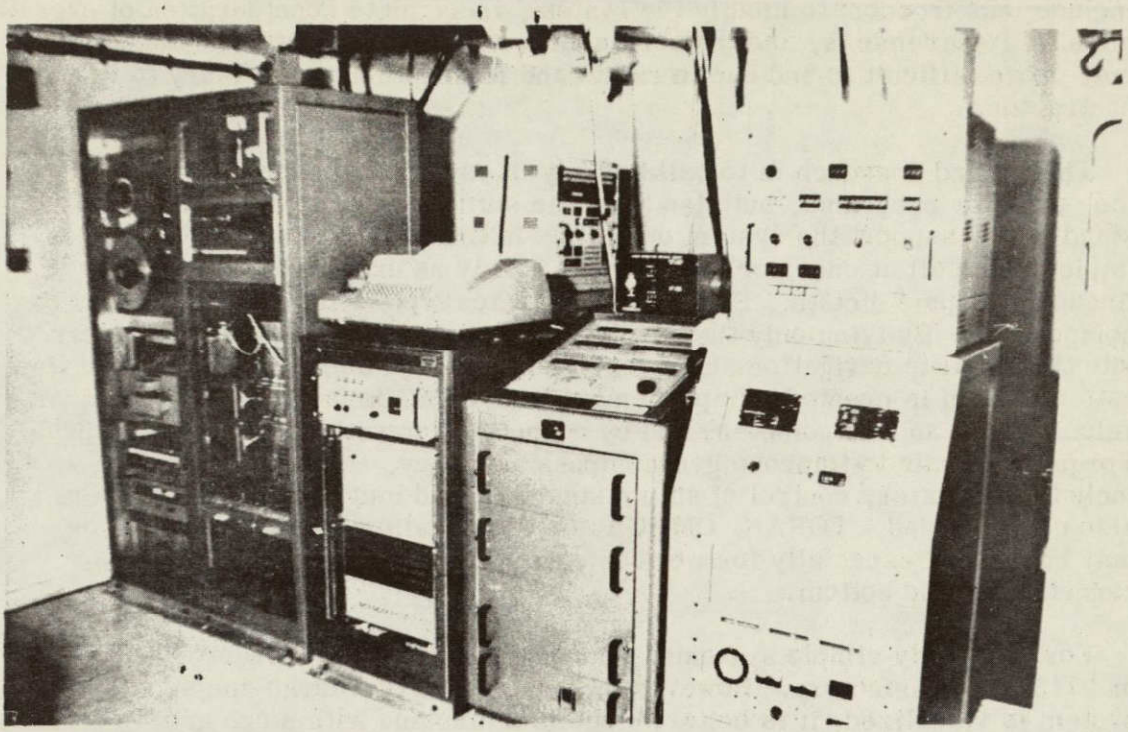

1069-2710
UNCLASSIFIED

Figure 10. Integrated Navigation System Developed by Western Geophysical Division of Litton Industries (Photograph courtesy of Western Geophysical)

EM speed log, 3) the Magnavox 702 satellite receiver with Hewlett Packard 2115 computer, 4) the Texas Instruments 2054 computer, 5) special interface equipment, and 6) a Doppler sonar navigator. The Texas Instruments computer is the central integration element, and future systems will eliminate the need for the extra Hewlett Packard computer. See Reference 4 for additional details.

Figure 10 shows one of the integrated navigation systems now in operation by the Western Geophysical Division of Litton Industries. From left to right are: 1) a magnetic tape recorder, 2) special interface equipment, 3) the Magnavox MX/702/hp satellite navigation system, 4) a Doppler sonar navigator, and 5) a Litton inertial navigation computer and display unit. In this system, the inertial system is the central integration element. All raw data is recorded for post-mission analysis. See Reference 5 for additional details.

From the user's point of view, it appears that there are only two practical approaches to an integrated navigation system. One is to vest complete responsibility for system design, installation, operation, and maintenance in a single systems contractor. In this way, the user in effect purchases navigation services from the contractor rather than having personnel who understand or support the system directly. Disadvantages of this approach

include less freedom to modify the system, incomplete consideration of overall mission requirements, and the sole-source operation/maintenance contract may prove difficult to end due to rights and information proprietary to the contractor.

The second approach is to build or buy the system components, including the computer programs, but also to obtain sufficient documentation to understand and to support the system directly. In this way, the system may be implemented all at once, or it may grow slowly as experience, need, and financial support dictate. Figure 11 illustrates typical integrated system components. By tying only the resolved velocity outputs of a Doppler sonar into the satellite navigation computer, a simple but effective integrated navigation system is created. Improvements can be made later by adding a velocimeter, an inclinometer, and by connecting directly to the gyrocompass. Torquing signals to improve gyrocompass accuracy, additional displays including a plotter, control of ship's steering, and magnetic data recorders also can be added. LORAN, OMEGA, or other radio navigation aids also may be useful, especially for work in deep water where Doppler sonar cannot reach the bottom.

For relatively simple systems, computers such as the Hewlett Packard 2114 or 2115 are satisfactory. However, where growth to a large and sophisticated system is visualized, it is better to obtain a machine with more growth potential, such as the Hewlett Packard 2116, as pictured in Figure 12.

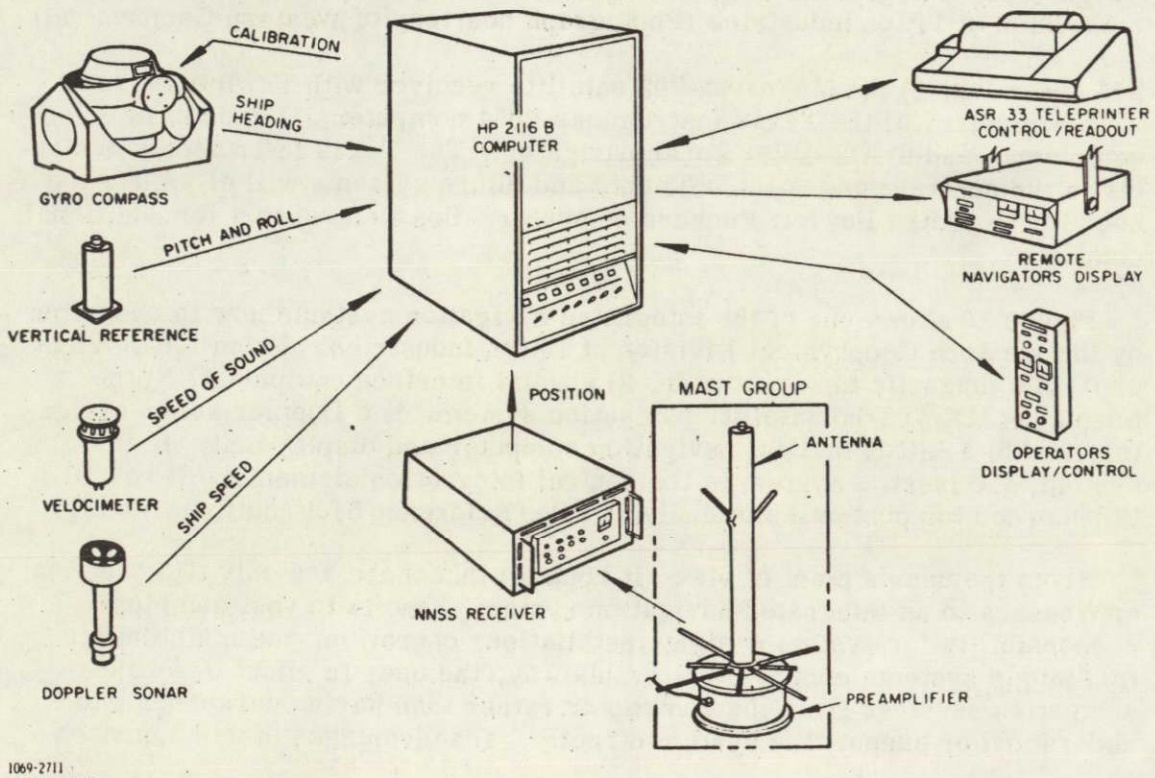

Figure 11. Typical Components for an Integrated Geophysical Navigation System

1069-2712
UNCLASSIFIED

Figure 12. Magnavox MX/702/hp with Hewlett Packard 2116 Computer for Expandable System Applications

This writer is convinced that a simple and direct approach to system integration is preferable to some of the more sophisticated schemes which have been proposed. In the first place, there is real benefit in understanding how the system works in simple cause and effect terms, rather than having its characteristics obscured by a complicated Kalman-type filter. The simple approach is especially helpful when troubleshooting a system to find which component is not performing properly. The simple approach also makes a simple change simple, rather than forcing a rework of the entire system filter equations. Second, when the inherent satellite position fix accuracy is 150 ft. RMS and when the dead reckoning equipment errors are either deterministic or clearly orthogonal, there is little or no accuracy advantage in using a Kalman filter compared to filtering separately each of the major error sources, e.g., the gyrocompass azimuth bias. Finally, it is clear that post-mission data anlysis will always give better accuracy than can be achieved in real time. (In real time, the position error is always greater just before a satellite fix. In post-mission analysis, the error before and after the fix is the same; the worst error is half-way between satellite fixes.) Therefore, complexity of field equipment and software should be limited to satisfying only the field navigational requirements. Raw data should be recorded for conducting a thorough post-mission analysis.

SATELLITE FIX ACCURACY

From the user's point of view, there are only three factors which influence satellite position fix accuracy. They are: 1) accuracy of expressing ship's motion, 2) accuracy of antenna height, and 3) adequacy of the satellite navigation equipment and fix program.

Expressing Ship's Motion

When satellite navigation is used independently, i.e., not as part of an integrated system, ship's motion is normally expressed by speed and heading entered manually through the Teleprinter. Both of these numbers will be somewhat in error. Errors may come from the instrumentation, from unknown wind and current effects, and/or from human error. Nevertheless, the position fix will be affected. Figure 13 shows the effect on one fix of a one-knot velocity error in each of eight compass directions.

Two points are clear. The fix error is greater when the velocity error is in a north-south direction, and the error is not trivial. References 2 and 3 discuss the error sensitivity in more detail. A good rule of thumb is to assume about 0.25 n.mi. of fix error for every knot of velocity error.

Except in integrated navigation systems, the velocity error is likely to be predominant. Integrated systems using Doppler sonar can achieve velocity errors of 0.5% or less, which at 10 knots is 0.05 kt. Using the 0.25 n.mi. per knot rule of thumb gives a resultant fix error of only 75 ft. for this example.

Antenna Height Accuracy

Unfortunately, the geoidal height map is not entirely accurate. It was developed through analysis of satellite tracking data, a process called satellite geodesy. However, the fine structure of geoidal height variation has very little

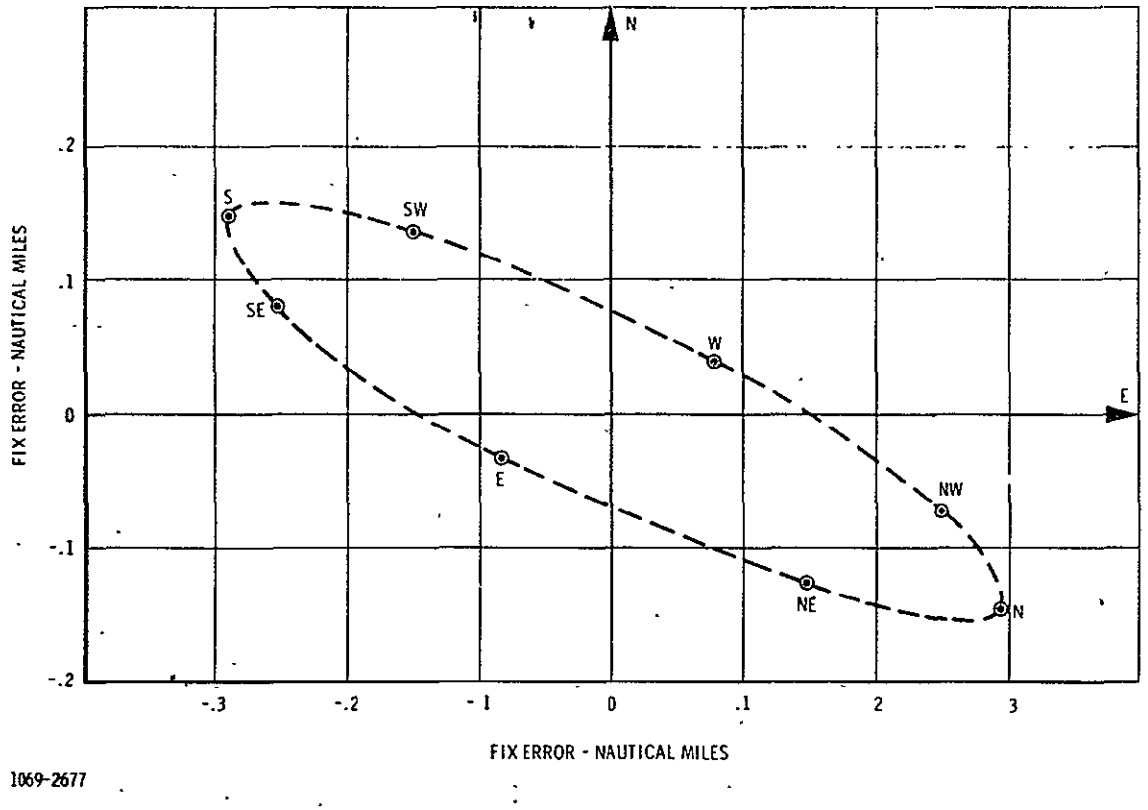

Figure 13. Effect of a One Knot Velocity Error on the Fix from a 53° Satellite Pass. Direction of Velocity Error is Noted Beside Each of Eight Fix Results. Satellite Was West of Receiver and Heading South.

effect on a satellite's motion as it passes 600 n.mi. overhead at a speed of nearly five miles per second. Therefore, errors of 20 meters or more exist in the map. Sensitivity to antenna height error is given by Figure 11 of Reference 2.

The Magnavox Company is developing a computer program capable of accurately determining antenna height as well as the latitude and longitude of a fixed antenna. Early results are very encouraging. The program is intended for land survey missions, but it also may prove useful in removing local bias error in the geoidal height map.

Basic Fix Accuracy

Figure 5 of Reference 3 is reproduced here as Figure 14. It shows the 268 ft. RMS fix accuracy which was being obtained in November, 1968. The MX/702/hp computer program which gave these results employed only two-minute Doppler counts, and these results are typical of all such two-minute Doppler programs. This same set of raw data also was processed by an experimental short Doppler program in an IBM 360-40 computer, and the accuracy was improved dramatically to 124 ft. RMS. In addition, five fixes which had been rejected by the two-minute program for having too little Doppler data were accepted by the short Doppler program and gave good position fixes. These results are shown in Figure 6 of Reference 3.

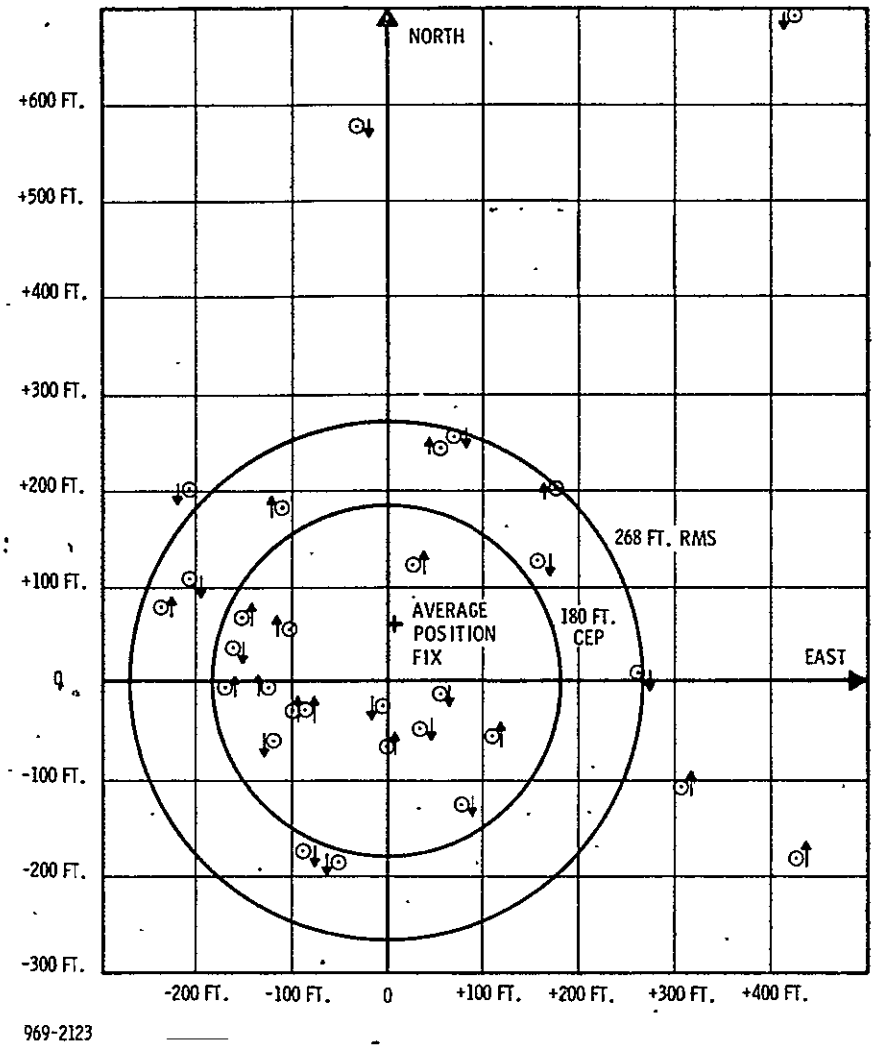

Figure 14. Bulls-eye Plot of 30 Fixes from the MX/702/hp Using a Two-Minute Doppler Program

In mid-August, 1969, the first short Doppler program was issued to all users of the MX/702/hp. The output from the MAPS-69227 program is illustrated in Figures 6 and 7, and typical accuracy results being obtained are shown in Figure 15. Although 168 ft. RMS represents a real step forward compared to the two-minute program, the goal of 124 ft. has not been reached. Work will continue toward this goal. Very recently an improvement was made which gave the 150 ft. RMS accuracy shown in Figure 16. This improvement will be released to users of MX/702/hp systems during November, 1969.

Several interesting facts can be learned from a study of Figures 14, 15, and 16. Note from Figure 15 that some of the fixes were taken while using an atomic (rubidium) reference oscillator and the rest were taken using the built-in crystal reference oscillator after a warm-up period of 48 hours. It is clear that there is absolutely no penalty from using the internal crystal oscillator.

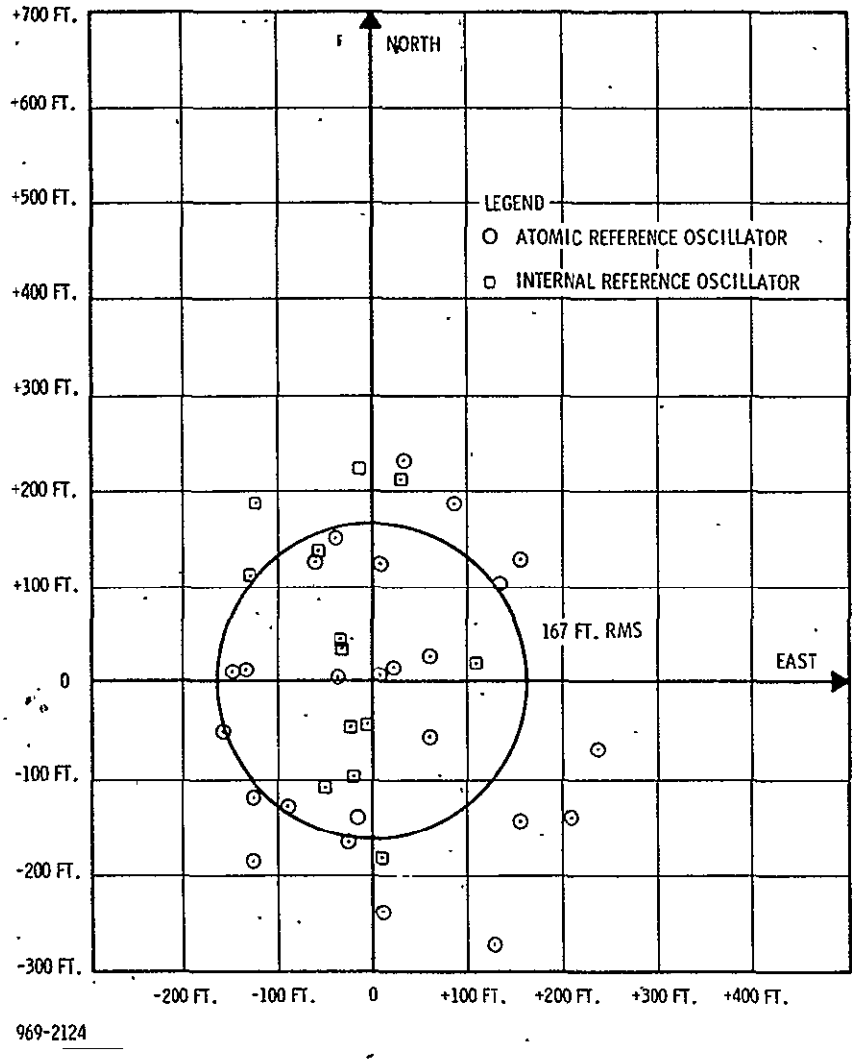

Figure 15. Bulls-eye Plot of 38 Fixes from the MX/702/hp Using the MAPS-69227 Short Doppler Program

Table I is a list of the RMS and CEP statistics from each of the bulls-eye plots. Note that the raw data for items 1 and 4 were identical, only the computer programs reducing the data were different. Also recall that the RMS statistic is influenced very strongly by a few large errors. On the other hand, the CEP, which is the radius of the circle containing exactly 50% of the fix results, is influenced strongly by a large number of very good results.

The MAPS-69227 results show only slight improvement of the CEP, but the RMS was much improved. In other words, the very best fix results from either program were not much different, but the short Doppler program did dramatically reduce the incidence and severity of occasional poor fixes. This is an important improvement in terms of increasing the reliability of obtaining good fix results.

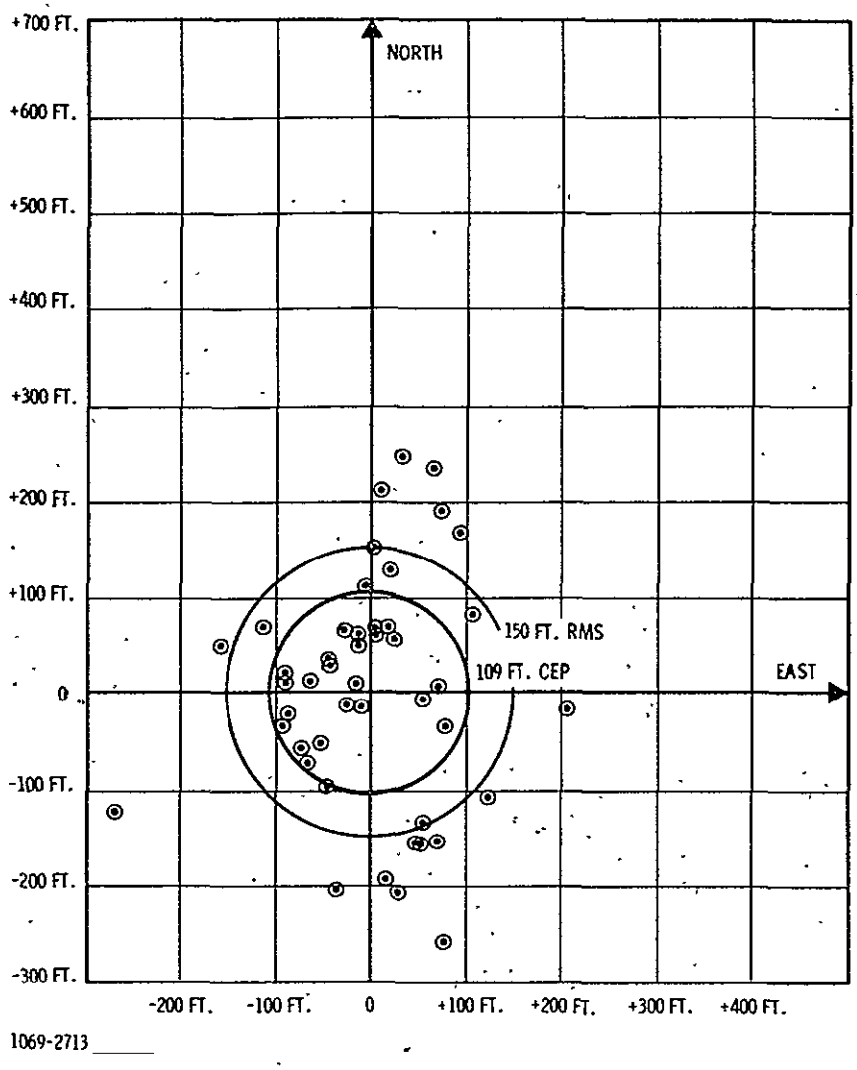

Figure 16. Bulls-eye Plot of 46 Fixes from the MX/702/hp Using an Improved Version of the Short Doppler Program

TABLE I
ACCURACY STATISTICS FOR THREE COMPUTER PROGRAMS

	RMS ft	CEP ft
1. Two-Minute Doppler Program	268	180
2. MAPS-69277 Short Doppler Program	168	158
3. Improved Short Doppler Program	150	109
4. Experimental Program	124	99

The most recent change to the MX/702/hp short Doppler program reduces the RMS error slightly, but it makes a strong improvement in the CEP. This means that a small error source has been eliminated so that the best fixes are now even better. With this improvement, the CEP is nearly as good as that of the experimental program. Further accuracy and fix reliability improvements can be expected.

REFERENCES

1. R.E. Doan and William M. Mebane, "Impact of Satellite Navigation on Marine Geophysical Surveys," presented at 39th Annual Meeting of the Society of Exploration Geophysicists, Calgary, Canada, 14-18 September, 1969.

2. Thomas A. Stansell, Jr., "The Navy Navigation Satellite System: Description and Status", NAVIGATION, Vol. 15, No. 3, Fall 1968.

3. Thomas A. Stansell, Jr., "An Integrated Geophysical Navigation System Using Satellite-Derived Position Fixes", Offshore Technology Conference Preprints, Vol. II, May 18-21, 1969.

4. Dr. David R. Reinhartsen, "The GEO NAV System", Marine Geodesy Symposium sponsored by the Marine Technology Society, November 3, 1969.

5. Alton B. Moody, "High Accuracy Offshore Navigation", Marine Geodesy Symposium sponsored by the Marine Technology Society, November 4, 1969.

APPENDIX IV

LINK CALCULATIONS

In this section power budgets have been computed for an ideal system, that is, one in which multipath does not significantly degrade the performance of the communication link. With the TDRS at an altitude of 22,300 miles and the user satellite maintained in a fixed orbit ranging from 100 miles to 1000 miles, the distance of the user/DRSS link varies from 21,300 miles to 26,750 miles. Primary consideration in this section is the uplink which assumes a carrier frequency in the band 14,875 to 15,350 MHz for the ground/TDRS link and a VHF carrier frequency of 400 MHz, and S-band carrier frequency ranging from 2,025 to 2,120 MHz, and a K-band carrier frequency in the band 13,250 to 13,725 MHz for the TDRS/user link.

The power requirements for each of the aforementioned communications links are presented in Tables A through D. Assumed in each table is a minimum and maximum system margin of 6 and 10 dB respectively; furthermore, the user antennas in all cases is assumed to have a 0 dB gain. Table A contains the power requirements for the TDRS/user link at 400 MHz. For this link a 16 dB TDRS antenna gain is assumed and the path loss varies from 175 dB to 176.8 dB, resulting in a minimum and maximum transmitter power requirement of 37.2 and 43.0 dbm respectively. For the S-band link the TDRS antenna gain is assumed to be 32 dB and the path loss variation of 189.4 to 192.0 dB. The available power at the receiver of the user spacecraft as shown in Table B varies from 67.4 $\frac{\text{dbm}}{\text{Hz}}$ to 81.3 $\frac{\text{dbm}}{\text{Hz}}$. The TDRS antenna gain for the TDRS/user K-band link presented in Table C, is assumed to be 48 dB, with a path loss ranging from

205.48 to 207.56 dB. The available receiver $\frac{C}{No}$ for this link is a maximum of 80.4 $\frac{dbm}{Hz}$ and a minimum of 92.24 $\frac{dbm}{Hz}$.

The power requirements for the ground/TDRS K-band link are presented in Table D. For this case a TDRS antenna gain of 49 dB is assumed and a minimum and maximum path loss of 206.4 and 208.54 dB respectively, resulting in an available receiver power level varying from 81.1 $\frac{dbm}{Hz}$ to 92.96 $\frac{dbm}{Hz}$.

TABLE A

Power Requirements for
TDRS/User Link

Carrier frequency = 400 MHz

Description	Max	Min	Remarks
$\frac{C}{N_o}$ Desired (dB-Hz)	40	40	
Margin Needed (dB)	10	6	
N_o = Noise Spectral Density $\frac{dbm}{Hz}$	-167.8	-167.8	
C = Carrier Power Required (dbm)	-117.8	-121.8	
G_t = User Antenna Gain (dB)	0	0	
G_r = DRSS Antenna Gain (dB)	16	16	
L_p = Path Loss (dB)	176.8	175	
P_t = Transmitter Power Required (dbm)	43.0	37.2	$P_t = C + L_p - G$
(watts)	20.0	5.2	

TABLE B

Power Requirements for
TDRS/User Link

Carrier frequency = 2025-2120

Description	Max	Min	Remarks
P_t = Transmitter Power Available (dbw)	20	10	
(dbm)	50	40	
G_t = User Antenna Gain (dB)	33.5	23.0	
G_r = DRSS Antenna Gain (dB)	32.0	32.0	
L_p = Path Loss (dB)	192.0	189.4	
C = Carrier Power Available (dbm)	-76.5	-94.4	$P_t - L_p + G_t + G_r$
Margin Needed (dB)	10	6	
N_o = Noise Spectral Density $\frac{dbm}{Hz}$	-167.8	-167.8	
$\frac{C}{N_o}$ Available at Input (dbm-Hz)	81.30	67.4	$C-M-N_o$

TABLE C

Power Requirements for
TDRS-User Link

Carrier frequency = 13250-13725

Description	Max	Min	Remarks
P_t = Transmitter Power Available (dbw) (dbm)	20 50	10 40	
G_t = User Antenna Gain (dB)	44	36	
G_r = DRSS Antenna Gain (dB)	48	48	
L_p = Path Loss (dB)	207.56	205.48	
C = Carrier Power Available (dbm)	-65.56	-81.48	$P_t - L_p + G_t + G_r$
Margin Needed (dB)	10	6	
N_o = Noise Spectral Density $\frac{dbm}{Hz}$	-167.8	-167.8	
$\frac{C}{N_o}$ Available at Input (dbm-Hz)	92.24	80.4	$C - M - N_o$

TABLE D

Power Requirements for
GND/TDRS Link

Carrier frequency = 14875-15350

Description	Max	Min	Remarks
P_t = Transmitter Power Available (dbw)	20	10	
(dbm)	50	40	
G_t = User Antenna Gain (dB)	44.7	36.7	
G_r = DRSS Antenna Gain (dB)	49	49	
L_p = Path Loss (dB)	208.54	206.4	
C = Carrier Power Available (dbm)	-64.84	-80.7	$P_t - L_p + G_t + G_r$
Margin Needed (dB)	10	6	
N_o = Noise Spectral Density $\frac{dbm}{Hz}$	-167.8	-167.8	
$\frac{C}{N_o}$ Available at Input (dbm-Hz)	92.96	81.1	$C - M - N_o$

APPENDIX V

TDRS POSITION ERROR ANALYSIS ASSUMING 3 RANGE MEASUREMENTS

The previous formulation can be easily modified to characterize the simpler case where the TDRS position is established from the range measurements from three stations. Using the previous notation, the incremental equation to be used for small-error analysis now reads

$$\delta r_j = \sum_{i=1}^{3} \alpha_{ij}(\delta x_i - \delta p_i^{(j)}) \qquad (j=1,2,3)$$

or

$$\sum_{i=1}^{3} \alpha_{ij}\, \delta x_i = \delta r_j + \sum_{i=1}^{3} \alpha_{ij}\, \delta p_i^{(j)} = \delta r_j + \delta \xi_j$$

If we denote by C the 3×3 directional-cosines matrix, i.e., $C_{ij} = \alpha_{ij}$, and also assume it to be non-singular, then the position error equations can be written as

$$\underset{\sim}{\delta x} = C^{-1}(\underset{\sim}{\delta r} + \underset{\sim}{\delta \xi})$$

where the first term represents a range-measurement error contribution, and the second term a station-location error contribution.

If we assume a common location error $\delta p_i^{(j)} = \delta p$ for all coordinates i and stations j, the bias TDRS position error due to this effect is given by

$$(\underset{\sim}{\delta x})_{k,\,\substack{\text{station}\\\text{location}}} = \delta p \sum_{i=1}^{3} [C(C^{-1})^T]_{ik}$$

In turn, the covariance matrix of the TDRS position error due to zero-mean, independent, range-measurement errors is specified by

$$K(\underset{\sim}{\delta x}) = C^{-1} K(\underset{\sim}{\delta r}) . (C^{-1})^T ; \quad K(\underset{\sim}{\delta r}) = \text{diag}\ (\sigma_i^2)$$

or

$$[K(\underset{\sim}{\delta x})]_{ij} = \sum_{k=1}^{3} \sigma_k^2 (C^{-1})_{ik} (C^{-1})_{jk}$$

so the individual coordinate-error variances are given by

$$\sigma^2(\delta x_j) = \sum_{k=1}^{3} \sigma_k^2 (C^{-1})_{jk}^2$$

Example 4

$X(0,0,h+R)$

$S_1(0,0,R)$

$S_2(0,R/\sqrt{2},\ R/\sqrt{2})$

$S_4(R/\sqrt{2},0,R/\sqrt{2})$

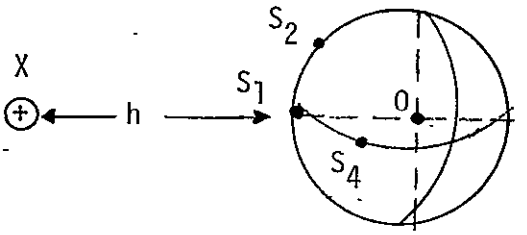

$$C = \begin{bmatrix} 0 & 0 & 1 \\ 0 & -R/\sqrt{2}D & 1-B \\ -R/\sqrt{2}D & 0 & 1-B \end{bmatrix} \qquad C^{-1} = \begin{bmatrix} \sqrt{2}D(1-B)/R & 0 & -\sqrt{2}D/R \\ \sqrt{2}D(1-B)/R & -\sqrt{2}D/R & 0 \\ 1 & 0 & 0 \end{bmatrix}$$

$$\sigma^2(\delta x_1) = \frac{2D^2(1-B)^2}{R^2}\ \sigma_1^2 + \frac{2D^2}{R^2}\ \sigma_4^2 \approx 69.8\ \sigma_1^2 + 70.8\ \sigma_4^2$$

$$\sigma^2(\delta x_2) = \frac{2D^2(1-B)^2}{R^2}\ \sigma_1^2 + \frac{2D^2}{R^2}\ \sigma_2^2 \approx 69.8\ \sigma_1^2 + 70.8\ \sigma_4^2$$

$$\sigma^2(\delta x_3) = \sigma_1^2$$

$$\frac{(\delta x_1)_p}{\delta p} = \frac{\sqrt{2}D}{R} - \frac{2\sqrt{2}D}{R}(1-B)-(1-B)D \approx -26$$

$$\frac{(\delta x_2)_p}{\delta p} = B \approx 0.0072$$

$$\frac{(\delta x_3)_p}{\delta p} = \frac{-R}{\sqrt{2}D} \approx -0.12$$

Example 5

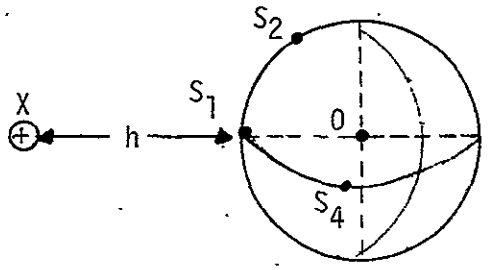

$X(0,0,h+R)$

$S_1(0,0,R)$

$S_2(0,\sqrt{3}R/2,R/2)$

$S_4(\sqrt{3}R/2,0,R/2)$

$$C = \begin{bmatrix} 0 & 0 & 1 \\ 0 & -\sqrt{3}R/2D'' & 1-B'' \\ -\sqrt{3}R/2D'' & 0 & 1-B'' \end{bmatrix}, \quad C^{-1} = \begin{bmatrix} \frac{2D''}{\sqrt{3}R}(1-B'') & 0 & -\frac{2D''}{\sqrt{3}R} \\ \frac{2D''}{\sqrt{3}R}(1-B'') & +\frac{2D''}{\sqrt{3}R} & 0 \\ +1 & 0 & 0 \end{bmatrix}$$

$$\sigma^2(\delta x_1) = \frac{4D''^2}{3R^2}(1-B'')^2\,\sigma_1^2 + \frac{4D''^2}{3R^2}\,\sigma_4^2 \approx 49.8\,\sigma_1^2 + 50.8\,\sigma_4^2$$

$$\sigma^2(\delta x_2) = \frac{4D''^2}{3R^2}(1-B'')^2\,\sigma_1^2 + \frac{4D''^2}{3R^2}\,\sigma_2^2 \approx 49.8\,\sigma_1^2 + 50.8\,\sigma_2^2$$

$$\sigma^2(\delta x_3) = \sigma_1^2$$

$$\frac{(\delta x_1)_p}{\delta p} = -\frac{2D''}{\sqrt{3}R} - \frac{4D''}{\sqrt{3}R}(1-B'') - (1-B'') \approx -22$$

$$\frac{(\delta x_2)_p}{\delta p} = B'' \approx 0.01$$

$$\frac{(\delta x_3)_p}{\delta p} = -\frac{\sqrt{3}R}{2D''} \approx -0.15$$

Example 6

$X(0,0,h+R)$

$S_2(0,R/\sqrt{2},R/\sqrt{2})$

$S_3(0,-R/\sqrt{2},R/\sqrt{2})$

$S_4(R/\sqrt{2},0,R/\sqrt{2})$

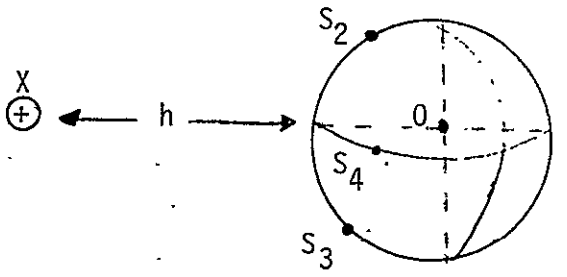

$$C = \begin{bmatrix} 0 & -R/\sqrt{2}D & 1-B \\ 0 & R/\sqrt{2}D & 1-B \\ -R/\sqrt{2}D & 0 & 1-B \end{bmatrix}, \quad C^{-1} = \begin{bmatrix} D/\sqrt{2}R & D/\sqrt{2}R & -\sqrt{2}D/R \\ -D/\sqrt{2}R & D/\sqrt{2}R & 0 \\ \frac{1}{2}(1-B)^{-1} & \frac{1}{2}(1-B)^{-1} & 0 \end{bmatrix}$$

$$\sigma^2(\delta x_1) = \frac{D^2}{2R^2}\sigma_2^2 + \frac{D^2}{2R^2}\sigma_3^2 + \frac{2D^2}{R^2}\sigma_4^2 \approx 17.7\,\sigma_2^2 + 17.7\,\sigma_3^2 + 70.8\,\sigma_4^2$$

$$\sigma^2(\delta x_2) = \frac{D^2}{2R^2}\sigma_2^2 + \frac{D^2}{2R^2}\sigma_3^2 \approx 17.7\,\sigma_2^2 + 17.7\,\sigma_3^2$$

$$\sigma^2(\delta x_3) = \frac{1}{4}(1-B)^{-2}\sigma_2^2 + \frac{1}{4}(1-B)^{-2}\sigma_3^2 \approx 0.254\,\sigma_2^2 + 0.254\,\sigma_3^2$$

$$\frac{(\delta x_1)_p}{\delta p} = -\frac{1}{2} - \frac{3\sqrt{2}D}{R}\,(1-B) \approx -18$$

$$\frac{(\delta x_2)_p}{\delta p} = \frac{1}{2}$$

$$\frac{(\delta x_3)_p}{\delta p} = -\frac{R}{2\sqrt{2}D}\,(1-B)^{-1} \approx -0.06$$

Example 7

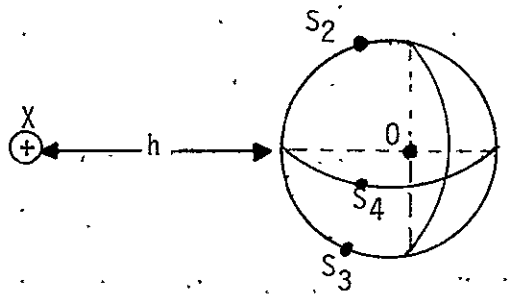

$X(0,0,h+R)$

$S_2(0,\sqrt{3}R/2,R/2)$

$S_3(0,-\sqrt{3}R/2,R/2)$

$S_4(\sqrt{3}R/2,0,R/2)$

$$C = \begin{bmatrix} 0 & -\frac{\sqrt{3}R}{2D''} & 1-B'' \\ 0 & \frac{\sqrt{3}R}{2D''} & 1-B'' \\ -\frac{\sqrt{3}R}{2D''} & 0 & 1-B'' \end{bmatrix}, \quad C^{-1} = \begin{bmatrix} \frac{D''}{\sqrt{3}R} & \frac{D''}{\sqrt{3}R} & -\frac{2D''}{\sqrt{3}R} \\ -\frac{D''}{\sqrt{3}R} & \frac{D''}{\sqrt{3}R} & 0 \\ \frac{1}{2}(1-B'')^{-1} & \frac{1}{2}(1-B'')^{-1} & 0 \end{bmatrix}$$

$$\sigma^2(x_1) = \frac{D''^2}{3R^2}\,\sigma_2^2 + \frac{D''^2}{3R^2}\,\sigma_3^2 + \frac{4D''^2}{3R^2}\,\sigma_4^2 \approx 12.7\,\sigma_2^2 + 12.7\,\sigma_3^2 + 50.8\,\sigma_4^2$$

$$\sigma^2(x_2) = \frac{D''^2}{3R^2}\,\sigma_2^2 + \frac{D''^2}{3R^2}\,\sigma_3^2 \approx 12.7\,\sigma_2^2 + 12.7\,\sigma_3^2$$

$$\sigma^2(x_3) = \frac{1}{4}(1-B'')^{-2}\,\sigma_2^2 + \frac{1}{4}(1-B'')^{-2}\,\sigma_3^2 \approx 0.255\,\sigma_2^2 + 0.255\,\sigma_3^2$$

$$\frac{(\delta x_1)_p}{\delta p} = -\frac{1}{2} - \frac{6D''}{\sqrt{3}R}\,(1-B'') \approx -21$$

$$\frac{(\delta x_2)_p}{\delta p} = \frac{1}{2}$$

$$\frac{(\delta x_3)_p}{\delta p} = -\frac{\sqrt{3}R}{4D^{11}}(1-B^{11})^{-1} \approx -0.07$$

Discussion of Results

If we assume a common rms range-measurement error σ for all stations, as well as a common station location error δp for all station coordinates, then the previous results can be conveniently summarized as shown in the table that follows. For the satellite-station geometries considered in the examples, the tabulated values indicate that the 3 range-differences measurement procedure yields greater error magnitudes than the 3-ranges measurement procedure. Moreover, the errors exhibit a stronger variation with the geometries in the range-differences procedures. Any other conclusions regarding the error dependence on the system geometry is difficult since no major patterns are evident; e.g., sometimes a change in geometry increases one corrdinate error at the expense of another. In any case, it should be understood that the analysis and results have been concentrated on a single measurement (the rms error was obtained by ensemble-averaging over the random error contribution with no time dependence considerations). Needless to say, any smoothing of consecutive range samples will affect the effective TDRS position error, and the actual orbital determination technique to be used should be included in the analysis for a proper perspective.

TDRS Location Error Results: 3 Range Measurements

	σ_{x_1}/σ	σ_{x_2}/σ	σ_{x_3}/σ
Example 4	11.8	11.8	1
Example 5	10.0	10.0	1
Example 6	10.3	6.0	0.71
Example 7	8.7	5.0	0.71

(a) Normalized TDRS R.M.S. Location Errors due to Station Range-Measurement Errors

	δ_{x_1}/δ_p	δ_{x_2}/δ_p	δ_{x_3}/δ_p
Example 4	-26	0.0072	-0.12
Example 5	-22	0.01	-0.15
Example 6	-18	0.5	-0.06
Example 7	-21	0.5	-0.07

(b) Normalized TDRS Location Errors due to Station Location Errors

THE COMPANY • GOVERNMENT AND INDUSTRIAL DIVISION